Universitat Internacional de Catalunya

uic
barcelona

Tesis doctoral

Strategies to induce vascularization:

angiogenesis stimulation and tissue engineering blood vessels

Èlia Bosch Rué

Strategies to induce vascularization: angiogenesis stimulation and tissue engineering blood vessels

Èlia Bosch Rué

PhD Thesis

Bioengineering Institute of Technology

Universitat Internacional de Catalunya

Barcelona 2021

Supervisor: Dr. Román Pérez

Doctorate program: Health Sciences

Research field: Biomedical Engineering / Bioengineering

uic
barcelona

Acknowledgments / Agraïments

Finalment arriba el moment de tancar aquesta etapa de doctorat, i és per això que m'agradaria dedicar unes paraules d'agraïments a totes aquelles persones que d'alguna manera o altre hi han format part i han fet possible la seva finalització.

A tots els membres del BIT. A en Román, director de tesi, per haver-me donat la oportunitat de realitzar la tesi doctoral. A en Luís, per haver-me donat un cop de mà sempre que has pogut, sobretot als inicis (que sempre són durs!). A la Barbara, perquè sempre transmets alegria a tothom, i durant aquests quasi 4 anys hem passat de companyes de laboratori a amigues. Espero que no deixis mai d'explicar els teus acudits! Per molt dolents que a vegades puguin ser, sempre ens arrenques un somriure. A Leire, por estar siempre dispuesta a ayudar por mucho trabajo que puedas tener. Muchas gracias por todos los ánimos y ayuda a lo largo de esta tesis. A la Bego, pels cafès i animar-me quan més ho he necessitat. A Maria M. i a la Raquel Rodríguez, que llegasteis en pack, como zipi y zape. Gracias por transmitir vuestro toque de humor y gracias por el soporte que me habéis dado. A les últimes incorporacions predoc, a la Marina, que tot i coincidir poc temps, m'has demostrat ser una bona persona i lluitadora, y a Raquel Rojas, recién llegada y ya transmites facilidad para trabajar. També m'agradaria donar les gràcies a persones que han passat pel BIT en algun moment o altre. En Joan, perquè sempre hi posaves una mica d'humor a les coses, i per ser el més liant del lab. No hi havia dia que no et caigués una caixa de gel pel terra! Gràcies pel suport i consells. A Bea Santiago, por tus consejos. A la Júlia, per les ganes i dedicació que hi posaves en els experiments, i fer que treballar amb tu fos fàcil.

També m'agradaria agraïr a la resta d'integrants del BIT, tot i el poc temps que hem coincidit. A Emilio, Jennifer i Xavier M., por transmitir vuestras ganas y motivación en hacer las cosas de la mejor manera posible. También agradecer a Maria G., Miguel M., Yolanda, Miguel C. y Alejandro. Finalmente, a Isabel, por su amabilidad en hacer las cosas.

A la Noelia N., per la teva senzillesa i naturalitat, i per ajudar-nos amb el que has pogut. A la Noelia G., per ajudar-me amb temes de papeleo d'una manera eficaç. I a Maria Arregui, per haver-me donat algun cop demà.

Al grup de Ciències Bàsiques, amb els que hem compartit laboratori durant bona part de la tesi. Especialment a la Núria, per l'alegria i optimisme que m'has transmès durant tot aquest temps. Per tots els teus ànims i suport durant tota aquesta etapa. I perquè hem passat a ser persones que comparteixen un lab, a fer créixer una amistat fora de la universitat. Moltes

gràcies a tu i en Martí per escoltar-me i ser-hi sempre. També agrair a la Marta Pérez, per ajudar-me sempre que ho he necessitat, i a l'Andrea, per fer tot lo possible per esterilitzar-me els estris a temps. També agrair a l'Helena, per donar un toc optimista inclús en les situacions més difícils. Després de parlar amb tu les coses semblen més fàcils. També a la Laura, per preguntar sempre com van les coses i fer que les hores de cultius passessin més ràpid.

Me gustaría agradecer también a las chicas del servicio de esterilización con gas plasma de la UIC. Por la amabilidad que tuvieron conmigo des del primer día, y por esterilizar mis "cachivaches" en tiempo récord.

I would like to thank in a very special way all the people which I cross my path during my research stay at Duke University. First of all, I would like to thank Professor George Truskey, for accepting me for a research stay of 6 months, and for his mentoring and supervision during this period. Not only I could learn a lot about TEBV perfusion and functional assessment, but new ways of thinking and working in a lab. Special thanks to Ana Truskey, for being so nice with me since the first day we met. I would like to thank you all the rides to farmer's market, where I could discover the best gluten and dairy free bread I have ever eaten! Thank you for being so nice with me. I would also like to thank Truskey's lab members. Ellery, Anandita and Nadia, you were so kind with me since the first day I arrived. Thanks for helping me with all I needed. Muath, thank you for helping me and for sharing your craziest ideas, it was nice working with you. I must admit that I miss your jokes, but I hope you have found another innocent person to joke with!. Jay, for all your commitment, dedication and persistance in the lab. I am sure you will be a great doctor. Catherine, my deskmate, for the little chit chats we had, thanks for being kind with me. Crystal, for always being nice with me. I would also like to thank the post-docs. Xu, I could learn a lot from you and I am very grateful for that. Qiao, although we barely coincided, you demonstrated me to be a nice person. Thanks to all of you, you made me feel as one more of your lab team. It was really nice to work with all of you.

Per altra banda, m'agradaria agrair també al grup de catalans i espanyols amb qui vam coincidir durant l'estada a USA. A la Mariona i en Nacho, per la vostra senzillesa, naturalitat, sempre disposats a ajudar i acollir-me des del primer moment. Gràcies també per les excursions i per fer-me descobrir el món del rocòdrom. D'aquí va sorgir una amistat que estic segura que no es perdrà mai. A la Carol, per la gran força de voluntat que em vas demostrar tenir. A l'Oriol i la Raquel, per acollir-me i fer-nos descobrir Durham i voltants, i una mica més de la cultura americana. I al petit Èric! Que amb el seu somriure ens alegrava i enamorava a tots. I finalmente a Mabel y Luís, por vuestro gran humor y alegrar todas las comidas que

tuvimos en Duke. De Luís pudimos aprender mucho de la "dieta" americana. Gràcies a tots per acollir-me com una més en el grup.

Als meus biomèdics! A en Riki, perquè ets un crack, gràcies per haver-me visitat a Durham, per mostrar tant d'interès i curiositat. Estic segura que arribaràs molt lluny! A la Lídia, durant tots aquests anys hem fet créixer una gran amistat. Per tots els anys que vam compartir pis, per tots els sopars i festes de la vila i no-vila, per les visites Girona i Calaf, per les excursions, pels estimats berenars al Jansana, i podria seguir. Moltes gràcies per tot. Moltes gràcies a tots dos pel vostre suport i ànims durant tota aquesta etapa, tot i estar en tres franges horàries diferents, sempre hem trobat el moment per reunir-nos.

A l'Imma, m'has demostrat ser una persona molt valenta, i arriscar-se per fer allò que realment t'agrada. Moltes gràcies per estar al meu costat sempre i per donar-me ànims quan més ho he necessitat!

Finalment, m'agradaria agrair d'una manera molt especial a la meva família. Als meus pares, pel vostre suport incondicional i per haver cregut sempre en mi sense dubtar en cap moment. Moltes gràcies per haver fet tot lo possible perquè pogués arribar fins aquí. A les meves germanes. A l'Anna, en certa manera sempre ens has anat obrint camí. Gràcies per tots els teus consells doctoratils i de la vida. A la Sara, perquè ets la que "se li en va més la pinça" i ets capaç d'alegrar-nos en els pitjors moments. Gràcies per els consells i suport que m'has donat. I a la Neus, que som com el dia i la nit, però a la vegada com carn i ungla des de que vam néixer. Moltes gràcies per ser-hi sempre, escoltar-me i aconsellar-me. També vull agrair als meus cunyats, per ser-hi també durant tot aquest procés. Als petits de la família: Emma, Jac, Júlia i Clàudia, perquè sou capaços d'alegrar a qualsevol! I de la vostra curiositat infinita m'heu fet aprendre molt. M'agradaria donar les gràcies a l'avi Andreu, per ensenyar-me que en aquesta vida no s'aconsegueix res sense esforç, i per la capacitat de cantar-nos cançons improvisades amb rima en un moment! "qui canta els mals espanta". M'agradaria també agrair als avis que ja no hi són. Especialment a la Padrina, que gairebé a mitja tesi ens vas deixar. Sempre has tingut un somriure i rialla per endavant, i ens has ensenyat que amb constància i esforç tot es pot aconseguir. El teu riure se'ns encomanava. Moltes gràcies per cuidar-nos a tots fins al final. També agrair a l'avi Pere, cada vegada que parlàvem amb tu apreníem noves coses sobre la vida. I a la iaia Amparo, amb esperit de lluita fins al final. Finalment, no em puc deixar d'agrair a en Nuc, amic incondicional, i el duo Pipa i Pepa, que fan el dia a dia més distret.

A la meva família política, en Josep i la Paquita. Moltes gràcies per cuidar-me des del primer moment i fer-me sentir com una més de la família. Gràcies també pel vostre suport durant tot

A la padrina,

La nostra àngel de la guarda.

Abstract

Angiogenesis, which results in a capillary network formation, is one of the crucial events that take place when there is tissue damage, being critical for successful tissue regeneration. It does not only allow the arrival of oxygen, nutrients and waste removal, but it also allows the arrival of progenitor cells necessary to induce tissue restoration. However, when there is an excessive damage, tissues are unable to regenerate by themselves. During the last decades, tissue engineering emerged as an alternative to improve tissue regeneration, with the combination of biomaterials (which serves as scaffolds), cells and/or stimulatory molecules. Therefore, one of the aims of tissue engineering is to incorporate stimulatory molecules within scaffolds to promote blood vessel formation for successful tissue regeneration and integration. Alternatively, there are some clinical situations in which high caliber vessels are needed instead of capillary network formation. An example would be with cardiovascular diseases (CVD), such as atherosclerosis or aneurysms, in which blood vessel replacement is needed. Autologous and xenogeneic grafts present some limitations, mainly risk of disease transmission and shortage of donors. Therefore, tissue engineered blood vessels (TEBVs) emerged as a promising alternative.

Regarding angiogenesis, generally, growth factors have been incorporated within scaffolds as molecules of choice to stimulate blood vessel formation. Although they have demonstrated a proper angiogenic response, they present some limitations, such as delicate handling properties and short half-life. As naturally found in human body, ions have demonstrated to be a promising alternative, being able to stimulate cellular functions, such as blood vessel formation. However, sometimes there is no consensus about the appropriate non-toxic and therapeutic doses, due to a lack of concentration screening studies before introducing them into the scaffolds. Regarding TEBVs, different approaches have been described for their development. However, they usually include several manufacturing steps and additional biomaterial patterning or additional stimulus to acquire native vascular cell alignment.

This thesis is focused on angiogenesis stimulation and TEBVs, divided in two main blocks: i) development of a drug delivery system (DDS) with the incorporation of ions to stimulate early phases of bone regeneration, including angiogenesis; ii) development of TEBVs through extrusion-based approach.

In the first part, an initial screening of different concentrations of therapeutic ions was performed to assess non-toxic and therapeutic concentrations in angiogenesis and osteogenesis, with endothelial cells (ECs) and human mesenchymal stem cells (hMSCs),

respectively. Results allowed establishing therapeutic doses of both ions for blood vessel formation, although they showed impairment when tested for osteogenic differentiation. These ions were then incorporated within a biomaterial to allow forming a DDS, showing that the incorporated therapeutic ions could have antibacterial and angiogenic potential, allowing a sequential delivery of both ions. The designed DDS consisted of a fiber like structure incorporating hydroxyapatite based microparticles which could potentially be used for bone tissue regeneration.

In the second part, TEBVs were successfully developed with extrusion-based approach in one single step procedure. Moreover, specific vascular cell types were incorporated, with high cell survival and presenting native cell alignment and some vasoactive functionality. Furthermore, we could improve their mechanical properties by extruding TEBVs with high concentrations of collagen, allowing their perfusion with arterial shear stress. Further studies are required to prove their functionality and maturation, with the potential to be used as blood vessel replacement or even vascular disease modeling.

Resum

L'angiogènesis, que dona lloc a la formació de xarxes capil·lars, és un dels esdeveniments més importants que té lloc quan hi ha dany als teixits, sent fonamental per aconseguir la regeneració dels teixits. No només permet l'arribada d'oxigen, nutrients i eliminació de residus, sinó que també permet l'arribada de cèl·lules progenitores necessàries per induir la restauració dels teixits. Tot i així, quan es produeix un dany gran, els teixits no poden regenerar-se per si mateixos. En les darreres dècades, l'enginyeria tissular va sorgir com una alternativa per millorar la regeneració de teixits, amb la combinació de biomaterials (que serveixen com a bastides), cèl·lules i/o molècules estimuladores. Així doncs, un dels objectius de l'enginyeria de teixits és la incorporació de molècules estimuladores en els biomaterials per promoure la formació de vasos sanguinis per aconseguir amb èxit la regeneració de teixits i la seva integració en l'hòspeda. Alternativament, hi ha algunes situacions clíniques en les que es necessita vasos sanguinis grans en comptes de xarxes capil·lars. Un exemple el trobem amb les malalties cardiovasculars, com l'arterioescleròsi o aneurismes, en els quals és necessari un recanvi del vas sanguini. Els empèlts autòlegs i xenogènics s'han usat com a material substitutori, però presenten algunes limitacions, principalment el risc de transmissió de malalties i escassetat de material o donants. Així doncs, l'enginyeria tissular de vasos sanguinis va sorgir com una alternativa prometedora.

Generalment, pel que fa l'angiogènesis, els factors de creixement s'han incorporat en els biomaterials com a molècules d'elecció per estimular la formació de vasos sanguinis. Tot i que han demostrat induir una resposta angiogènica adequada, presenten algunes limitacions, com ara propietats delicades per la seva manipulació i una vida de curta durada. Per altra banda, els ions, que es troben de manera natural en el cos humà, han demostrat ser una alternativa prometedora, ja que són capaços d'estimular funcions cel·lulars com seria la formació de vasos sanguinis. Tanmateix, no hi ha un ampli consens respecte les concentracions apropiades que no siguin tòxiques i que indueixin un efecte terapèutic, degut a la falta d'estudis previs on es faci un cribatge abans d'introduir-los en els biomaterials. Pel que fa a l'enginyeria tissular de vasos sanguinis, s'han descrit diferents metodologies per desenvolupar-los. Tot i així, aquests mètodes inclouen diversos passos i l'addició de patrons addicionals en els biomaterials o estímuls addicionals per induir l'alineament cel·lular similar als vasos nadius.

Aquesta tesi es centra en l'estimulació de l'angiogènesi i l'enginyeria tissular de vasos sanguinis, dividida en dos blocs principals: i) el desenvolupament d'un sistema d'alliberació de fàrmacs amb la incorporació de ions per estimular fases primerenques de la regeneració de

l'ós, incloent l'angiogènesi; ii) el desenvolupament de vasos sanguinis per enginyeria tissular mitjançant un mètode basat en l'extrusió.

En la primer part, es va fer inicialment un cribatge amb diferents concentracions de dos tipus de ions terapeutics per determinar quin rang de concentracions no eren tòxiques i tenien un efecte terapèutic en l'angiogenesi i l'osteogènesis, usant cèl·lules endotelials i cèl·lules mesenquimals humanes, respectivament. Els resultats obtinguts van permetre establir un rang de concentracions terapèutiques dels dos ions per la formació de vasos sanguinis, però van mostrar un efecte deleteri quan es van usar per induir la diferenciació òssia. Posteriorment, es va desenvolupar un sistema d'alliberació de fàrmacs on es van incorporar aquests ions, demostrant que els ions terapèutics incorporats poden tenir un potencial antimicrobià i angiogènic, permetent l'alliberació seqüencial d'ambdós ions. El sistema d'alliberació de fàrmacs dissenyat consistia en una estructura similar a una fibra incorporant micropartícules amb contingut d'hidroxiapatita que potencialment es podria utilitzar per la regeneració de teixit ossi.

En la segona part, els vasos sanguinis desenvolupats per enginyeria tissular van ser creats satisfactoriament mitjançant el mètode d'extrusió, involucrant un sol pas. A més a més, es va poder incorporar els tipus cel·lulars vasculars específics, amb una alta taxa de viabilitat i presentant l'alineament cel·lular nadiu i certa functionalitat vasoactiva. Posteriorment, es va poder millorar les propietats mecàniques extruint aquests vasos amb concentracions altes de col·lagen, permetent la seva perfusió amb un *shear stress* arterial. Es requereixen estudis addicionals per demostrar la seva funcionalitat i maduració, amb el potencial de ser usats com a reemplaçament de vasos sanguinis o, fins i tot, com a model de malalties vasculars.

Original publications

- **Bosch-Rué E**, Delgado LM, Gil FJ, Perez RA. Direct extrusion of individually encapsulated endothelial and smooth muscle cells mimicking blood vessel structures and vascular native cell alignment. *Biofabrication*. 2020;13(1).

- **Bosch-Rué E**, Díez-Tercero L, Giordano B, Delgado LM, Bosch BM, Hoyos-Nogués M, Mateos-Timoneda MA, Tran P, Gil FJ, Perez RA. Ion delivery strategies for mimicking the osteogenic development induction. *Frontiers in Cell and Developmental Biology* (submitted).

- Zhang Q*, **Bosch-Rué E***, Perez RA, Truskey GA. Bio-fabrication of tissue engineering vascular systems. *APL Bioengineering* (submitted). *Joint first authorship

Congress Participation

- Díez-Tercero L., Delgado LM., **Bosch-Rué E.**, Pérez RA. *Engineering immunomodulatory matrixes for dual release of ions and drugs for bone regeneration applications.* World Biomaterial Congress 2020; Oral communication; Glasgow, Scotland; 11/12/2020-15/12/2020

- **Bosch-Rué E.**, Delgado LM., Pérez RA. *Engineering blood vessel like structures: a preliminary study.* TERMIS EU 2019; Oral communication; Rhodes, Greece: 27/05/2019-31/05/2019.

- **Bosch-Rué E.**, Delgado LM., Perez RA. *Engineering blood vessel like structures for tissue engineering*. Annual event of Biomed PhDay – III edition; Oral communication; Barcelona, Spain; 18th of January 2019.

- Giordano-Kelhoffer B., Delgado, L.M., **Bosch-Rué E.**, Hoyos-Nogués, M., Perez, R.A. *Therapeutic microcarriers for bone tissue engineering in Dentistry*. Annual event of Biomed PhDay – III edition; Oral communication; Barcelona, Spain; 18th of January 2019.

Table of contents

Abbreviations

Ach: acetylcholine

ADSC: adipose-derived stem cells

ALP: alkaline phosphatase

Ang-1: angiopoietin-1

ASC: adult stem cells

BaG: Bioactive glasses

BM: basement membrane

BM-MNC: bone marrow-derived mononuclear stem cells

BMP: bone morphogenetic protein

BSP: bone sialoprotein

BTE: bone tissue engineering

CaP: calcium phosphate

CBP: CREB-binding protein

CVD: cardiovascular disease

DDS: drug delivery system

EC: endothelial cells

ECM: extracellular matrix

EPC: endothelial progenitor cells

ESC: embryonic stem cells

FGF: fibroblast growth factor

FIH: factor-inhibiting HIF-1

GF: growth factor

GF: growth factors

HA: hydroxyapatite

HASMC: human aortic smooth muscle cells

HGPS: Hutchinson-Gilford Progeria Syndrome

HIF-1α: hypoxia-inducible factor 1-alpha

hNDF: human neonatal dermal fibroblast

HRE: hypoxia response element

HUVEC: human umbilical vein endothelial cells

IGF: insulin growth factor

iPSC: induced pluripotent stem cells

MMP: matrix metalloproteases

MPS: microphysiological systems

MSC: human mesenchymal stem cells

NO: nitric oxide

OC: osteocalcin

OPN: osteopontin

OSX: osterix

PBS: phosphate buffered saline

PCL: poly-Ɛ-caprolactone

PDGF: plateled-derived growth factor

PECAM-1: platelet endothelial cell adhesion molecule-1

PGA: polyglycolic acid

PHD: prolyl-4-hydroxylase

Phe: phenylephrine

PLA: polylactic acid

PLCL: poly(L-lactic acid-*co*-Ɛ-caprolactone)

PLGA: poly(lactide-*co*-glycolide acid)

PLLA: poly-L-lactic acid

ROS: reactive oxygen species

Runx-2: runt-related transcription factor - 2

SDF-1: stromal derived factor-1

SMCs: smooth muscle cells

TCP: tricalcium phosphate

TEBV: tissue engineered blood vessels

TGF-β: transforming growth factor β

TGF-β: transforming growth factor-β

UTS: ultimate tensile strength

VEGF: vascular endothelial growth factor

VHL: von Hippel-Lindau

VTE: vascular tissue engineering

α-SMA: alpha-smooth muscle actin

β-TCP: β-tricalcium phosphate

CHAPTER 1

Introduction

CHAPTER 1. Introduction

The formation of new blood vessels after tissue damage is a critical event for the success of tissue regeneration. When there is an excessive damage, the native regenerative capacity of the body is unable to restore vascularization, leading to tissue necrosis and cell death. For this reason, tissue engineering emerged, using the combination of biomaterials, cells and/or stimulatory molecules. One of its main aims is the stimulation of scaffold vascularization for successful tissue regeneration. For this purpose, it is important to know the mechanisms that trigger blood vessel formation. Alternatively, other clinical situations require the development of high caliber vessels, such as arteries. This would be the case of cardiovascular diseases, in which blood vessel replacement is needed to restore normal blood flow and avoid tissue ischemia.

This chapter will introduce the structure and main components of human vascular system as well as the mechanisms by which blood vessel formation occurs. The importance of tissue vascularization will be introduced with bone tissue. The main components and strategies of tissue engineering will be briefly described, and special attention will be given on drug delivery systems and tissue engineered blood vessels.

1.1.   Human vascular system

Human body is composed of different type of cells that together create tissues and subsequently organs. For proper function and survival, these organs need a nutrient and oxygen supply, and removal of cell waste at the same time. The main responsible of nourishment and waste removal is the circulatory system, composed of different types of blood vessels.

1.1.1. Types of blood vessels

Vascular system is a closed circulatory system composed of different types of blood vessels that differ in size: arteries (0,1-10 mm), arterioles (10-100 μm), capillaries (4-10 μm), venules (10-100 μm) and veins (0,1- >1 mm) (1) **(Figure 1)**. Generally, blood vessel wall is composed of cell and matrix fibers organized in three tunica (intima, media and adventitia), although there are some differences between them. In the next section, the three main layers of arteries will be described, and differences between the other vascular structures will be mentioned.
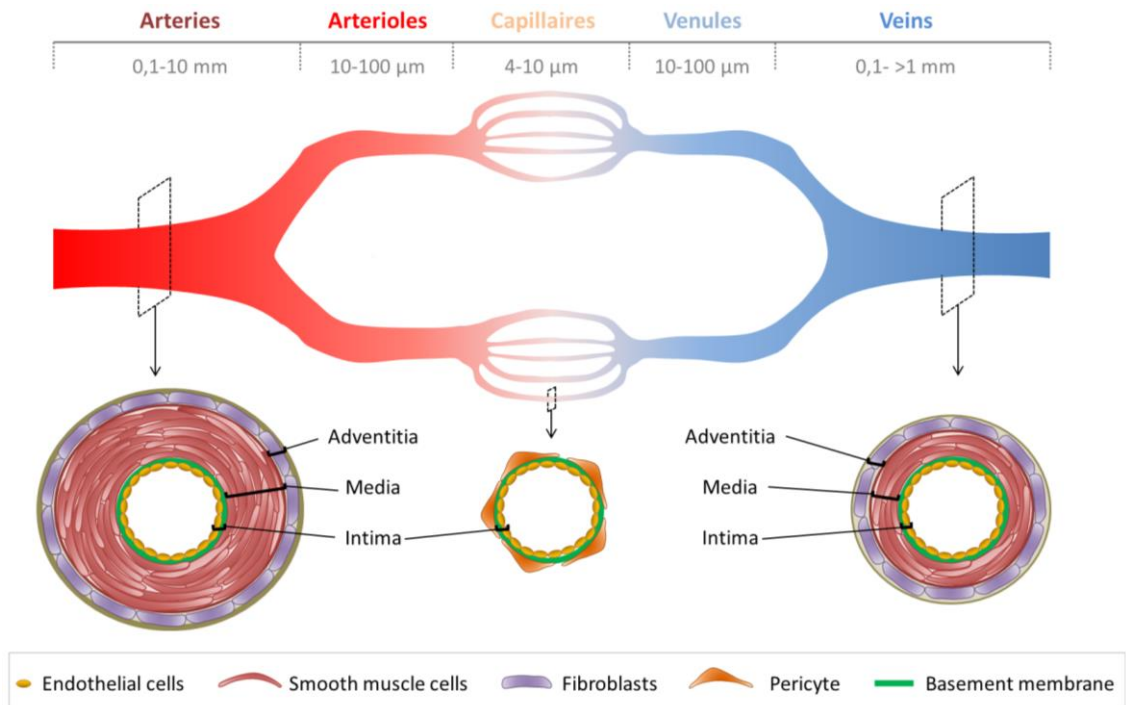
Figure 1. Vascular system. Schematic representation of blood vessels types, sizes and structures.

1.1.2. Architecture of blood vessels

1.1.2.1. Tunica intima

Tunica intima is the innermost layer of arterial wall. It comprises an endothelium, a basal lamina and internal elastic lamina. The endothelium consists of a monolayer of endothelial cells (EC) aligned in the longitudinal axis of the vessel due to the shear stress produced by the blood flow (2)(3). One of the functions of the tunica intima is due to the glycoprotein constituting the glycocalyx, found on the surface of EC, which confers anti-thrombogenic properties to the lumen of the vessel (4). A part from that, endothelium is also responsible for the vascular permeability, which would be defined as the sieve of plasma content from the lumen into the wall, where molecules smaller than 40 kDa can diffuse through the wall whereas larger molecules would require other active and selective mechanisms (5)(6). Furthermore, EC control the vascular tone through the synthesis and release of nitric oxide (4)(7). Adjacent to ECs there is the basal lamina, mainly composed of collagen type IV and laminin (8), which is secreted by EC during development or injury. Basal lamina is supported by the internal elastic lamina, mostly constituted by elastic fibers, providing flexibility and stability for EC (3).

All types of blood vessels have tunica intima with a continuous monolayer of EC, but the main difference is that in capillaries EC can also be fenestrated or discontinuous (9), depending on the tissue.

1.1.2.2. Tunica media

Tunica media is the second layer of the vessel wall. It is mainly composed of smooth muscle cells (SMCs) which are concentrically arranged and provide the necessary mechanical strength and contractility, acting as effectors of vascular tone due to paracrine loop found between EC and SMCs (10). Another important function of SMCs is the deposit of extracellular matrix (ECM). ECM is mainly composed of elastin and collagen type I, which correspond to ~50 wt% of the vessel's dry weight (11), organized in lamellar units. Each lamellar unit consists of a circumferential fenestrated sheet of elastin fibers connected with other lamellar units through interlamellar elastin connections. SMCs, collagen type I and proteoglycans are distributed between the layers of elastin fibers (12). Although elastin has a low tensile strength, it operates as an elastic reservoir and distributes stress uniformly throughout the wall and collagen fibers (11). The outer part of tunica media is the external elastic lamina that provides structural support.

Tunica media is thicker in arteries compared to veins, with a thickness that can reach 500 µm compared to medium-sized veins, which is described to be around 20-50 µm. Going downstream in the vasculature, arterioles possess about 2-3 layers of SMCs and venules consist of 1-2 layers (13). Finally, capillaries do not have tunica media, and instead they have pericytes abutting the single layer of ECs and basement membrane. Another important difference is that the regulation of vascular tone is specific for arteries and can also occur in the arteriole level (9).

1.1.2.3. Tunica adventitia

Tunica adventitia is the outermost layer of the vessel wall. It is constituted by fibroblast and myofibroblasts which deposit an ECM rich in collagen. The collagenous fibers are generally arranged circumferentially and its high content offers a high mechanical stability preventing the rupture of the vessel at high pressures (11). Adventitia also contains the vasa vasorum, which consists of small blood vessels that nourish cells populating the vessel wall. Interestingly, it also contains residential progenitor cells with the potential to differentiate in different cell types such as EC and SMCs, amongst others (14).

Not all types of blood vessels have adventitia. For instance, capillaries and cerebral vessels lack this layer (13). Other differences are found regarding the components of adventitia. For example, some large veins such as vena cava, have another cell type in adventitia, specifically SMCs. A part from that, vasa vasorum is only present in arteries where the media contains more than 29 lamellar units (4), which corresponds to a wall thickness above 200 μm.

1.2. Blood vessel formation

During the natural formation of vascular network two processes can be distinguished: vasculogenesis and angiogenesis. Vasculogenesis takes place in the early embryonic development and consists in *de novo* formation of blood vessel from angioblasts (mesoderm-derived endothelial precursors), which differentiate into EC and form a primitive capillary network (15). Later in the development and postnatally, vascular formation occurs via angiogenesis, defined as the formation of blood vessels from pre-existing ones (16). In this later case, new vessel formation can mainly take place through sprouting angiogenesis **(Figure 2A)**, where EC form sprouts from the pre-existing vessel and elongate towards an angiogenic stimulus (hypoxic signal), or by intussusceptive angiogenesis **(Figure 2B)**, where protrusive extensions of the endothelium are inserted in the lumen of the capillaries and split them (17). After the formation of capillaries, a process known as arteriogenesis can occur, triggered mainly by fluid shear stress, where mural cells (pericytes and/or SMCs) are recruited and enwrap EC tubules providing stability, controlling the perfusion and increasing the diameter and wall thickness (18).
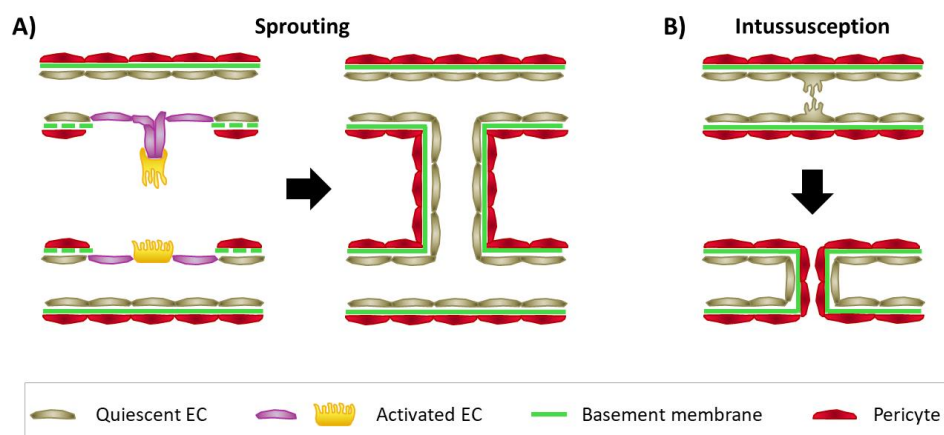
Figure 2. Strategies of blood vessel formation. A) sprouting angiogenesis; B) Intussusception angiogenesis.

In the rest of the thesis, the term angiogenesis will refer to sprouting angiogenesis, which represents a substantial fraction of blood vessel development and it is the most studied one.

1.2.1. Induction of angiogenesis

Angiogenesis is a complex process regulated by spatiotemporal presence of growth factors triggered by a hypoxic signal, where HIF-1α plays a pivotal role. Under normoxic conditions, HIF-1α is hydroxylated at two proline residues by prolyl-4-hydroxylase (PHD) (19) (**Figure 3A**). This increases the affinity of von Hippel-Lindau (VHL) to HIF-1α, which ubiquitinates it inducing proteosomal degradation. The proline hydroxylation of HIF-1α is recognized by factor-inhibiting HIF-1 (FIH), which induces another hydroxylation to asparagine residue, inhibiting the interaction with transcriptional co-activators (p300 and CREB-binding protein (CBP)). Under hypoxic conditions, there is no oxygen available for proline hydroxylation and HIF-1α translocates into the nucleus, where is associated with HIF-1β and p300/CBP **(Figure 3B)**. Then, this complex binds to a DNA region termed hypoxia response element (HRE) and several genes involved in angiogenesis are transcribed, such as vascular endothelial growth factor (VEGF), triggering the activation of EC to evoke blood vessel formation.
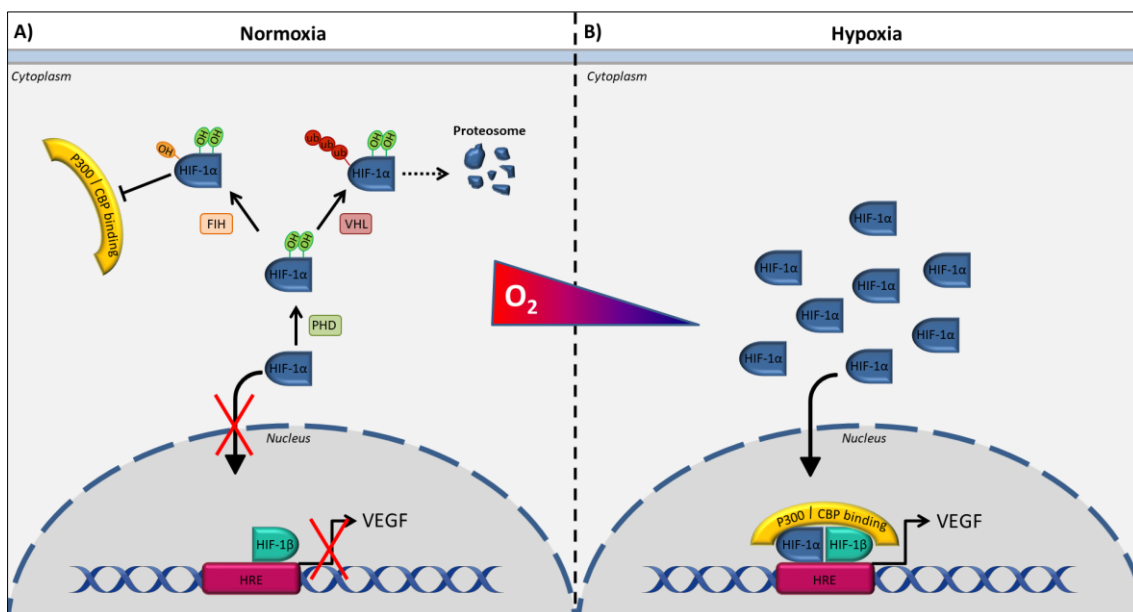
Figure 3. Schematic representation of hypoxic signal pathway. A) Under normoxic conditions, HIF-1α is hydroxylated by PHD and FIH, and ubiquitinated by VHL, inducing proteosomal degradation of HIF-1α. B) Under hypoxic conditions, hydroxylation can not be performed and HIF-1α translocates into the nucleus where it is associated with p300 and CBP. This complex binds to HRE and transcribes genes involved in angiogenesis. Abbreviations: hypoxia-inducible factor 1-alpha (HIF-1α); prolyl-4-hydroxylase (PHD); factor-inhibiting HIF-1 (FIH); von Hippel-Lindau (VHL); CREB-binding protein (CBP); hypoxia response element (HRE); vascular endothelial growth factor (VEGF).

1.2.2. Angiogenesis steps

As previously described, low concentration of oxygen induces the translocation of HIF-1α into the nucleus and the transcription of genes involved in angiogenesis such as VEGF (20). Subsequently, the delivery of VEGF from hypoxic cells triggers the activation of quiescent EC into tip and stalk phenotype (**Figure 4A)**. These phenotypes are transient and are only expressed when angiogenesis takes place. Tip cell phenotype dictates the amount of sprouts and the direction of migration, whereas stalk cell phenotype lengthens the sprout and form capillary lumen (21). EC receiving more VEGF signal become tip cells and inhibit their neighbor EC to acquire this phenotype and in turn, induce their specification to stalk cell phenotype. Tip cells are enriched with matrix metalloproteases (MMPs), such as MT-MMP1, which mediates basement membrane (BM) degradation (22). BM degradation exposes collagen type I which promotes EC proliferation and migration. At the same time, ECs deliver Angiopoietin-2 (Ang-2) which causes the detachment of mural cells (23), therefore allowing ECs migration towards VEGF gradient. While tip cells migrate, stalk cells proliferate, establish cell junction (VE-cadherin) with neighboring cells, produce basement membrane components to assure the integrity of the sprout and form the lumen of the vessel **(Figure 4B)**. Two models have been described for lumen formation (24) **(Figure 4C)**. One of them describes the formation of intracellular (pinocytic) vacuoles which are fused with vacuoles of neighboring cells, resulting in the formation of a lumen. In the other model, EC defines first the apical-basal polarity. Then, the apical membrane, which would correspond to lumen surface, is negatively charged with glycoproteins, consequently opening up the lumen due to repulsive signal. Once the lumen is formed, as a next step, tip cells contact with other tip cells establishing junctions to consolidate the connection, therefore adding new vessels into the existing vascular network **(Figure 4D)**. With the lumen formation, the onset of blood flow increases the oxygen concentration, which reduces de VEGF expression and shifts activated ECs towards a quiescent phenotype. In order to become functional, blood vessels must mature, which involves the recruitment of mural cells and deposition of ECM (25) **(Figure 4E)**. ECs deliver the plateled-derived growth factor (PDGF), which induce mural cells proliferation and migration. Furthermore, ECs delivers transforming growth factor β (TGF-β), which similar to PDGF, promotes the proliferation and migration of mural cells, and also leads to their differentiation and production and deposition of ECM. Finally, mural cells produce Angiopoietin-1 (Ang-1), which stabilizes vessels by promoting pericyte adhesion and tightening ECs junctions.
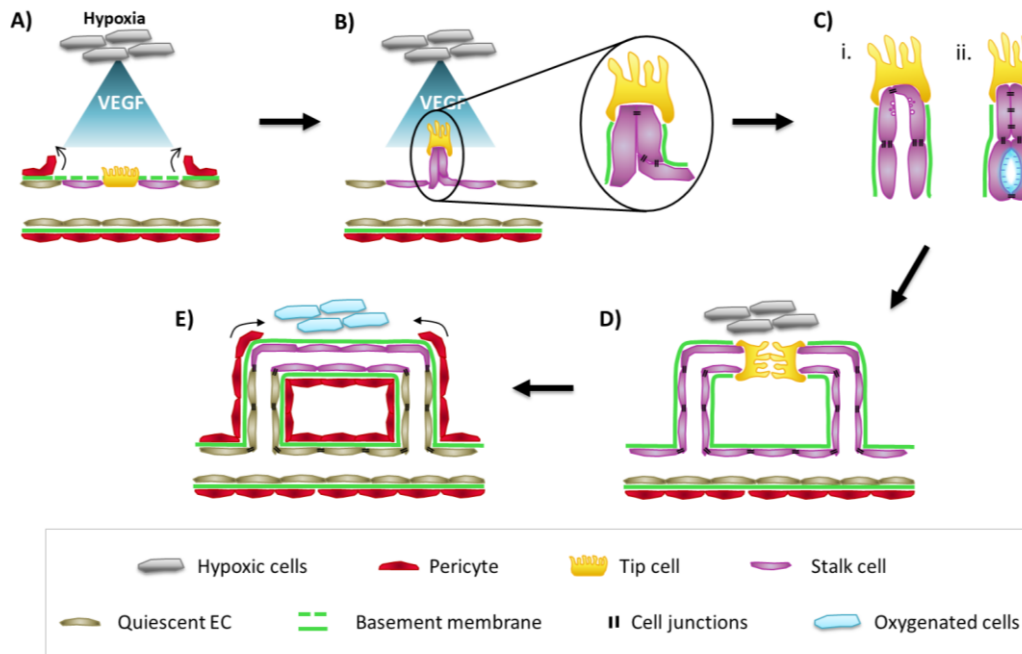
Figure 4. Schematic representation of blood vessel formation. a) Hypoxic cells deliver VEGF and activate EC towards tip or stalk phenotype. b) While tip cells migrate, stalk cells proliferate, establish cell junctions with neighboring cells and synthetizes basement membrane. c) Lumen vessel formation can occur through the fusion of vacuoles (i) or by the repulsion of negatively charged glycoproteins of the lumen surface (ii). d) Tip cells contact with other tip cells, connecting the newly formed vessels. e) The onset of blood flow induces the EC switch towards a quiescent state, and the delivery of PDGF and TGF-β for the recruitment of mural cells and ECM synthesis and deposition.

1.2.3. Importance of angiogenesis in bone regeneration

Angiogenesis or blood vessel formation is one of the crucial events that take place when there is tissue damage, being critical for successful tissue regeneration (26). It not only allows the arrival of oxygen, nutrients and waste removal, but it also allows the arrival of progenitor cells necessary to induce tissue restoration. For instance, it has been recognized in bone fracture healing process the importance of blood supply as a key component for a successful bone regeneration, with a poor bone regeneration outcome when angiogenesis was not completely restored (27). A part from that, blood supply also serves as a source of calcium and phosphate, two key components for bone mineralization (explained in detail in the next section). Moreover, as previously mentioned, blood vessel formation enables the arrival of mesenchymal stem cells (MSCs), which undergoes to osteogenic differentiation and hence, new bone formation (28).

1.3.   Bone tissue

1.3.1. Bone function

Bones are innervated and vascularized organs involved in many body functions, for instance: i) provide structural support for the body; ii) protect internal structures and organs; iii) locomotion; iv) provide maintenance of mineral homeostasis through its reserve of calcium and phosphate ions and by regulating the concentration of some electrolytes in the blood; and v) provides blood cell formation through hematopoiesis within bone marrow (29).

1.3.2. Bone structure and composition

From a macroscopic point of view, bone tissue is organized into cancellous bone (also known as trabecular or spongy bone) and cortical bone (also known as compact bone) (30) **(Figure 5)**. Cortical bone is a dense and nearly solid tissue found in the peripheral regions. It is highly mineralized and is important for structural and mechanical properties. Surrounding the outer surface of cortical bone is the periosteum layer, which contains blood vessels, osteoblasts and osteoprogenitor cells that are activated during bone growth and repair (31). Conversely, cancellous bone is an interconnected porous network with higher surface area compared to cortical bone, localized in the interior of bones, neighboring marrow cavity. It is involved in the homeostasis of calcium and acid/base regulation.
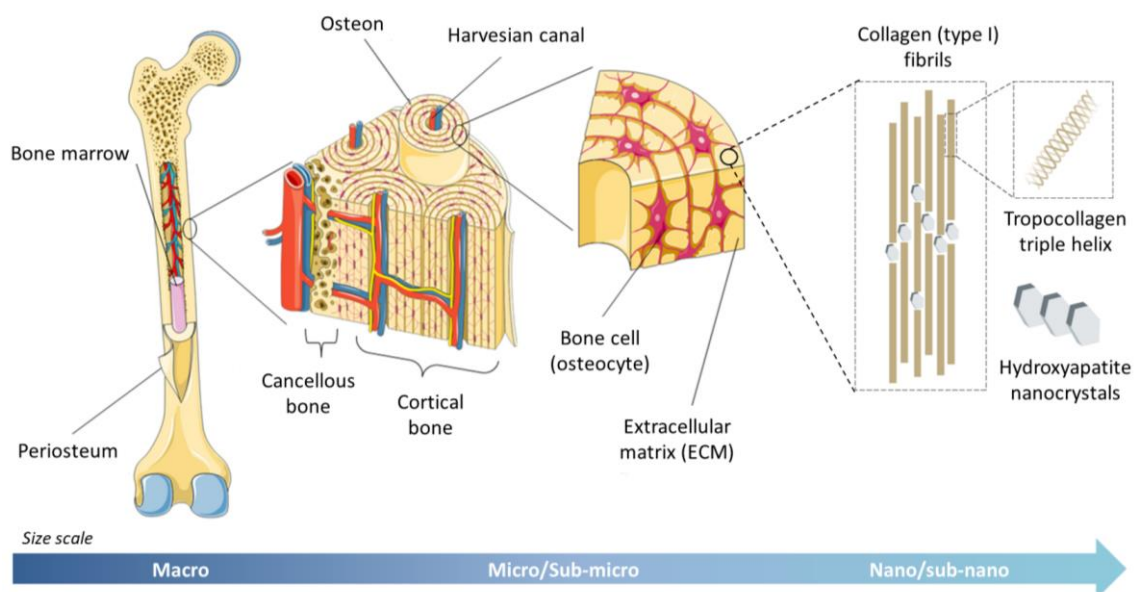
Figure 5. Schematic overview of bone structure and components. Representation of different parts and components in the macro (cortical and cancellous bone), micro/sub-micro (osteons) and nano/sub-nano level (collagen and hydroxyapatite crystals). Figure modified from (32,33).

In a microscopic level, cortical and cancellous bone are organized in osteon structures. Cortical osteons are called Harvesian systems, whereas cancellous osteons are called packets with less hierarchical structure (29). Cortical osteons are composed of cells and ECM organized in a lamellar pattern, surrounding the Harvesian canal which contains nerves and blood vessels. In a nano-size level, the lamellar structure is formed by collagen (type I) fibrils which are laid down in alternating orientations. Calcium and phosphate are present in bone ECM in the form of hydroxyapatite crystals (HA), which precipitate within and between collagen fibrils. Both collagen and HA are the main organic protein and inorganic mineral, respectively, present in the bone, and together account for 95% of bone dry weight (34).

1.3.3. Bone cell components

Bon tissue presents three main cell types (35), as shown in **Figure 6**:

- **Osteoblasts:** they are cuboidal cells derived from mesenchymal stem cells (MSCs) and are located along the bone surface. They are known for their bone forming function, as they synthetize and deposit osteoid (unmineralized collagen) and promote its mineralization through the deposition of calcium and phosphate as HA crystals. Through this process, osteoblasts eventually become surrounded and trapped by mineralized bone matrix, where they mature into oscteocyte phenotype.

- **Bone lining cells:** they are quiescent flat-shaped osteoblasts on bone surface where bone resorption or formation does not occur.

- **Osteocytes:** they possess a dendritic morphology and are derived from MSC through osteoblast differentiation. They are the most abundant bone cell type (90-95% of total bone cells). Osteocytes remain connected with other osteocytes and bone lining cells through gap junctions, creating an extensive network known as lacunar-canalicular network, where they perform intercellular transport of small signaling molecules. Moreover, the lacunar-canalicular network is in close proximity to vasculature, allowing the exchange of nutrients, oxygen and waste.
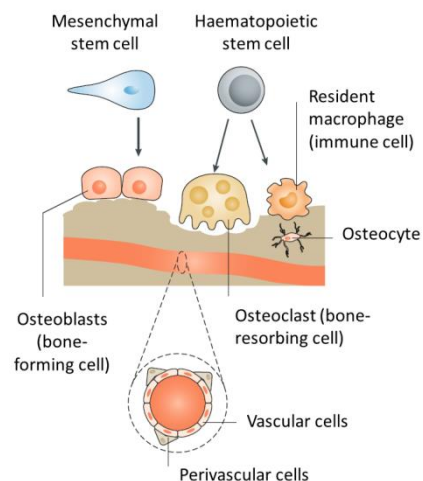
Figure 6. Main cellular components of bone. Bone principal cell components are osteoblasts, osteocytes and osteoclasts. Figure adapted from (33).

- **Osteoclasts:** they are large mononucleated cells derived from mononuclear cells of the hematopoietic stem cell lineage. The plasmatic membrane of osteoclasts which is in contact with bone matrix folds and forms a ruffled border, releasing lysosomal enzymes and acids. Consequently, protein and mineral components of the underlying bone matrix are digested and delivered. This process is known as resorption and helps to maintain calcium levels from blood.

Figure 7. Bone remodeling. Schematic representation of the main phases of bone remodeling. This figure was produced using Servier Medical Art (http://smart.servier.com/).
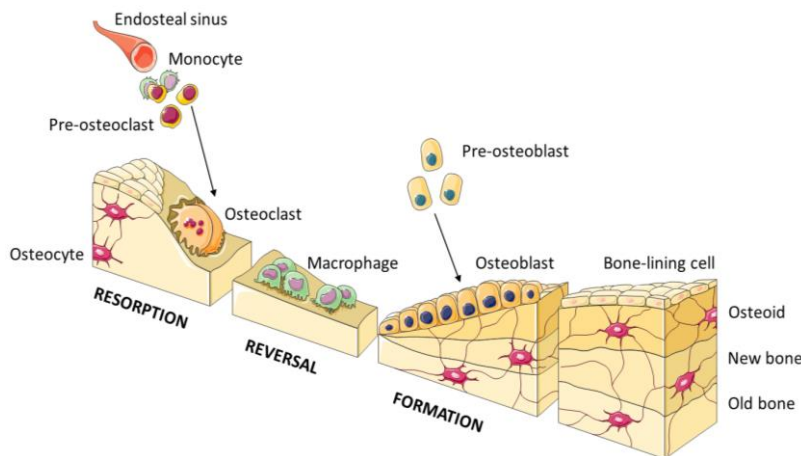
Bone is a dynamic tissue which is continuously remodeled through lifetime to regulate mineral homeostasis and skeletal size, shape and structural integrity (36). Remodeling process consist of three phases (**Figure 7**): i) resorption, where osteoclasts digest old bone; ii) reversal, where mononuclear cells (macrophage-like cells) appear on bone surface and prepare it for osteoblasts migration and differentiation; iii) formation, when osteoblasts form new bone until the resorbed bone is replaced for new one.

1.3.3.1. Osteogenic differentiation

The transition process from MSCs to osteoblastic lineage can be divided into 4 phases: proliferation, differentiation, matrix deposition and mineralization. This process is tightly regulated by transcription factors and proteins in a spatio-temporal manner, as schematically illustrated in **Figure 8**. Initially, MSCs are induced to differentiate into osteoprogenitor cells under the influence of some growth factors such as bone morphogenetic proteins (BMPs). After an active proliferation phase, osteoprogenitor cells express two transcription factors which are absolutely essential for osteoblast differentiation and function: runt-related transcription factor-2 (Runx-2) and Osterix (OSX) (37). On the one hand, Runx-2 induces the commitment of MSCs to osteogenic lineage. On the other hand, both Runx-2 and OSX regulate the gene expression of major bone matrix proteins during osteoblast differentiation. As they mature and acquire the pre-osteoblast phenotype, they start to produce abundant matrix proteins such as collagen type I (COL1), which is deposited as osteoid or non-mineralized bone

matrix. Additionally, they also begin to express alkaline phosphatase (ALP), involved in the mineralization of ECM with phosphates that, together with calcium, form hydroxyapatite crystals (38). When pre-osteoblasts mature and fully differentiate into osteoblasts, they express high levels of bone sialoprotein (BSP) and osteocalcin (OC). BSP is a non-collagenous protein that binds to collagen and acts as a nucleus for the formation of hydroxyapatite crystal. OC is the most abundant non-collagenous protein considered the promoter or initiator of calcium deposition (29). After the mineralization process, the osteoblasts become bone lining cells, while another subset of osteoblasts become surrounded by its own deposition of ECM and terminally differentiate to osteocytes, playing a role in bone cell communication.
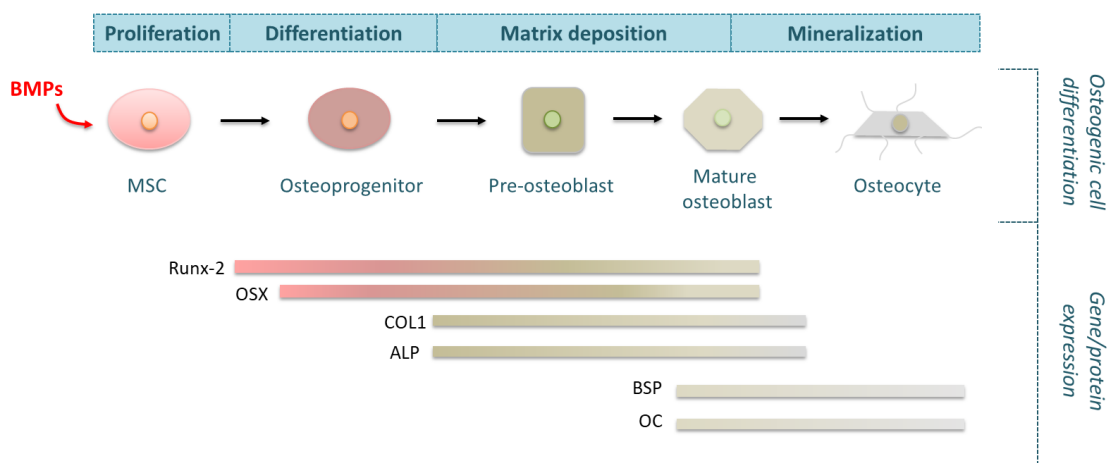
Figure 8. Osteogenic differentiation process. Schematic representation of osteoblast differentiation steps indicating the main transcription factors or proteins involved in each phase.

1.3.4. Bone regeneration steps

Bone is able to regenerate in response to trauma and fractures. During bone regeneration there is a multistep process, which can be divided in four phases (inflammation, angiogenesis, chemotaxis and osteogenesis), where many biomolecules are involved on each stage (**Figure 9**). In a fracture healing, there is first an inflammatory phase mediated through interleukine-1 (IL-1), Il-6 and tumour necrosis factor α (TNF-α), and then an anti-inflamatory phase mediated by Il-4, IL-10 and IL-13, which promotes first bone remodelling followed by bone formation, respectively (39). Then, angiogenesis restoration is carried out with the stimulation of some growth factors such as vascular endothelial growth factor (VEGF), fibroblast growth factor (FGF) and platelet-derived growth factor (PDGF), amongst others (40). The newly formed vessels allow the rapid access of metabolites and the recruitment of progenitor stem cells, through chemotactic factors such as stromal derived factor 1 (SDF-1) (41), and there, they

undergo the osteogenic differentiation with the stimulation of some growth factors such as BMPs, FGFs, PDGFs and insulin-like growth factors (IGFs) (42).
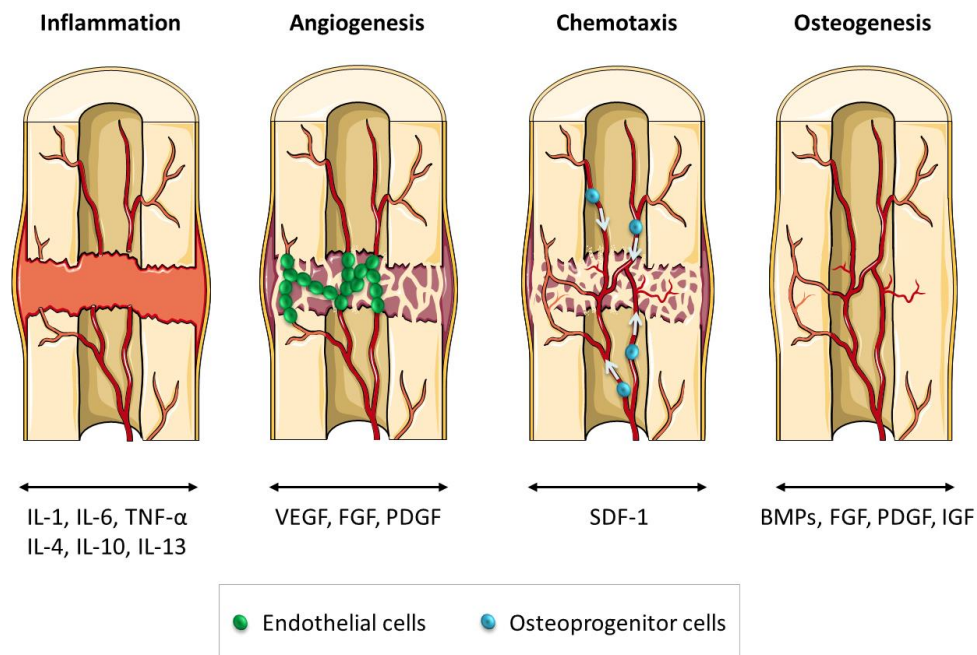
Figure 9. Bone regeneration steps in bone fracture healing. The four main phases are represented with the main growth factors involved in each one. This figure was produced using Servier Medical Art (http://smart.servier.com/).

Although bone tissue possesses a regenerative capacity, it is only sufficient for the healing of small size damage, such as cracks and small fractures. Bone defects exceeding ≥ 2.5 cm (considered the critical size threshold) are unable to regenerate without aid (43). The main cause for the inability to regenerate the tissue is due to lack of vascularization, especially in the inner site of the defect zone, where the lack of oxygen leads to necrosis and cell death. Large defects caused by traumatic injury, tumor resection or congenital defects amongst others, require clinical intervention for healing. For instance, the use of autologous bone grafts has been used to treat large defects, which are osteoconductive and osteoinductive, which refer to their ability to allow and induce bone growth, respectively. Furthermore, they are as well biocompatible and non-immunogenic, therefore avoiding an immune response. However, they have some disadvantages, such as morbidity, available amount of the graft and an elevated cost related to the surgeries (42,44). Allogeneic bone grafts, derived from human donors, have also been used, but they have immunogenicity issues and rejection reactions, as well the possible risk of diseases transmission (44,45). As an alternative to natural bone grafts, synthetic grafts have emerged, which can be further enhanced with tissue engineering strategies, providing limitless supply and no risk of pathogen transmission.

1.4. Tissue engineering

The term of tissue engineering was originally introduced by Langer and Vacanti as an interdisciplinary field involving the principles of biology and engineering to create functional tissues or organs *in vitro* to replace the damaged ones as an alternative of donor material (46). Generally, tissue engineering uses a combination of biomaterials (which serve as scaffolds), cells and stimulatory molecules.

1.4.1. Components of tissue engineering

1.4.1.1. Biomaterials

Biomaterials serve as a temporary scaffold allowing tissue ingrowth providing an appropriate 3D extracellular matrix for cells. At the same time, they can contain stimulatory molecules which induce cell migration, proliferation and/or differentiation.

Generally, an ideal scaffold should degrade in a similar rate to the regeneration rate. At the same time, they must be biocompatible, porous (to allow cell ingrowth, nutrient diffusion and development of vascular structures) and allow a customized shape to fill the tissue defect. More specifically for bone regeneration, it should also be able to promote the differentiation of progenitor cells to an osteoblastic lineage and to have mechanical properties of the bone to be regenerated.

Commonly, biomaterials can be classified in terms of composition or morphology.

1.4.1.1.1. Composition of biomaterials

- **Ceramics:** ceramics are inorganic and non-metallic materials widely used for bone regeneration. The most common ones are calcium phosphate (CaP), specially HA, β-tricalcium phosphate (β-TCP) and biphasic calcium phosphate (BCP), which is a mixture of HA and β-TCP (47). These materials are similar to the mineral phase of native bone, being attractive for their use as bone scaffolds, as they are biocompatible and able to induce osteoblast differentiation and growth (48). Moreover, they generally display high compressive strength. Bioactive glasses (BaG) are another example of ceramic materials which, similar to CaP, can release soluble ions, such as silica or calcium, which can stimulate both angiogenesis and osteogenesis (49,50). As a general drawback, ceramic materials are brittle. Although some of them resorbs fast, such as

β-TCP , others are slowly resorbed, such as HA (51), although it can depend on the crystallinity.

- **Metallic:** metal-based materials haven been the choice for load-bearing applications due to their good physical properties (high strength, fatigue resistance and machining properties). The most used is titanium, presenting a good biocompatibility and mechanical strength and also being resistant to corrosion (52,53). However, metals are not biodegradable, and their mainly use are for prosthesis and dental implants.

- **Polymers:** polymers have been widely used in tissue engineering due to their similarities with ECM, biocompatibility and biodegradability properties. However, they generally possess poor mechanical properties and its use is limited for high load-bearing scaffolds applications (54). Polymers can be classified as natural or synthetic according to their source:

  o **Natural polymers:** they include proteins and polysaccharides mainly found in tissue ECM, therefore, they are advantageous due to their biocompatibility and inherent biological domains, facilitating cell adhesion, proliferation and differentiation (55). Examples of natural polymers are collagen, chitosan, alginate, gelatin, fibroin, elastin, amongst others. Collagen is one of the most used for bone and blood vessel formation, as it is one of the main components of both ECM.

  o **Synthetic polymers:** they can be synthesized under controllable conditions compared to natural polymers. Therefore, their mechanical strength, degradation rate and microstructure are more predictable and reproducible. They usually have better mechanical properties than natural polymers. Example of synthetic polymers are poly(lactic acid) (PLA), poly(glycolic acid) (PGA), polycaprolactone (PCL) (54). However, they present some disadvantages, such as poor biocompatibility, release of acidic products because of their degradation and an early loss of mechanical properties during degradation (56).

- **Composites:** composite materials are the blend of minimum two materials with the purpose of integrating their advantageous characteristics and minimize their individual drawbacks (57). For instance, these combinations can improve the poor biocompatibility of synthetic polymers when combined with natural polymers. As another example, the combination of ceramics with synthetic polymers, for instance CaP with PLA, could enhance the angiogenic response compared with materials alone (58). Alternatively, mechanical properties and biological performance can also be

improved with the combination of ceramics and natural polymers, such as CaP with collagen for bone regeneration purposes (59).

1.4.1.1.2.   Morphology of biomaterials

- **Porous scaffolds:** porous scaffolds, such as fiber-based scaffolds, are the most used in tissue engineering due to their resemblance with ECM. They contain interconnected pores that allow nutrient and molecule diffusion, tissue in-growth and development of vascular structures, a key process for tissue regeneration (60). The main methods used to obtain porous scaffolds are solvent-casting, freeze drying, 3D printing and electrospinning (60–62).

- **Microparticles and nanoparticles:** microparticles are considered micro-scaffolds generally with sphere form, ranging from 100-400 µm. They can support cell growth and thus, they can be used as microcarriers and placed into the site of defect. A part from that, they can also encapsulate stimulatory molecules such as growth factors and be used as a drug delivery system (63).They can be obtained by water-in-oil emulsion, water-in-oil-in water emulsion, microsphere gelation, electrospraying, amongst others (64). On the other side, nanoparticles, ranging from 20 to 200 nm, can penetrate into cells and are mainly used as a drug or gene delivery system (65)(66). They are generally synthesized by chemical routes (67).

- **Hydrogels:** hydrogels are 3D polymer network with micropores which trap a significant aqueous medium. Cells can be incorporated within it as they are soft and provide a cell-friendly 3D matrix similar to native tissues (64). They are usually made of natural polymers, supporting cell adhesion and migration (68). Signaling molecules can also be incorporated within them as a drug delivery system, and be released to stimulate surrounding cells. Hydrogels are formed through either covalent or non-covalent bonds, and can be modulated into various shapes (69).

1.4.1.2.   Cells

Cells play an important role in tissue healing and regeneration as they are one of the main components of a tissue. Cells can be incorporated within the scaffold or they can be recruited from the host tissue using specific stimulatory molecules (70). When using cells with the engineered construct, they can be from autologous, allogeneic or xenogeneic source. An autologous source is preferable to avoid immune reactions. However, allogeneic or xenogeneic

source, as well as immortalized cell lines, can also be used, but just as a tool for investigating specific aspects of cell behavior with scaffolds (71).

When using autologous source, they can be terminally differentiated mature cells. However, they present a limited proliferation capability, loss of phenotype and dedifferentiation when expanded *in vitro*. As an alternative, stem cells are a promising source as they can be maintained with their self-renewal properties (which allow them to proliferate indefinitely maintaining their undifferentiated state) and they have the potential to differentiate in more than one specialized cell type. More specifically, for bone regeneration purposes, stem cell source such as bone marrow-derived mesenchymal stem cells (BM-MSCs), adipose-derived stem cells (ASCs), embryonic stem cells (ESCs) and induced pluripotent stem cells (iPSCs) have been used. However, MSCs are considered the best choice because of their osteogenic differentiation potential and because they are easy accessible from multiple tissues of patients as autologous source, thus, avoiding immune response (72). In the case of vascular network formation, stem cell source such as MSCs, which have been demonstrated to differentiate to ECs under specific conditions (73), or endothelial progenitor cells (EPCs), which can be isolated from peripheral blood and can be differentiated to ECs (74,75), are considered good candidates for vascularization of engineered constructs.

1.4.1.3.   Stimulatory molecules

1.4.1.3.1.   *Growth factors*

Growth factors (GF) are found in all tissues and are involved in the stimulation of cell growth, proliferation, migration and differentiation. They are delivered by cells and can be stored in ECM and released after tissue injury. Many GF have been described to direct angiogenesis and osteogenesis during bone regeneration. Therefore, it is believed that, in addition to mimic the ECM structure, scaffolds should incorporate stimulatory molecules such as GF.

During the angiogenic phase of bone regeneration, several GF are described to be involved, being the main ones VEGF, FGF and PDGF. As previously described, VEGF stimulates the proliferation and migration of ECs resulting in the formation of tubular structures (76). FGF regulates many stages of angiogenesis, from BM degradation to EC proliferation, migration and reformation of BM (77). The main role described for PDGF is the recruitment of pericytes towards new blood vessels for their stabilization and maturation (78,79). Alternatively, several growth factors have also been described to be involved in the osteogenic phase of bone regeneration, such as BMPs, FGF and IGF. BMPs are the most known GF involved in bone

regeneration. They trigger osteogenic differentiation of osteoprogenitor cells and MSCs (80). Between different members of BMPs family, BMP-2 is considered to have a key role in the expression of osteogenic markers (81). FGFs, specifically basic FGF (bFGF) (also known as FGF-2), a part from being involved in angiogenesis, it is thought to promote osteoblast cell proliferation (82). IGF is described to act as a mitogenic factor inducing osteoblast growth and proliferation (83). Although GFs have had clinical success, they present some limitations such as low stability, short circulating half-life and high cost. Hence, low-cost and more stable alternatives have been considered, such as the use of therapeutic ions.

1.4.1.3.2. Ions

Some ions have been described to be therapeutically relevant, presenting similar effects as GFs when incorporated into scaffolds for tissue regeneration purposes (39). More specifically, they are described to be able to stimulate some cellular functions, such as angiogenesis, osteogenesis, anti-imlamatory responses, amongst others (39). Therefore, they are considered an attractive alternative.

Some ions have been used to induce angiogenesis, such as copper, cobalt and silicon. All of them act mimicking hypoxic conditions into the cells due to the inhibition of hydroxylation and ubiquitination of HIF-1α, consequently stabilizing and accumulating HIF-1α (84–89). This, in turn, up-regulates the expression of some angiogenic factors such as VEGF and triggers blood vessel formation. Other ions also showed promising results in angiogenic stimulation, such as boron and strontium, although their mechanism of action are unknown (90,91).

Bone regeneration can also be enhanced with ions such as silicon, zinc, strontium or magnesium. Silicon is described to be implicated in the mineralization process (92) whereas zinc is mainly involved in osteoblast proliferation and differentiation (93,94). Alternatively, the inhibition of osteoclast activity and up-regulation of Runx-2 has been described with strontium, inducing osteogenic differentiation (95). Finally, magnesium is shown to induce osteogenic differentiation, up-regulating some proteins such as BMP-2 and collagen, and induce matrix mineralization (96,97). Although copper and cobalt have also been reported to be beneficial and induce osteogenic differentiation (98,99), controversial results are found in the literature with opposite results (100–102). Therefore, more studies are needed in order to elucidate their osteogenic therapeutic effects.

1.4.2. Approaches in tissue engineering

Two main approaches are utilized to develop engineered constructs (70) as shown in **Figure 10**, which are not mutually exclusive and can be combined:

i) **Drug delivery constructs:** biomaterials used as scaffolds for growth factor/drug delivery device. In this strategy, upon implantation cells are recruited to the scaffold zone and are able to form matrix on and throughout the scaffold.

ii) **Cell delivery constructs:** biomaterials used as scaffolds where specific cells of the tissue to be regenerated are seeded. Then, these cells lay down specific matrix for the tissue to be regenerated for later transplantation.
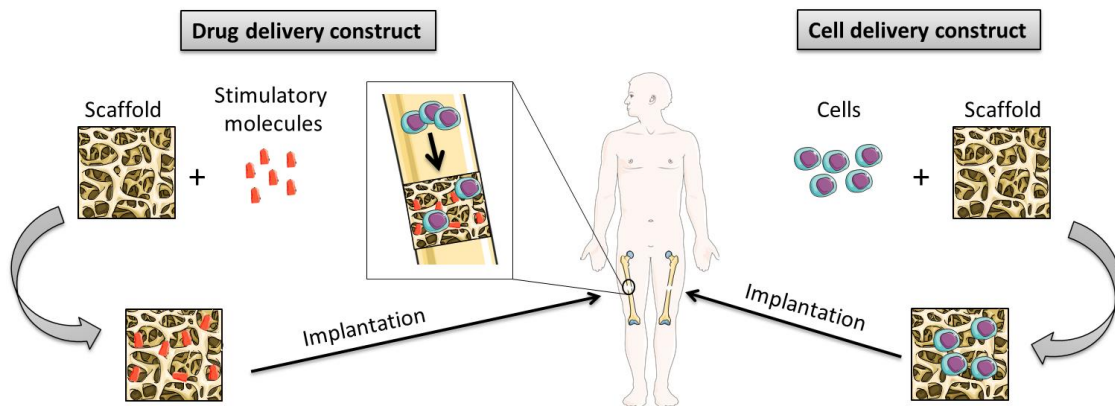
Figure 10. Tissue engineering approaches. Schematic representation of two main approaches of tissue engineering: drug and cell delivery constructs.

During tissue regeneration, different growth factors are involved stimulating different regeneration phases in a sequential manner, as previously described with bone regeneration (inflammation, angiogenesis, chemotaxis and osteogenesis). The generation of vascular network is crucial for the restoration of blood flow in ischemic tissues and achieve a successful regeneration (26). Previous studies demonstrated the need to induce the formation of vascular structures in scaffolds for an *in vivo* successful bone regeneration (103), whereas poor angiogenesis was identified as the main reason of implant failure. Therefore, one of the main challenges of bone tissue engineering is the development of blood vessels to ensure cell viability and regeneration in the core of scaffolds once implanted and hence, bone repair. Thus, tissue engineering strategies that allow sequential release of molecules to stimulate, for example, an angiogenic phase followed by an osteogenic phase, are considered to be more effective for tissue performance and it can be achieved using drug delivering systems (DDS), specifically with dual or multi delivery systems.

Alternatively, some situations would require the development and incorporation of large vessels in the scaffolds, such as arterioles or arteries, that could form capillary networks within the scaffold and at the same time, could be anastomosed with the vasculature of the patient. This would be the case, for example, of locally advanced tumors that invade nearby structures like main arteries or veins of the organ, and their resection would compromise their structure. Another example would be big fractures affecting main arterioles or arteries. This would allow concurrently a direct perfusion after implantation. Other situations could benefit from the development of large vessels, such as in cardiovascular diseases, where obstruction of vessels due to atherosclerosis or dilation of vessels due to aneurisms requires their replacement to allow a proper blood flow. In these cases, cell delivery approach would be more appropriate, using biomaterials to recreate the microarchitecture of blood vessels and incorporating specific vascular cell types within it, a process known as tissue engineered blood vessels (TEBV).

1.5. Drug delivery strategies

Direct injection or systematic local supplementation of GF results in low availability due to their rapid degradation *in vivo*, short half-life in physiological conditions and inactivation and/or degradation by enzymes. Furthermore, raising their doses to increase their availability results in ectopic or adverse effects. For this reason, drug delivery systems (DDSs) are considered an alternative promising approach.

DDSs are defined as a device that enables a controlled release of a therapeutic substance (growth factor, ion or others) in a targeted area without reaching non-target cells, tissues or organs (104). DDSs can deliver one or more molecules. In the later case, their release can be controlled in a time-dependent manner mimicking the sequentially involvement of signaling molecules that take place during tissue regeneration.

As previously described, biomaterials used for drug delivery can be from different compositions (ceramics, natural or synthetic polymers, composites) and different morphologies (fibers, micro/nanoparticles, hydrogels), which can be combined providing multiple DDSs designs, as shown in **Figure 11.**
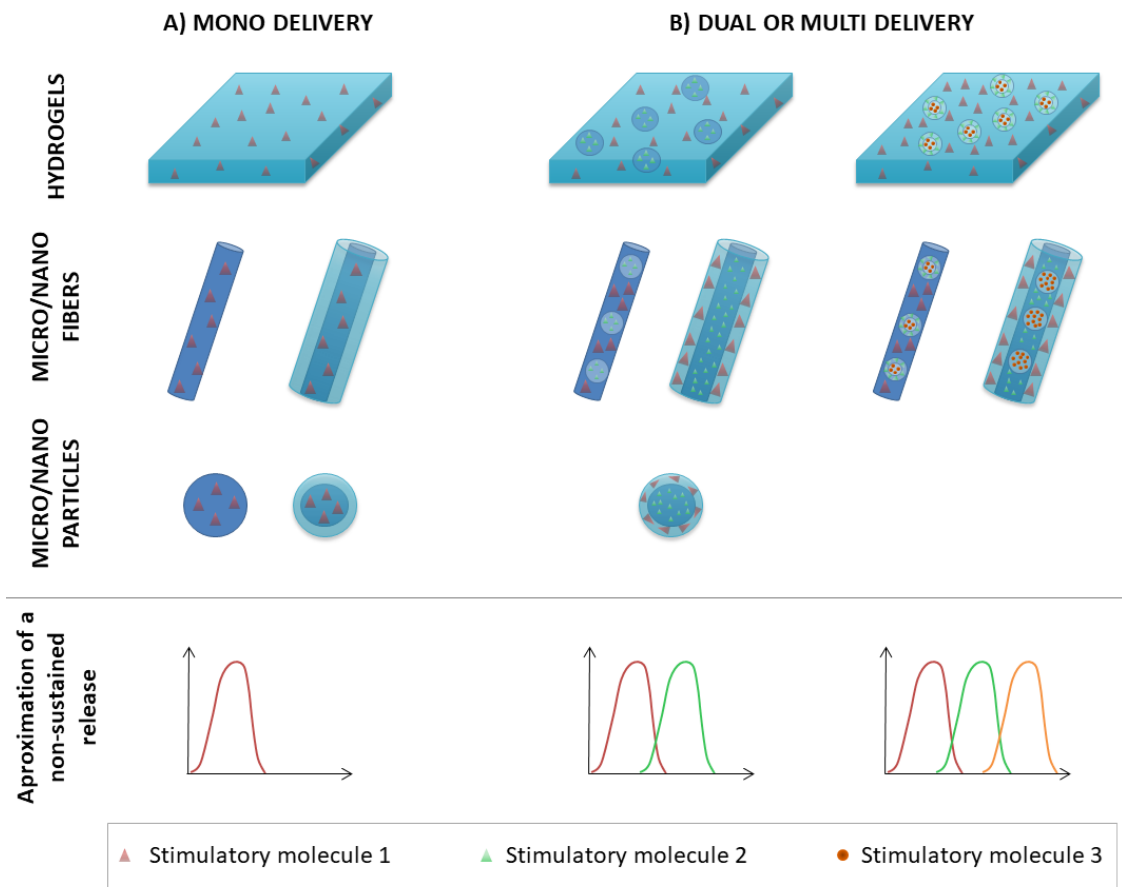
Figure 11. Examples of drug delivery systems for sequential molecules release. Different combinations of scaffold morphologies are schematized for the delivery of one or more stimulatory molecules.
To simplify the figure, we assumed that the delivery of a molecule from a hydrogel, fiber or microparticle is the same, but it should be noted that the pattern release would be different. The purpose of the figure is to show different release of the molecule depending on the drug delivery system compartmentalization.

The delivery of stimulatory molecules can rely on different incorporation methods within the scaffold, such as non-covalent or covalent binding or even the use of micro- or nanoparticles as therapeutic molecule reservoir:

- **Non-covalent binding:** in this case, bioactive molecules and therapeutics are incorporated by physical entrapment, adsorption or formation of ionic complexes (105). Generally, with this incorporation method, the delivery is achieved by passive diffusion and it leads to an initial uncontrolled burst release. Conversely, if stimulatory molecules are encapsulated in the core of core-shell structures, a more controlled and sustained release is achieved (106,107).

- **Covalent binding:** this requires the modification of stimulatory molecules, such as proteins, to contain reactive functional groups (thiols, acrylates, azides, amongst others) which react with polymer matrices (108). In this case, the release is mediated

by hydrolysis, reduction reactions or enzymatic cleavage mediated by cells, reducing the burst release and prolonging the release over time.

- **Micro-/nanoparticles:** the incorporation of micro- or nanoparticles loaded with therapeutic molecules and embedded within scaffolds can result on a more precise control of their release and achieve a long-term sustained release (109).

Other parameters that can influence the release of the molecules are the crosslinking properties of the materials. For instance, when the crosslinking of a polymer is increased, this leads to a decrease mesh size, which in turn, lowers the diffusion rate of the therapeutic agent (110,111). The degree of crosslinking also affects the degradation rate and therefore, the release of the encapsulated molecule. Physical shape and size also affects the release rate. For instance, higher microsphere size generally allows a controlled and more sustained release than smaller microsphere size (112).

Furthermore, DDSs not only allows the incorporation of one single therapeutic molecule, but can incorporate two or more bioactive molecules and release them in a sequential manner when different morphologies and/or composition of scaffolds are combined. Examples of different combination of scaffolds are shown in **Figure 11**.

1.5.1. Mono delivery

Different encapsulation strategies can be accomplished for the encapsulation and delivery of one single stimulatory molecule, as shown in **Figure 11A,** such us in a hydrogel, in a micro/nano fiber or in a micro/nanoparticle. Furthermore, they can be encapsulated in the core of core-shell structures for a more sustained release (107). Encapsulation of GF within these structures have been widely used to stimulate angiogenesis or osteogenesis. For instance, VEGF loaded in the core of core/shell electrospun fibers composed of dextran in the core and poly(lactide-*co*-glycolide acid) (PLGA) in the shell, had a sustained release for more than 28 days showing an excellent activity on the performance of endothelial cells (113). Alternatively, BMP-2 incorporated in the poly(ethylene glycol) (PEG) core surrounded by PCL shell, showed an almost zero order release with a higher osteogenic gene expression both *in vitro* and *in vivo* studies compared to non-loaded fibers (106). In a similar way, ions have been incorporated in the scaffolds and achieved promising therapeutic outcomes. For instance, copper was added as a coating in calcium phosphate (CaP) scaffolds by immersion with graphene oxide-copper solution followed by a vacuum dehydration. This enabled a slow and sustained release of copper, and significantly increased the amount of rat bone-marrow MSCs

that adhered after 12h, compared to calcium phosphate scaffolds alone. Moreover, it incremented the expression of HIF1-α in BMSCs, which induced the release of VEGF *in vitro*, showing as well enhanced vascularization in an *in vivo* cranial bone defect compared to control (114). As another example, the release of strontium incorporated in bioactive glasses scaffold showed an enhancement of osteogenic differentiation of MSCs compared to un-doped scaffolds (115).

1.5.2. Dual or multi delivery

Because tissue repair involves multiple events and biofactors, the delivery of just one therapeutic molecule often do not produce satisfactory outcomes. Thus, delivery of more than one molecule seems to be more appropriate when regeneration steps want to be mimicked. In order to deliver them in a sequential manner, the development of different compartments within the scaffold is needed. This is achieved with core-shell structures or incorporating one delivery system within another. In the last case, the incorporated biomaterial should be at least smaller in structure than the outer scaffolds. Usually, the incorporated structures include micro/nanoparticles or even small-diameter fibers. With this scaffold structures, usually, the molecules incorporated in the outer part of the scaffold are firstly released, whereas molecules encapsulated in the inner part are delivered afterwards. Examples of some strategies for dual delivery scaffolds are shown in **Figure 11B**. Following these strategies, dual drug delivery systems have been developed to stimulate an angiogenic followed by osteogenic response to improve bone regeneration. For instance, composite scaffold made of alginate fibers embedded in PLA matrix was developed, where VEGF was loaded in alginate and BMP-2 in the PLA matrix, aiming a first release of VEGF followed by BMP-2 (116). There was an increased release of VEGF after 7 days and thereafter, an increase of BMP-2 was observed up to 28 days. When implanted in a femoral bone mouse defect, a significantly increase of bone regeneration was observed compared to non-loaded scaffolds. Incorporation of two ions in scaffolds also proved to be positive for angiogenesis and osteogenesis. As an example, the incorporation and subsequently release of silicon and magnesium from tricalcium phosphate (TCP) scaffolds improved both, blood vessel and bone formation in a rat bone defect model compared to TCP alone (117). Both ions are found as trace elements in the mineral phase of bone, and have been described to have individually positive effects either in angiogenesis and osteogenesis, demonstrating their synergistic effect when combined together (117). Moreover, combination of GF with ions also showed promising results, as reported with fibrous scaffolds composed of collagen-based core incorporating BMP-2 and alginate-based

shell containing cobalt. Cobalt ions were quickly released within a week, whereas BMP-2 had a sustained release over several weeks to months (118). Cobalt could increase angiogenic genes such as VEGF and HIF-1α, as well as VEGF protein secretion *in vitro*. Alternatively, BMP-2 up-regulated osteogenic genes such as ALP, BSP and OC as well as OC protein secretion. Further, *in vivo* experiments with rat calvarium defect model showed a significantly new bone formation when both molecules were combined together compared to their individual incorporation.

1.6. Tissue engineered blood vessels (TEBV)

1.6.1. Clinical need to develop TEBV

In recent years, different needs to develop tissue engineered blood vessels (TEBV) have emerged: i) for scaffold vascularization for a successful integration; ii) for replacement of injured vessels due to cardiovascular diseases (CVDs); iii) for drug testing and model vascular diseases.

1.6.1.1. Scaffold vascularization

Failure of engineered grafts is described in large engineered constructs (with a thickness more than 200 μm) lacking of any functional vasculature, where the supply of nutrients and oxygen is compromised and cells are subjected to hypoxia and, eventually, cell death (119). As an alternative improvement, the introduction of a vasculature within engineered scaffolds *in vitro* has been proposed, demonstrating an increase of cell survival and scaffold integration *in vivo* (120). However, the anastomosis of the capillary structures of the scaffold with the vasculature of the patient is not possible. Furthermore, microvessel physiological growth rate is not faster than 5 μm/h, resulting in the inosculation (connection) of two microvascular networks from hours to days (121), compromising cell survival and vasculature structure in the initial time-course after implantation. For this reason, the incorporation of a macrovascular structure (tissue engineered blood vessel) that can be microsurgically anastomosed to the patient is desirable for direct perfusion after implantation (122), which will enable at the same time *in vitro* perfusion of the construct, described to be necessary for the maturation of the vasculature and successful perfusion after implantation without leakages (123).

1.6.1.2. Blood vessel replacement

According to World Health Organization (WHO), cardiovascular diseases (CVDs) are the principal cause of worldwide death, representing 31% of global death (124). The main etiology of CVDs is atherosclerosis, characterized by the narrowing and occlusion of blood vessels due to the accumulation of fatty and fibrous material, known as atherosclerotic plaque, in the inner layer of arteries (125), leading to end tissue ischemia. The most prevalent treatments for CVDs include stents and bypass surgery. The use of stents inevitably cause damage to the endothelium and vessel wall giving place to a cascade of events involving the activation of platelets, thrombus formation and inflammatory reaction. The delivery of cytokines and growth factors by macrophages and platelets subsequently activates smooth muscle cell proliferation leading to a re-narrowing of the vessel, known as restenosis (126). The multiple implants of stents finally requires a vessel replacement with autologous ones such as saphenous vein, mammary artery or radial artery (127–129). However, autologous source is not always possible due to previous harvest or because of the inherent disease of the patient. In addition to that, it has been reported vein grafts failures and reoperations after 10-15 years of intervention (130,131). For all these reasons, special attention has emerged in developing TEBV as an alternative graft to perform bypass.

1.6.1.3. Drug testing and model vascular diseases

TEBV also catch the eye for novel drug testing and development of vascular diseases. Novel drugs and molecules are constantly being discovered although prior to clinical trials these drugs are tested *in vitro* and *in vivo* with two-dimensional (2D) cell cultures and animal models, respectively. However, 2D cell cultures grown on plastic or matrix protein coating cannot resemble the native extracellular matrix (ECM) found in *in vivo* tissues, leading to abnormal functionality or dedifferentiation compared with 3D cell culture (132). Furthermore, drug responses in animals are often not predictive of human responses due to differences in metabolic and signaling mechanisms, precluding some drugs as candidates for human clinical trials (133). Due to the costly and time-consuming process of drug development and lack of efficacy and toxicity of a substantial number of drugs, the development of microphysiological systems (MPS) have gained interest in the last few years. MPS consist of perfused tissue engineered 3D organ constructs with human cells that recreate the structure and function of a human organ, which may be used to mimic the physiology, allowing to accurately model diseases and hence to allow predicting drug responses (134,135). One example of MPS are TEBVs, which can be used to model some vascular diseases. For instance, a model of

Hutchinson-Gilford Progeria Syndrome (HGPS), which is caused by a mutation in the Lamin A/C that induce smooth muscle cells (SMCs) senescence and loss in the cardiovascular system, has been developed with TEBV using induced pluripotent stem cell (iPSC)-derived SMCs from a HGPS patient (136). A part from that, new drugs can be tested in these *in vitro* diseases models which provides a better representation of the disease phenotype compared to 2D tissue culture. Moreover, it has been described that some drugs can have secondary negative effects. For instance, chemotherapeutic drugs can induce vascular damage with loss of vasodilation effects and suppressed anti-inflammatory and vascular reparative functions. At the end, these effects trigger the development of hypertension, thrombosis and atherogenesis (137,138). In this regard, TEBV has also been proposed for the evaluation and screening of pharmaceutical drug candidates for toxicity and efficacy.

1.6.2. Development of TEBV

Some criteria should be achieved when developing TEBV in order to obtain functional vessels in a similar way as found in native conditions: i) appropriate mechanical stability, being able to stand pulsatile pressure without rupture; ii) biocompatible and non-thrombogenic, avoiding immune response and presenting a proper patency; iii) biodegradable, allowing the production of new ECM by cells in a similar rate as reabsorption; iv) vasoactive, being able to vasoconstrict or vasodilate when appropriate stimulus are present. All this characteristics can be achieved depending on the biomaterials used as scaffolds to allow cell proliferation, the appropriate cell source and the methodology used to develop TEBV, which are described in the next subsections.

1.6.2.1. Biomaterials

Scaffolds play an important role in TEBV development, as it aims to provide the appropriate 3D structure for cell proliferation, migration and synthesis of ECM proteins. Ideally, the scaffold should be biodegradable, being resorbed in culture *in vitro* or *in vivo* after implantation and substituted for the tissue generated by cells. Moreover, it should provide appropriate mechanical stability to withstand physiological blood pressure. Diverse materials have been used including natural, synthetic polymers and the combination of them.

1.6.2.1.1. Natural polymers

Significant attention has received natural polymers as they have proper biological cues to allow cell adhesion and proliferation. The most used for TEBV development is collagen, which together with elastin are the two main components of vascular ECM (139). Particularly, in 1986

Weinberg and Bell developed the first TEBV with collagen gel with the three main tunica of blood vessels (140). In this first attempt, TEBVs did not show proper mechanical and burst strength even when a Dacron mesh was added for structural support, obtaining a burst strength of 120-180 mmHg in comparison to 2000-3000 mmHg obtained in physiological vessels such as saphenous vein and internal mammary artery (141). Afterwards, many efforts have been carried out to improve the mechanical properties of collagen gel. For instance, the use of cross-linking agents such as gluteraldehyde, procyanidins, genipin amongst others, which resulted in an increase of mechanical features compared to collagen alone (142,143). Moreover, controlling the alignment of collagen fibers in a microscopic level is also described to enhance its mechanical properties (144,145). As an alternative, fibrin has also been used to develop TEBV as it possesses a higher mechanical properties, being able to withstand physiological blood pressure when implanted *in vivo* and also being able to induce collagen and elastin synthesis in SMCs (146–148). Other natural polymers used in a less extent for TEBV development includes silk fibroin (149,150), alginate (151,152) and chitosan (153).

In general, the main disadvantage of natural polymers is their low mechanical properties compared to synthetic polymers. This can be improved with the aid of bioreactors, which stimulates cells to deposit extracellular matrix and also induces blood vessel maturation and functionality (154,155). Another promising approach would be the use of high concentrations of collagen, from 12 to 24 mg/mL, as it has been recently demonstrated to ameliorate the mechanical features and allowing cell survival despite its high concentration (156).

As an alternative, decellularization of native vessels from autologous or xenogeneic source have also been used, as they preserve the natural protein structure and organization of native blood vessels and maintain similar mechanical properties (157). However, autologous source is not always possible and with xenogeneic vessels the completely removal of immunogenic molecules still remains a challenge and can give immune responses (158).

1.6.2.1.2.   Synthetic polymers

Synthetic polymers also gains attention, specially biodegradable synthetic polymers rather than non-degradable ones, due to their biocompatibility, mechanical properties, and porosity (159). Amongst the widely used are degradable polyesters composed of glycolide and lactide and their co-polymers, such as polyglycolic acid (PGA), poly-L-lactic acid (PLLA) and poly-Ɛ-caprolactone (PCL). In 1999, Niklason *et al* were the first to develop functional TEBV with PGA scaffold, providing successful results in terms of mechanical properties, reporting rupture strength to 2000 mmHg at 8 weeks of pulsatile culture as well as demonstrating contractile

response to pharmacological agents such as endothelin-1 and prostaglandin $F_{2\alpha}$ (160). Furthermore, TEBV remained patent with no evidence of stenosis or dilation after 24 days post implantation. Later on, other studies using PGA for TEBV development emerged (161), even in human clinical trials (162). Other synthetic polymers with a slower degradation rate also showed promising results for vascular applications. For example, in an *in vivo* study using vascular grafts made of PCL, after 12 weeks of implantation they were full patent with no thrombosis or aneurysmal dilation. Furthermore, infiltration of cells and new ECM deposition could be demonstrated manifesting scaffold remodeling (163).

Although synthetic polymers seem promising due to their inherent mechanical properties, they have some drawbacks. For instance, the lack of bioactivity which has been addressed with the incorporation of adhesion peptides on the surface of the polymer with extracellular matrix proteins or derivatives (164), for example with the addition of gelatin coating to PGA scaffolds (165). Another concern is the toxic products derived from their hydrolysis, which can affect cell viability and proliferation. For example, the hydrolysis of PGA derives in acidic products, creating localized areas of low pH, described to alter the proliferation of SMCs and their differentiation state to a synthetic phenotype instead of contractile (166).

1.6.2.1.3. Combination of polymers

Due to the good bioactive properties of natural polymers and good mechanical properties of synthetic polymers, in the lasts years a combination of both have been applied to improve the outcome of TEBV development. Multiple types of combinations have been described due to the number of natural and synthetic polymers available. For instance, a monolayer composite scaffold made from PCL and gelatin fibers resulted in a surface wettability transformation from hydrophobic to hydrophilic, improving human MSC adhesion and spreading compared to PCL alone (167). Furthermore, results from tensile modulus and strength test were equivalent to human coronary arteries, although they presented an inferior ultimate tensile strength.

Bilayered TEBV constructs have also been developed. For instance with a polymer blend of PCL and collagen, which allowed EC adhesion in the inner layer and infiltration of SMC to the outer layer, and presented sufficient mechanical properties to withstand physiological blood pressures (168). Similar results were observed in a later study where a mixture of collagen and chitosan was used for inner and outer layer, and the composite Poly(l-lactide-co-caprolactone) (P(LLA-CL)) as the middle layer (169). Despite the proper cell adhesive motifs of collagen, special attention has to be considered when using it, as it can initiate the coagulation cascade and thrombus formation. For this reason, when introducing collagen to the scaffold, some

researches added non-thrombogenic polymers to the scaffold, such for example poly(1,8-octanediol citrate) (POC) (170), which proved to be hemocompatible and allow EC attachment. Other strategies include the encapsulation of antithrombotic proteins within the scaffold. For instance, a vascular scaffold made with the combination of collagen, chitosan and poly(L-lactic acid-*co*-Ɛ-caprolactone) (PLCL) encapsulating heparin resulted in good cell biocompatibility with antiplatelet adhesion and mechanical properties similar to native blood vessels, in terms of tensile and suture retention strength, burst pressure and compliance (171).

As a further step, tri-layered TEBV has also been developed using hybrid polymers. As an example, a TEBV with an inner and outer layer made of PLCL and collagen and middle layer made of PLGA with silk fibroin was developed, in which HUVEC and SMCs could proliferate and organize well *in vitro* (172). Furthermore, *in vivo* results showed biodegradation of the scaffold and infiltration of cells with an increase of collagen production after 10 weeks of implantation.

Altogether, the choice of the biomaterial is an important decision as it will dictate the properties of the scaffold and the subsequently success of the vascular graft. The combination of natural and synthetic polymers seems an appropriate approach due to the sum of their individual beneficial properties as are bioactivity, biocompatibility, biodegradation and mechanical stability.

1.6.2.2. Cell source

The ideal cells for vascular tissue engineering should be from an autologous source to avoid immune reaction, they should also be able to proliferate within the construct and differentiate to a mature phenotype and finally, they should be easy to harvest. Since vascular tissue engineering field arose, different sources of cells have been used to populate vascular scaffolds: from terminally differentiated cells to embryonic and adult stem cells and even induced pluripotent stem cells.

1.6.2.2.1. Differentiated somatic cells

Somatic cells such as EC, SMCs and fibroblasts can be obtained from patients, for example from saphenous veins or mammary arteries (173,174). The advantage of this source is that these cells can be seeded in a vascular scaffold and it avoids the risk of immune response upon implantation. The isolation of endothelial cells is mainly addressed for the endothelialization of TEBV scaffold to achieve anti-thrombogenic properties and good patency, leaving the tunica media and/or adventitia for recellularization with host cells upon implantation. For instance, l'Heureux *et al* isolated fibroblasts from skin biopsy to develop TEBV scaffold through sheet

rolling method, and subsequently seeded endothelial cells isolated from saphenous vein into the lumen (175). After 8 months of *in vivo* implantation, these TEBV demonstrated a confluent endothelium with anti-thrombogenic properties and a proper mechanical stability. Furthermore, SMCs were observed in the media of TEBV suggesting recruitment and remodeling of this layer with host cells, with synthesis of collagen and elastic fibers. Other studies, a part from using autologous EC also used autologous SMCs with biodegradable scaffolds, for instance SMCs isolated from bovine aorta and seeded in a chemically modified PGA scaffold (160).

Despite the advantage of using terminally differentiated autologous cells to avoid immune rejection, there are some disadvantages using this cell source. For instance, there are technical challenges associated with the harvest of these cells, as well as limit availability because patients with CVD might not have enough healthy tissue. Moreover, somatic differentiated cells have reduced proliferation prolonging the *ex vivo* culture expansion in order to obtain enough cells. In this regard, stem cells haven been proposed as an alternative due to their less limited proliferation capacity.

1.6.2.2.2.   Embryonic stem cells (ESC)

It has been long said that embryonic stem cells (ESC), derived from the inner cell mass of blastocyst stage embryo, have a huge potential for tissue engineering and regenerative medicine. ESC are pluripotent, being able to differentiate into all three germ layer linages under proper stimulus, and have indefinite self-renewal capacity (176). In vascular tissue engineering, the differentiation of ESC to endothelial cells gained much attention than smooth muscle cells. For instance, ESC differentiated to endothelial cells were able to engraft in the microvasculature of mouse ischemic hind limb and improve its perfusion (177). In another study, endothelial cells derived from ESC and implanted in a tissue-engineered vessel model in SCID mice with a mesenchymal precursor cell line were able to form cord-like networks with luminal structures and integrated with host vasculature (178).

Although ESC seems a promising source of cells for vascular engineering, it also presents some drawbacks. The main problems of using ESC are derived from ethic issues, as ESC can be considered a human being, and this has limited their use for research and clinical applications (179). Apart from that, these cells are usually acquired from a donor, so the risk of immune response exists. Therefore, the use of other sources of stem cells, such as adult stem cells, has been proposed.

1.6.2.2.3. Adult stem cells (ASC)

In order to overcome ethical concerns, adult stem cells have been proposed as an alternative to ESC since they can be harvested from patient's own tissues and, in addition, overcome immune responses. Moreover, similar to ESC, they possess self-renewal capacities, however they are multipotent stem cells, therefore, they can differentiate to a less wide specific cell types. Different types of adult stem cells haven been used in vascular tissue engineering, such as mesenchymal stem cells (MSC), bone marrow-derived mononuclear stem cells (BM-MNC), endothelial progenitor cells (EPC) and adipose derived stem cells (ADSC).

MSC are derived from mesenchyme, that arises from mesoderm, and are found in many tissues within the body, such as bone marrow (180). These cells are able to differentiate to EC and SMC in special conditions (73,181). As MSC have a higher proliferation rate than terminally differentiated cells, they are preferable to be used in their multipotent state. For instance, MSC seeded in the lumen of PCLA vascular scaffolds differentiated to EC under shear stress conditions (182). This results are in concordance with a later study where MSC were also seeded in a vascular scaffold made of PLLA and collagen and they could also be differentiated to EC (183). Numerous studies reported that mechanical stimulus such as cyclic stretch could differentiate MSC to SMC and thus, be used for vascular engineering as cyclic stretch is an stimulus present in physiological conditions (184,185). Referent to this, a study demonstrated the use of human MSC as a good candidate as SMC source. These cells were cultured in TEBV scaffolds made of PGA and coated with fibronectin and showed their differentiation toward SMCs due to cyclic strain stimulus and specific growth factors (186). Other studies incorporated EC and SMC previously differentiated into TEBV scaffolds. For example, after MSC differentiation, EC and SMC were seeded in decellularized arterial scaffold and implanted *in vivo* in an ovine model. Non seeded TEBV occluded within two weeks, whereas TEBV containing cells were non-thrombogenic, patent and presented appropriated mechanical stability for 5 months (187). The main disadvantage of using MSC is the method of harvesting them from patients, as aspiration of bone marrow is an invasive technique.

BM-MNCs have been considered another potential source because of the large number that can be obtained from bone marrow aspiration from the iliac crest. BM-MNC includes numerous lineages and differentiated stages of cells and high levels of cytokines, which has been considered to help in regeneration of tissues. The first study using BM-MNC in vascular grafts *in vivo* was reported by Matsumura *et al*, in which BM-MNC were pre-labeled with a green fluorescent, seeded in PLLA TEBV scaffold and implanted in inferior cava of dogs. TEBV

showed no stenosis or obstruction up to two years, and early time points showed their differentiation towards EC and SMC, demonstrating their contribution to the establishment of TEBV (188). Despite this direct beneficial effect when used in TEBV, the mechanism of how they actually contributed is not clear. Contrary to the previous investigation, in an *in vivo* animal study it could be observed the disappearance of these cells within a few days of implantation. However, the authors noticed an increase of monocyte chemo-attractant protein-1 with an early monocyte recruitment, and a repopulation of the TEBV with host EC and SMC, suggesting a possible vascular remodeling due to inflammatory process (189). There are some human clinical trials also reporting the use of BM-MNCs as a promising source. For instance, PLLA or PGA combined with PLCL scaffolds seeded with BM-MNC were implanted as extracardiac cavopulmonary conduits in pediatric patients with single ventricle physiology. After 5.8 years follow up, there was no evidence of aneurysm, graft rupture, infection or ectopic calcification (190), and these results were maintained after 11.1 years follow up period (191). The mechanisms underlying how these cells proliferate, differentiate and contribute to TEBV remodeling remain elusive and arises a debate about if BM-MNC truly contribute to vascular tissue formation with a direct differentiation to SMC and EC. A special consideration should be taken when using these cells, as they should be from an autologous source to avoid immune responses due to the presence of B and T cells within this population.

EPC is another cell type used in vascular engineering. They are unipotent stem cells with the ability to differentiate and mature into a specific cell type, in particular into endothelial cells lining the lumen of blood vessels. EPC can be obtained from umbilical cord blood or adult peripheral blood, and depending the method used to isolate them two populations can be obtained known as early and late-outgrowth EPC (74). Contrary to early-outgrowth EPC, late-growth EPC have been reported to be functionally similar to human aortic endothelial cells (HAECs) and considered a promising source of adult stem cells for cardiovascular therapies (192). Furthermore, these cells presented a mild inflammatory response without signs of rejection when used from allogeneic source, due to their low expression of MHC class I and no expression of MHC class II molecules, widening the window for a non-autologous source (193). There are some studies using EPC as an EC source. For instance, early studies expanded EPC *ex vivo* after isolating them from sheep's peripheral blood, and then they were seeded onto decellularized porcine iliac vessels and implanted as a carotid interposition graft in sheeps. After 150 days, these vascular grafts remained patent and could induce NO-mediated vasodilation similar as arterial endothelial cells, whereas non-seeded grafts occluded within 15 days (194). Their anti-thrombotic properties were assessed in later studies. For instance,

titanium tubes used for stent purposes seeded with EPC, after 3 days of *in vivo* implantation were free of clot, whereas non seeded scaffolds were completely occluded or partially thrombosed (195). In concordance with this results, decellularized scaffolds seeded with EPC and implanted as porcine carotid artery also showed patency at 30 days, resisting clotting and intimal hyperplasia (186). To give another example, EPC cultured in TEBV scaffolds made of PCL and chitosan also remained patent after 3 months when implanted into carotid arteries of dogs (196). All these results demonstrate the capacity of EPC to differentiate into EC forming a monolayer in the lumen of TEBV scaffolds with anti-thrombotic properties, thus becoming a promising source as EC cells for vascular tissue engineering. Furthermore, their harvesting is less invasive compared to MSC and makes them even more attracting.

Finally, ADSCs are another type of adult stem cells tested for vascular engineering. ADSCs can be isolated from adipose tissues, precisely from stromal vascular fraction, from procedures such as liposuction, abdominoplasty, amongst others, being their harvest easier than MSC. Similar to MSC, ADSCs have self-renewal properties and multipotential differentiation (197) and can be differentiated to vascular cells with appropriate biochemical and biomechanical stimulus. For instance, ADSCs exhibited EC phenotype when cultured with endothelial cell growth supplements and physiological shear stress force (198), obtaining better results when the shear stress was gradually introduced (199). When EC derived from ADSC were seeded in vascular scaffolds and implanted *in vivo* in a carotid artery of canine animal, they appeared to be mildly thrombogenic, possibly related to the lack of eNOS expression, suggesting that they might not be fully differentiated to an EC phenotype (198). On the other side, ADSCs were able to acquire SMCs phenotype when cultured with a combination of transforming growth factor-β1 (TGF-β1) and bone morphogenetic protein-4 (BMP4), with expression of SMC-related markers (200). Furthermore, once differentiated they were seeded in PGA scaffolds and subjected to pulsatile stimulation in a bioreactor for 8 weeks. After this period, compared to static scaffolds, there was a well-organized structure with an increase of collagen deposition similar to native vessels and improved mechanical properties. In a slightly different approach, in another study ADSC were seeded directly into TEBV scaffold made of PLGA and fibrin prior to their differentiation (201). Mechanical stimulation was carried out with pulsatile stimulus out for 2 weeks, together with the presence of some growth factors such as plateled-derived growth factor BB (PDGF-BB), TGF-β1 and basic fibroblasts growth factor (bFGF). The biomechanical and biochemical stimulus induced ADSC differentiation towards SMC-like cells.

Although ADSC seems a choice for vascular engineering, certainty that these cells can differentiate to a mature EC and SMCs is not completely clear. A previously study reported a

mild thrombogenic properties of EC-derived ADSC, suggesting that they were not completely differentiated (198). Moreover, there are some studies reporting that microvascular cells derived from ADSCs increased the development of intimal hyperplasia (202,203) and decreased patency (204), in a dog, rat and rabbit model, respectively. Furthermore, these cells were reported to not be able to differentiate into SMCs in elderly patients or with diseases such as diabetes, which are considered candidate patients for vascular treatments (205). For all these reasons, more studies are needed to confirm their capacity to differentiate to mature vascular cells.

Between the ASC previously described, the most promising source are MSC, due to their ability to differentiate to EC and SMC and lack of inflammatory response. The main pitfall of using MSC is derived from harvesting technique, which is considered invasive for the patients. EPC are also a good candidate to be used as EC, but it would require the use of other cell source for SMC differentiation, as EPC alone cannot generate a completely and functional TEBV. In the lasts years, the use of iPSC have gained a lot of attention, as despite having the advantages of MSC, their method of harvest is not invasive.

1.6.2.2.4. Human induced pluripotent stem cells (hiPSC)

The noteworthy work from Yamanaka *et al* demonstrating that cells with an embryonic-like state could be obtained by reprograming adult differentiated cells opened an encouraging source to obtain a variety of cell lineages (206). These cells, known as induced pluripotent stem cells (iPSC) can be generated from a diversity of tissues such as skin, fat, amongst others, and can be highly expanded *in vitro* with a superior proliferative ability compared to both adult primary and stem cells. Therefore, iPSC presents unlimited autologous source without the ethical problems related with the use of ESC. Similar to ESC, iPSCs possess indefinite self-renewal capacities and can be differentiated into cells from the three embryonic germ layers (207). Related to vascular tissue engineering, iPSC can differentiate into blood-vessel related cells such as EC and SMC under specific supplemented media, exhibiting mature functional properties (208). Moreover, in the case of EC derived from iPSC, the exposure of shear stress similar to physiological conditions on EC with a bioreactor system could specify them to an arterial lineage, as demonstrated with the up-regulation of EphrinB2 and Notch1 arterial markers (209). Furthermore, they present the plasticity of mature primary vascular endothelium, responding to diverse pro-inflammatory stimuli and maintaining a dynamic barrier (210). On the other hand, SMC differentiated from iPSC acquired a mature phenotype being able to contract when stimulated with carbachol and also up-regulate specific collagen

genes and matrix metalloproteinase under cytokine stimulation (211). Moreover, when seeded into PLLA scaffolds and implanted in mice, SMC could maintain their phenotype and demonstrated vascular tissue formation with collagen extracellular matrix deposition. In another study, SMC differentiated from iPSC showing positivity for alpha-smooth muscle actin (α-SMA) and calponin were seeded onto tubular PGA scaffolds in bioreactors and a functional TEBV with abundant collagen deposition was obtained after 8-9 week, with mechanical properties that enabled suture as an *in vivo* graft (165). However, the TEBV could only stand 500 mmHg and was dilated after 2 weeks of implantation, suggesting that SMC were no matured or differentiated enough. To solve this problem, a later study introduced incremental pulsatile stretching and optimized TEBV medium (containing TGF-β1 without PDGF-BB) prior to implantation to further mature SMC phenotype obtaining a mechanical strength (1400 mmHg of rupture pressure) comparable to saphenous veins (212). When TEBV were implanted *in vivo,* they showed to be patent without luminal dilation, maintaining mechanical and contractile functions. So these studies demonstrate the ability to differentiate iPSC towards mature and functional EC and SMCs when appropriate biochemical and biomechanical stimulus are applied.

An interesting approach of generating iPSC from patient's cells is the possibility to generate vascular model diseases. For instance, the use of skin fibroblasts from patients with Hutchinson-Gilford Progeria Syndrome (HGPS) were used to obtain iPSC and differentiate them to SMC (HGPS iSMC) and embedded in collagen TEBV to model a vascular HGPS (136). In this case, as EC, healthy EPC were used derived from cord blood to isolate the effect of HGPS iSMC. Interestingly, TEBV with HGPS iSMC presented a reduced vasoactivity and increased medial wall thickness, calcification and apoptosis compared with healthy iSMC or MSC TEBVs, which are key features of HGPS. Furthermore, they were able to respond to certain drugs. In a later study, EC derived from iPSC from patients with HGPS (HGPS iEC) were also introduced in the TEBV, together with HGPS iSMC (213). Although iEC aligned with flow, they manifested a low flow-responsive gene expression, altered NOS3 levels and a reduced vasoconstriction and vasodilation. When iEC were placed with healthy iSMC, there was only observed a reduced vasodilation, indicating that EC might also have a role in HGPS, and demonstrating the use of iPSC to model vascular diseases as a promising platform for further studies in a molecular pathophysiology level or for drug testing.

All these promising results demonstrate a huge potential of using iPSC as an autologous unlimited source for vascular tissue engineering without ethical issues or immune problems, able to obtain multiple cell fates. Safety concerns arise from human iPSC generation through

the use of viruses for human clinical purposes. Advanced integration-free reprogramming alternatives are emerging to avoid these concerns, such us the use of non-integrated plasmids, mRNA, small molecules, amongst others, which might be the key for future human applications (214).

1.6.2.3. Approaches

When developing a TEBV, it is important to reproduce the native architecture of blood vessels with their three main layers (tunica intima, media and adventitia) with specific cell types in each one of them. Since the first TEBV developed in 1986, different approaches have emerged to develop tubular structures to obtain arterial TEBV. The main methods can be classified in the following groups: sheet rolling, matrix molding, electrospinning and 3D bioprinting (**Figure 12**).
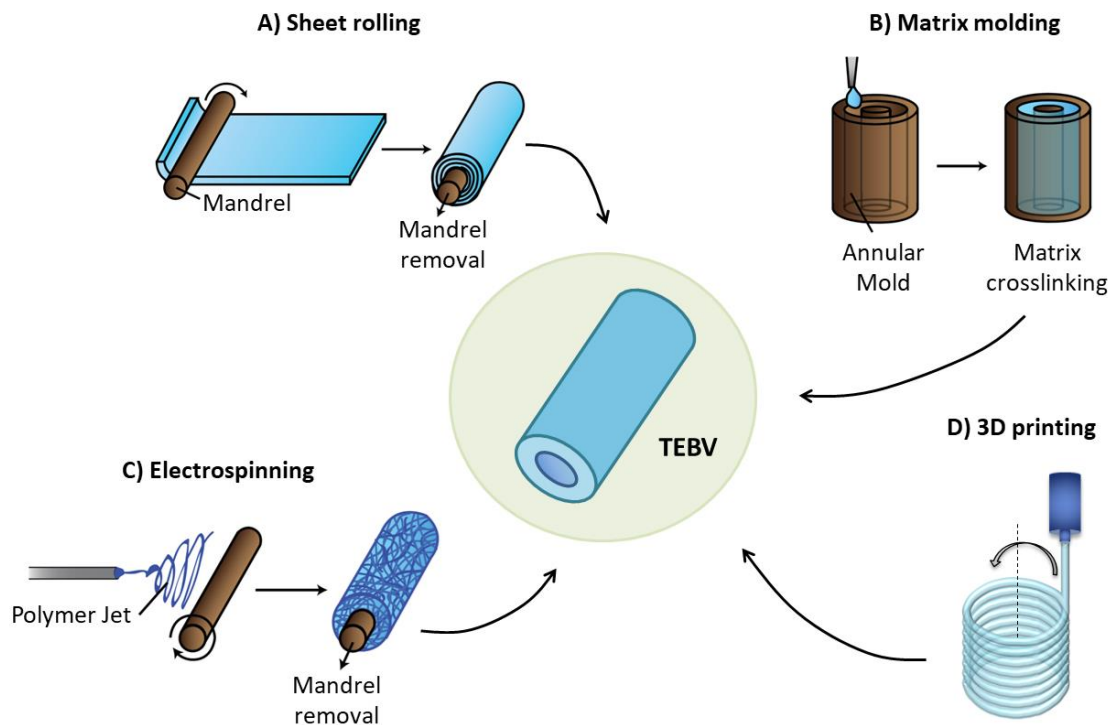
Figure 12. Approaches to tissue engineer blood vessels. Representation of the main four methods to obtain tubular structures for tissue engineered blood vessels: A) Sheet rolling; B) Matrix molding; C) Electrospinning and; D) 3D printing. Figure adapted and modified from (215).

1.6.2.4. Sheet rolling

Sheet rolling method is based on a sheet of cells (scaffold-free) or a sheet of biomaterial with or without cells (with scaffold) which is rolled over a mandrel to obtain a tubular structure (**Figure 12A**).

One of the first methods to obtain a TEBV was using scaffold-free sheet rolling (also known as tissue engineering by self-assembly (TESA)), pioneered by l'Heureux *et al*, in which cells are cultured with soluble factors to induce ECM deposition. For instance, in this first approach, SMC and fibroblasts were cultured with a supplementation of sodium ascorbate during 30 days to induce ECM formation. After this period, sheets of ECM with cells were formed and they were manually peeled off and wrapped around a perforated tubular mandrel, rolling SMC sheet first as a media layer. After one week of maturation with a bioreactor, fibroblast sheet was rolled around SMC layer as adventitia layer and matured for 8 weeks allowing the fuse of layers. After this interval, the mandrel was removed and endothelial cells were seeded in the lumen of the tube, obtaining a three-layered TEBV (216). The burst pressure obtained was similar to human vessels, being above 2000 mmHg. Moreover, cells expressed matured markers such as desmin in SMC or von Willebrand factor in EC, and the endothelium was functional being able to inhibit platelet adhesion *in vitro*. Following the same procedure with slight modifications (an internal acellular membrane instead of medial layer), TEBV were implanted in canine, nude rats and primate animal models (175). TEBVs were mechanical stable and anti-thrombogenic during 8 months. *In vivo* remodeling occurred, with the formation of basement membrane, the presence of α-actin positive cells in the media, indicating the presence of SMC, with vasa vasorum formation and deposition of elastin and collagen. Mechanical properties were improved when continuous sheet containing SMC and fibroblasts contiguously were rolled on a mandrel in a single step (217). A part from that, circumferential alignment of cells from medial layer could be achieved by seeding them onto PDMS substrates with nanogratings of 350 nm line width, 700 nm pitch and 250 nm depth (218). The scaffold free or TESA approach showed promising results in early clinical trials when TEBV were used as arteriovenous shunts for hemodialysis access, being the primary patency rate 78% during the first month and 60% after 6 months of implantation (219).

Some drawbacks using this method have been mentioned. For instance, with this approach, the cell sheet has to be manually peeled of, which can lead to potential sites of bursting due to tearing. This problem can be solved with a thermo-responsive culture surface, specifically with poly(N-isopropylacrylamide) (PIPAAM). At 37ºC, PIPAAM is hydrophobic and cells can adhere and proliferate, whereas at 32ºC, PIPAAM becomes hydrophilic, inducing spontaneous cell detachment (220). Therefore, detachment of cell sheet is achieved by simply reducing the temperature, without mechanical or enzyme treatment, maintaining cell-to-cell junctions. Another concern is the long time required to obtain a functional TEBV, which is around 8 months. To solve this, a strategy to air-dry and froze the entire fibroblast layer after

maturation, and defrost and seed with autologous endothelial cells when needed was proposed as a possibility to indefinitely store autologous tissues for a patient (221). This strategy was used to obtain TEBV as arteriovenous fistula and after eight weeks postoperatively the grafts functioned without complications, reducing the final surgery preparation to less than 2 weeks.

Sheet rolling using scaffolds have also been reported in the literature. For instance, different cell types were seeded contiguously on a stretched PDMS membrane. Once the end of a membrane was released, the membrane was rolled up forming a tubular structure with different layers and different cell types on each layer resembling the native structure of vessels (222). Interestingly, the longitudinal or circumferential alignment of cells could be controlled by the microgrooves on the surface of PDMS membrane. However, no mechanical tests were reported in this study. In another study, EC and SMC were seeded onto decellularized human amniotic membranes demonstrating initial binding. After rolling the SMC membrane and perfusing it with a bioreactor, the laminate structure bounded tightly together forming a uniform tubular construct with mechanical properties similar to human carotid arteries (223). The ECM composition was also similar to native vessels, but no functional properties were reported. Similar to scaffold-free, other procedure modifications have been introduced to roll the biomaterial sheet into tubular structure, such as the use of thermo-responsive shape-memory scaffolds. For instance, a sheet made of poly(lactide-glycolide-trimethylene carbonate (PLGATMC) with a surface coating of aligned nanofibrous membrane of PLGA with chitosan for cell adhesion and proliferation (224). The sheet was temporarily planar at 20ºC and SMCs were seeded. After cell adhesion, the sheet was placed at 37ªC and self-rolled to small-diameter tube. An advantage of this method is the possibility to control the alignment of cells through surface scaffold patterning. Further studies are required in order to elucidate both mechanical and functional properties of TEBVs using scaffold sheet rolling.

1.6.2.4.1. *Matrix molding*

Weinberg and Bell develop the first TEBV using the matrix molding approach (140). The most widely used biomaterials in this method are natural polymers. This method mainly consists on using molds to create tubular structures (**Figure 12B**). For instance, Weinberg and Bell used collagen mixed with SMC and Syedain *et al* used a suspension of dermal fibroblasts with fibrin. In both cases, the mixtures were injected in an annular mold and after crosslinking, a tubular structure was obtained (140) with promising results when used as lamb artery replacement (225). In a similar way, TEBV construct was obtained when a gel solution with human neonatal

dermal fibroblasts (hNDF) and collagen type I was cross-linked within a 3 mL syringe with a mandrel in the center of it (226). Subsequent plastic compression and water removal was performed to increase collagen fiber density with 0,8 µm membrane filter and Kim Wipes. The obtained TEBV were functional and mechanically strong to stand physiological shear stress. Other creative and sophisticated alternatives have been developed. For instance, Want *et al* developed a three step procedure which consisted of a 3D-printing a cylinder structure as a positive mold, immersing it on PDMS to generate a negative mold and injecting water inside and freeze it. Then, the cylinder ice was demolded from PDMS and dip coated in dissolved tropoelastin and re-freezed. Afterwards, the structure was lyophilized, being the ice used as a sacrificial material and obtaining a tubular structure of protein (227). Interestingly, depending on the time dipping the ice, thicker wall structures could be obtained, being 5 seconds the limit before ice started to melt. Dual layered structures can also be achieved using matrix molding. For example, using a glass capillary, a glucose-coated tungsten wire in the middle of the glass capillary and silicon tubes to each end of it, as previously reported (228). A gel collagen solution with cells was injected into the inner space of the mold and then, the mold was placed in DMEM at 37ºC to allow collagen gelification. After that, the tungsten wire was replaced for a thinner one, and a gel collagen solution was inserted in the space between the cross-linked collagen and the thinner wire. After its gelification, the wire was removed and a double-layer collagen TEBV structure was obtained.

1.6.2.4.2. Electrospinning

Electrospinning technique is a method that allows the formation of micro or nanofibrous scaffolds which resembles the ECM. Briefly, the method consists of a syringe loaded with a polymer which is pumped at a slow injection speed by a syringe pump. A high direct current voltage is applied in the polymer generating a large electric field inducing the formation of cone shape liquid droplet known as Taylor cone. Due to the high voltage, a liquid jet of polymer is generated from Taylor cone and travels onto a collector. The collector has the opposite polarity of the polymer and hence, it attracts the fibers. As the liquid travels to the collector, the solvent is evaporated and solid fibers are deposit on the collector (229). If the collector is a rotating cylinder, tubular scaffolds are obtained for TEBV development (**Figure 12C**). Due to the high voltage used in this approach, cells are seeded *a posteriori* onto the scaffold. Synthetic polymers and combinations of them are widely used with this technology, being the most utilized PCL and PLA (230,231). However, combinations of synthetic with natural polymers, such as collagen (232,233), elastin (234,235), gelatin (236,237) and silk fibroin (238), have also been used in order to improve biocompatibility, reporting higher cell

population and proliferation. An interesting feature of this method is the possibility to modulate the fiber diameter by several material and processing parameters, such as viscosity, molecular weight of the polymer, flow rate amongst others, which in turn modulates the porosity of the scaffold. Porosity is a characteristic which is important for TEBV permeability, nutrient and oxygen diffusion, and cell infiltration. In this sense, micro size fibers generates a more porous structure compared with nano sized fibers (239). Using different fiber diameter, Ju *et al* developed a bi-layered construct with different pore size, achieved by nano-scale fibers in the inner layer, which allowed EC adhesion, and higher diameter fiber in the outer layer, which allowed SMC infiltration with homogenous distribution (168). Tri-layered structures have also been developed with this approach. For instance, McClure *et al* electrospinned blends of PCL with collagen and elastin with different weight ratios for each layer, presenting mechanical properties such as burst pressure, compliance, amongst others in the range of native artery (240). In another study, hybrid material composed of PLA/PCL was deposit as the inner and outer layer, and as a middle support layer, a combination of PU with PCL was electrospinned, providing sufficient strength and elasticity for vascular graft (241). HUVEC and SMCs were seeded in the inner and outer layers, respectively, presenting a high viability over 90%. Remarkably, the outer circumferential aligned PLA/PCL fibers guided SMCs in circumferential oriented direction. This feature has been demonstrated in other studies, where EC and SMC can be aligned in the direction of the fibers. For example, Wu *et al,* using a three-step electrospinning method, produced a tri-layered vascular graft which consisted of axially aligned PLCL-collagen fibers as the inner layer, circumferentially oriented PLGA-silk fibroin yarns as the middle layer, and random PLCL-collagen fibers as the outer layer to hold the entire tubular structure (172). HUVEC and SMCs could be oriented along the fibers direction in the inner and middle layer, respectively. Therefore, with the electrospinning approach the alignment of cells and porosity of the scaffolds can be controlled.

1.6.2.4.3. *3D bioprinting*

3D bioprinting, also known as additive manufacturing, allows the development of 3D customizable structures from 2D stacking layers, generally using a computer-aided layer-by-layer deposition of bioink (composed of cells and biomaterials) (**Figure 12D**). In vascular tissue engineering field, 3D printing allows the development of a wide range of tubular structures and sizes, from arteries to small arteriole-size, as well as branched structures or even the incorporation of vascular networks within scaffolds for tissue regeneration. The bioinks employed should possess some criteria, such as guarantee cell survival or the property to switch from a liquid to a solid state once printed, with enough mechanical properties to

maintain the printed structure (242). The most widely used bioink is alginate, due to its rapid crosslinking properties, although other hydrogels such as collagen, gelatin, fibrin and their combinations have been utilized. There are three main modalities within 3D printing: extrusion, inkjet and laser-assisted 3D printing (243), being the extrusion-based the most used.

1.6.2.4.3.1. Extrusion-based bioprinting

With extrusion-based 3D bioprinting, a filament shape bioink is continuously extruded using pneumatic or mechanical (piston or screw) force (244). Briefly, pressurized air is used with pneumatic force to displace the bioink contained in the 3D printing nozzle, whereas an electric motor connected to the piston or screw induces their movement and so, the displacement of the bioink (**Figure 13A**). One of the main advantages of extrusion-based approach is the possibility to use high viscosity bioinks as well as high cell density, in comparison with the other two modalities (243).
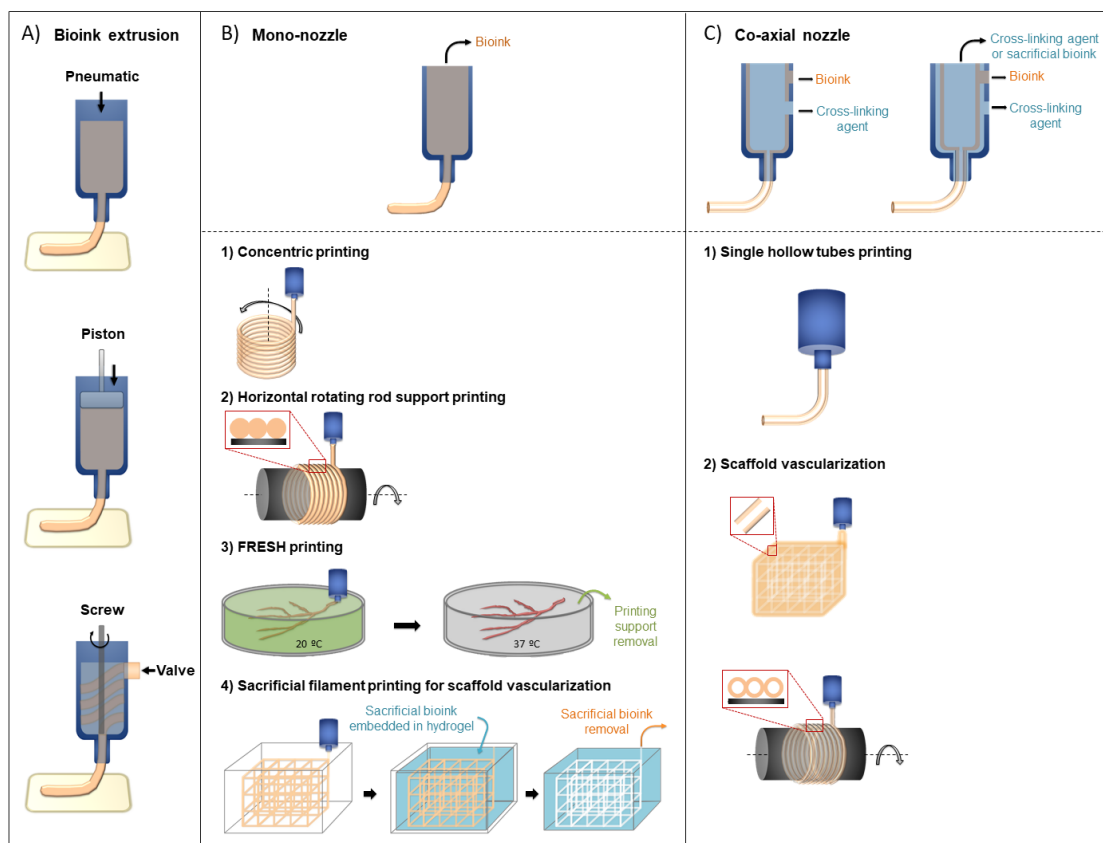
Figure 13. Strategies to develop vascular conduits using extrusion-based 3D printing. (A) Extrusion 3D printing uses pneumatic or mechanical (piston or screw) forces to extrude continuous material. (B) Using mono-nozzle print head, tubular vascular structures can be obtained through B1) concentric vertical printing; B2) horizontal printing on the surface of a rotating rod; B3) using a hydrogel support bath known as freeform reversible embedding of suspended hydrogels (FRESH); B4) the use of sacrificial bioinks embedded within hydrogels. (C) Using co-axial nozzles as the print head, C1) hollow tubular structures can be obtained directly and C2) if organized in 3D structure, vascularized scaffolds can be developed.

Using a concentric pattern in the vertical plane, hydrogels can be extruded obtaining large tubular structures, as represented in **Figure 13 B1**. As an example, Tan and Yeong obtained 15 mm length and 6 mm radius tubular structures, which are considered clinically relevant (245). However, following this printing pattern, short stacking length structures can be obtained, and developing multiple concentric layers mimicking the architecture of native vessels is challenging. Alternatively, horizontal rotating rod or cylinder has been used, depositing the hydrogel on their surface (**Figure 13 B2**). Freeman *et al* extruded a cell-laden hydrogel composed of a mixture of neonatal human dermal fibroblasts, gelatin and fibrinogen on the surface of a rotating rod (246). Then, the vascular construct was cross-linked with thrombin and cultured for 60 days. At the end of the culture, the burst pressure achieved was 1110 mmHg, which corresponds to half burst pressure of human saphenous vein. Multilayered vascular constructs can also be printed with horizontal rotating rod, as demonstrated by Jang *et al*. First, PCL was extruded as the inner layer followed by the extrusion of alginate with endothelial cells as middle layer. Then, PCL was extruded above as the outer layer, resulting in a three-layered tubular structure (247). Finally, to ensure alginate crosslinking, the construct was submerged in calcium chloride bath and subsequently implanted into bilateral carotid and femoral arteries of a canine model. After two weeks, endothelialization took place, with a patency of 64.3% and protection against inflammation in cell loaded constructs.

The abovementioned strategies are satisfactory when simple hollow tubular structures want to be develop, but presents limitations when more complex branched structures want to be manufactured. To this end, Hinton *et al* introduced an alternative approach to obtain 3D sophisticated constructs termed as freeform reversible embedding of suspended hydrogels (FRESH) (**Figure 13 B3**). More specifically, the bioink is extruded at 20ºC into a support bath containing a secondary hydrogel, also known as fugitive ink, which provides mechanical support avoiding the spread of the bioink during printing process, thus maintaining its printed structure. Thereafter, the temperature is raised up to 37ºC, which leads to hydrogel support bath melting leaving behind only the 3D printed vascular structure (248). Gelatin microparticles used as support bath allowed the development of bifurcated tubes using different bioinks such as alginate, collagen type I and fibrin. Furthermore, more sophisticated structures such as branched coronary artery of 4.5 cm length, <1mm wall thickness and a lumen diameter ranging from 1 to 3 mm could be printed with alginate. In a later study, using collagen type I, a coronary artery-size vessel was printed and perfused during 5 days with murine C2C12 casted around the structure, demonstrating active remodeling of the construct and high viability of cells (156).

While developing vascular structures is an adequate approach for certain clinical scenarios, vasculature structure is an indispensable step for tissue regeneration. For this reason, when an engineered scaffold is constructed for the regeneration of specific tissues, the introduction of a pre-vasculature inside is a necessary step for the success of the graft once implanted, as previously mentioned (120). This approach is limited to other technologies previously described but can be guaranteed with 3D printing technology. For this purpose, Miller *et al* introduced the use of acellular fugitive bioinks to create vascular channels within scaffolds (249). Commonly, filamentous network structures are printed with sacrificial hydrogels (i.e., Pluronic®, alginate, gelatin, agarose) and are consequently embedded in a hydrogel containing cells from a desired tissue to be regenerated, such as osteogenic progenitors or hepatocytes, to mention a few (249,250). Afterwards, sacrificial bioinks are dissolved by chemical reactions or thermal modifications, leaving empty channels where EC can be sedded (**Figure 13 B4**) (251). For instance, Kolesky *et al* used Pluronic® as a fugitive ink and MSC-laden hydrogel to print network structures and casted a hydrogel containing gelatin, fibrin and human neodermal fibroblasts around it. Then, the temperature was lowered at 4ºC and it was perfused with cold cell culture media, removing Pluronic® and seeding HUVEC thereafter (250). The scaffold presented a mature vascular network after 6 weeks of perfusion, with an endothelium providing a barrier function. Moreover, the scaffold was designed for bone regeneration and perfusing it with osteogenic differentiation media induced MSC differentiation towards osteogenic phenotype. However, the incorporation of larger vessels within the scaffold that can be anastomosed to the vasculature of the patient is desirable for a direct perfusion after implantation.

A novel strategy is to adapt 3D printing with a coaxial nozzle to allow the formation of hollowed microtubular constructs in one step process instead of layer-by-layer (**Figure 13 C1**). One of the most common hydrogels reported in the literature using this approach is alginate with calcium chloride as the cross-linking agent due to its instantly crosslinking properties. Generally, coaxial nozzles usually have an inner core were the cross-linking agent is extruded and allows a rapid crosslinking of the outer shell hydrogel, resulting in stable hollow microtube structure (152,252). The possibility of cross-linking the hydrogel in two directions have been reported by other studies, adding an extra outer shell in the coaxial nozzle (253). The dimensions of the core-shell nozzles determine the dimensions of the tubular structures. An advantage of this approach is that, with a short period of time, long hollowed conduits can be obtained. For instance, Gao *et al* developed a microvessel in one step procedure using a blend of EPC with alginate and vascular-tissue-derived decellularized extracellular matrix (254). In

addition, this TEBV could be perfused and endothelialized *in vitro*, and when implanted *in vivo* in a mouse ischemic limb model, increase of neovascularization and recovering of the ischemic limb was reported. Furthermore, these vascular constructs can be organized in a 3D structure, resulting in scaffolds with vasculature, successfully supporting proliferation and maturation of vascular cells (252) (**Figure 13 C2**). Moreover, when these hollowed structures are deposed on the surface of a rotating rod, two-level fluid channels is developed, including a macro-channel in the middle of the tubular construct with micro channels in their wall. As an example, Gao *et al* printed two layers encapsulating three different cell types: fibroblasts on the outer layer, smooth muscle cells in the middle layer and HUVEC cells seeded on the surface of the inner layer, mimicking the native blood vessel architecture and reporting a cell viability over 90% (151).

1.6.2.4.3.2. Inkjet bioprinting

Another modality of 3D bioprinting is inkjet bioprinting, also known as drop-based bioprinting. In this case, contrary to the extrusion method, the bioink is deposited drop-by-drop with the use of thermal or piezoelectric forces
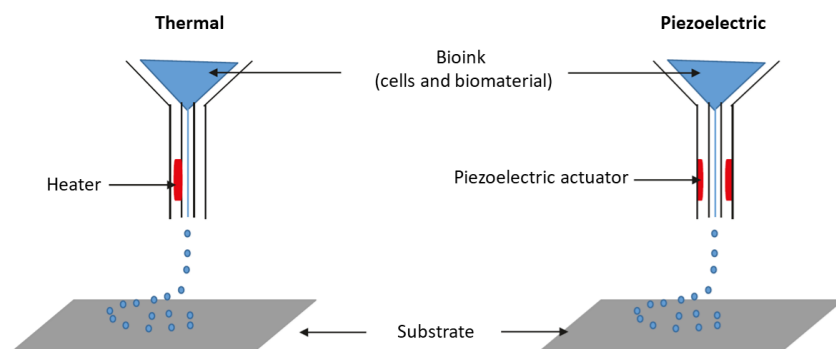
Figure 14. Inkjet 3D printing. With thermal inkjet, the print head is electrically heated producing pressure pulses that force droplets of the bioink through the nozzle. With piezoelectric inkjet, the bioink breaks into droplets due to acoustic waves generated by a piezoelectric actuator. Figure adapted from (255).

(243) (**Figure 14**). To put it briefly, in thermal inkjet bioprinting pulses of pressure are generated by heating the print head, inducing the generation of droplets, whereas in piezoelectric inkjet, the bioink breaks into droplets due to acoustic waves generated by piezoelectric crystal. A requisite of using inkjet bioprinting is the use of low viscosity bioinks to avoid nozzle clogging and preferably with quickly cross-linking properties to form a solid structure after printing. This requirement reduces the number of bioinks to be used, being alginate the most widely used together with its composites (256), with several studies reporting the development of tubular structures as mentioned below.

Similar to extrusion method, single tubular structures are obtained when circular printing pattern is applied in the vertical axis (257). To improve the construction stability during

printing process, some studies report the use of hydrophobic and high density fluid support such as fluorocarbons, which do not mix with the printing material and preserve the printed structure, with the possibility to create branched tubular structures (258,259). Likewise, tubular structures can also be printed along the horizontal axis. In this case, although cross-sectional deformation has been reported due to droplet impact force, gravity and buoyant force (260), it can be avoid printing the tubular structure with a predictive compensation, involving non-circular printing resulting in a circular shape (261). Despite alginate is the hydrogel most used in the abovementioned studies, it is limited in terms of providing a friendly environment for cell spreading. Few studies attempted to use other hydrogels successfully generating vascular conduits. For instance, Schöneber *et al* reported an *in vitro* blood vessel model with tri-layered structure using inkjet 3D bioprinting along horizontal axis. Sacrificial gelatin with HUVEC was printed as the inner core followed by a deposition of fibrin and smooth muscle cells as tunica media. Finally, casting a hydrogel containing fibroblasts, fibrin and collagen around the previous structure formed the tunica adventitia. Perfusion of this structure with physiological flow conditions resulted in functional vessels expressing VE-cadherin, smooth muscle actin and an increase of collagen type IV deposition, with a monolayer of endothelial cells preserving the barrier function (262). Although inkjet 3D printing has mainly focused on building tubular structures, few studies reported promising results developing microvascular networks. For instance, a bioink composed of human microvascular endothelial cells (HMVEC) and thrombin dispensed on fibrinogen resulted in the alignment and proliferation of HMVEC forming confluent micro-sized tubular structures resembling capillaries (263). In another study, three different bioinks composed of bovine aortic endothelial cells, canine smooth muscle cells and human amniotic fluid-derived stem cells were used to develop an alginate-collagen scaffold. After *in vivo* implantation, the construct was able to mature and function with adequate vascularization (264).

1.6.2.4.3.3. Laser-assisted bioprinting

Laser assisted bioprinting is a nozzle free printing strategy, being less common than extrusion and inkjet 3D printing in vascular engineering field. This modality consists in directing a pulse laser through a "ribbon" structure containing the bioink. The ribbon comprises an upper energy absorbing material layer (e.g., gold or titanium) and a lower bioink layer containing hydrogel and/or cells. Laser pulses focus on the absorbing layer generating a high pressure bubble that push the bioink towards a collector substrate located below the ribbon (243) (**Figure 15**). This modality presents a high degree of precision and resolution of the printed construct and can be used with high-viscosity bioink. However the preparation of ribbon is

time consuming and the viability of cells is lower compared with the other 3D printing modalities (265).
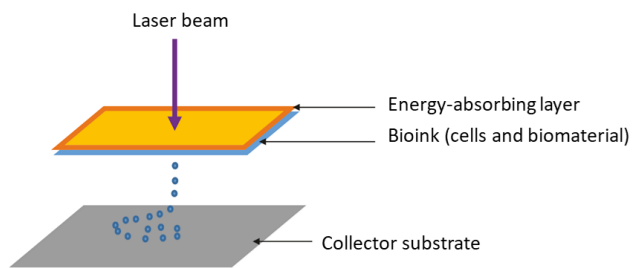
Figure 15. Laser-assisted 3D printing. A pulse of laser beam is directed on absorbing substrate generating a high pressure bubble that push the bioink towards a collector substrate. Figure adapted from (255).

Limited number of published studies is found in the literature using laser-assisted bioprinting for vascular conduits development (266). In general, they are focused in printing pattern structures with vascular cells to induced vascularization of engineered constructs. For instance, 3D patterned HUVEC and human umbilical vein smooth muscle cells (HUVSMC) on Matrigel substrate resulted in a well-defined and interconnected vascular structures *in vitro* (267). In a similar way, a recent study could successfully pre-organize endothelial cells on collagen hydrogels containing osteoprogenitor cells forming a capillary-like network (268). When implanted *in vivo*, a significant increase in vascularization and bone regeneration rate was observed in pre-patterned endothelial scaffolds compared to random seeding (269). Another significant result was observed when HUVEC and human MSC were pre-patterned on a polyester urethane urea (PEUU) cardiac patch. *In vivo* implantation showed increased vessel formation and integration with murine vascular system, with a significant functional improvement of infarcted hearts (270).

1.7.   References

1.   Tortora GJ. Principles of anatomy & physiology / Gerard J. Tortora, Bryan H. Derrickson. 13th ed. Hoboken N.J.: Wiley; 2011.

2.   Dewey CF, Bussolari SR, Gimbrone MA, Davies PF. The dynamic response of vascular endothelial cells to fluid shear stress. J Biomech Eng. 1981;103(3):177–85.

3.   MK P, R T. The vascular system. An overview of structure and function. J Pharmacol Toxicol Methods. 2000;44(2):334–40.

4.   Levy BI, Tedgui A. Morphologic Aspects of the Large Artery Vascular Wall. In: Biology of the arterial wall. 1999. p. 3–12.

5.   Egawa G, Nakamizo S, Natsuaki Y, Doi H, Miyachi Y, Kabashima K. permeability in mice using two-photon. 2013;1–6.

6.   Claesson-Welsh L. Vascular permeability - The essentials. Ups J Med Sci. 2015;120(3):135–43.

7.   Tousoulis D, Kampoli A-M, Tentolouris Nikolaos Papageorgiou C, Stefanadis C. The Role of Nitric Oxide on Endothelial Function. Curr Vasc Pharmacol. 2012;10(1):4–18.

8.   Jayadev R, Sherwood DR. Basement membranes. Curr Biol. 2017;27(6):R207–11.

9.   Potente M, Mäkinen T. Vascular heterogeneity and specialization in development and disease. Nat Rev Mol Cell Biol. 2017;18(8):477–94.

10.   Lilly B. We have contact: Endothelial cell-smooth muscle cell interactions. Physiology. 2014;29(4):234–41.

11.   Wagenseil J, Mecham R. Vascular Extracellular Matrix and Arterial Mechanics. Physiolocial Rev. 2009;89(3):957–89.

12.   Chen H, Kassab G. Microstructure-Based Biomechanics of Coronary Arteries in Health and Disease. J Biomech. 2016;49(12):2548–59.

13.   Rhodin JAG. Architecture of the Vessel Wall. In: Comprehensive Physiology. 1980. p. 1–31.

14.   Majesky MW, Dong XR, Hoglund V, Daum G, Mahoney WM. The adventitia: A progenitor cell niche for the vessel wall. Cells Tissues Organs. 2011;195(1–2):73–81.

15.   Risau W, Flame I. Vasculogenesis. Annu Rev Cell Dev Biol. 1995;11:73–91.

16.   Swift MR, Weinstein BM. Arterial-venous specification during development. Circ Res. 2009;104(5):576–88.

17.   Hinsbergh VWM van. Angiogenesis: Basics of Vascular Biology. In: Vascularization for Tissue Engineering and Regenerative Medicine. 2016. p. 1–29.

18.   Carmeliet P. Mechanisms of angiogenesis and arteriogenesis. Nat Med. 2000;6(4):389–95.

19.   Krock BL, Skuli N, Simon MC. Hypoxia-Induced Angiogenesis: Good and Evil. Genes and Cancer. 2011;2(12):1117–33.

20.   Forsythe JA, Jiang BH, Iyer N V, Agani F, Leung SW, Koos RD, et al. Activation of vascular endothelial growth factor gene transcription by hypoxia-inducible factor 1. Mol Cell Biol. 1996;16(9):4604–13.

21.   Gerhardt H. VEGF and endothelial guidance in angiogenic sprouting. Organogenesis. 2008;4(4):241–6.

22.   De Smet F, Segura I, De Bock K, Hohensinner PJ, Carmeliet P. Mechanisms of vessel branching: Filopodia on endothelial tip cells lead the way. Arterioscler Thromb Vasc Biol. 2009;29(5):639–49.

23.   Huang H, Bhat A, Woodnutt G, Lappe R. Targeting the ANGPT-TIE2 pathway in malignancy. Nat Rev Cancer. 2010;10(8):575–85.

24.   Potente M, Gerhardt H, Carmeliet P. Basic and therapeutic aspects of angiogenesis. Cell. 2011;146(6):873–87.

25.   Jain RK. Molecular regulation of vessel maturation. Nat Med. 2003;9(6):685–93.

26.   Banfi A, Holnthoner W, Martino MM, Ylä-Herttuala S. Editorial: Vascularization for Regenerative Medicine. Front Bioeng Biotechnol. 2018;6:1–2.

27.   Dickson K, Katzman S, Delgado E, Contreras D. Delayed Unions and Nonunions of Open Tibial Fractures. Correlation With Arteriography Results. Clin Orthop Relat Res. 1994;302:189–93.

28.   Stegen S, van Gastel N, Carmeliet G. Bringing new life to damaged bone: The importance of angiogenesis in bone repair and regeneration. Bone. 2015;70:19–27.

29.   Clarke B. Normal bone anatomy and physiology. Clin J Am Soc Nephrol. 2008;3 Suppl 3:S131–9.

30.   Liu Y, Luo D, Wang T. Hierarchical Structures of Bone and Bioinspired Bone Tissue Engineering. Small. 2016;12(34):4611–32.

31.   Buck DW, Dumanian GA. Bone biology and physiology: Part I. the fundamentals. Plast Reconstr Surg. 2012;129(6):1314–20.

32.   Meng Bao C le, Y.L. E, S.K. M, Liu Y, Choolani M, K.Y. J. Advances in Bone Tissue Engineering. In: Regenerative Medicine and Tissue Engineering. 2013. p. 599–614.

33.   Koons GL, Diba M, Mikos AG. Materials design for bone-tissue engineering. Nat Rev Mater. 2020;1–20.

34.   Qu H, Fu H, Han Z, Sun Y. Biomaterials for bone tissue engineering scaffolds: A review. RSC Adv. 2019;9(45):26252–62.

35.   Florencio-Silva R, Sasso GRDS, Sasso-Cerri E, Simões MJ, Cerri PS. Biology of Bone Tissue: Structure, Function, and Factors That Influence Bone Cells. Biomed Res Int. 2015;(421746).

36.   Hadjidakis DJ, Androulakis II. Bone remodeling. Ann N Y Acad Sci. 2006;1092:385–96.

37.   Dirckx N, Van Hul M, Maes C. Osteoblast recruitment to sites of bone formation in skeletal development, homeostasis, and regeneration. Birth Defects Res Part C - Embryo Today Rev. 2013;99(3):170–91.

38.   Wennberg C, Hessle L, Lundberg P, Mauro S, Narisawa S, Lerner UH, et al. Functional characterization of osteoblasts and osteoclasts from alkaline phosphatase knockout mice. J Bone Miner Res. 2000;15(10):1879–88.

39.   Perez RA, Seo SJ, Won JE, Lee EJ, Jang JH, Knowles JC, et al. Therapeutically relevant aspects in bone repair and regeneration. Mater Today. 2015;18(10):573–89.

40.   Krishnan L, Willett NJ, Guldberg RE. Vascularization strategies for bone regeneration. Ann Biomed Eng. 2014;42(2):432–44.

41.   Lau TT, Wang D-A. Stromal cell-derived factor-1 (SDF-1): homing factor for engineered regenerative medicine. Expert Opin Biol Ther. 2011;11(2):189–97.

42.   Dimitriou R, Jones E, McGonagle D, Giannoudis P V. Bone regeneration: current concepts and future directions. BMC Med. 2011;9(16):1–10.

43.   Schemitsch EH. Size Matters: Defining Critical in Bone Defect Size! J Orthop Trauma. 2017;31(10):S20–2.

44. Henkel J, Woodruff MA, Epari DR, Steck R, Glatt V, Dickinson IC, et al. Bone Regeneration Based on Tissue Engineering Conceptions — A 21st Century Perspective. Bone Res. 2013;1(3):216–48.

45. Roberts TT, Rosenbaum AJ. Bone grafts, bone substitutes and orthobiologics: the bridge between basic science and clinical advancements in fracture healing. Organogenesis. 2012;8(4):114–24.

46. Langer R, Vacanti JP. Tissue Engineering. Science (80-). 1993;260:920–6.

47. Amin AMM, Ewais EMM. Bioceramic scaffolds. In: Scaffolds in Tissue Engineering - Materials, Technologies and Clinical Applications. 2017. p. 49–74.

48. Shih YR V., Hwang Y, Phadke A, Kang H, Hwang NS, Caro EJ, et al. Calcium phosphate-bearing matrices induce osteogenic differentiation of stem cells through adenosine signaling. Proc Natl Acad Sci U S A. 2014;111(3):990–5.

49. Mao C, Chen X, Miao G, Lin C. Angiogenesis stimulated by novel nanoscale bioactive glasses. Biomed Mater. 2015;10(2):25005.

50. Baino F, Hamzehlou S, Kargozar S. Bioactive glasses: Where are we and where are we going? J Funct Biomater. 2018;9(25).

51. Gao C, Deng Y, Feng P, Mao Z, Li P, Yang B, et al. Current progress in bioactive ceramic scaffolds for bone repair and regeneration. Int J Mol Sci. 2014;15(3):4714–32.

52. Takemoto M, Fujibayashi S, Neo M, Suzuki J, Kokubo T, Nakamura T. Mechanical properties and osteoconductivity of porous bioactive titanium. Biomaterials. 2005;26(30):6014–23.

53. Simon M, Lagneau C, Moreno J, Lissac M, Dalard F, Corrosion GB, et al. Corrosion resistance and biocompatibility of a new porous surface for titanium implants. Eur J Oral Sci. 2005;113(6):537–45.

54. Shi C, Yuan Z, Han F, Zhu C, Li B. Polymeric biomaterials for bone regeneration. Ann Jt. 2016;1(27):1–14.

55. Nosrati H, Pourmotabed S, Sharifi E. A review on some natural biopolymers and their applications in angiogenesis and tissue engineering. J Appl Biotechnol Reports. 2018;5(3):81–91.

56. Gunatillake PA, Adhikari R, Gadegaard N. Biodegradable synthetic polymers for tissue engineering. Eur Cells Mater. 2003;5:1–16.

57. Lee EJ, Kasper FK, Mikos AG. Biomaterials for Tissue Engineering. Ann Biomed Eng. 2014;42(2):323–37.

58. Aguirre A, González A, Navarro M, Castaño Ó, Planell JA, Engel E. Control of microenvironmental cues with a smart biomaterial composite promotes endothelial progenitor cell angiogenesis. Eur Cells Mater. 2012;24:90–106.

59. Yu HS, Jin GZ, Won JE, Wall I, Kim HW. Macrochanneled bioactive ceramic scaffolds in combination with collagen hydrogel: A new tool for bone tissue engineering. J Biomed Mater Res - Part A. 2012;100 A(9):2431–40.

60. Perez RA, Mestres G. Role of pore size and morphology in musculo-skeletal tissue

regeneration. Mater Sci Eng C. 2016;61:922–39.

61.   Turnbull G, Clarke J, Picard F, Riches P, Jia L, Han F, et al. 3D bioactive composite scaffolds for bone tissue engineering. Bioact Mater. 2018;3(3):278–314.

62.   Mikos AG, Temenoff JS. Formation of highly porous biodegradable scaffolds for tissue engineering. Electron J Biotechnol. 2000;3(2):114–9.

63.   Perez RA, El-Fiqi A, Park JH, Kim TH, Kim JH, Kim HW. Therapeutic bioactive microcarriers: Co-delivery of growth factors and stem cells for bone tissue engineering. Acta Biomater. 2014;10(1):520–30.

64.   Perez RA, Jung CR, Kim HW. Biomaterials and Culture Technologies for Regenerative Therapy of Liver Tissue. Adv Healthc Mater. 2017;6(2).

65.   Vieira S, Vial S, Reis RL, Oliveira JM. Nanoparticles for bone tissue engineering. Biotechnol Prog. 2017;33(3):590–611.

66.   Darweesh RS, Ayoub NM, Nazzal S. Gold nanoparticles and angiogenesis: Molecular mechanisms and biomedical applications. Int J Nanomedicine. 2019;14:7643–63.

67.   Rane AV, Kanny K, Abitha VK, Thomas S. Methods for Synthesis of Nanoparticles and Fabrication of Nanocomposites. In: Synthesis of Inorganic Nanomaterials. Elsevier Ltd.; 2018. p. 121–39.

68.   Nsiah BA, Moore EM, Roudsari LC, Virdone NK, West JL. Angiogenesis in hydrogel biomaterials. In: Biosynthetic Polymers for Medical Applications. Elsevier Ltd; 2016. p. 189–203.

69.   Slaughter B V., Khurshid SS, Fisher OZ, Khademhosseini A, Peppas NA. Hydrogels in Regenerative Medicine. Adv Mater. 2009;21(32–33):3307–29.

70.   Howard D, Buttery LD, Shakesheff KM, Roberts SJ. Tissue engineering: Strategies, stem cells and scaffolds. J Anat. 2008;213(1):66–72.

71.   Kartsogiannis V, Ng KW. Cell lines and primary cell cultures in the study of bone cell biology. Mol Cell Endocrinol. 2004;228(1–2):79–102.

72.   Yousefi A, James PF, Akbarzadeh R, Subramanian A, Flavin C, Oudadesse H. Prospect of Stem Cells in Bone Tissue Engineering: A Review. Stem Cells Int. 2016;2016:6180487.

73.   Oswald J, Boxberger S, Joergensen B, Bornhaeuser M, Ehninger G, Werner C. Mesenchymal Stem Cells can be differentiated into endothelial cells in vitro. Stem Cells. 2004;22:377–84.

74.   Hur J, Yoon CH, Kim HS, Choi JH, Kang HJ, Hwang KK, et al. Characterization of Two Types of Endothelial Progenitor Cells and Their Different Contributions to Neovasculogenesis. Arterioscler Thromb Vasc Biol. 2004;24(2):288–93.

75.   Kaushal S, Amiel GE, Guleserian KJ, Shapira OM, Perry T, Sutherland FW, et al. Functional Small Diameter Neovessels using Endothelial Progenitor Cells Expanded Ex Vivo. Nat Med. 2001;7(9):1035–40.

76.   Ferrara N. Role of vascular endothelial growth factor in regulation of physiological angiogenesis. Am J Physiol - Cell Physiol. 2001;280(6):C1358–66.

77. Presta M, Dell'Era P, Mitola S, Moroni E, Ronca R, Rusnati M. Fibroblast growth factor/fibroblast growth factor receptor system in angiogenesis. Cytokine Growth Factor Rev. 2005;16(2):159–78.

78. Morita I, Murota SI, Sakaguchi M. Three isoforms of platelet-derived growth factors all have the capability to induce angiogenesis in vivo. Biol Pharm Bull. 1994;17(12):1686–8.

79. Lindahl P, Johansson BR, Levéen P, Betsholtz C. Pericyte loss and microaneurysm formation in PDGF-B-deficient mice. Science (80-). 1997;277(5323):242–5.

80. Beederman M, Lamplot JD, Nan G, Wang J, Liu X, Yin L, et al. BMP signaling in mesenchymal stem cell differentiation and bone formation. J Biomed Sci Eng. 2013;6(8A):32–52.

81. Sun J, Li J, Li C, Yu Y. Role of bone morphogenetic protein-2 in osteogenic differentiation of mesenchymal stem cells. Mol Med Rep. 2015;12(3):4230–7.

82. Charoenlarp P, Rajendran AK, Iseki S. Role of fibroblast growth factors in bone regeneration. Inflamm Regen. 2017;37(1):1–7.

83. De Witte TM, Fratila-Apachitei LE, Zadpoor AA, Peppas NA. Bone tissue engineering via growth factor delivery: from scaffolds to complex matrices. Regen Biomater. 2018;5(4):197–211.

84. Feng W, Ye F, Xue W, Zhou Z, Kang YJ. Copper regulation of hypoxia-inducible factor-1 activity. Mol Pharmacol. 2009;75(1):174–82.

85. Yuan Y, Hilliard G, Ferguson T, Millhorn DE. Cobalt inhibits the interaction between hypoxia-inducible factor-α and von Hippel-Lindau protein by direct binding to hypoxia-inducible factor-α. J Biol Chem. 2003;278(18):15911–6.

86. Wu C, Zhou Y, Fan W, Han P, Chang J, Yuen J, et al. Hypoxia-mimicking mesoporous bioactive glass scaffolds with controllable cobalt ion release for bone tissue engineering. Biomaterials. 2012;33(7):2076–85.

87. Li H, Chang J. Stimulation of proangiogenesis by calcium silicate bioactive ceramic. Acta Biomater. 2013;9(2):5379–89.

88. Dashnyam K, Jin G-Z, Kim J-H, Perez R, Jang J-H, Kim H-W. Promoting angiogenesis with mesoporous microcarriers through a synergistic action of delivered silicon ion and VEGF. Biomaterials. 2017 Feb;116:145–57.

89. Dashnyam K, El-Fiqi A, Buitrago JO, Perez RA, Knowles JC, Kim HW. A mini review focused on the proangiogenic role of silicate ions released from silicon-containing biomaterials. J Tissue Eng. 2017;8:1–13.

90. Balasubramanian P, Hupa L, Jokic B, Detsch R, Grünewald A, Boccaccini AR. Angiogenic potential of boron-containing bioactive glasses: in vitro study. J Mater Sci. 2017;52(15):8785–92.

91. Gu Z, Xie H, Li L, Zhang X, Liu F, Yu X. Application of strontium-doped calcium polyphosphate scaffold on angiogenesis for bone tissue engineering. J Mater Sci Mater Med. 2013;24(5):1251–60.

92. Han P, Wu C, Xiao Y. The effect of silicate ions on proliferation, osteogenic

differentiation and cell signalling pathways (WNT and SHH) of bone marrow stromal cells. Biomater Sci. 2013;1(4):379–92.

93. He M, Chen X, Cheng K, Weng W, Wang H. Enhanced Osteogenic Activity of TiO2Nanorod Films with Microscaled Distribution of Zn-CaP. ACS Appl Mater Interfaces. 2016;8(11):6944–52.

94. Jin G, Cao H, Qiao Y, Meng F, Zhu H, Liu X. Osteogenic activity and antibacterial effect of zinc ion implanted titanium. Colloids Surfaces B Biointerfaces. 2014;117:158–65.

95. Peng S, Zhou G, Luk KDK, Cheung KMC, Li Z, Lam WM, et al. Strontium promotes osteogenic differentiation of mesenchymal stem cells through the Ras/MAPK signaling pathway. Cell Physiol Biochem. 2009;23(1–3):165–74.

96. Yoshizawa S, Brown A, Barchowsky A, Sfeir C. Magnesium ion stimulation of bone marrow stromal cells enhances osteogenic activity, simulating the effect of magnesium alloy degradation. Acta Biomater. 2014;10(6):2834–42.

97. Díaz-Tocados JM, Herencia C, Martínez-Moreno JM, Montes de Oca A, Rodríguez-Ortiz ME, Vergara N, et al. Magnesium Chloride promotes Osteogenesis through Notch signaling activation and expansion of Mesenchymal Stem Cells. Sci Rep. 2017;7(1):1–12.

98. J.Rodríguez P, Ros S, Gonzlez M. Modulation of the proliferation and differentiation of human mesenchymal stem cells by copper. J Cell Biochem. 2002;85(1):92–100.

99. Kulanthaivel S, Roy B, Agarwal T, Giri S, Pramanik K, Pal K, et al. Cobalt doped proangiogenic hydroxyapatite for bone tissue engineering application. Mater Sci Eng C. 2016;58:648–58.

100. Li S, Wang M, Chen X, Li SF, Li-Ling J, Xie HQ. Inhibition of osteogenic differentiation of mesenchymal stem cells by copper supplementation. Cell Prolif. 2014;47(1):81–90.

101. Drynda A, Drynda S, Kekow J, Lohmann C, Bertrand J. Differential Effect of Cobalt and Chromium Ions as Well as CoCr Particles on the Expression of Osteogenic Markers and Osteoblast Function. Int J Mol Sci. 2018;19(10):3034.

102. Birgani ZT, Gharraee N, Malhotra A, Van Blitterswijk CA, Habibovic P. Combinatorial incorporation of fluoride and cobalt ions into calcium phosphates to stimulate osteogenesis and angiogenesis. Biomed Mater. 2016;11(1).

103. Yu H, VandeVord PJ, Mao L, Matthew HW, Wooley PH, Yang SY. Improved tissue-engineered bone regeneration by endothelial cell mediated vascularization. Biomaterials. 2009;30(4):508–17.

104. Bruschi ML. Modification of drug release. In: Strategies to Modify the Drug Release from Pharmaceutical Systems. 2015. p. 15–28.

105. De Witte TM, Fratila-Apachitei LE, Zadpoor AA, Peppas NA. Bone tissue engineering via growth factor delivery: From scaffolds to complex matrices. Regen Biomater. 2018;5(4):197–211.

106. Zhu H, Yu D, Zhou Y, Wang C, Gao M, Jiang H, et al. Biological activity of a nanofibrous barrier membrane containing bone morphogenetic protein formed by core-shell electrospinning as a sustained delivery vehicle. J Biomed Mater Res - Part B Appl Biomater. 2013;101B(4):541–52.

107. Perez RA, Kim HW. Core-shell designed scaffolds for drug delivery and tissue engineering. Acta Biomater. 2015;21:2–19.

108. Lienemann PS, Lutolf MP, Ehrbar M. Biomimetic hydrogels for controlled biomolecule delivery to augment bone regeneration. Adv Drug Deliv Rev. 2012;64(12):1078–89.

109. Wang Z, Wang K, Lu X, Li M, Liu H, Xie C, et al. BMP-2 encapsulated polysaccharide nanoparticle modified biphasic calcium phosphate scaffolds for bone tissue regeneration. J Biomed Mater Res - Part A. 2015;103(4):1520–32.

110. Reinhart CT, Peppas NA. Solute diffusion in swollen membranes. Part II. Influence of crosslinking on diffusive properties. J Memb Sci. 1984;18:227–39.

111. Carbinatto FM, de Castro AD, Evangelista RC, Cury BSF. Insights into the swelling process and drug release mechanisms from cross-linked pectin/high amylose starch matrices. Asian J Pharm Sci. 2014;9(1):27–34.

112. Chen W, Palazzo A, Hennink WE, Kok RJ. Effect of particle size on drug loading and release kinetics of gefitinib-loaded PLGA microspheres. Mol Pharm. 2017;14(2):459–67.

113. Jia X, Zhao C, Li P, Zhang H, Huang Y, Li H, et al. Sustained release of VEGF by coaxial electrospun dextran/PLGA fibrous membranes in vascular tissue engineering. J Biomater Sci Polym Ed. 2011;22(13):1811–27.

114. Zhang W, Chang Q, Xu L, Li G, Yang G, Ding X, et al. Graphene Oxide-Copper Nanocomposite-Coated Porous CaP Scaffold for Vascularized Bone Regeneration via Activation of Hif-1α. Adv Healthc Mater. 2016;5(11):1299–309.

115. Santocildes-Romero ME, Crawford A, Hatton P V., Goodchild RL, Reaney IM, Miller CA. The osteogenic response of mesenchymal stromal cells to strontium-substituted bioactive glasses. J Tissue Eng Regen Med. 2015;9(5):619–31.

116. Kanczler JM, Ginty PJ, White L, Clarke NMP, Howdle SM, Shakesheff KM, et al. The effect of the delivery of vascular endothelial growth factor and bone morphogenic protein-2 to osteoprogenitor cell populations on bone formation. Biomaterials. 2010;31(6):1242–50.

117. Bose S, Tarafder S, Bandyopadhyay A. Effect of chemistry on osteogenesis and angiogenesis towards bone tissue engineering using 3D printed scaffolds. Ann Biomed Eng. 2017;45(1):261–72.

118. Perez RA, Kim JH, Buitrago JO, Wall IB, Kim HW. Novel therapeutic core-shell hydrogel scaffolds with sequential delivery of cobalt and bone morphogenetic protein-2 for synergistic bone regeneration. Acta Biomater. 2015;23:295–308.

119. Jain RK, Au P, Tam J, Duda DG, Fukumura D. Engineering vascularized tissue. Nat Biotechnol. 2005;23(7):821–3.

120. Levenberg S, Rouwkema J, Macdonald M, Garfein ES, Kohane DS, Darland DC, et al. Engineering vascularized skeletal muscle tissue. Nat Biotechnol. 2005;23(7):879–84.

121. Laschke MW, Menger MD. Vascularization in tissue engineering: Angiogenesis versus inosculation. Eur Surg Res. 2012;48(2):85–92.

122. Rouwkema J, Khademhosseini A. Vascularization and Angiogenesis in Tissue

Engineering: Beyond Creating Static Networks. Trends Biotechnol. 2016;34(9):733–45.

123.   Price GM, Wong KHK, Truslow JG, Leung AD, Acharya C, Tien J. Effect of Mechanical Factors on the Function of Engineered Human Blood Microvessels in Microfluidic Collagen Gels. Biomaterials. 2010;31(24):6182–9.

124.   World Health Organization. Cardiovascular diseases (CVDs) [Internet]. 2017. Available from: https://www.who.int/news-room/fact-sheets/detail/cardiovascular-diseases-(cvds)

125.   Libby P, Buring JE, Badimon L, Hansson GK, Deanfield J, Bittencourt MS, et al. Atherosclerosis. Nat Rev Dis Prim. 2019;5(56):1–18.

126.   Chaabane C, Otsuka F, Virmani R, Bochaton-Piallat ML. Biological responses in stented arteries. Cardiovasc Res. 2013;99(2):353–63.

127.   Sabik JF. Understanding saphenous vein graft patency. Circulation. 2011;124(3):273–5.

128.   Gu CX, Yang JF, Zhang HC, Wei H, Li LK. Off-pump coronary artery bypass grafting using a bilateral internal mammary artery Y graft. J Geriatr Cardiol. 2012;9(3):247–51.

129.   Verma S, Szmitko PE, Weisel RD, Bonneau D, Latter D, Errett L, et al. Should radial arteries be used routinely for coronary artery bypass grafting? Circulation. 2004;110(5):40–6.

130.   Wan S, George SJ, Berry C, Baker AH. Vein graft failure: Current clinical practice and potential for gene therapeutics. Gene Ther. 2012;19(6):630–6.

131.   Owens CD, Gasper WJ, Rahman AS, Conte MS. Vein graft failure. J Vasc Surg. 2015;61(1):203–16.

132.   Baker BM, Chen CS. Deconstructing the third dimension – how 3D culture microenvironments alter cellular cues. J Cell Sci. 2012;125(13):3015–24.

133.   Dehne EM, Hasenberg T, Marx U. The ascendance of microphysiological systems to solve the drug testing dilemma. Futur Sci OA. 2017;3(2).

134.   Wikswo JP. The relevance and potential roles of microphysiological systems in biology and medicine. Exp Biol Med. 2014;239(9):1061–72.

135.   LA L, DA T. Microphysiological Systems (" Organs-on-Chips ") for Drug. CTS-Clinical Transl Sci. 2017;10(4):237–9.

136.   Atchison L, Zhang H, Cao K, Truskey GA. A Tissue Engineered Blood Vessel Model of Hutchinson-Gilford Progeria Syndrome Using Human iPSC-derived Smooth Muscle Cells. Sci Rep. 2017;7(1):1–12.

137.   Cameron AC, Touyz RM, Lang NN. Vascular Complications of Cancer Chemotherapy. Can J Cardiol. 2016;32(7):852–62.

138.   Soultati A, Mountzios G, Avgerinou C, Papaxoinis G, Pectasides D, Dimopoulos MA, et al. Endothelial vascular toxicity from chemotherapeutic agents: Preclinical evidence and clinical implications. Cancer Treat Rev. 2012;38(5):473–83.

139.   Miranda-Nieves D, Chaikof EL. Collagen and Elastin Biomaterials for the Fabrication of Engineered Living Tissues. ACS Biomater Sci Eng. 2017;3(5):694–711.

140. Weinberg CB, Bell E. A blood vessel model constructed from collagen and cultured vascular cells. Science (80-). 1986;231(4736):397–400.

141. Konig G, McAllister TN, Dusserre N, Garrido SA, Iyican C, Marini A, et al. Mechanical properties of completely autologous human tissue engineered blood vessels compared to human saphenous vein and mammary artery. Biomaterials. 2009;30(8):1542–50.

142. Wang X, Ma B, Chang J. Preparation of decellularized vascular matrix by co-crosslinking of procyanidins and glutaraldehyde. Biomed Mater Eng. 2015;26(1–2):19–30.

143. Delgado LM, Fuller K, Zeugolis DI. Collagen Cross-Linking: Biophysical, Biochemical, and Biological Response Analysis. Tissue Eng - Part A. 2017;23(19–20):1064–77.

144. Matthews JA, Wnek GE, Simpson DG, Bowlin GL. Electrospinning of collagen nanofibers. Biomacromolecules. 2002;3(2):232–8.

145. Lin J, Shi Y, Men Y, Wang X, Ye J, Zhang C. Mechanical Roles in Formation of Oriented Collagen Fibers. Tissue Eng Part B Rev. 2020;26(2):116–28.

146. Swartz DD, Russell JA, Andreadis ST. Engineering of fibrin-based functional and implantable small-diameter blood vessels. Am J Physiol - Hear Circ Physiol. 2005;288(3 57-3):1451–60.

147. Long JL, Tranquillo RT. Elastic fiber production in cardiovasular tissue-equivalents. Matrix Biol. 2003;22(4):339–50.

148. Gui L, Boyle MJ, Kamin YM, Huang AH, Starcher BC, Miller CA, et al. Construction of tissue-engineered small-diameter vascular grafts in fibrin scaffolds in 30 days. Tissue Eng - Part A. 2014;20(9–10):1499–507.

149. Lovett M, Eng G, Kluge JA, Cannizzaro C, Vunjak-Novakovic G, Kaplan DL. Tubular silk scaffolds for small diameter vascular grafts. Organogenesis. 2010;6(4):217–24.

150. Enomoto S, Sumi M, Kajimoto K, Nakazawa Y, Takahashi R, Takabayashi C, et al. Long-term patency of small-diameter vascular graft made from fibroin, a silk-based biodegradable material. J Vasc Surg. 2010;51(1):155–64.

151. Gao Q, Liu Z, Lin Z, Qiu J, Liu Y, Liu A, et al. 3D Bioprinting of Vessel-like Structures with Multi-level Fluidic Channels 3D Bioprinting of Vessel-like Structures with Multi-level Fluidic Channels. ACS Biomater Sci Eng. 2017;3(3):399–408.

152. Zhang Y, Yu Y, Ozbolat IT. Direct bioprinting of vessel-like tubular microfluidic channels. J Nanotechnol Eng Med. 2013;4(2):1–7.

153. Aussel A, Montembault A, Malaise S, Foulc MP, Faure W, Cornet S, et al. In Vitro Mechanical Property Evaluation of Chitosan-Based Hydrogels Intended for Vascular Graft Development. J Cardiovasc Transl Res. 2017;10(5–6):480–8.

154. Eoh JH, Shen N, Burke JA, Hinderer S, Xia Z, Schenke-layland K, et al. Enhanced elastin synthesis and maturation in human vascular smooth muscle tissue derived from induced-pluripotent stem cells. Acta Biomater. 2017;52:49–59.

155. Oikonomou E, Tsalamandris S, Mourouzis K, Tousoulis D. Biology of the Vessel Wall. Coronary Artery Disease. Elsevier Inc.; 2017. 3–12 p.

156. Lee A, Hudson AR, Shiwarski DJ, Tashman JW, Hinton TJ, Yerneni S, et al. 3D bioprinting

of collagen to rebuild components of the human heart. Science (80-). 2019;365(6452):482–7.

157.   Dahl SLM, Koh J, Prabhakar V, Niklason LE. Decellularized native and engineered arterial scaffolds for transplantation. Cell Transplant. 2003;12(6):659–66.

158.   Rieder E, Steinacher-Nigisch A, Weigel G. Human immune-cell response towards diverse xenogeneic and allogeneic decellularized biomaterials. Int J Surg. 2016;36:347–51.

159.   Anju S, Prajitha N, Sukanya VS, Mohanan P V. Complicity of degradable polymers in health-care applications. Mater Today Chem. 2020;16:100236.

160.   L. E. Niklason, J. Gao, W. M. Abbott, K. K. Hirschi, S. Houser, R. Marini RL. Functional arteries grown in vitro. Science (80-). 1999;284:489–93.

161.   Williams C, Wick TM. Perfusion bioreactor for small diameter tissue-engineered arteries. Tissue Eng. 2004;10(5–6):930–41.

162.   Kirkton RD, Santiago-Maysonet M, Lawson JH, Tente WE, Dahl SLM, Niklason LE, et al. Bioengineered human acellular vessels recellularize and evolve into living blood vessels after human implantation. Sci Transl Med. 2019;11(485).

163.   Nottelet B, Pektok E, Mandracchia D, Tille JC, Walpoth B, Gurny R, et al. Factorial design optimization and in vivo feasibility of poly(ε-caprolactone)-micro- and nanofiber-based small diameter vascular grafts. J Biomed Mater Res - Part A. 2009;89(4):865–75.

164.   Ye Q, Zund G, Jockenhoevel S, Schoeberlein A, Hoerstrup SP, Grunenfelder J, et al. Scaffold precoating with human autologous extracellular matrix for improved cell attachment in cardiovascular tissue engineering. ASAIO J. 2000;46(6):730–3.

165.   Gui L, Dash BC, Luo J, Qin L, Zhao L, Yamamoto K, et al. Implantable tissue-engineered blood vessels from human induced pluripotent stem cells. Biomaterials. 2016;102:120–9.

166.   Higgins SP, Solan AK, Niklason LE. Effects of polyglycolic acid on porcine smooth muscle cell growth and differentiation. J Biomed Mater Res - Part A. 2003;67(1):295–302.

167.   Jiang YC, Jiang L, Huang A, Wang XF, Li Q, Turng LS. Electrospun polycaprolactone/gelatin composites with enhanced cell–matrix interactions as blood vessel endothelial layer scaffolds. Mater Sci Eng C. 2017;71:901–8.

168.   Ju YM, Choi JS, Atala A, Yoo JJ, Lee SJ. Bilayered scaffold for engineering cellularized blood vessels. Biomaterials. 2010;31(15):4313–21.

169.   Huang C, Geng X, Qinfei K, Xiumei M, Al-Deyab SS, El-Newehy M. Preparation of composite tubular grafts for vascular repair via electrospinning. Prog Nat Sci Mater Int. 2012;22(2):108–14.

170.   Motlagh D, Allen J, Hoshi R, Yang J, Lui K, Ameer G. Hemocompatibility evaluation of poly(diol citrate) in vitro for vascular tissue engineering. J Biomed Mater Res Part A. 2007;82A(4):907–16.

171.   Yin A, Luo R, Li J, Mo X, Wang Y, Zhang X. Coaxial electrospinning multicomponent functional controlled-release vascular graft: Optimization of graft properties. Colloids Surfaces B Biointerfaces. 2017;152:432–9.

172. Wu T, Zhang J, Wang Y, Li D, Sun B, El-Hamshary H, et al. Fabrication and preliminary study of a biomimetic tri-layer tubular graft based on fibers and fiber yarns for vascular tissue engineering. Mater Sci Eng C. 2018;82:121–9.

173. Grenier G, Rémy-Zolghadri M, Guignard R, Bergeron F, Labbé R, Auger FA, et al. Isolation and culture of the three vascular cell types from a small vein biopsy sample. Vitr Cell Dev Biol - Anim. 2003;39(3–4):131–9.

174. Buijtenhuijs P, Buttafoco L, Poot AA, Daamen WF, van Kuppevelt TH, Dijkstra PJ, et al. Tissue engineering of blood vessels: characterization of smooth-muscle cells for culturing on collagen-and-elastin-based scaffolds. Biotechnol Appl Biochem. 2004;39(2):141–9.

175. L'Heureux N, Dusserre N, Konig G, Victor B, Keire P, Wight TN, et al. Human tissue-engineered blood vessels for adult arterial revascularization. Nat Med. 2006;12(3):361–5.

176. Rippon HJ, Bishop AE. Embryonic stem cells. Cell Prolif. 2004;37:23–34.

177. F. HN, Hiroshi N, Christoph P, Abhijit D, Yasodha N, Felix F, et al. Embryonic stem cell-derived endothelial cells engraft into the ischemic hindlimb and restore perfusion. Arterioscler Thromb Vasc Biol. 2010;30(5):984-U224.

178. Wang ZZ, Au P, Chen T, Shao Y, Daheron LM, Bai H, et al. Endothelial cells derived from human embryonic stem cells form durable blood vessels in vivo. Nat Biotechnol. 2007;25(3):317–8.

179. Volarevic V, Markovic BS, Gazdic M, Volarevic A, Jovicic N, Arsenijevic N, et al. Ethical and safety issues of stem cell-based therapy. Int J Med Sci. 2018;15(1):36–45.

180. Han Y, Li X, Zhang Y, Han Y, Chang F, Ding J. Mesenchymal Stem Cells for Regenerative Medicine. Cells. 2019;8(8):886.

181. Gu W, Hong X, Le Bras A, Nowak WN, Bhaloo SI, Deng J, et al. Smooth muscle cells differentiated from mesenchymal stem cells are regulated by microRNAs and suitable for vascular tissue grafts. J Biol Chem. 2018;293(21):8089–102.

182. Dong J De, Gu YQ, Li CM, Wang CR, Feng ZG, Qiu RX, et al. Response of mesenchymal stem cells to shear stress in tissue-engineered vascular grafts. Acta Pharmacol Sin. 2009;30(5):530–6.

183. Jia L, Prabhakaran MP, Qin X, Ramakrishna S. Stem cell differentiation on electrospun nanofibrous substrates for vascular tissue engineering. Mater Sci Eng C. 2013;33(8):4640–50.

184. DW H, TM M, DA V. Characterization of the response of bone marrow-derived progenitor cells to cyclic strain: implications for vascular tissue-engineering applications. Tissue Eng - Part A. 2004;10:361–9.

185. Ghazanfari S, Tafazzoli-Shadpour M, Shokrgozar MA. Effects of cyclic stretch on proliferation of mesenchymal stem cells and their differentiation to smooth muscle cells. Biochem Biophys Res Commun. 2009;388(3):601–5.

186. Gong Z, Niklason LE. Small-diameter human vessel wall engineered from bone marrow-derived mesenchymal stem cells (hMSCs). FASEB J. 2008;22(6):1635–48.

187. Zhao Y, Zhang S, Zhou J, Wang J, Zhen M, Liu Y, et al. The development of a tissue-engineered artery using decellularized scaffold and autologous ovine mesenchymal stem cells. Biomaterials. 2010;31(2):296–307.

188. Matsumura G, Miyagawa-Tomita S, Shin'Oka T, Ikada Y, Kurosawa H. First evidence that bone marrow cells contribute to the construction of tissue-engineered vascular autografts in vivo. Circulation. 2003;108(14):1729–34.

189. Roha JD, Sawh-Martinez R, Brennan MP, Jay SM, Devine L, Rao DA, et al. Tissue-engineered vascular grafts transform into mature blood vessels via an inflammation-mediated process of vascular remodeling. Proc Natl Acad Sci U S A. 2010;107(10):4669–74.

190. Hibino N, McGillicuddy E, Matsumura G, Ichihara Y, Naito Y, Breuer C, et al. Late-term results of tissue-engineered vascular grafts in humans. J Thorac Cardiovasc Surg. 2010;139(2):431-436.e2.

191. Sugiura T, Matsumura G, Miyamoto S, Miyachi H, Breuer CK, Shinoka T. Tissue-engineered vascular grafts in children with congenital heart disease: intermediate term follow-up. Semin Thorac Cardiovasc Surg. 2018;30(2):175–9.

192. Brown MA, Wallace CS, Angelos M, Truskey GA. Characterization of umbilical cord blood-derived late outgrowth endothelial progenitor cells exposed to laminar shear stress. Tissue Eng - Part A. 2009;15(11):3575–87.

193. Ladhoff J, Fleischer B, Hara Y, Volk HD, Seifert M. Immune privilege of endothelial cells differentiated from endothelial progenitor cells. Cardiovasc Res. 2010;88(1):121–9.

194. Kaushal S, Amiel GE, Guleserian KJ, Shapira OM, Perry T, Sutherland FW, et al. Functional small diameter neovessels using endothelial progenitor cells expanded ex vivo. Nat Med. 2010;7(9):1035–40.

195. Jantzen AE, Lane WO, Gage SM, Jamiolkowski RM, Haseltine JM, Galinat LJ, et al. Use of autologous blood-derived endothelial progenitor cells at point-of-care to protect against implant thrombosis in a large animal model. Biomaterials. 2011;32(33):8356–63.

196. Zhou M, Qiao W, Liu Z, Shang T, Qiao T, Mao C, et al. Development and in vivo evaluation of small-diameter vascular grafts engineered by outgrowth endothelial cells and electrospun chitosan/poly(ε- caprolactone) Nanofibrous Scaffolds. Tissue Eng - Part A. 2014;20(1–2):79–91.

197. Dai R, Wang Z, Samanipour R, Koo KI, Kim K. Adipose-Derived Stem Cells for Tissue Engineering and Regenerative Medicine Applications. Stem Cells Int. 2016;2016.

198. Fischer LJ, McIlhenny S, Tulenko T, Golesorkhi N, Zhang P, Larson R, et al. Endothelial differentiation of adipose-derived stem cells: Effects of endothelial cell growth supplement and shear force. J Surg Res. 2009;152(1):157–66.

199. McIlhenny SE, Hager ES, Grabo DJ, Dimatteo C, Shapiro IM, Tulenko TN, et al. Linear shear conditioning improves vascular graft retention of adipose-derived stem cells by upregulation of the α5β 1 integrin. Tissue Eng - Part A. 2010;16(1):245–55.

200. Wang C, Cen L, Yin S, Liu Q, Liu W, Cao Y, et al. A small diameter elastic blood vessel wall prepared under pulsatile conditions from polyglycolic acid mesh and smooth

muscle cells differentiated from adipose-derived stem cells. Biomaterials. 2010;31(4):621–30.

201. Wang X, Sui S. Pulsatile culture of a poly(DL-lactic-co-glycolic acid) sandwiched cell/hydrogel construct fabricated using a step-by-step mold/extraction method. Artif Organs. 2011;35(6):645–55.

202. Arts CHP, Hedeman Joosten PPA, Blankensteijn JD, Staal FJT, Ng PYY, Heijnen-Snyder GJ, et al. Contaminants from the transplant contribute to intimal hyperplasia associated with microvascular endothelial cell seeding. Eur J Vasc Endovasc Surg. 2002;23(1):29–38.

203. Lin CH, Hsia K, Tsai CH, Ma H, Lu JH, Tsay RY. Decellularized porcine coronary artery with adipose stem cells for vascular tissue engineering. Biomed Mater. 2019;14(4).

204. Arts CH, De Groot PG, Attevelt N, Heijnen-Snyder GJ, Verhagen HJ, Eikelboom BC, et al. In vivo transluminal microvascular endothelial cell seeding on balloon injured rabbit arteries. J Cardiovasc Surg (Torino). 2004 Apr;45(2):129–37.

205. Krawiec JT, Weinbaum JS, St. Croix CM, Phillippi JA, Watkins SC, Rubin JP, et al. A cautionary tale for autologous vascular tissue engineering: Impact of human demographics on the ability of adipose-derived mesenchymal stem cells to recruit and differentiate into smooth muscle cells. Tissue Eng - Part A. 2015;21(3–4):426–37.

206. Takahashi K, Yamanaka S. Induction of Pluripotent Stem Cells from Mouse Embryonic and Adult Fibroblast Cultures by Defined Factors. Cell. 2006;126(4):663–76.

207. Yilmaz A, Benvenisty N. Defining Human Pluripotency. Cell Stem Cell. 2019;25(1):9–22.

208. Patsch C, Challet-meylan L, Thoma EC, Urich E, Sullivan JFO, Grainger SJ, et al. Generation of vascular endothelial and smooth muscle cells from human pluripotent stem cells. Nat Cell Biol. 2016;17(8):994–1003.

209. Sivarapatna A, Ghaedi M, Le A V., Mendez JJ, Qyang Y, Niklason LE. Arterial specification of endothelial cells derived from human induced pluripotent stem cells in a biomimetic flow bioreactor. Biomaterials. 2015;53:621–33.

210. Adams WJ, Zhang Y, Cloutier J, Kuchimanchi P, Newton G, Sehrawat S, et al. Functional vascular endothelium derived from human induced pluripotent stem cells. Stem Cell Reports. 2013;1(2):105–13.

211. Wang Y, Hu J, Jiao J, Liu Z, Xhou Z, Zhao C, et al. Engineering vascular tissue with functional smooth muscle cells derived from human iPS cells and nanofibrous scaffolds. Biomaterials. 2014;35(32):8960–9.

212. Luo J, Qin L, Zhao L, Gui L, Ellis MW, Huang Y, et al. Tissue-Engineered Vascular Grafts with Advanced Mechanical Strength from Human iPSCs. Cell Stem Cell. 2020;26(2):251-261.e8.

213. Atchison L, Abutaleb NO, Snyder-Mounts E, Gete Y, Ladha A, Ribar T, et al. iPSC-Derived Endothelial Cells Affect Vascular Function in a Tissue-Engineered Blood Vessel Model of Hutchinson-Gilford Progeria Syndrome. Stem Cell Reports. 2020;14(2):325–37.

214. Liu G, David BT, Trawczynski M, Fessler RG. Advances in Pluripotent Stem Cells: History, Mechanisms, Technologies, and Applications. Stem Cell Rev Reports. 2020;16(1):3–32.

215. Song HG, Rumma RT, Ozaki CK, Edelman ER, Chen CS. Vascular Tissue Engineering : Progress , Challenges , and Clinical Promise. Cell Stem Cell. 2018;22(3):340–54.

216. L'Heureux N, Pâquet S, Labbé R, Germain L, Auger FA. A completely biological tissue-engineered human blood vessel. FASEB J. 1998;12(1):47–56.

217. Gauvin R, Ahsan T, Larouche D, Lévesque P, Dubé J, Auger FA, et al. A novel single-step self-assembly approach for the fabrication of tissue-engineered vascular constructs. Tissue Eng - Part A. 2010;16(5):1737–47.

218. Jung Y, Ji H, Chen Z, Fai Chan H, Atchison L, Klitzman B, et al. Scaffold-free, Human Mesenchymal Stem Cell-Based Tissue Engineered Blood Vessels. Sci Rep. 2015;5(15116):1–9.

219. McAllister TN, Maruszewski M, Garrido SA, Wystrychowski W, Dusserre N, Marini A, et al. Effectiveness of haemodialysis access with an autologous tissue-engineered vascular graft: a multicentre cohort study. Lancet. 2009;373(9673):1440–6.

220. Shimizu T, Yamato M, Isoi Y, Akutsu T, Setomaru T, Abe K, et al. Fabrication of pulsatile cardiac tissue grafts using a novel 3-dimensional cell sheet manipulation technique and temperature-responsive cell culture surfaces. Circ Res. 2002;90(3):E40–8.

221. Wystrychowski W, Cierpka L, Zagalski K, Garrido S, Dusserre N, Radochonski S, et al. Case study: First implantation of a frozen, devitalized tissueengineered vascular graft for urgent hemodialysis access. J Vasc Access. 2011;12(1):67–70.

222. Yuan B, Jin Y, Sun Y, Wang D, Sun J, Wang Z, et al. A Strategy for Depositing Different Types of Cells in Three Dimensions to Mimic Tubular Structures in Tissues. Adv Mater. 2012;24(7):890–6.

223. Amensag S, McFetridge PS. Rolling the human amnion to engineer laminated vascular tissues. Tissue Eng - Part C Methods. 2012;18(11):903–12.

224. Chen M, Li L, Xia L, Zhang F, Jiang S, Hu H, et al. Temperature Responsive Shape-Memory Scaffolds with Circumferentially Aligned Nanofibers for Guiding Smooth Muscle Cell Behavior. Macromol Biosci. 2020;20(2):1–11.

225. Syedain Z, Reimer J, Lahti M, Berry J, Johnson S, Tranquillo RT. Tissue engineering of acellular vascular grafts capable of somatic growth in young lambs. Nat Commun. 2016 Sep 27;7.

226. Fernandez CE, Yen RW, Perez SM, Bedell HW, Povsic TJ, Reichert WM, et al. Human vascular microphysiological system for in vitro drug screening. Sci Rep. 2016;6(21579):1–14.

227. Wang R, Ozsvar J, Aghaei-Ghareh-Bolagh B, Hiob MA, Mithieux SM, Weiss AS. Freestanding hierarchical vascular structures engineered from ice. Biomaterials. 2019;192:334–45.

228. Itai S, Tajima H, Onoe H. Double-layer perfusable collagen microtube device for heterogeneous cell culture. Biofabrication. 2019;11(1).

229. Hasan A, Memic A, Annabi N, Hossain M, Paul A, Dokmeci MR, et al. Electrospun Scaffolds for Tissue Engineering of Vascular Grafts. Acta Biomater. 2014;10(1).

230. Pham QP, Sharma U, Mikos AG. Electrospun poly (ε-caprolactone) microfiber and multilayer nanofiber/microfiber scaffolds: Characterization of scaffolds and measurement of cellular infiltration. Biomacromolecules. 2006;7(10):2796–805.

231. Vaz CM, van Tuijl S, Bouten CVC, Baaijens FPT. Design of scaffolds for blood vessel tissue engineering using a multi-layering electrospinning technique. Acta Biomater. 2005;1(5):575–82.

232. Lee SJ, Liu J, Oh SH, Soker S, Atala A, Yoo JJ. Development of a composite vascular scaffolding system that withstands physiological vascular conditions. Biomaterials. 2008;29(19):2891–8.

233. Niu G, Criswell T, Sapoznik E, Lee S, Soker S. The influence of cross-linking methods on the mechanical and biocompatible properties of vascular scaffold. J Sci Appl Biomed. 2013;1(1):1–7.

234. Stitzel J, Liu J, Lee SJ, Komura M, Berry J, Soker S, et al. Controlled fabrication of a biological vascular substitute. Biomaterials. 2006;27(7):1088–94.

235. Lee SJ, Yoo JJ, Lim GJ, Atala A, Stitze J. In vitro evaluation of electrospun nanofiber scaffolds for vascular graft application. J Biomed Mater Res Part A. 2007;83A(4):999–1008.

236. Lee J, Yoo JJ, Atala A, Lee SJ. The effect of controlled release of PDGF-BB from heparin-conjugated electrospun PCL/gelatin scaffolds on cellular bioactivity and infiltration. Biomaterials. 2012;33(28):6709–20.

237. Detta N, Errico C, Dinucci D, Puppi D, Clarke DA, Reilly GC, et al. Novel electrospun polyurethane/gelatin composite meshes for vascular grafts. J Mater Sci Mater Med. 2010;21(5):1761–9.

238. Yu E, Mi H-Y, Zhang J, Thomson JA, Lih-Sheng T. Development of Biomimetic Thermoplastic Polyurethane/Fibroin Small-Diameter Vascular Grafts via a Novel Electrospinning Approach. J Biomed Mater Res part A. 2018;106(4):985–96.

239. Soliman S, Sant S, Nichol JW, Khabiry M, Traversa E, Khademhosseini A. Controlling the porosity of fibrous scaffolds by modulating the fiber diameter and packing density. J Biomed Mater Res - Part A. 2011;96 A(3):566–74.

240. McClure MJ, Sell SA, Simpson DG, Walpoth BH, Bowlin GL. A three-layered electrospun matrix to mimic native arterial architecture using polycaprolactone, elastin, and collagen: A preliminary study. Acta Biomater. 2010;6(7):2422–33.

241. Liu K, Wang N, Wang W, Shi L, Li H, Guo F, et al. A bio-inspired high strength three-layer nanofiber vascular graft with structure guided cell growth. J Mater Chem B. 2017;5(20):3758–64.

242. Valot L, Martinez J, Mehdi A, Subra G. Chemical insights into bioinks for 3D printing. Chem Soc Rev. 2019;48(15):4049–86.

243. Murphy S V., Atala A. 3D bioprinting of tissues and organs. Nat Biotechnol. 2014;32(8):773–85.

244. Hospodiuk M, Moncal KK, Dey M, Ozbolat IT. Extrusion-based biofabrication in tissue engineering and regenerative medicine. In: 3D Printing and Biofabrication. 2016. p.

255–81.

245. Tan YSE, Yeong WY. Concentric bioprinting of alginate-based tubular constructs using multi-nozzle extrusion-based technique. Int J bioprinting. 2015;1(1):49–56.

246. Freeman S, Ramos R, Alexis P, Zhou L, Reeser K, Jin S, et al. A bioink blend for rotary 3D bioprinting tissue engineered small-diameter vascular constructs. Acta Biomater. 2019;95:152–64.

247. Jang EH, Kim J-H, Lee JH, Kim D-H, Youn Y-N. Enhanced biocompatibility of multi-layered, 3D bio-printed artificial vessels composed of autologous mesenchymal stem cells. Polymers (Basel). 2020;12(3).

248. Hinton TJ, Jallerat Q, Palchesko RN, Park JH, Grodzicki MS, Shue HJ, et al. Three-dimensional printing of complex biological structures by freeform reversible embedding of suspended hydrogels. Sci Adv. 2015;1(9).

249. Miller JS, Stevens KR, Yang MT, Baker BM, Nguyen DHT, Cohen DM, et al. Rapid casting of patterned vascular networks for perfusable engineered three-dimensional tissues. Nat Mater. 2012;11(9):768–74.

250. Kolesky DB, Homan KA, Skylar-Scott MA, Lewis JA. Three-dimensional bioprinting of thick vascularized tissues. Proc Natl Acad Sci U S A. 2016;113(12):3179–84.

251. Bertassoni LE, Cecconi M, Manoharan V, Nikkhah M, Hjortnaes J, Cristino AL, et al. Hydrogel bioprinted microchannel networks for vascularization of tissue engineering constructs. Lab Chip. 2014;14(13):2202–11.

252. Gao Q, He Y, Fu J, Liu A, Ma L. Coaxial nozzle-assisted 3D bioprinting with built-in microchannels for nutrients delivery. Biomaterials. 2015;61:203–15.

253. Jia W, Gungor-Ozkerim PS, Zhang YS, Yue K, Zhu K, Liu W, et al. Direct 3D bioprinting of perfusable vascular constructs using a blend bioink. Biomaterials. 2016;106:58–68.

254. Gao G, Lee JH, Jang J, Lee DH, Kong JS, Kim BS, et al. Tissue Engineered Bio-Blood-Vessels Constructed Using a Tissue-Specific Bioink and 3D Coaxial Cell Printing Technique: A Novel Therapy for Ischemic Disease. Adv Funct Mater. 2017;27(33):1–12.

255. Dzobo K, Thomford NE, Senthebane DA, Shipanga H, Rowe A, Dandara C, et al. Advances in Regenerative Medicine and Tissue Engineering : Innovation and Transformation of Medicine. Stem Cells Int. 2018;2018(2495848).

256. Pataky K, Braschler T, Negro A, Renaud P, Lutolf MP, Brugger J. Microdrop printing of hydrogel bioinks into 3D tissue-like geometries. Adv Mater. 2012;24(3):391–6.

257. Nakamura M, Nishiyama Y, Henmi C, Iwanaga S, Nakagawa H, Yamaguchi K, et al. Ink jet three-dimensional digital fabrication for biological tissue manufacturing: Analysis of alginate microgel beads produced by ink jet droplets for three dimensional tissue fabrication. J Imaging Sci Technol. 2008;52(6):0602011–6.

258. Blaeser A, Duarte Campos DF, Weber M, Neuss S, Theek B, Fischer H, et al. Biofabrication Under Fluorocarbon: A Novel Freeform Fabrication Technique to Generate High Aspect Ratio Tissue-Engineered Constructs. Biores Open Access. 2013;2(5):374–84.

259. Duarte Campos DF, Blaeser A, Weber M, Jäkel J, Neuss S, Jahnen-Dechent W, et al. Three-dimensional printing of stem cell-laden hydrogels submerged in a hydrophobic high-density fluid. Biofabrication. 2013;5(1).

260. Xu C, Zhang Z, Christensen K, Huang Y, Fu J, Markwald RR. Freeform Vertical and Horizontal Fabrication of Alginate-Based Vascular-Like Tubular Constructs Using Inkjetting. J Manuf Sci Eng Trans ASME. 2014;136(6):1–9.

261. Xu C, Christensen K, Zhang Z, Huang Y, Fu J, Markwald RR. Predictive compensation-enabled horizontal inkjet printing of alginate tubular constructs. Manuf Lett. 2013;1(1):28–32.

262. Schöneberg J, De Lorenzi F, Theek B, Blaeser A, Rommel D, Kuehne AJC, et al. Engineering biofunctional in vitro vessel models using a multilayer bioprinting technique. Sci Rep. 2018;8(1):1–13.

263. Cui X, Boland T. Human microvasculature fabrication using thermal inkjet printing technology. Biomaterials. 2009;30(31):6221–7.

264. Xu T, Zhao W, Zhu JM, Albanna MZ, Yoo JJ, Atala A. Complex heterogeneous tissue constructs containing multiple cell types prepared by inkjet printing technology. Biomaterials. 2013;34(1):130–9.

265. Bishop ES, Mostafa S, Pakvasa M, Luu HH, Lee MJ, Wolf JM, et al. 3-D bioprinting technologies in tissue engineering and regenerative medicine: Current and future trends. Genes Dis. 2017;4(4):185–95.

266. Xiong R, Zhang Z, Chai W, Huang Y, Chrisey DB. Freeform drop-on-demand laser printing of 3D alginate and cellular constructs. Biofabrication. 2015;7(4):45011.

267. Wu PK, Ringeisen BR. Development of human umbilical vein endothelial cell (HUVEC) and human umbilical vein smooth muscle cell (HUVSMC) branch/stem structures on hydrogel layers via biological laser printing (BioLP). Biofabrication. 2010;2(1).

268. Kérourédan O, Bourget JM, Rémy M, Crauste-Manciet S, Kalisky J, Catros S, et al. Micropatterning of endothelial cells to create a capillary-like network with defined architecture by laser-assisted bioprinting. J Mater Sci Mater Med. 2019;30(2).

269. Kérourédan O, Hakobyan D, Rémy M, Ziane S, Dusserre N, Fricain JC, et al. In situ prevascularization designed by laser-assisted bioprinting: Effect on bone regeneration. Biofabrication. 2019;11(4).

270. Gaebel R, Ma N, Liu J, Guan J, Koch L, Klopsch C, et al. Patterning human stem cells and endothelial cells with laser printing for cardiac regeneration. Biomaterials. 2011;32(35):9218–30.

CHAPTER 2

Objectives

CHAPTER 2. Objectives

The main aim of this thesis is the development of vascularization through the stimulation of angiogenesis to improve bone regeneration or through tissue engineering blood vessels for blood vessel replacement treatment or scaffold vascularization. Two specific objectives were established:

1. To develop a dual ion delivery system to stimulate early phases of bone regeneration, focusing on angiogenesis (chapter 3 and 4).
2. To develop a tissue engineered blood vessel-like structure (chapter 5, 6 and 7).

These two main objectives can be divided in several sub-objectives:

1. **To develop a dual ion delivery system to stimulate early phases of bone regeneration, focusing on angiogenesis.**
   1.1. To assess therapeutic concentrations of two therapeutic ions (**chapter 3**).
      1.1.1. To determine non-toxic concentrations of two therapeutic ions in endothelial and osteoprogenitor cells.
      1.1.2. To study their potential to induce *in vitro* angiogenesis and osteogenesis with endothelial and osteoprogenitor cells.
      1.1.3. To study their potential to induce *in vitro* angiogenesis and osteogenesis when combined together.
   1.2. To develop a dual delivery system for the release of two ions (**chapter 4**).
      1.2.1. To optimize the parameters to obtain alginate-hydroxyapatite microparticles.
      1.2.2. To optimize the development of alginate fibers that allows the encapsulation of alginate-hydroxyapatite microparticles.
      1.2.3. To optimize the amount of microparticles that can be embedded in alginate monofibers preserving stability.
      1.2.4. To optimize crosslinking ion concentrations to achieve the release of therapeutic doses.
2. **To develop a tissue engineered blood vessel-like structure**.
   2.1. To develop a tissue engineered blood vessel-like (TEBV) structure with extrusion method (**Chapter 5).**
      2.1.1. To optimize biomaterials concentrations and processing parameters to obtain a stable hollowed dual-layered structure using alginate and collagen.

2.1.2. To assess endothelial cells viability and behavior encapsulated in the inner layer of the TEBV construct.

2.1.3. To assess smooth muscle cells viability and behavior encapsulated in the outer layer of the TEBV construct.

2.1.4. To assess co-culture viability and distribution of cells within TEBV construct.

2.2. To assess functionality of alginate/collagen TEBV (**Chapter 6 – Duke University collaboration**)

2.2.1. To set up a perfusion system and flow rate parameters for our TEBVs.

2.2.2. To assess mechanical stability of TEBVs.

2.2.3. To assess functionality of TEBVs.

2.3. To increase the mechanical properties of tissue engineered blood vessel-like structure providing appropriate cell environment for cells (**Chapter 7**).

2.3.1. To develop a suitable bath support that allows the tubular structure maintenance of the extruded collagen.

2.3.2. To optimize collagen concentration and extrusion parameters.

2.3.3. To assess viability of co-cultured endothelial and smooth muscle cells within the TEBV construct.

2.3.4. To evaluate the endothelial and smooth muscle cells distribution within TEBV construct.

CHAPTER 3

Copper and cobalt as potential inducers of angiogenesis and osteogenesis

CHAPTER 3. Copper and cobalt as potential inducers of angiogenesis and osteogenesis

3.1.   Introduction

Bone regeneration is a multi-step process involving different events such as inflammation of damaged zone, blood vessel formation, recruitment of osteoprogenitor cells to the zone of healing and their subsequent osteogenic differentiation for bone formation (1). On time and coordinated blood vessel formation (angiogenesis) is crucial to achieve successful bone regeneration.

As detailed in chapter 1, big fractures cannot be completely regenerated as it exceeds the regenerative capacity of bone. In order to enhance this process and promote complete regeneration, different strategies have been developed in combination with bone scaffolds to guide tissue formation: the use of growth factors and the use of active metal ions. Growth factors are naturally found in the body during regenerative processes and have been extensively used in tissue engineering (2). However, they have delicate handling properties and short half-life. Ions are also present in the human body at low concentrations or as trace elements, presenting high stability. Interestingly, ions have been tested in different *in vitro* and *in vivo* studies demonstrating their capacity to regulate cellular functions, for instance in angiogenesis and osteogenesis processes, inducing therapeutic effects similar to other biologically relevant molecules such as growth factors (3,4). Therefore, in the last years, ions have been considered a promising alternative.

In relation to angiogenic stimulation, copper (Cu^{2+}) and cobalt (Co^{2+}) have been proposed as good candidates, as both ions are described to mimic hypoxic conditions by up-regulating hypoxia inducible factor-1α (HIF-1α). This, in turn, up-regulates angiogenic-related genes such as VEGF, and therefore, triggering blood vessel formation (5,6). Different studies have incorporated these ions within scaffolds in order to deliver them and stimulate a proper angiogenic response (7). Although, in general, results show a successful therapeutic response, they are not conclusive in terms of the optimum concentrations of Cu^{2+} or Co^{2+} that are non-toxic and induce or enhance angiogenic response. This is because of the delivery of these ions from the scaffolds, which generally do not follow a zero order kinetics. Ions present a more burst release instead, delivering different doses through time (8–12). At the same time, depending on scaffold composition, they can deliver other ions, which difficult the elucidation

of the therapeutic effect of individual ions. In this sense, studies which include these ions into the cell culture medium as a salt, and hence, present a constant concentration during cell culture time, provide a more direct data about the effect of the ions into the cells. However, published studies show discrepancies with respect to non-toxic concentrations of Cu^{2+} or Co^{2+} that at the same time, induce and angiogenic response with endothelial cells. For instance, on the one hand, regarding Cu^{2+} cytotoxicity, Guo-fu Hu *et al*., reported non-toxic concentrations and dose-dependent increase of HUVEC proliferation from 1 to 500 μM (13). Conversely, another study reported HUVEC viability and growth up to 100 μM, whereas higher concentrations were described to be cytotoxic (14). Contrary to these results, Stähli C *et al*., showed a decreased viability and metabolic activity in a dose-dependent manner from ≈10 to 190 μM (15). In relation to angiogenic gene response induced by Cu^{2+}, some studies report an increase of HIF-1α and VEGF (5), whereas others do not observe an increase of HIF-1α (16) or VEGF (14) expression. On the other hand, regarding Co^{2+} cytotoxicity, Zan *et al*., described viability and increased proliferation in a dose-dependent manner up to 200 μM (17). Similarly, another study reported 150 μM concentration to be non-toxic with proliferation rate comparable to normoxic conditions (18). However, other authors showed contrary results. More specifically, Peters *et al*., described a concentration-dependent reduction in cell number from 10 to 700 μM, with significant proliferation impairment beyond 100 μM (19). With regards to angiogenic gene response induced by Co^{2+}, some authors describe an increase of both HIF-1α and VEGF expression (17,20), whereas others describe a reduction of HIF-1α expression (19).

In relation to osteogenic differentiation, some studies incorporated Cu^{2+} or Co^{2+} in scaffolds and showed an enhanced osteogenic differentiation (21,22). However, as previously mentioned, the release usually is not constant through time and other ions can be delivered, which makes difficult to isolate the osteogenic effect of each ion. Therefore, studies incorporating these ions into the cell culture media can provide more reliable information about their particular therapeutic effect. However, few studies with controversial results are found in the literature regarding non-toxic concentrations and enhanced osteogenic differentiation with mesenchymal stem cells (MSCs). For instance, when Cu^{2+} was supplemented into the cell culture media, J. Rodríguez *et al*., described viable concentrations for MSCs up to 250 μM, although proliferation was reduced with 5 μM or higher doses (23). However, another study reported concentrations higher of 10 μM to be toxic for MSCs (24). Respect to osteogenic gene expression, while some authors report an early ALP expression (23), others describe a significant down-regulation of Runx-2, ALP, OC, OPN, amongst others

(24). In reference to Co^{2+} supplementation into the cell culture media, there is lack of studies in the literature. However, we found a study reporting a decrease of MSCs proliferation when Co^{2+} concentrations were increased (from 10 to 100 µM) (25). At the same time, authors reported a down-regulation in a dose-dependent manner of Runx-2, ALP and BSP, although they describe an up-regulation of OPN gene. Therefore, it is not clear whether Cu^{2+} or Co^{2+} can enhance the osteogenic differentiation.

All in all, despite there are some studies incorporating Cu^{2+} or Co^{2+} into the cell culture medium, there is some controversy surrounding the appropriate non-toxic and therapeutic concentrations of these ions for angiogenic and osteogenic response.

3.2.   Objectives

The aim of this chapter was to screen a range of non-toxic concentrations of two hypoxic mimicking ions (copper and cobalt) and their potential to induce angiogenesis and/or osteogenesis in endothelial cells and osteoprogenitor cells, respectively. As secondary objective of this chapter, we wanted to assess the effect of the combined ions in angiogenesis.

3.3.   Materials & Methods

3.3.1. Angiogenic response

3.3.1.1.   Cell culture

Human Umbilical Vein Endothelial Cells (HUVEC; Lonza) were used to assess the angiogenic response. For cell expansion, HUVEC were seeded at a density of 2500 cells/cm^2 and maintained with endothelial growth medium-2 bulletkit (EGM-2) (Lonza; Ref. H3CC-3162), containing VEGF, rhFGF-B, rhEGF, r-IGF-I, hydrocortisone, ascorbic acid, gentamicin sulfate, amphotericin-B and 2% FBS. HUVEC cells were passaged using 0,25% Trypsin-EDTA (Gibco) when they reached 70-85% confluence. Cells were maintained in standard culture conditions (37ºC and 5% CO_2). Passages equal or below P5 were used for subsequently assays. For the culture of cells with cell culture media supplemented with ions, two types of cell culture mediums were tested: i) basal medium (Lonza; Ref. CC-3156), supplemented with 2% FBS and amphotericin-B; ii) and EGM-2 medium, previously described.

3.3.1.2. Culture of HUVEC in the presence of copper, cobalt or both

The influence of different ion concentrations on HUVEC was assessed using the mediums mentioned above supplemented with $CuCl_2$ and/or $CoCl_2$ (both from Sigma-Aldrich). For Cu^{2+} and Co^{2+} supplementation, concentrations of 0, 0.1, 1, 10, 100 and 200 µM and 0, 0.5, 5, 25, 50 and 100 µM were assessed, respectively, for viability and proliferation assays. For further morphology, gene expression and tubule formation Matrigel® assays, non-toxic concentrations were used, which were concentrations with cell viability over 80%. HUVEC were seeded in a density of 5000 cels/cm^2 for all the assays, except for the Matrigel® assay, in which 70.000 cels/cm^2 were used. After 24h of seeding, cultivation with ion supplemented medium started for a total of 7 days, with change of media every two days. The same assays were performed to assess the effect of both ions combined together. In this case, the highest concentration which showed a therapeutic effect for each ion and half of the highest concentrations were used.

3.3.1.3. Cell cytotoxicity and proliferation assay

Viability and number of cells was assessed using a commercially colorimetric available kit, specifically the Cell Counting Kit-8 (CCK-8) (Sigma-Aldrich). This kit contains a water-soluble tetrazolium salt WST-8 which is reduced by dehydrogenases of cells, resulting in a yellow-colored product (formazan). The amount of formazan generated is considered directly proportional to the number of viable cells, and has an absorbance spectrum peak at 450-460 nm. CCK-8 was performed according to manufacturer's instructions. Briefly, at time points of 2 and 7 days after medium supplementation with ions, CCK-8 solution was added in each well and incubated with cells for 3 hours. After this period, supernatant was placed in a 96 well plate (Greiner bio-one) and the absorbance was read at 450 nm using a multi-detection microplate reader (Synergy HT, BioTek). For viability, results were normalized with the control medium, which did not contained supplemented ion. Viability percentages over 80% were considered non-toxic. For proliferation, a known number of cells (2000, 4000, 8000, 10 000, 20 000 and 30 000) were plated to obtain a standard curve to extrapolate the respective number of cells in day 2 and 7.

3.3.1.4. Cell morphology with phalloidin

Cell morphology and organization was performed by immunofluorescence of actin filament staining with phalloidin (Acti-stain 488 fluorescent phalloidin, Cytoskeleton, Inc). For this purpose, 24 well plate coverslips were autoclaved and placed in each well. Then, 20 µL of 1% sterilized gelatin (Sigma-Aldrich) was added on the surface of each coverslip and incubated at

room temperature for 30 min. Afterwards, the excess of gelatin was aspirated and 24 well plates were placed in the incubator at 37ºC for 30 minutes. After this incubation period, cell culture media was added and HUVEC were seeded in each well. At the time points of 0 (just before adding supplemented media), 2 and 7 days after medium supplementation, cells were rinsed with PBS 1X and subsequently fixed with 4% PFA during 20 min at room temperature. Then, cells were rinsed three times with PBS 1X and permeabilized with 0,5% Triton-100x/PBS for 10 min. After three washes with PBS 1X, samples were incubated with 100 nM Acti-stain phalloidin (Cytoskeleton, Inc) for 30 min protected from light. Then, after PBS 1X rinsing, cells were incubated with DAPI (NucBlue Fixed Cell stain DAPI, LifeTechnologies) for 5 min. Finally, cells were rinsed one last time with PBS 1X and then, cover slips were detached from 24 well plate and mounted on a microscope slide with Fluoromount-G (BioNova). Samples were kept in the dark at 4ºC and they were visualized by confocal laser microscopy (Leica SP8, LAS X software version 3.5.5.19976). Excitation/emission wavelengths were 480/520 nm for phalloidin and 405/460 for DAPI. Images were processed with the same confocal software (LAS X Life Science software, Leica).

3.3.1.5. Gene expression RT-qPCR

Gene expression was analyzed by quantitative real time polymerase chain reaction (qPCR). At time points of 2 and 7 days after medium supplementation, cell pellets were collected using 0,25% Trypsin-EDTA (Gibco) and spin centrifugation of 1500 rpm for 5 min. Short time points of 1, 2, 4, 10 and 24h were also assessed. Then, total RNA was isolated from cells using NucleoSpin RNA Kit (Macherey-Nagel) including DNAse treatment step following manufacturer's instructions. Quantification of isolated RNA was performed using a microvolume plate (Take 3) to measure absorbance ratio of wavelengths 260/280 nm in a microplate reader (Synergy HT Multi-detection Microplate Reader, BioTek). A ratio of ~2 was considered pure RNA. Reverse-transcription (RT) of RNA to cDNA was performed using Transcriptor First Strand cDNA Synthesis Kit (Roche) following manufacturer's instructions using T100 Thermal Cycler (Bio-Rad). For the amplification and quantification of cDNA targets, QuantiNova SYBR Green PCR kit (Qiagen) was used following manufacturer's instructions. Briefly, 20 ng of cDNA per reaction were amplified under the following conditions: an initial heat activation step of 2 min at 95ºC followed by 40 cycles of denaturation for 5s at 95ºC and annealing/extension for 10s at 60ºC, using a CFX96 Real-Time PCR Detection System (Bio-Rad). The primers sequences used for vascular endothelial growth factor (VEGF), hypoxia-inducible factor 1-alpha (HIF-1α), platelet endothelial cell adhesion molecule-1 (PECAM-1) and the endogen gen beta-actin (β-Actin) are listed in **Table 1**. To normalize data, β-Actin was used as

internal reference for each reaction. Relative expression was calculated using the $2^{-\Delta\Delta Ct}$ method and all data were expressed as fold-changes compared to control of day 0.

Table 1. List of primers sequences used for cDNA amplification in RT-qPCR.

	Gene	Primer	Sequence (5'-3')
Endogen	β-Actin	Forward	AGAGCTACGAGCTGCCTGAC
		Reverse	AGCACTGTGTTGGCGTACAG
Angiogenic	VEGF	Forward	CCCACTGAGGAGTCCAACAT
		Reverse	AAATGCTTTCTCCGCTCTGA
	HIF-1α	Forward	TGCTCATCAGTTGCCACTTC
		Reverse	TCCTCACACGCAAATAGCTG
	PECAM-1	Forward	TCAAATGATCCTGCGGTATTC
		Reverse	CCACCACCTTACTTGACAGGA

3.3.1.6. Matrigel assay for tubular formation

In vitro tubular formation analysis was performed using Matrigel® Growth Factor Reduced (GFR) (Corning® Matrigel®, Ref. 734-0268) with HUVEC cells in 96 well plates. First, 75 µL of Matrigel were transferred in each well and incubated for 10 min at room temperature. After this period, plates were incubated in a humidified incubator at 37ºC for 30 min. Then, 75 µL of cell culture media was added in each well. Supplemented media contained doubled the final desired ion concentration. Plates were incubated 30 min at 37ºC. Then, 70.000 cells/cm^2 were added in each well with a volume of 75 µL. At the time points of 4 and 8h, cells were rinsed once with PBS 1X and fixed with 4% PFA for 30 min. Afterwards, cells were rinsed three times and stored at 4ºC with PBS 1X. There were three triplicates per condition and three fields per well were photographed using an inverted microscope coupled with a camera (Nikon Eclipse TS2-S-SM) and its software (IC Measure software). The phase contrast images were analyzed using the freely Angiogenesis Analyzer plugin of Image J. Number of nodes, number of meshes and number and total tubule length were analyzed.

3.3.2. Osteogenic response

3.3.2.1. Cell culture

Human Bone Marrow-derived Mesenchymal Stem Cells (hBM-MSC; ATCC) were used to assess the osteogenic response. For cell expansion, hBM-MSC were seeded at a density of 5000 cells/cm^2 and maintained with basal mesenchymal stem cell medium (ATCC; Ref. PCS-500-030)

supplemented with mesenchymal stem cell growth kit (ATCC; Ref. PCS-500-041), which contained 2.4 mM rhIGF-1, 5 ng/mL rhFGF-b, 2.4 mM L-Alanyl-L-Glutamine, 7% of FBS and 1% penicillin-streptomycin. When confluence reached approximately 80%, hBM-MSC were passaged using 0,25% Trypsin-EDTA (Gibco). Cells were maintained in standard culture conditions (37ºC and 5% CO_2). hBM-MSC equal or below P5 were used for later assays. For the culture of cells with cell culture media supplemented with ions, , osteogenic differentiation media was used, which consisted of basal mesenchymal stem cell medium (ATCC; Ref. PCS-500-030) supplemented with 10 mM β-Glycerolphosphate, 50 μg/mL ascorbic acid, 100 nM dexamethasone, 10% FBS and 1% penicillin-streptomycin.

3.3.2.2. Culture of hBM-MSC in the presence of copper or cobalt

The same procedure explained in section *3.3.1.2* was followed.

3.3.2.3. Cell cytotoxicity and proliferation assay

The same procedure explained in section *3.3.1.3* was followed.

3.3.2.4. Cell morphology with phalloidin

The same procedure explained in section *3.3.1.4* was followed.

3.3.2.5. Gene expression RT-qPCR

The same procedure explained in section *3.3.1.*5 was followed. The primers sequences used for run-related transcription factor-2 (Runx-2), alkaline phosphatase (ALP), osteocalcin (OC) and the endogen gen beta-actin (β-Actin) are listed in **Table 2**.

Table 2. List of primers sequences used for cDNA amplification in RT-qPCR.

	Gene	Primer	Sequence (5'-3')
Endogen	β-Actin	Forward	AGAGCTACGAGCTGCCTGAC
		Reverse	AGCACTGTGTTGGCGTACAG
Osteogenic	RUNX-2	Forward	CCCGTGGCCTTCAAGGT
		Reverse	CGTTACCCGCCATGACAGTA
	ALP	Forward	GGAACTCCTGACCCTTGACC
		Reverse	TCCTGTTCAGCTCGTACTGC
	OC	Forward	CGCCTGGGTCTCTTCACTAC
		Reverse	CTCACACTCCTCGCCCTATT

3.3.3. Statistical analysis

Statistical analysis was performed using SPSS software (SPSS v21, IBM). Kruskal-Wallis and Mann Whitney U non-parametric tests were used to compare viability, proliferation, gene expression and tubule formation (number of nodes, meshes and total tubule length) between experimental groups of the same time point and between time points for each experimental condition (data represented as mean ± standard deviation; n=4 for viability and proliferation and n=3 for gene expression and Matrigel assay for each condition). Spearman non-parametric test was used to study the correlation between HIF-1α and VEGF gene expression. Control samples were cells without any supplementation ion in cell culture media.

3.4. Results

3.4.1. Role of copper and cobalt in angiogenesis

3.4.1.1. Viability and proliferation

In order to elucidate the ion concentrations which are not cytotoxic, HUVEC cells were cultivated under different copper (Cu^{2+}) and cobalt (Co^{2+}) concentrations. Additionally, their viability effect was tested with both basal and growth media, to find out which one was more appropriate to use for further assays. Generally, we could observe an increase of detached cells and cell debris, and a decrease number of cells when HUVEC were cultivated with basal medium (BM) compared to growth medium (GM). Moreover, when Cu^{2+} or Co^{2+} were added in both cell culture mediums, a reduction of cells was observed in a dose-dependent manner during culture time, which was more evident when HUVEC were cultured with BM.

Results of viability and proliferation assays were in accordance with the observations of cell culture. More specifically, when HUVEC cells were cultured with BM supplemented with Cu^{2+}, there was an increase of viability and cell number with lower concentrations (up to 1 µM) at day 2 (**Figure 1A** and **1B**). However, longer culture time revealed a significant decrease in viability and cell number for all concentrations tested in a dose-dependent manner, with the exception of 0.1 µM which had a significant increase in cell number. Alternatively, when HUVEC were cultured with GM supplemented with Cu^{2+}, they presented a proper viability with Cu^{2+} concentrations up to 10 µM (**Figure 1C**). Moreover, cell number was also significantly increased during culture time with all concentrations tested (**Figure 1D**). Nevertheless, Cu^{2+} concentrations ≥10 µM presented significantly lower cell number compared to control at day 7. It is worth to mention that viable concentrations of Cu^{2+} allowed to practically double cell

number from day 2 to day 7 with GM, whereas a slightly increase in cell number was observed with BM, presenting considerable lower cell number compared to GM. For this reason, we considered to use GM for the subsequent assays.
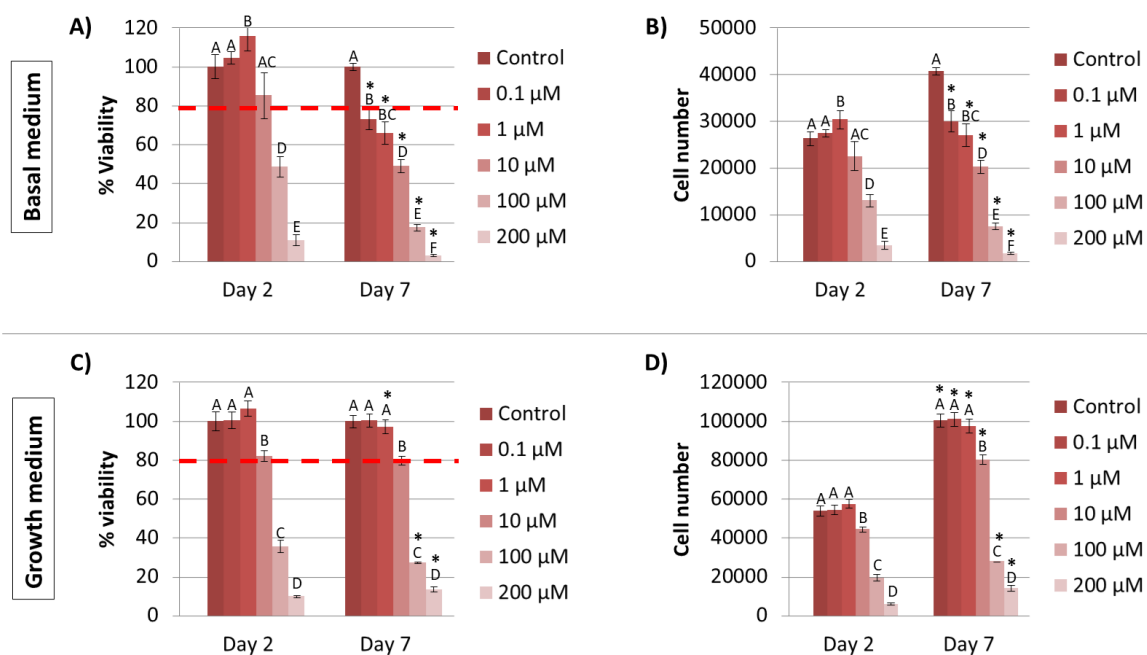
Figure 1. HUVEC viability and proliferation with Cu^{2+} cell culture media supplementation. A) HUVEC viability and B) cell number cultured with Cu^{2+} supplementation with basal medium (BM); C) HUVEC viability and D) cell number cultured with Cu^{2+} supplementation with growth medium (GM). Statistics is represented with letters when comparisons were made between the different experimental groups within the same time point. Same letters represent no significant differences (p>0.05), whereas different letters represent statistical differences (p<0.05). Differences between time points for each experimental condition is represented with * (p<0.05).

Regarding HUVEC culture with BM supplemented with Co^{2+}, at day 2, concentrations up to 25 µM demonstrated not being toxic for cells (**Figure 2A**) and same cell number was obtained with concentrations up to 5 µM (**Figure 2B**). However, during culture time, viability was reduced for all concentrations tested at day 7 compared to day 2, being significantly lower compared to control of the same time point. Interestingly, HUVEC cells demonstrated their capacity to proliferate with concentrations up to 5 µM at day 7 compared to day 2, whereas higher concentrations showed lower cell number (**Figure 2B**). However, all concentrations tested had lower cell number compared to their time point control. Alternatively, when HUVEC cells were cultured with GM supplemented with Co^{2+}, concentrations up to 50 µM demonstrated not being toxic for HUVEC at the end of culture (**Figure 2C**). Intriguingly, cell number significantly increased for all conditions from day 2 to day 7, although all concentrations were significantly lower compared to time point control (**Figure 2D**). Similar to previously mentioned with Cu^{2+}, HUVEC cell number was reduced to half with control

conditions with BM compared to GM, and it was even lower when Co^{2+} was added and increased. For this reason, we also decided to use GM for the subsequent assays.
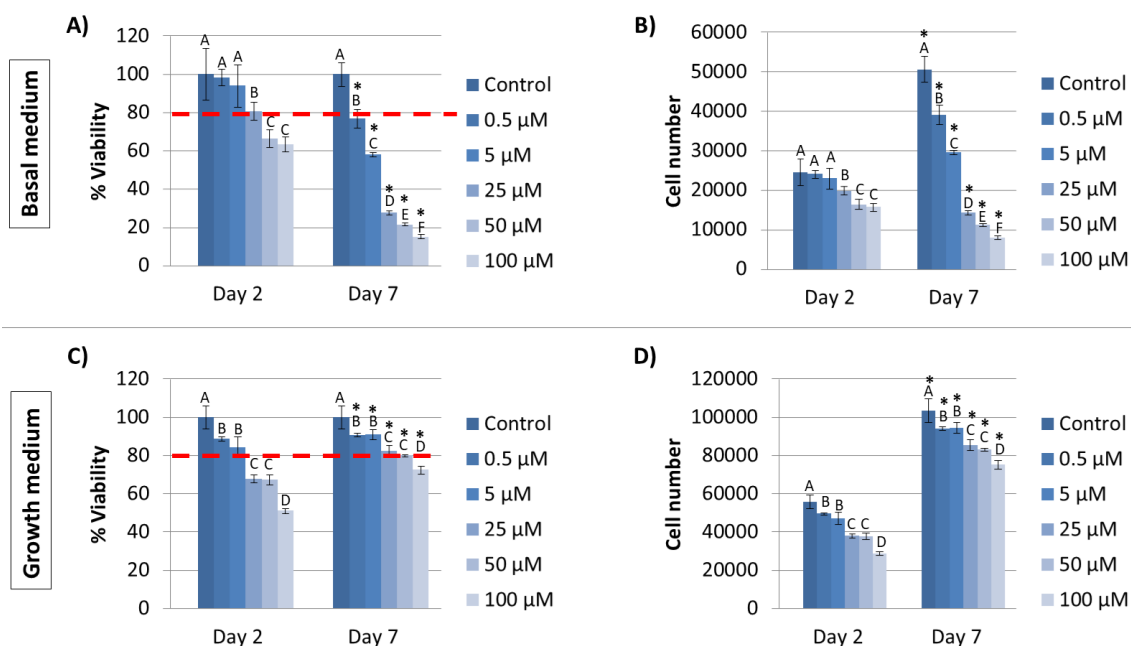

Figure 2. HUVEC viability and proliferation with Co^{2+} cell culture media supplementation. A) HUVEC viability and B) cell number cultured with Co^{2+} supplementation with basal medium (BM); C) HUVEC viability and D) cell number cultured with Co^{2+} supplementation with growth medium (GM).
Statistics is represented with letters when comparisons were made between the different experimental groups within the same time point. Same letters represent no significant differences ($p>0.05$), whereas different letters represent statistical differences ($p<0.05$). Differences between time points for each experimental condition is represented with * ($p<0.05$).

Based on viability results, for the subsequent assays ion concentrations of 0.1, 1 and 10 µM for Cu^{2+} and 0.5, 5, 25 and 50 µM for Co^{2+} were used, as demonstrated to be non-toxic for HUVEC.

3.4.1.2. HUVEC morphology

The influence of both ions on cell morphology and arrangement were evaluated with actin filament staining. Regarding Cu^{2+} supplementation, at early time points from 0 to 2 days some cells acquired an elongated phonotype, with no apparent differences between experimental groups and control (**Figure 3**). In addition, there was a substantial increase of cell proliferation, almost reaching cell confluence in all conditions, although it seemed to be less cells with 10 µM condition. At day 7, cells reached confluence and started to grow and proliferate over the monolayer. With the concentration of 10 µM, there were less number of cells. These observations are in accordance with cell number results (**Figure 1D)**.
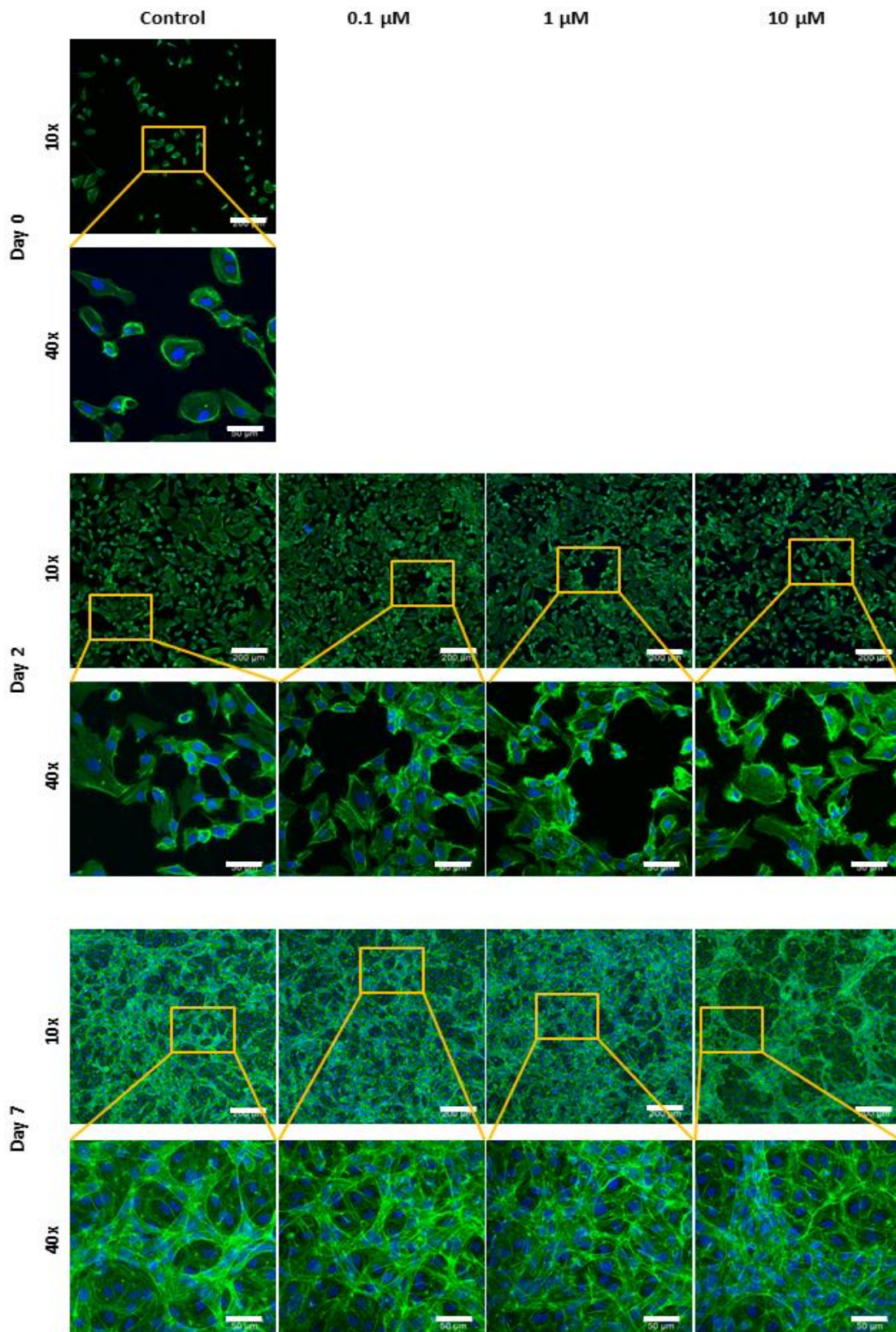
Figure 3. Morphology of HUVEC cultured with different concentrations of Cu^{2+}. Scale bar = 200 µm and for magnification 50 µm.

With regards to Co^{2+} addition, some HUVEC cells also presented an elongated morphology and increased their number at day 2 compared to day 0 (**Figure 4**). With concentrations of 25 and 50 µM it seemed to be less cells compared to control, reaching almost confluence. At day 7, HUVEC reached confluence and some cells proliferated over the monolayer. With 50 µM Co^{2+} concentration there was less cell number compared to control. These observations are in accordance with cell number (**Figure 2D**).
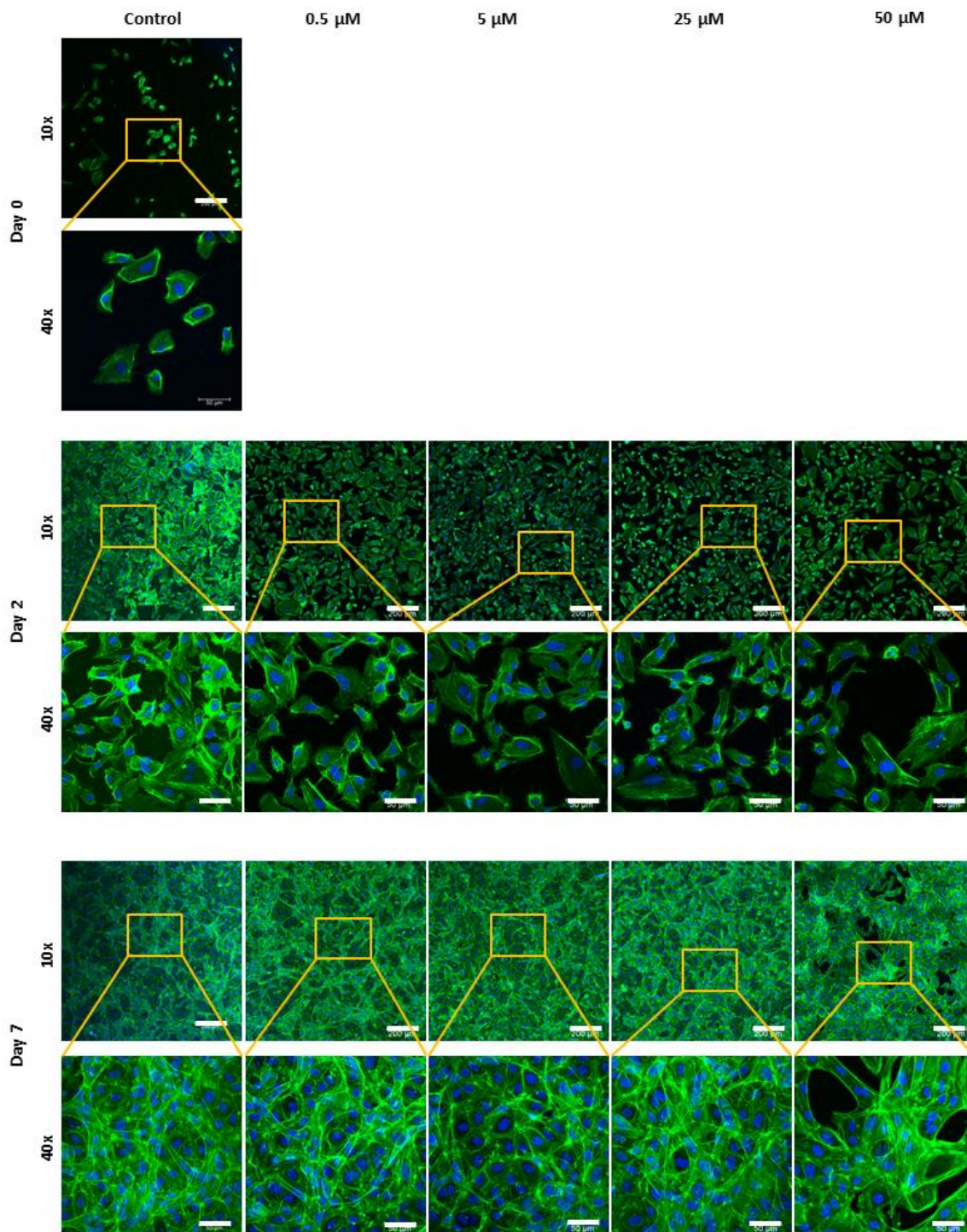
Figure 4. Morphology of HUVEC cultured with different concentrations of Co^{2+}. Scale bar = 200 µm and for magnification 50 µm.

3.4.1.3. Ion influence on angiogenesis gene expression

To further assess the potential of Cu^{2+} and Co^{2+} in stimulating angiogenic response in HUVEC, we analyzed the expression of three principal genes involved in the angiogenic response: HIF-

1α, VEGF and PECAM-1. For this purpose, it was first analyzed the expression profile in a short period of hours (1, 2, 4, 10 and 24h), and subsequently, in longer periods (2 and 7 days).

In general, within the initial hours, HUVEC cultured with Cu^{2+} showed a progressive increase of HIF-1α expression in all experimental conditions (**Figure 5A**). Interestingly, 10 μM concentration showed a constant increased up to 24h compared to other conditions, with significant higher expression at 10h compared to control. Regarding VEGF expression profile, there was an increase of VEGF expression up to 2h and a progressively decrease up to 24h for all conditions tested (**Figure 5B**). More in detail, 1 and 10 μM presented similar VEGF expression compared to control up to 10h, whereas 0.1 μM had a lower expression profile. It is worth to mention that all Cu^{2+} concentrations induced a significantly higher VEGF expression within 1h compared to control. Finally, different profiles were observed with PECAM-1 expression (**Figure 5C**). More in detail, all conditions showed an increase of PECAM-1 up to 4h, and a slight reduction up to 10h. However, 1 and 10 μM showed a second increase up to 24h, whereas control and 0.1 μM did not present this trend. A summary of statistical analysis results of gene expression comparison between experimental groups for each time point is shown in **Table 3**.
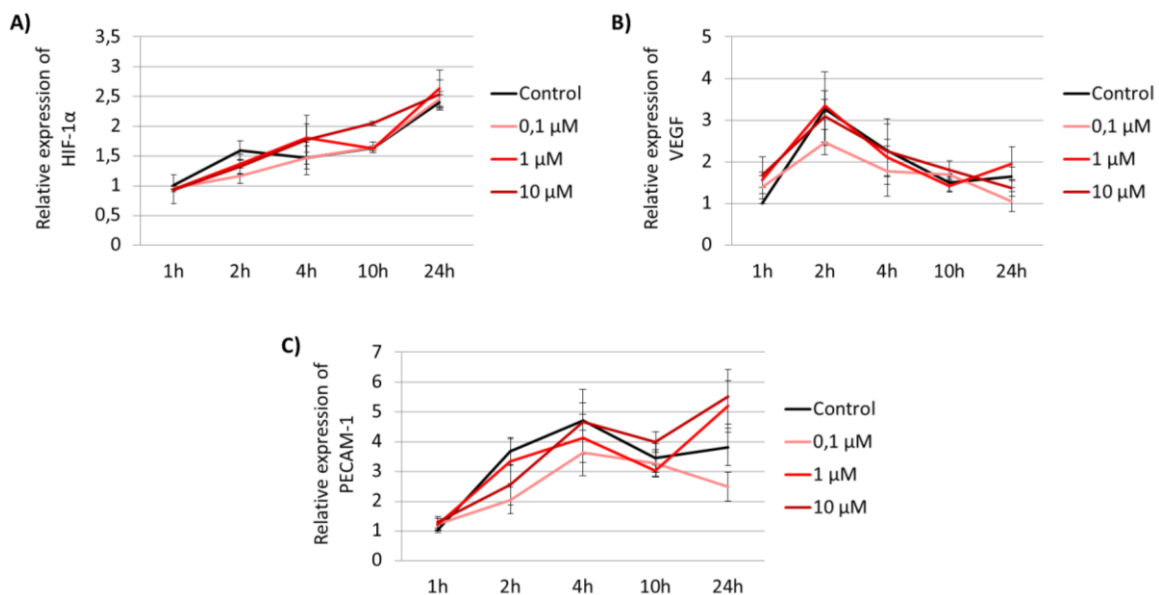
Figure 5. HUVEC gene expression profile within short time points. Different Cu^{2+} concentrations were evaluated at 1, 2, 4, 10 and 24h for the gene expression of A) HIF-1α, B) VEGF and C) PECAM-1. Data represented correspond to fold-changes compared to 1h control.

Table 3. Statistics summary of HUVEC gene expression profile cultured with Cu^{2+} within short time. Comparisons between experimental groups of each time point. Symbols represent *= significant differences ($p<0.05$); ns = non-significant differences ($p>0.05$).

		HIF-1α			VEGF			PECAM-1		
		0,1 µM	1 µM	10 µM	0,1 µM	1 µM	10 µM	0,1 µM	1 µM	10 µM
1h	Control	*	ns	*	*	*	*	*	ns	*
	0,1 µM		ns	ns		ns	ns		ns	ns
	1 µM			ns			ns			ns
	10 µM									
2h	Control	*	ns	*	ns	ns	ns	*	ns	*
	0,1 µM		ns	ns		*	ns		*	ns
	1 µM			ns			ns			ns
	10 µM									
4h	Control	ns	ns	ns	ns	ns	ns	ns	ns	ns
	0,1 µM		ns	ns		ns	ns		ns	ns
	1 µM			ns			ns			ns
	10 µM									
10h	Control	ns	ns	*	ns	ns	ns	ns	ns	ns
	0,1 µM		ns	*		*	ns		ns	ns
	1 µM			*			*			*
	10 µM									
24h	Control	ns	ns	ns	*	ns	ns	*	ns	*
	0,1 µM		ns	ns		*	*		*	*
	1 µM			ns			ns			ns
	10 µM									

In later time points, at day 2, HUVEC HIF-1α expression analysis revealed similar expression with no significant differences between all experimental conditions (**Figure 6A**). Later on, at day 7, HIF-1α expression was significantly increased with the lowest concentration of 0.1 µM. Regarding VEGF expression at day 2, all Cu^{2+} concentrations significantly increased its expression compared to control, in a dose-dependent manner (**Figure 6B**). Remarkably, 10 µM concentration induced more than two-fold VEGF expression compared to control, and at the same time, it was significantly higher than VEGF expression induced by 0.1 and 1 µM. Interestingly, at day 7 lower concentrations, 0.1 and 1 µM, induced a higher VEGF expression compared to control. It is worth to mention that 0.1 µM induced two-fold VEGF expression compared to control, but at the same time, it induced almost three times more VEGF expression compared to day 2. Finally, the expression of PECAM-1 remained the same for all

experimental conditions at day 2 and was significantly increased in a dose-dependent manner by 0.1 and 1 µM at day 7 (**Figure 6C**).
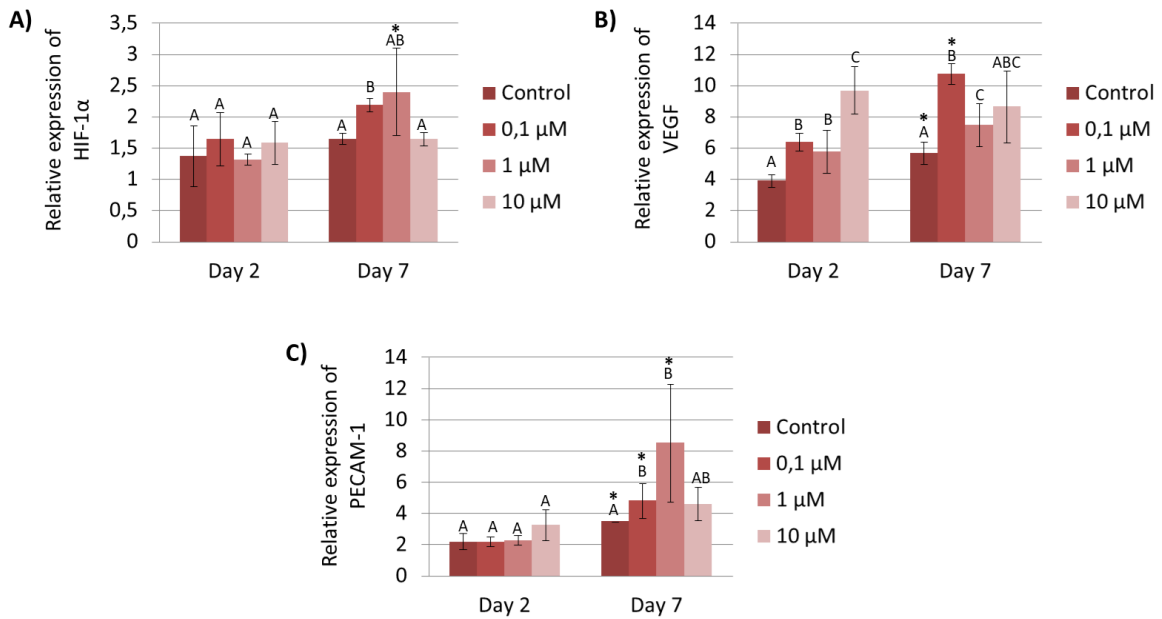
Figure 6. HUVEC gene expression. Different Cu^{2+} concentrations were evaluated at 2 and 7 days for the gene expression of A) HIF-1α, B) VEGF and C) PECAM-1. Data represented correspond to fold-changes compared to Day 0 control.

Statistics is represented with letters when comparisons were made between the different experimental groups within the same time point. Same letters represent no significant differences (p>0.05), whereas different letters represent statistical differences (p<0.05). Differences between time points for each experimental condition is represented with * (p<0.05).

We further assessed if there was a correlation between HIF-1α and VEGF expression (**Table 4**). Although it was found a significant correlation at 2 and 4h, there was no significant and strong correlation between the gene expression of HIF-1α and VEGF.

Table 4. HIF-1α and VEGF expression correlation results with Cu^{2+} supplementation. Symbols: ns=non-significant (p>0.05); *=p<0.05; **=p<0.01.

Time point	R-value	p-value
1h	0.376	ns
2h	0.650	*
4h	0.895	**
10h	0.336	ns
24h	0.357	ns
2 days	0.476	ns
7 days	0.490	ns

When HUVEC were cultured with Co^{2+} supplementation, results of HIF-1α expression within initial hours revealed a general progressive increase up to 24h for all experimental conditions (**Figure 7A**). More in detail, at 1h, the higher concentrations of 25 and 50 µM significantly

increase HIF-1α expression compared to control. Although all conditions followed a similar trend, it was observed that the control, 0.5 and 25 μM conditions significantly up-regulated HIF-1α expression at 2h compared to 5 and 50μM. Regarding VEGF expression, results show an increase up to 2h and a progressive decrease up to 24h with control, 0.5 and 25 μM (**Figure 7B**). Alternatively, 5 and 50 μM showed a progressive decrease of VEGF expression up to 24h. It is worth to mention that at 1h all Co^{2+} concentrations tested induced a higher VEGF expression compared to control. Finally, PECAM-1 expression presented different patterns with different Co^{2+} concentrations and time course (**Figure 7C**). A summary of statistical analysis results of gene expression comparison between experimental groups for each time point is shown in **Table 5**.
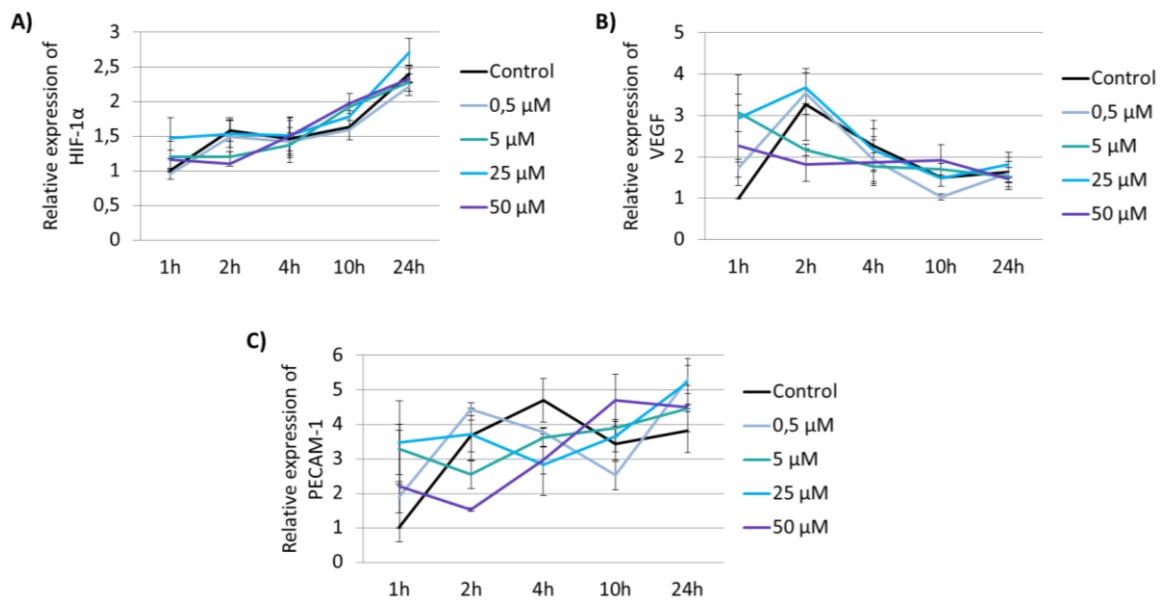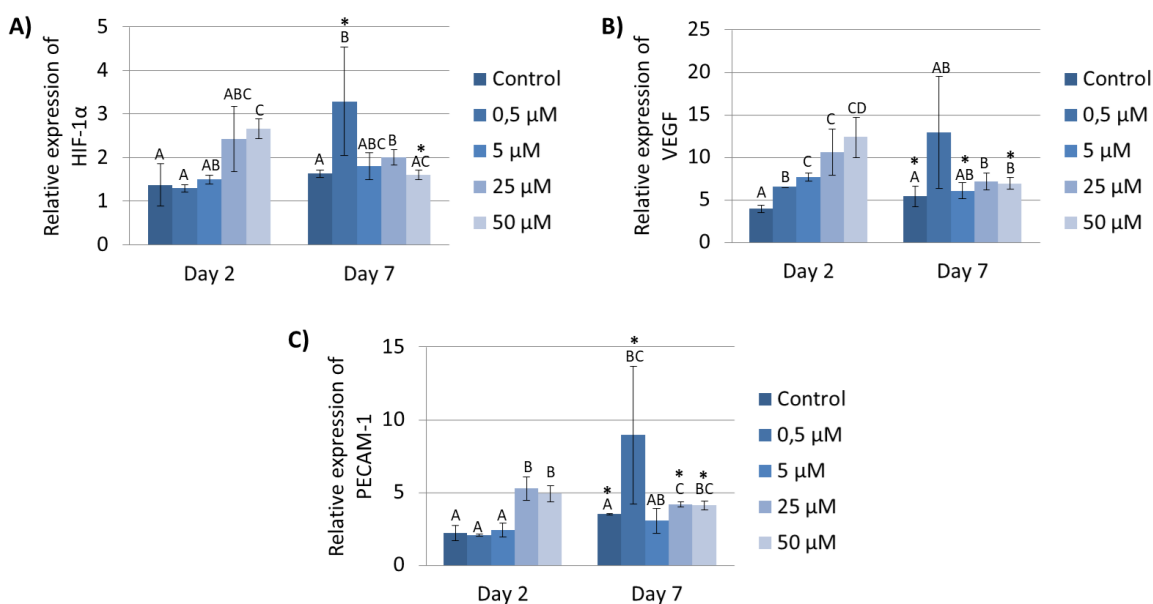

Figure 7. HUVEC gene expression within short time points. Different Co^{2+} concentrations were evaluated at 1, 2, 4, 10 and 24h for the gene expression of A) HIF-1α, B) VEGF and C) PECAM-1. Data represented correspond to fold-changes compared to 1h control.

Table 5. Statistics of HUVEC gene expression profile cultured with Co^{2+} within short time. Comparisons between experimental groups of each time point. Symbols represent *= significant differences ($p<0.05$); ns = non-significant differences ($p>0.05$)

		HIF-1α				VEGF				PECAM-1			
		0.5 μM	5 μM	25 μM	50 μM	0.5 μM	5 μM	25 μM	50 μM	0.5 μM	5 μM	25 μM	50 μM
1h	Control	ns	ns	*	*	*	*	*	*	*	*	*	ns
	0.5 μM		ns	*	*		*	*	ns		*	*	ns
	5 μM			ns	ns			ns	ns			ns	ns
	25 μM				*				ns				ns
	50 μM												
2h	Control	ns	*	ns	*	ns	ns	ns	*	*	*	ns	*
	0.5 μM		ns	ns	*		*	ns	*		*	ns	*
	5 μM			*	*			*	ns			*	*
	25 μM				*				*				*
	50 μM												
4h	Control	ns	ns	ns	ns	ns	ns	ns	ns	*	*	*	*
	0.5 μM		ns	ns	ns		ns	ns	ns		ns	ns	*
	5 μM			ns	ns			ns	ns			ns	*
	25 μM				ns				ns				ns
	50 μM												
10h	Control	ns	*	ns	*	*	ns	ns	ns	ns	ns	ns	*
	0.5 μM		*	ns	*		*	*	*		*	*	*
	5 μM			ns	ns			ns	ns			ns	ns
	25 μM				ns				ns				ns
	50 μM												
24h	Control	*	ns	ns	ns	ns	ns	ns	ns	*	ns	*	ns
	0.5 μM		ns	*	ns		ns	ns	ns		ns	ns	*
	5 μM			ns	ns			ns	ns			ns	ns
	25 μM				ns				ns				ns
	50 μM												

In later time points, at day 2, HUVEC HIF-1α expression analysis showed a gradual increase in a dose-dependent manner, although only 50 μM induced a significant up-regulation compared to control (**Figure 8A**). Later on, at day 7, the expression profile was reversed. More in detail, the lowest concentration of 0.5 μM induced a significant increase of HIF-1α expression compared to day 2 and compared to time point control. On the other side, 50 μM showed a down-regulation of HIF-1α at day 7 compared to day 2. Similar trend was observed with VEGF expression. At day 2, there was a significantly up regulation of VEGF for all concentrations tested in a dose-dependent manner, with the expression doubled with 25 and 50 μM compared to time point control (**Figure 8B**). At day 7, although 25 and 50 μM showed a down-regulation of their expression compared to day 2, VEGF expression was significantly higher than control. Finally, PECAM-1 expression at day 2 and 7 was significantly up regulated by

higher concentrations, specifically 25 and 50 µM (**Figure 8C**). Additionally, at day 7, the concentration of 0.5 µM also induced an up-regulation.

Figure 8. HUVEC gene expression. Different Co^{2+} concentrations were evaluated at 2 and 7 days for the gene expression of A) HIF-1α, B) VEGF and C) PECAM-1. Data represented correspond to fold-changes compared to Day 0 control.
Statistics is represented with letters when comparisons were made between the different experimental groups within the same time point. Same letters represent no significant differences (p>0.05), whereas different letters represent statistical differences (p<0.05). Differences between time points for each experimental condition is represented with * (p<0.05).

We further assessed if there was a correlation between HIF-1α and VEGF expression (**Table 6**). Statistical results show significant and strong correlation between the expression of these two genes.

Table 6. HIF-1α and VEGF expression correlation results with Co^{2+} supplementation. Symbols: ns=non-significant (p>0.05); *=p<0.05; **=p<0.01.

Time point	R-value	p-value
1h	0.670	**
2h	0.793	**
4h	0.321	ns
10h	0.806	**
24h	0.606	*
2 days	0.791	**
7 days	0.614	*

3.4.1.4. Tubule formation ability

The ability of Cu^{2+} and Co^{2+} to promote formation of tubular-like structures was further assessed by culturing HUVEC on Matrigel substrate. In general, with Cu^{2+} supplementation, thicker tubular structures were observed in comparison with control samples with phase contrast images at 4 and 8 hours (**Figure 9A**). The results of number of nodes, number of meshes and total tube length analysis showed a similar pattern, demonstrating a slight increase with 0.1 and 10 µM at 4h and with 0.1 and 1µM at 8h compared to time point control (**Figure 9B-D**). Nevertheless, these increases were not statistically significant compared to control samples or the rest of experimental groups for the same time point.
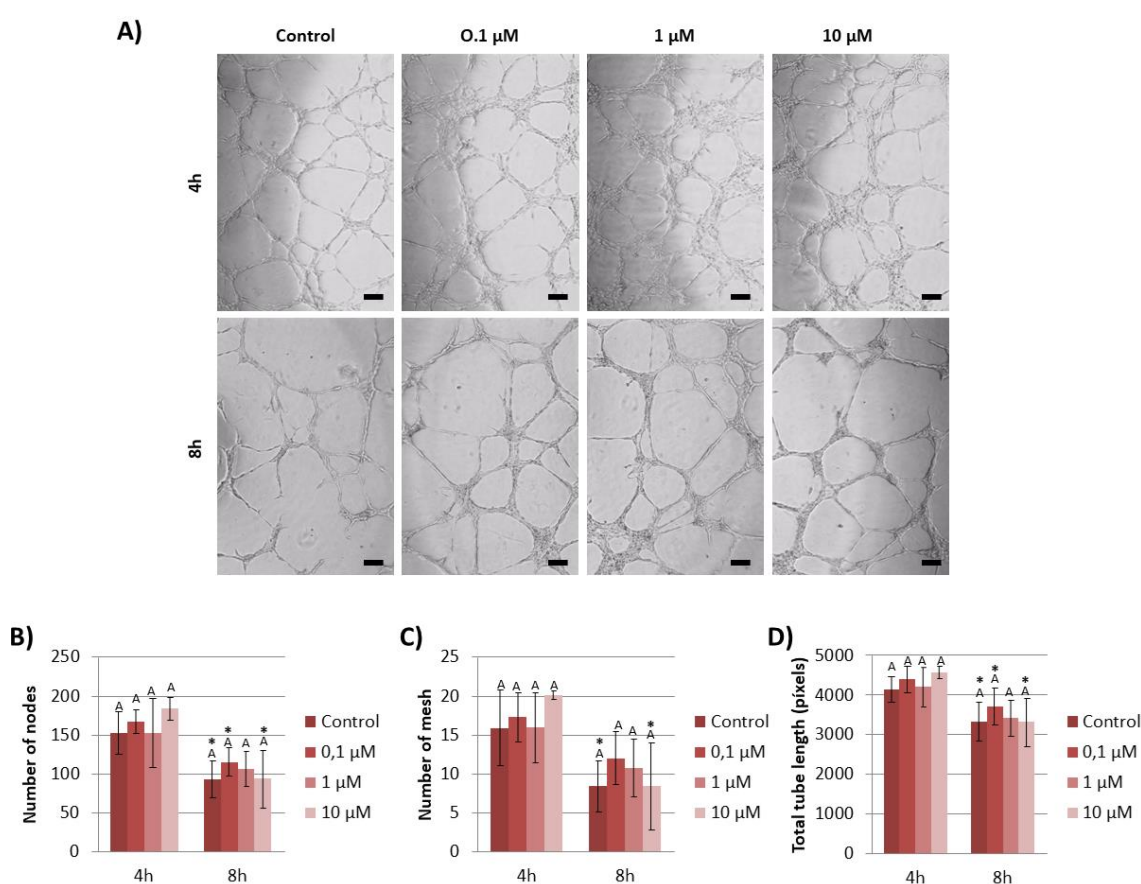
Figure 9. Effects of Cu^{2+} on tubule formation assay with HUVEC. A) Images of tubules formed under different concentrations of Cu^{2+} (0, 0.1, 1 and 10 µM) at 4 and 8 hours. B) Analysis of number of nodes, C) meshes and D) total tube length of HUVEC under different Cu^{2+} concentrations at 4 and 8 hours. Scale bar = 50 µm.
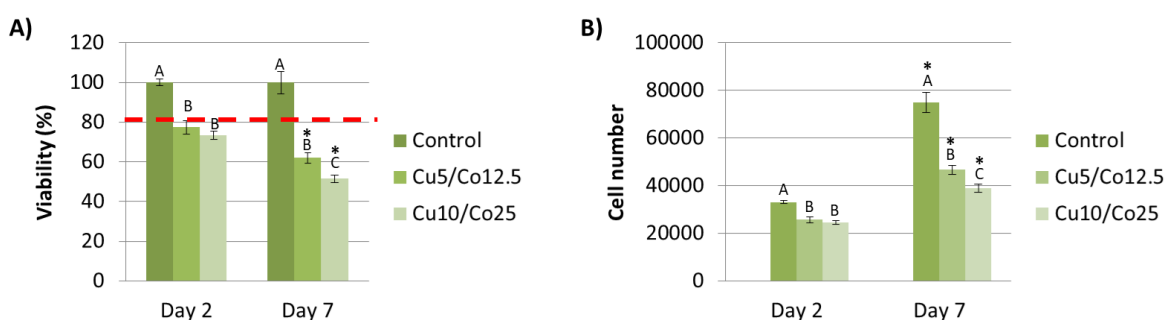Statistics is represented with letters when comparisons were made between the different experimental groups within the same time point. Same letters represent no significant differences (p>0.05). Differences between time points for each experimental condition is represented with * (p<0.05).

The assessment of Co^{2+} influence in tubule-like structures formation showed, in general, broken vascular structures with 50 µM concentration at 4 and 8h (**Figure 10 A**). Moreover,

control at 8h also showed broken vascular network. Similar to Cu^{2+}, similar pattern was obtained with the analysis of number of nodes, meshes and total tube length. More specifically, a slightly increase of these three parameters were achieved with 0.5, 5 and 25 µM at 4 and 8h, although these higher values were not statistically significant compared to time point controls (**Figure 10B-D**). However, a significant impairment on tubule formation resulted with 50 µM.
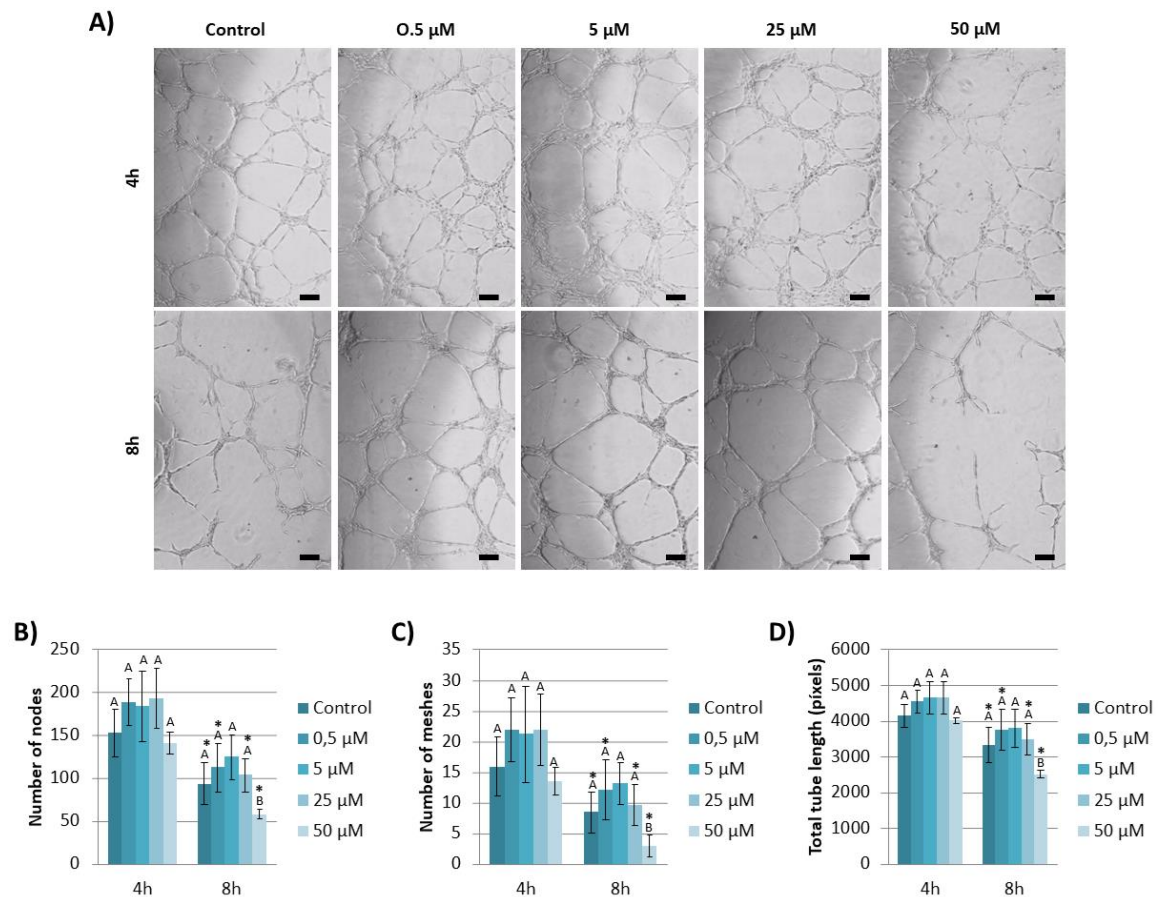
Figure 10. Effects of Co^{2+} on tubule formation assay with HUVEC. A) Images of tubules formed under different concentrations of Co^{2+} (0, 0.5, 5, 25 and 50 µM) at 4 and 8 hours. B) Analysis of number of nodes, C) meshes and D) total tube length of HUVEC under different Co^{2+} concentrations at 4 and 8 hours. Scale bar = 50 µm.
Statistics is represented with letters when comparisons were made between the different experimental groups within the same time point. Same letters represent no significant differences (p>0.05), whereas different letters represent statistical differences (p<0.05). Differences between time points for each experimental condition is represented with * (p<0.05).

3.4.1.5.   Influence of dual ion culture on viability and proliferation

Additionally to the individual ion evaluation in angiogenesis response, we wanted to elucidate if the combination of both ions could have synergistic or deleterious effects. To this purpose, we selected the concentration of 10 µM of Cu^{2+}, which demonstrated an important increase of

VEGF at early time points, and the concentration of 25 µM of Co^{2+}, which also showed a significant improvement of VEGF and PECAM-1 at early and later time points. This combination was coded as Cu10/Co25. As we considered the possibility that the combination of these two higher concentrations could be cytotoxic for cells, we also assessed the combination of half of these concentrations, being 5 µM for Cu^{2+} and 12.5 µM for Co^{2+}, coded as Cu5/Co12.5.

Results obtained with viability analysis showed that cells cultured with Cu5/Co12.5 and Cu10/Co25 reached a viability of almost 80% at day 2, but it was reduced down to 62% and 52% at day 7, respectively, being significantly lower compared to control (**Figure 11A**). Regarding cell number, both combinations of ions resulted in a significant decreased compared to control at both 2 and 7 days (**Figure 11B**). However, cell number increased from day 2 to day 7, suggesting that HUVEC cells were able to proliferate, almost doubling cell number.

Figure 11. HUVEC viability and cell number with Cu^{2+} and Co^{2+} supplementation. A) Viability and B) cell number of HUVEC under different combinations of Cu^{2+} and Co^{2+}. Abbreviations: Cu5/Co12.5 = 5 µM of Cu^{2+} and 12.5 µM of Co^{2+}; Cu10/Co25 = 10 µM of Cu^{2+} and 25 µM of Co^{2+}.
Statistics is represented with letters when comparisons were made between the different experimental groups within the same time point. Same letters represent no significant differences (p>0.05), whereas different letters represent statistical differences (p<0.05). Differences between time points for each experimental condition is represented with * (p<0.05).

3.4.1.6. Cell morphology under dual ion culture

The influence of the combination of both ions on HUVEC morphology and organization was also evaluated with actin filament staining. From day 0 to day 2 there was an increase of HUVEC cells with no apparent differences between experimental conditions (**Figure 12**). At day 7, control samples reached confluence and HUVEC cells grew over it. Regarding both combination of ions, although we observe the presence of more cells at day 7 compared to day 2, there were less number of cells compared to control. These observations are in accordance with previous results of proliferation.
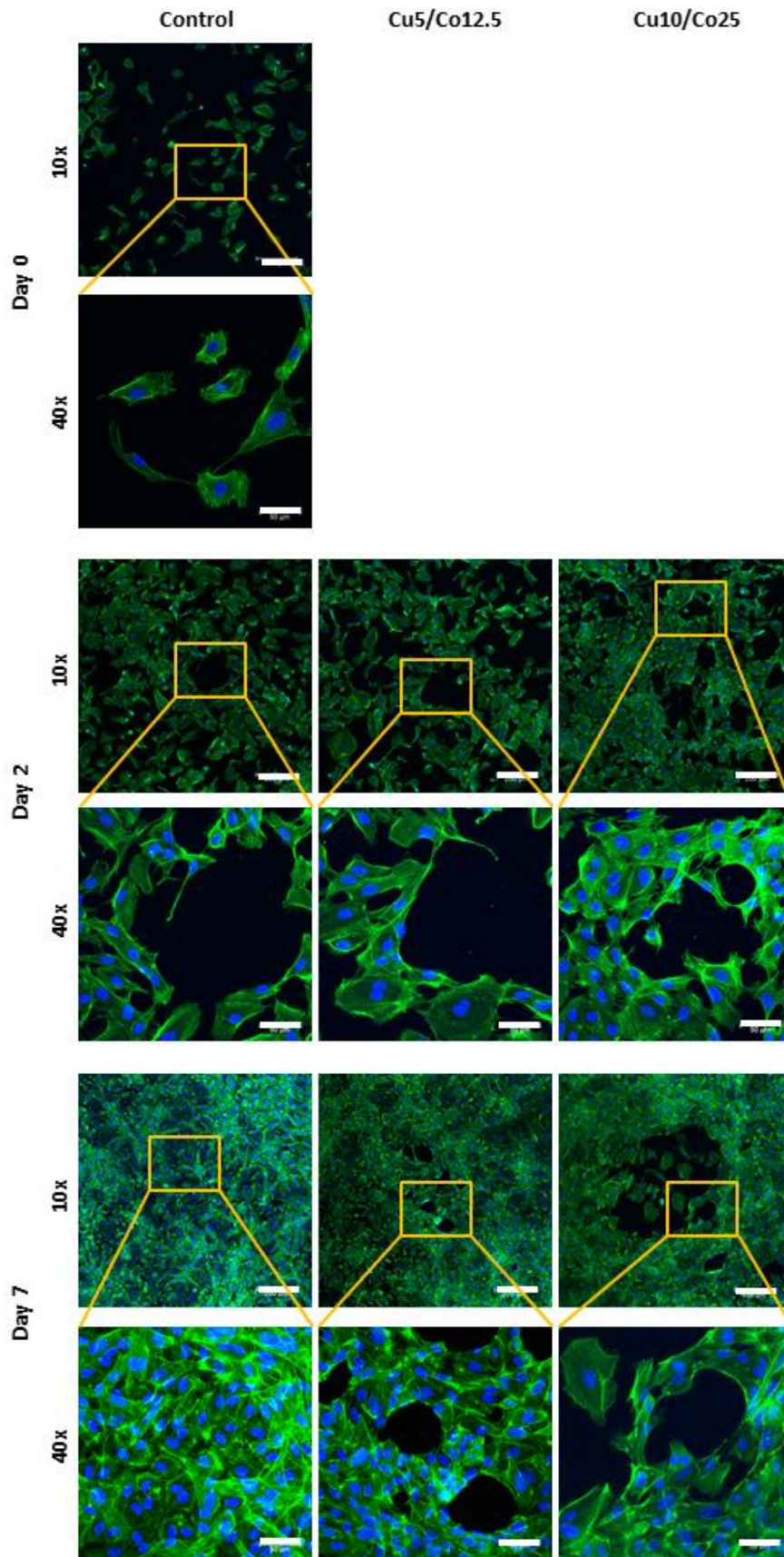
Figure 12. Morphology of HUVEC cultured with different concentrations of Cu^{2+} and Co^{2+}. Abbreviations: Cu5/Co12.5 = 5 µM of Cu^{2+} and 12.5 µM of Co^{2+}; Cu10/Co25 = 10 µM of Cu^{2+} and 25 µM of Co^{2+}. Scale bar = 200 µm and for magnification 50 µm.

3.4.1.7. Influence of dual ion culture on angiogenic gene expression

Surprisingly, the evaluation of angiogenic gene expression did not show any significant up or down-regulation of HIF-1α, VEGF or PECAM-1 for any of the combinations tested compared to control samples (**Figure 13A-C**).
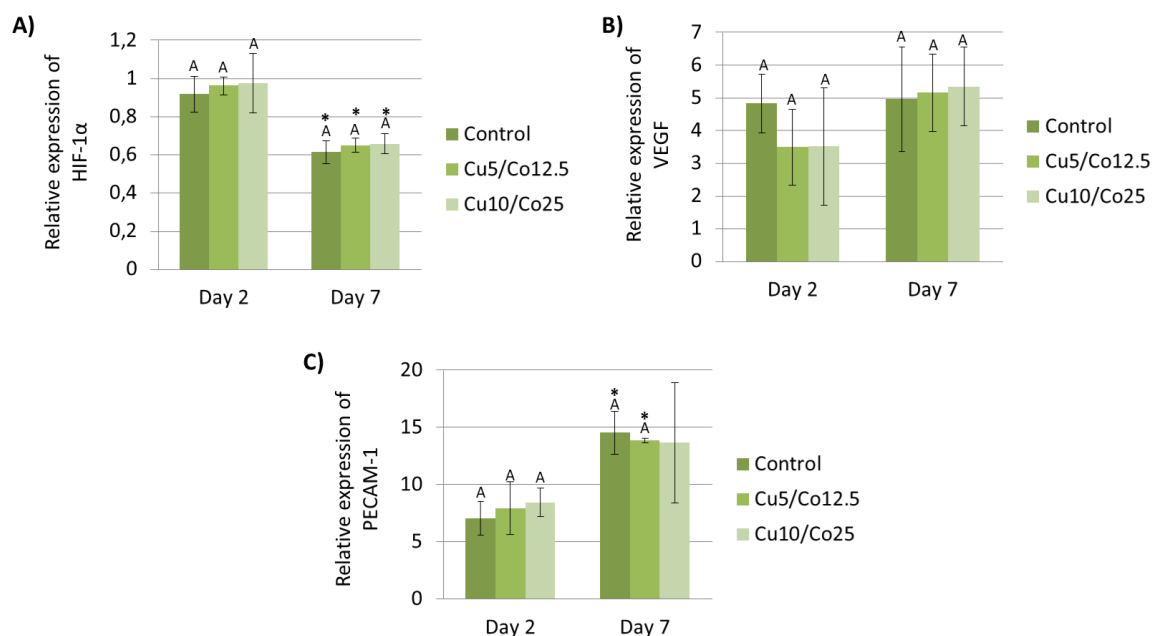
Figure 13. HUVEC gene expression. Different Cu^{2+} and Co^{2+} concentrations were evaluated at 2 and 7 days for the gene expression of A) HIF-1α, B) VEGF and C) PECAM-1. Data represented correspond to fold-changes compared to Day 0 control. Abbreviations: Cu5/Co12.5 = 5 μM of Cu^{2+} and 12.5 μM of Co^{2+}; Cu10/Co25 = 10 μM of Cu^{2+} and 25 μM of Co^{2+}.
Statistics is represented with letters when comparisons were made between the different experimental groups within the same time point. Same letters represent no significant differences (p>0.05). Differences between time points for each experimental condition is represented with * (p<0.05).

3.4.1.8. Tubule formation ability under dual ion culture

As a final assessment, tubule formation capability of HUVEC under both ion combinations was also assessed with Matrigel as a substrate. Apparently, with phase contrast images no differences seemed to be between all conditions tested (**Figure 14A**). Results of the analysis of number of nodes, number of meshes and total tube length resulted in non-statistically significant differences between experimental groups for each time point, confirming the previous observations (**Figure 14B-D**).
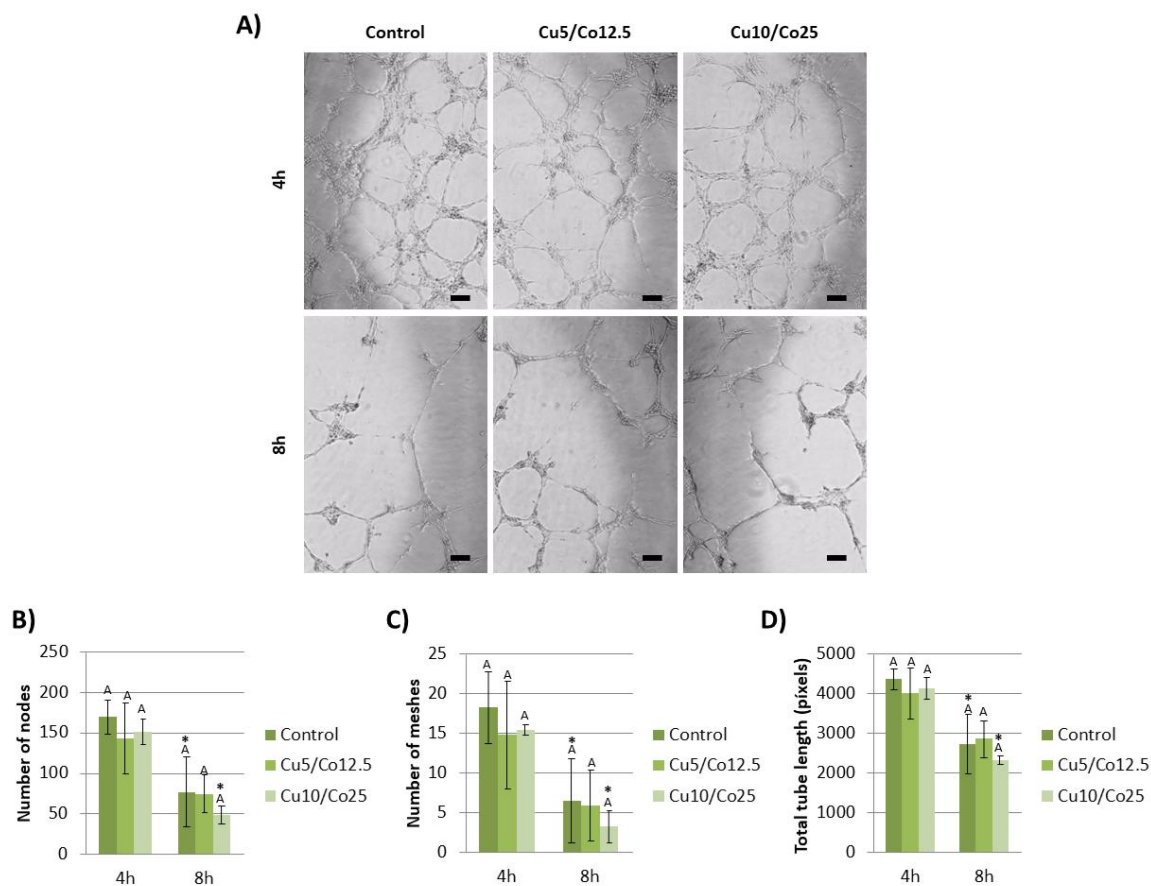
Figure 14. Effects of Cu^{2+} and Co^{2+} on tubule formation assay with HUVEC. A) Images of tubules formed under different concentrations of Cu^{2+} and Co^{2+} at 4 and 8 hours. B) Analysis of number of nodes, C) meshes and D) total tube length of HUVEC at 4 and 8 hours. Abbreviations: Cu5/Co12.5 = 5 μM of Cu^{2+} and 12.5 μM of Co^{2+}; Cu10/Co25 = 10 μM of Cu^{2+} and 25 μM of Co^{2+}. Scale bar = 50 μm. Statistics is represented with letters when comparisons were made between the different experimental groups within the same time point. Same letters represent no significant differences (p>0.05). Differences between time points for each experimental condition is represented with * (p<0.05).

3.4.2. Role of copper and cobalt in osteogenesis

3.4.2.1. Viability and proliferation

hBM-MSC viability analysis revealed non-toxic concentrations of Cu^{2+} up to 10 μM at the end of cell culture (**Figure 15A**). Interestingly, at day 7 significant increase in viability was observed with 0.1 and 1 μM compared to time point control and compared to day 2. Regarding cell number, although at day 2 the conditions of 0.1 and 1 had the same cell number as control, at day 7 there was a significant increase compared to time point control of day 7. Moreover, these conditions also presented an increase from day 2 to day 7 (**Figure 15B**). Higher concentrations of 100 and 200 μM resulted in a significant decrease in cell number compared to control time point. It is worth to mention that there was no proliferation of control cells from day 2 to day 7.
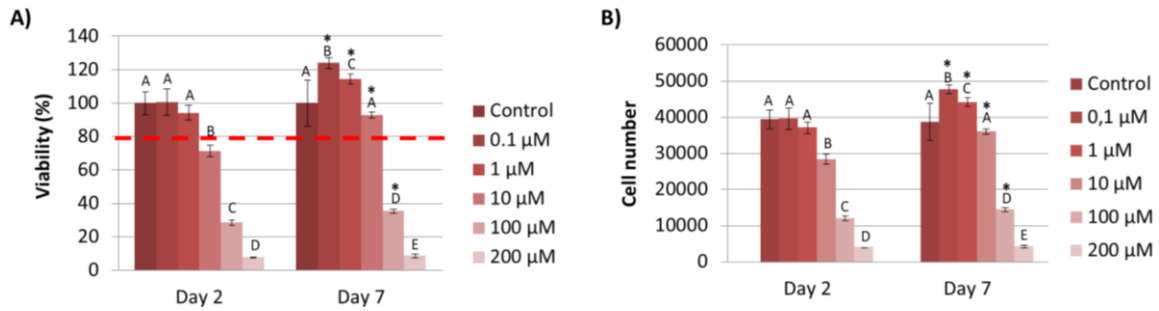
Figure 15. hBM-MSC viability and proliferation with Cu^{2+} cell culture media supplementation. A) Viability and B) proliferation of HUVEC under different Cu^{2+} concentrations (0, 0.1, 1, 10, 100 and 200 µM) at day 2 and 7.
Statistics is represented with letters when comparisons were made between the different experimental groups within the same time point. Same letters represent no significant differences (p>0.05), whereas different letters represent statistical differences (p<0.05). Differences between time points for each experimental condition is represented with * (p<0.05).

Conversely, when hBM-MSC were cultured with Co^{2+} cell culture media supplementation, none of the concentrations tested induced any cytotoxicity at 2 or 7 days, even with the highest concentration of 100 µM (**Figure 16A**). Regarding proliferation, all Co^{2+} concentrations tested induced an increase of cell number from day 2 to day 7, whereas no significant differences were found with control (**Figure 16B**).
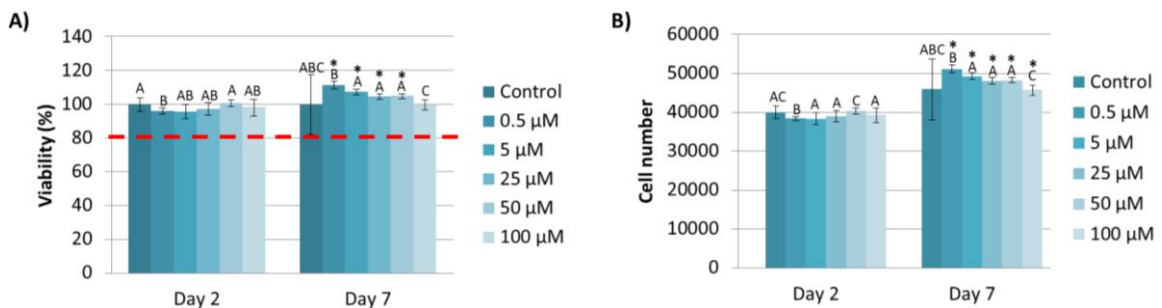
Figure 16. hBM-MSC viability and proliferation with Co^{2+} cell culture media supplementation. A) Viability and B) proliferation of HUVEC under different Co^{2+} concentrations (0, 0.5, 5, 25, 50 and 100 µM) at day 2 and 7.
Statistics is represented with letters when comparisons were made between the different experimental groups within the same time point. Same letters represent no significant differences (p>0.05), whereas different letters represent statistical differences (p<0.05). Differences between time points for each experimental condition is represented with * (p<0.05).

3.4.2.2. hBM-MSC morphology

To further assess hBM-MSC morphology, actin cytoskeleton filament staining was performed. During time course, cells undergo from a fibroblast-like phenotype to more enlarged phenotype with parallel actin stress fibers extended across the entire cytoplasm, with no apparent cytoskeleton disorganization with both ions supplementation (**Figure 17** and **Figure**

94

18). With Cu^{2+} supplementation, no apparent differences seemed to be between conditions (**Figure 17**), although with the presence of Co^{2+} a reduction of number of hBM-MSC or less wide cell morphology was observed with 50 µM at day 7 compared to control (**Figure 18**).
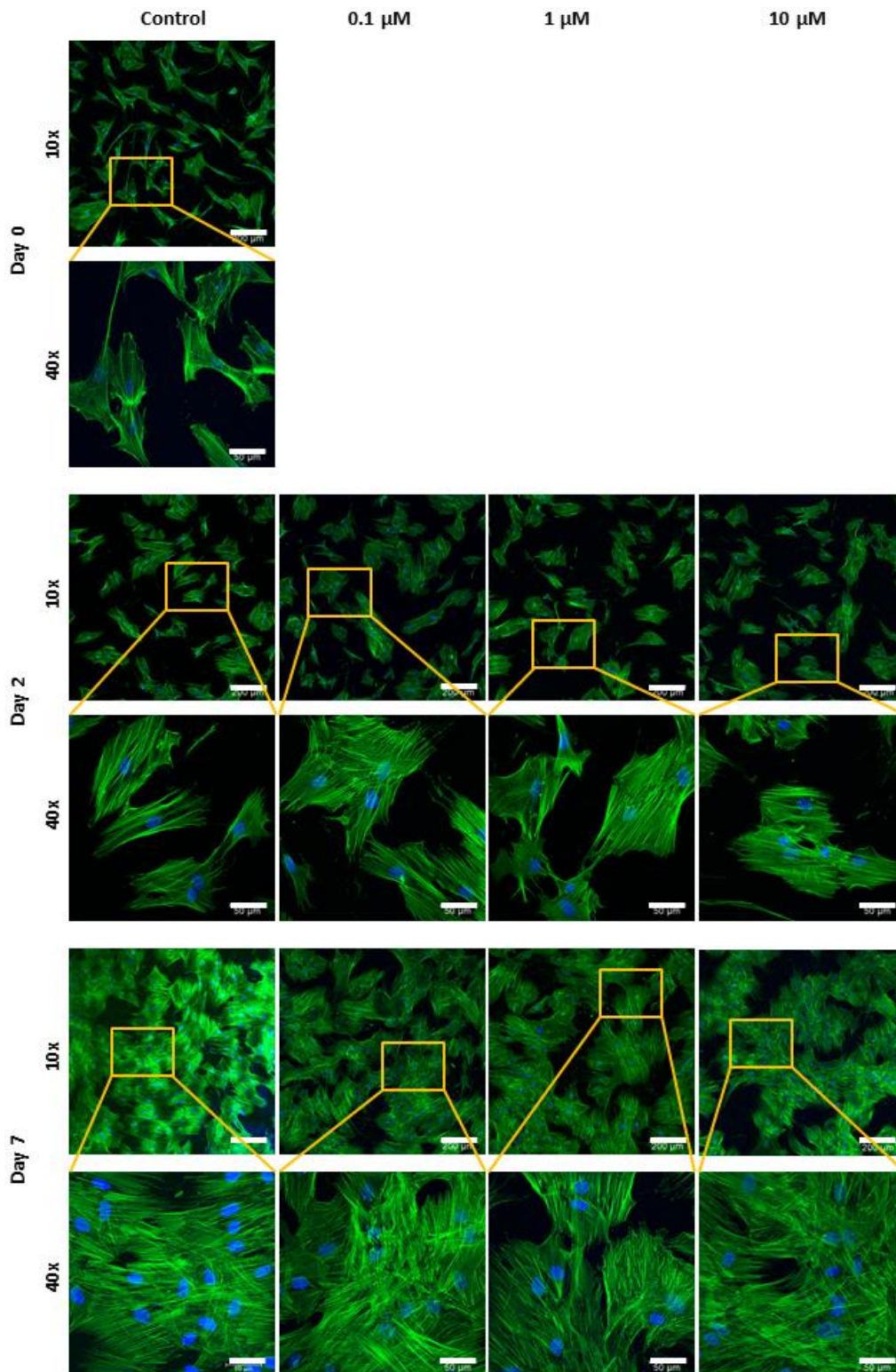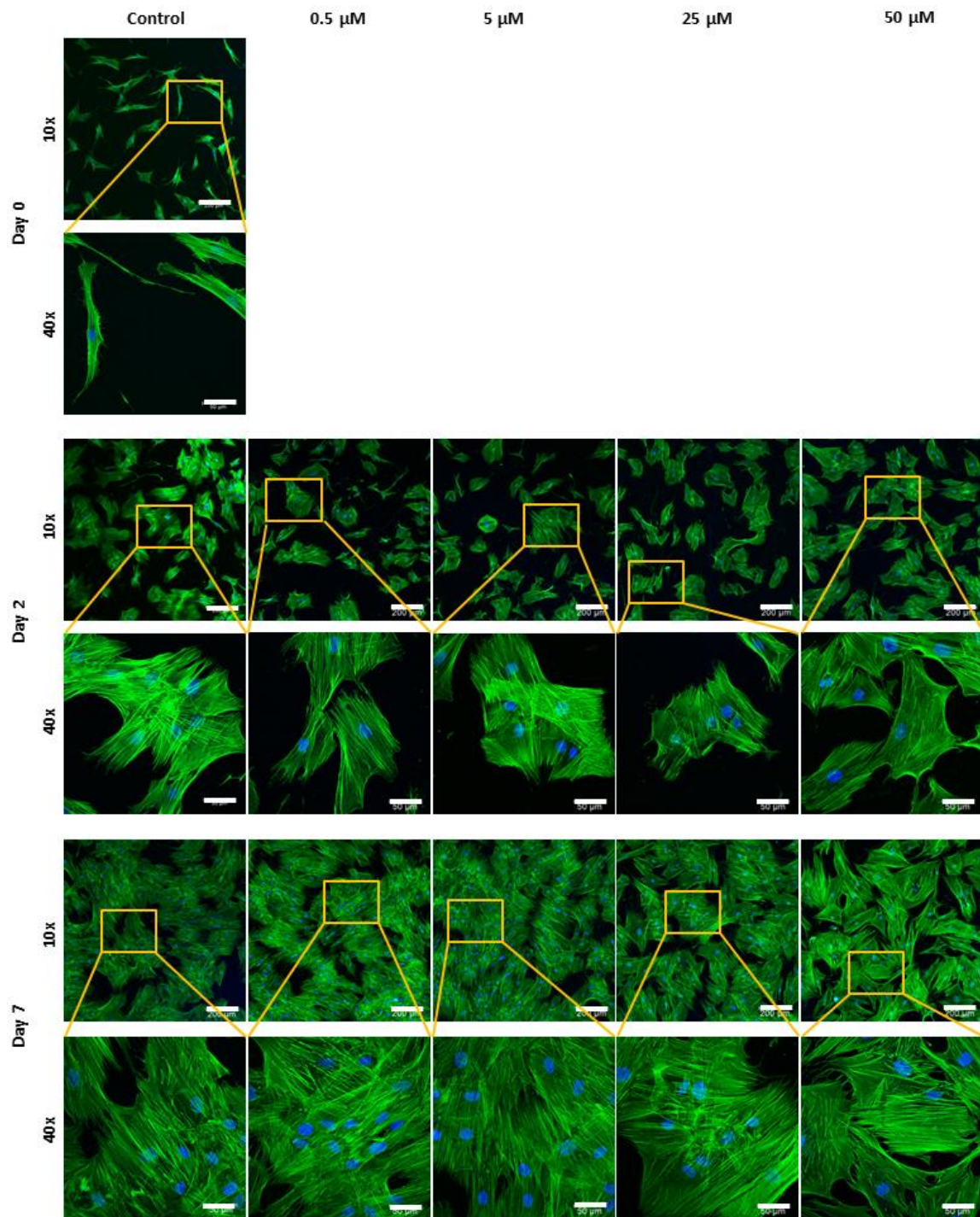

**Figure 17. Morphology of hBM-MSC cultured with different concentrations of Cu^{2+}.** Scale bar = 200 µm and for magnification 50 µm.

Figure 18. Morphology of hBM-MSC cultured with different concentrations of Co^{2+}. Scale bar = 200 μm and for magnification 50 μm.

3.4.2.3. Ion influence on osteogenic gene expression

To further assess the potential of Cu^{2+} and Co^{2+} in stimulating osteogenic differentiation in hBM-MSC, we analyzed the expression of three main genes involved in different stages of bone differentiation: Runx-2, ALP and OC, as early, middle and later osteogenic differentiation markers, respectively.

Gene expression analysis at day 2 of hBM-MSC cultured with Cu^{2+} resulted in a general increase of Runx-2 (**Figure 19A**). More in detail, the concentrations of 0.1 and 10 µM induced a significant increase compared to control. By contrast, at day 7 the condition 0.1 µM significantly down-regulated Runx-2, whereas the rest of Cu^{2+} concentrations tested induced similar expression compared to control. Interestingly, regarding ALP expression, 0.1 µM promoted an early significant up-regulation, whereas there were no significant differences among the rest experimental groups (**Figure 19B**). However, at day 7, although all Cu^{2+} concentrations were able to up-regulate ALP expression compared to day 2, it was significantly lower compared to control of day 7. Finally, despite OC expression was increased from day 2 to day 7, no significant differences were found between experimental groups compared to their respective time point control (**Figure 19C**).
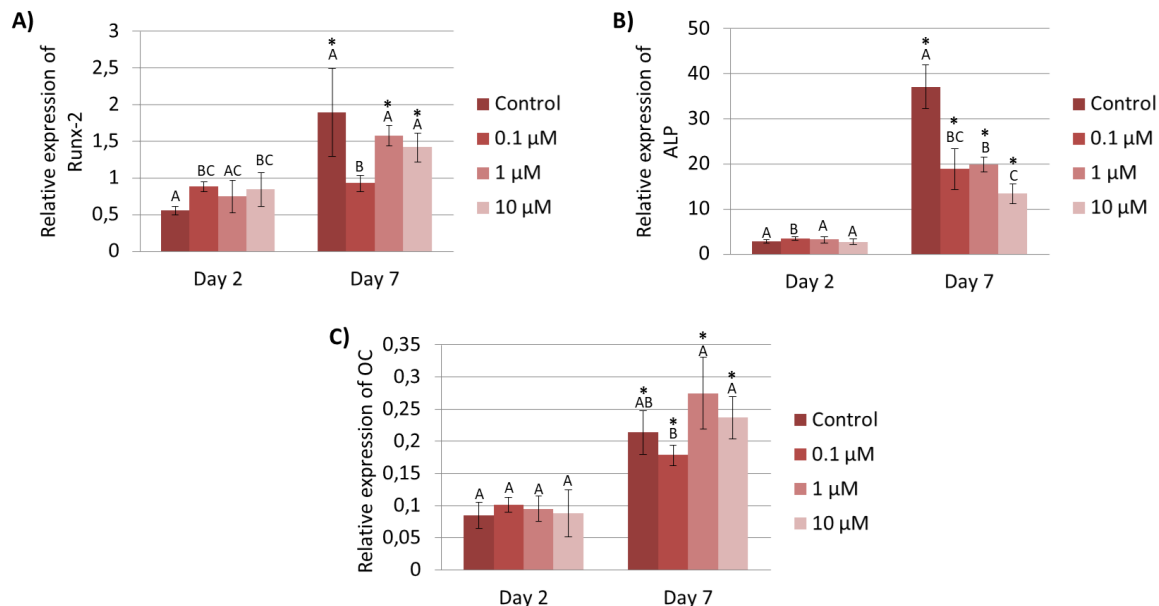
Figure 19. hBM-MSC gene expression. Different Cu^{2+} concentrations were evaluated at 2 and 7 days for the gene expression of A) Runx-2, B) ALP and C) OC. Data represented correspond to fold-changes compared to Day 0 control.
Statistics is represented with letters when comparisons were made between the different experimental groups within the same time point. Same letters represent no significant differences (p>0.05), whereas different letters represent statistical differences (p<0.05). Differences between time points for each experimental condition is represented with * (p<0.05).

Regarding the analysis of gene expression with the presence of Co^{2+}, results at day 2 revealed a significant up-regulation of Runx-2 with the highest concentration of 50 µM compared to control (**Figure 20A**). At day 7, there was a significant down-regulation of Runx-2 with 5 µM compared to control, whereas no significant differences were observed with the rest of conditions. Regarding ALP, at day 2 Co^{2+} supplementation did not alter its expression, but a significant down-regulation in a dose-dependent manner was induced beyond 5 µM at day 7, indicating a suppression of ALP expression (**Figure 20B**). Unexpectedly, although Co^{2+} decreased the ALP expression at later time point, the expression of OC was significantly up-regulated at day 2 by 25 µM and at day 7 by 0.5 µM (**Figure 20C**).
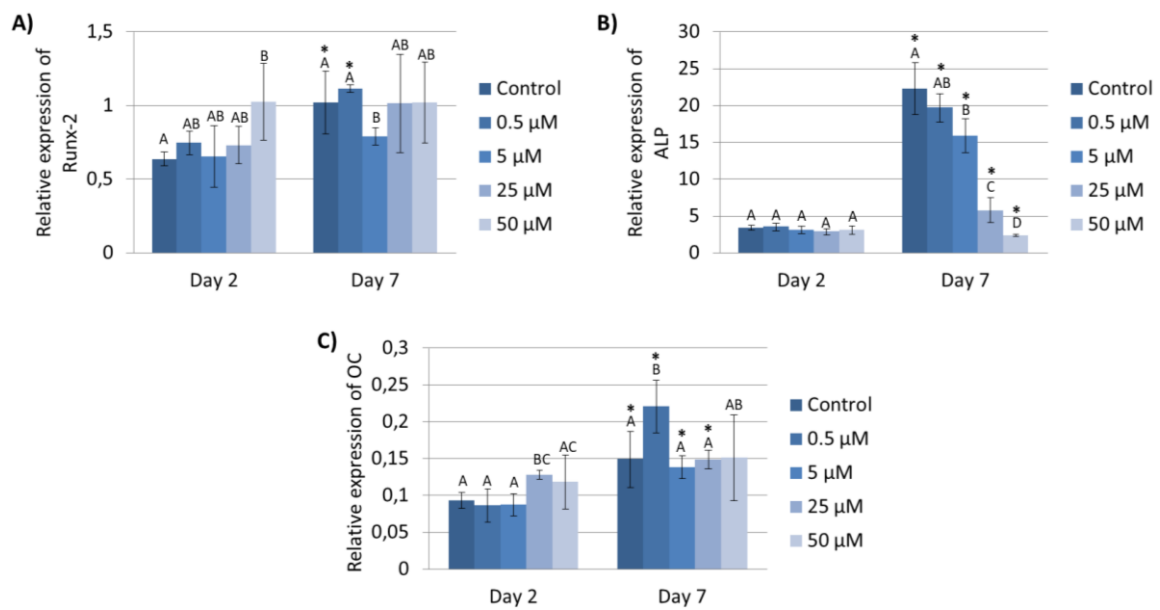
Figure 20. hBM-MSC gene expression. Different Co^{2+} concentrations were evaluated at 2 and 7 days for the gene expression of A) Runx-2, B) ALP and C) OC. Data represented correspond to fold-changes compared to day 0 control.
Statistics is represented with letters when comparisons were made between the different experimental groups within the same time point. Same letters represent no significant differences (p>0.05), whereas different letters represent statistical differences (p<0.05). Differences between time points for each experimental condition is represented with * (p<0.05).

3.5. Discussion

3.5.1. Role of copper and cobalt in angiogenesis

In the first part of this chapter, the role of Cu^{2+} and Co^{2+} on angiogenesis was investigated. First of all, we wanted to elucidate if we could use a reduced growth factor media, referred as basal medium (BM), instead of growth factor supplemented media (GM) to better isolate the effect of ions on the angiogenic response. HUVEC cultured with BM resulted in a lower cell number

compared to GM, with or without Cu^{2+} and Co^{2+} supplementation (**Figure 1B** and **C; Figure 2B** and **C**). Moreover, all Cu^{2+} and Co^{2+} concentrations tested resulted toxic for HUVEC cells with BM (**Figure 1A** and **2A**), whereas concentrations up to 10 µM of Cu^{2+} and 50 µM of $Co^{2+}$ were non-toxic for HUVEC cultured with GM (**Figure 1C** and **2C**). The low viability and proliferation of HUVEC with BM might be due to the reduced growth factor content, which is needed to allow their proliferation. Therefore, we decided to use GM for the rest of experiments, as it would ensure cell viability for subsequent analysis.

Regarding HUVEC proliferation with GM, we could observe a reduction with higher concentrations in a dose-dependent manner either with Cu^{2+} or Co^{2+} (**Figure 1D** and **Figure 2D**). Decrease of cell proliferation and viability with high concentration of ions might be due to cellular toxicity induced by reactive oxygen species (ROS). In the presence superoxide ($\cdot O_2$-) (produced by the mitochondria during cellular respiration) or reducing agents, such as glutathione (GSH) or ascorbic acid (generally found in cells with a concentration of 5 mM (26) and in cell culture media that we used for the experiments, respectively), Cu^{2+} can be reduced to Cu^+, which in turn, can catalyze the formation of hydroxyl radicals ($OH^\cdot$) from hydrogen peroxide (H_2O_2) (produced during normal cell metabolism (27)), through Haber-Weiss reaction (28):

$$\cdot O_{2-} + Cu^{2+} \rightarrow O_2 + Cu^+$$

$$Cu^+ + H_2O_2 \rightarrow Cu^{2+} + OH^- + OH^\cdot$$
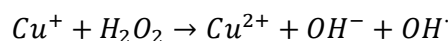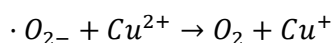
Similarly, Co^{2+} has also been described to be involved in ROS formation (29,30). More specifically, with the presence of oxygen, Co^{2+} might generate the radical intermediate Co^+-$OO^\cdot$ species (31):

$$Co^{2+} + O_2 \rightarrow Co^+ + O_2^\cdot \rightarrow Co^+ - OO^\cdot$$
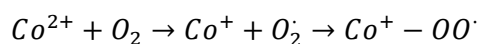
With the presence of superoxide dismutase enzyme (SOD) (an antioxidant enzyme present in cells (32)), it can catalyze the decomposition of Co^+-$OO^\cdot$ species to H_2O_2 and Co^+:

$$Co^+ - OO^\cdot \rightarrow H_2O_2 + Co^+$$
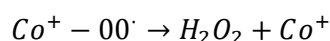
Finally, it was proposed that Co^+ could participate in the formation of $OH^\cdot$ radicals through Fenton reaction:

$$Co^+ + H_2O_2 \rightarrow Co^{2+} + OH^\cdot + OH^-$$
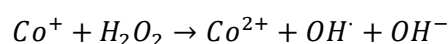
Results of HUVEC viability when both ions were combined support the proposed equations of ROS generation by Cu^{2+} or Co^{2+} discussed in the literature. More in detail, HUVEC viability was considerably reduced (**Figure 11A**), compared to viability with individual culture ions (**Figure 1C** and **Figure 2C**). As observed in ROS generation equations, Cu^{2+} generates O_2, whereas Co^{2+} consumes it. Therefore, there is the possibility that the presence of both ions might feedback the formation of ROS. Furthermore, it is widely reported that the generation of ROS can result in DNA damage, lipid peroxidation, depletion of protein sulfhydryls and other effects that leads to apoptosis of cells (31), and that might explain the decreased proliferation of cells when the concentrations of ions were increased. To confirm low viability and proliferation due to ROS formation, further studies including quantification of ROS species will need to be undertaken.

Comparing viability and proliferation results of HUVEC cultured with Cu^{2+} with published ones, we found similarities with another study. Stähli *et al.* reported a decreased HUVEC viability when cultured with concentrations equivalent to 7, 21 and 63 µM compared to control (15). However, our results differ from other studies reporting viability of HUVEC up to 50 µM (14) or 500 µM (13), or another study where bovine endothelial cells could proliferate with concentrations equivalent to 160 and 315 µM, without any statistically significant decrease respect to control cells (33). Regarding Co^{2+}, few studies are reported. Similar to our results, Peters *et al.*, described a proliferation decrease in a dose-concentration manner with concentrations of 10, 50, 100, 300 and 700 µM, with half cell number with 700 µM compared to control (19). Conversely, Tao Zan *et al* reported an enhanced proliferation of EC in a dose-dependent manner with Co^{2+} concentrations of 50, 100 and 200 µM (17). There are different results found in the literature regarding viability and proliferation of HUVEC with Cu^{2+} or Co^{2+}. However, the cause of this variability is still unknown.

Regarding the gene expression induced by Cu^{2+} and Co^{2+}, it is generally reported that both ions can enhance the angiogenic response by the stabilization and increase of HIF-1α, which in turn triggers VEGF transcription (5,6). Our results demonstrated that, in a wide overview, with Cu^{2+} supplementation it seems that higher concentrations (10 µM) of Cu^{2+} have a significant contribution in angiogenesis at early times observed with VEGF and PECAM-1 expression, whereas lower concentrations (0.1 and 1µM) seems to have a more therapeutic effect at later stage. However, statistical analysis revealed no correlation between HIF-1α and VEGF expression. Our findings are in agreement with a previous study. More specifically, authors suggested that Cu^{2+} might be required for the binding of HIF-1α to HRE sequence of target genes such as VEGF, but its deprivation did not affect the expression or stability of HIF-1α but it did decrease VEGF expression (16). This might explain why we could observe an increase of

VEGF although it was not correlated with HIF-1α expression. However, further studies are required to elucidate the mechanism of action of Cu^{2+} in angiogenic gene expression. In addition to this, it has been described that PECAM-1 is involved in endothelial cell migration and angiogenesis (34–36), and a reduction of blood vessel formation was reported when being inhibited (37). Here, we observed a significant increase of PECAM-1 expression with higher doses at early times (10 µM at 24h) and with lower doses at later times (0.1 and 1 µM at day 7), further suggesting an enhancement of angiogenic response with Cu^{2+}. Gene expression results seem to be in accordance with results obtained with tubule formation assay (**Figure 9**). Although there were no statistically significant differences, we could observe an increase of number nodes, number of meshes and total tube length with 0.1 and 10 µM at an early time of 4h, with higher values with 10 µM, whereas at a later time, at 8h, the lowest concentration of 0.1 µM seemed to have higher values.

Regarding results of gene expression induced by Co^{2+}, although lower concentrations can enhance the angiogenic response at specific times, it seems that higher concentrations of 25 and 50 µM enhance the response either at 2 and 7 days through the increase of HIF-1α, VEGF and PECAM-1 expression. Remarkably, we found a strong and significant correlation between HIF-1α and VEGF expression. These results are similar to a previous study demonstrating that Co^{2+} induced increased HIF-1α and VEGF expression in a dose-dependent manner, although the concentrations that they used were higher, specifically 50, 100 and 200 µM (17). Authors mentioned that Co^{2+} act as prolyl hydroxylation inhibitor, hence inhibiting HIF-1α degradation and stabilizing it, with subsequent VEGF expression. Moreover, the up-regulation of PECAM-1 expression with high concentrations further indicates an enhancement of angiogenic response. Alternatively, the results obtained from tubule formation assay indicated that Co^{2+} seemed to have an effect in vascular structure formation. It was observed an increase of number of nodes, number of meshes and total tube length with 0.5, 5 and 25 µM at early time of 4h, and with the lowest concentrations of 0.5 and 5 µM at later time of 8h. However these increases were not statistically significant. Importantly, the highest concentration of 50 µM induced an impairment of angiogenesis at 8h. This impairment was in accordance with a previous study where the in-vitro capillary formation of human EC was impaired with Co^{2+} concentrations of 50, 100 and 300 µM (19). The authors hypothesized that Co^{2+} exposure could induce interference of integrin signaling, which is normally regulated by divalent metal ions such as Ca^{2+}, Mg^{2+} and Mn^{2+}. Integrins recognize and respond to a variety of extracellular matrix proteins (38) and their signaling interference can lead to an impairment of EC adhesion (39),

which might be an explanation for the impairment of vascular network structures formation with the highest concentration of Co^{2+}.

Finally, as we observed an enhanced angiogenic response with individual culture of Cu^{2+} and Co^{2+} with HUVEC, we further evaluated the response when combined together. As far as we know, no previous studies are reported analyzing the role of these two ions combined together, neither as cell culture media supplement or as delivered from scaffolds. To our surprise, we could not observe any significant up or down-regulation of HIF-1α, VEGF or PECAM-1 between conditions during all time course of the experiment (**Figure 13**), or any significant difference of number of nodes, number of meshes and total tube length with the *in vitro* tubule formation assay compared to control (**Figure 14**). As we observed differences when both ions were cultured individually, these results point to the likelihood that both ions are mutually inhibiting each other when being together. Future research on elucidating the exact mechanisms by which Cu^{2+} and Co^{2+} induce the angiogenic response might extend the explanation of our inhibition results found when combined together.

3.5.2. Role of copper and cobalt in osteogenesis

As we wanted to elucidate the effect of Cu^{2+} and Co^{2+} in osteogenic differentiation, we cultured hBM-MSC with osteogenic medium, as MSC can differentiate towards other cell lineages. Differences between both ions were observed in viability, proliferation and osteogenic gene expression.

Regarding Cu^{2+} supplementation, hBM-MSC showed viability with concentrations up to 10 μM, whereas higher concentrations demonstrated to be toxic for them (**Figure 15A**). These results are in accordance with another study, which reported cytotoxic effects of Cu^{2+} with concentrations over 10 μM (24). The reduced viability with higher concentrations can be due to the ability of Cu^{2+} to form ROS, as mentioned earlier. Interestingly, at day 7 we observed a significant increased viability with 0.1 and 1 μM compared to control, and more surprisingly, viability of hBM-MSC with 10 μM was higher than HUVEC. Regarding Co^{2+} supplementation, all concentrations tested up to 100 μM did not show any cytotoxic effect at day 2 and 7 (**Figure 16A**). These results are similar to a previous published study, in which hMSC did not present toxicity for concentrations up to 200 μM, although a slight reduction was observed with 400 μM at 48h (40). In general, hBM-MSC showed higher viability when cultured with Cu^{2+} or Co^{2+} compared to HUVEC cells. It has been demonstrated that MSC are resistant to oxidative stimuli by constitutively expressing antioxidant enzymes, mainly SOD (involved in the formation of H_2O_2 from $O_2^{\cdot-}$), catalase (CAT) and glutathione peroxidase (GPx) (both involved in the

formation of H_2O and O_2 from H_2O_2) (41). Other studies demonstrated MSCs antioxidant activity by their administration to animal models associated with oxidative stress, resulting in a reduction of ROS levels (41). Therefore, that might explain why viability was higher, as MSCs have enhanced antioxidant properties. This is more evident when hBM-MSC were cultured with Co^{2+} compared to Cu^{2+}. The reason why Co^{2+} is less harmful is not clearly understood, but we hypothesized that the kinetic reaction with Cu^{2+} might be higher than Co^{2+}.

During MSC differentiation, there is a first high proliferation phase followed by a specific osteogenic differentiation where the proliferation rate is reduced. Control samples with osteogenic differentiation media showed no proliferation from day 2 to day 7, suggesting their bone differentiation commitment. However, in general, non-toxic concentrations of Cu^{2+} or Co^{2+} revealed a slight increase in cell number (**Figure 15B** and **Figure 16B**). This could be explained at some extend due to hypoxic conditions. On one hand, it has been previously described that MSC can maintain their proliferation capacity in hypoxic conditions, whereas in normoxic conditions they stop proliferating and start differentiating (42,43). On the other hand, several studies reported Co^{2+} and Cu^{2+} as hypoxia mimicking ions, increasing HIF-1α expression in MSC (8,22,44). In turn, HIF-1α has been described to activate a battery of genes, amongst them some involved in cell proliferation (45). Therefore, we hypothesized that hBM-MSC cultured with Cu^{2+} or Co^{2+} might induced hypoxic-mimic conditions and eventually maintained proliferation. However, further studies involving HIF-1α and cell cycle under these ions with MSC are required to confirm this hypothesis. Despite there was statistically significant increase in cell number from day 2 to day 7 with Cu^{2+} or Co^{2+} supplementation, it could be considered a subtle increase, suggesting a commitment to osteogenic differentiation. In this line, hBM-MSC gene expression results showed an early expression of Runx-2 at day 2 either with Cu^{2+} or Co^{2+} supplementation (**Figure 19A** and **Figure 20A**), indicating an early commitment. Although a significant increase of OC expression was observed only with Co^{2+} supplementation (**Figure 20C**), both ions resulted in ALP suppression in a dose-dependent manner (**Figure 19B** and **Figure 20B**), suggesting an osteogenic differentiation impairment. This ALP suppression is in accordance to a previous study where authors observed a decrease in ALP activity in a dose-dependent manner compared to non-supplemented cell culture media (46). Authors referred to another study for a possible explanation. More specifically, Hsu *et al*. demonstrated that HIF-1α stabilization due to hypoxia or $CoCl_2$ treatment, induced hMSCs osteogenic differentiation impairment caused by the switch from aerobic to anaerobic metabolism (47). Same authors previously demonstrated that metabolic switch from anaerobic

to aerobic is required for osteogenic differentiation (48). Therefore, Cu^{2+} and Co^{2+}, described to mimic hypoxia, might not provide the proper environment to allow hMSC differentiation.

3.6.   Conclusions

To summarize, we could observe that Cu^{2+} and Co^{2+} ions seem to enhance the angiogenic response in HUVEC cells with different concentrations, although results showed that some concentrations are more beneficial in different time points than others. However, further studies analyzing the expression of these markers in a protein level are necessary to validate the conclusions that are drawn from angiogenic gene expression results. Regarding the osteogenic response, although early gene expression results indicate an early commitment of hBM-MSC when cultured with Cu^{2+} or Co^{2+}, later time points indicate a clear suppression of osteogenic differentiation. Therefore, these results are not conclusive whether Cu^{2+} or Co^{2+} induce osteogenic therapeutic response. Further studies including protein expression and extending culture period time up to 21 days would provide more information about both ions effect in osteogenic response.

3.7.   References

1.   Newman MR, Benoit DSW. Local and targeted drug delivery for bone regeneration. Curr Opin Biotechnol. 2016;40:125–32.

2.   Caballero Aguilar LM, Silva SM, Moulton SE. Growth factor delivery: Defining the next generation platforms for tissue engineering. J Control Release. 2019;306:40–58.

3.   Mouriño V, Cattalini JP, Boccaccini AR. Metallic ions as therapeutic agents in tissue engineering scaffolds: An overview of their biological applications and strategies for new developments. J R Soc Interface. 2012;9(68):401–19.

4.   Perez RA, Seo SJ, Won JE, Lee EJ, Jang JH, Knowles JC, et al. Therapeutically relevant aspects in bone repair and regeneration. Mater Today. 2015;18(10):573–89.

5.   Martin F, Linden T, Katschinski DM, Oehme F, Flamme I, Mukhopadhyay CK, et al. Copper-dependent activation of hypoxia-inducible factor (HIF)-1: Implications for ceruloplasmin regulation. Blood. 2005;105(12):4613–9.

6.   Yuan Y, Hilliard G, Ferguson T, Millhorn DE. Cobalt inhibits the interaction between hypoxia-inducible factor-α and von Hippel-Lindau protein by direct binding to hypoxia-inducible factor-α. J Biol Chem. 2003;278(18):15911–6.

7.   Kargozar S, Baino F, Hamzehlou S, Hill RG, Mozafari M. Bioactive Glasses: Sprouting Angiogenesis in Tissue Engineering. Trends Biotechnol. 2018;36(4):430–44.

8.   Zhang W, Chang Q, Xu L, Li G, Yang G, Ding X, et al. Graphene Oxide-Copper Nanocomposite-Coated Porous CaP Scaffold for Vascularized Bone Regeneration via

Activation of Hif-1α. Adv Healthc Mater. 2016;5(11):1299–309.

9. Rath SN, Brandl A, Hiller D, Hoppe A, Gbureck U, Horch RE, et al. Bioactive copper-doped glass scaffolds can stimulate endothelial cells in co-culture in combination with mesenchymal stem cells. PLoS One. 2014;9(12):1–24.

10. Kulanthaivel S, Roy B, Agarwal T, Giri S, Pramanik K, Pal K, et al. Cobalt doped proangiogenic hydroxyapatite for bone tissue engineering application. Mater Sci Eng C. 2016;58:648–58.

11. Quinlan E, Partap S, Azevedo MM, Jell G, Stevens MM, O'Brien FJ. Hypoxia-mimicking bioactive glass/collagen glycosaminoglycan composite scaffolds to enhance angiogenesis and bone repair. Biomaterials. 2015;52(1):358–66.

12. Deng Z, Lin B, Jiang Z, Huang W, Li J, Zeng X, et al. Hypoxia-mimicking cobalt-doped borosilicate bioactive glass scaffolds with enhanced angiogenic and osteogenic capacity for bone regeneration. Int J Biol Sci. 2019;15(6):1113–24.

13. Hu GF. Copper stimulates proliferation of human endothelial cells under culture. J Cell Biochem. 1998;69(3):326–35.

14. Li S, Xie H, Li S, Kang YJ. Copper stimulates growth of human umbilical vein endothelial cells in a vascular endothelial growth factor-independent pathway. Exp Biol Med. 2012;237(1):77–82.

15. Stähli C, Muja N, Nazhat SN. Controlled copper ion release from phosphate-based glasses improves human umbilical vein endothelial cell survival in a reduced nutrient environment. Tissue Eng - Part A. 2013;19(3–4):548–57.

16. Feng W, Ye F, Xue W, Zhou Z, Kang YJ. Copper regulation of hypoxia-inducible factor-1 activity. Mol Pharmacol. 2009;75(1):174–82.

17. Zan T, Du Z, Li H, Li Q, Gu B. Cobalt chloride enhances angiogenic potential of CD133 cells. Front Biosci. 2012;17:2247–58.

18. Nakayama M, Takahashi K, Kitamuro T, Yasumoto KI, Katayose D, Shirato K, et al. Repression of heme oxygenase-1 by hypoxia in vascular endothelial cells. Biochem Biophys Res Commun. 2000;271(3):665–71.

19. Peters K, Schmidt H, Unger RE, Kamp G, Pröls F, Berger BJ, et al. Paradoxical effects of hypoxia-mimicking divalent cobalt ions in human endothelial cells in vitro. Mol Cell Biochem. 2005;270(1–2):157–66.

20. Chai YC, Mendes LF, van Gastel N, Carmeliet G, Luyten FP. Fine-tuning pro-angiogenic effects of cobalt for simultaneous enhancement of vascular endothelial growth factor secretion and implant neovascularization. Acta Biomater. 2018;72:447–60.

21. Wu C, Zhou Y, Xu M, Han P, Chen L, Chang J, et al. Copper-containing mesoporous bioactive glass scaffolds with multifunctional properties of angiogenesis capacity, osteostimulation and antibacterial activity. Biomaterials. 2013;34(2):422–33.

22. Perez RA, Kim JH, Buitrago JO, Wall IB, Kim HW. Novel therapeutic core-shell hydrogel scaffolds with sequential delivery of cobalt and bone morphogenetic protein-2 for synergistic bone regeneration. Acta Biomater. 2015;23:295–308.

23.   J.Rodríguez P, Ros S, Gonzlez M. Modulation of the proliferation and differentiation of human mesenchymal stem cells by copper. J Cell Biochem. 2002;85(1):92–100.

24.   Li S, Wang M, Chen X, Li SF, Li-Ling J, Xie HQ. Inhibition of osteogenic differentiation of mesenchymal stem cells by copper supplementation. Cell Prolif. 2014;47(1):81–90.

25.   Schröck K, Lutz J, Mändl S, Hacker MC, Kamprad M, Schulz-Siegmund M. Co(II)-mediated effects of plain and plasma immersion ion implanted cobalt-chromium alloys on the osteogenic differentiation of human mesenchymal stem cells. J Orthop Res. 2015;33(3):325–33.

26.   Pizzorno J. Glutatione! Integr Med. 2014;13(1):8–12.

27.   Alim I, Haskew-Layton RE, Aleyasin H, Guo H, Ratan RR. Spatial, temporal, and quantitative manipulation of intracellular hydrogen peroxide in cultured cells. 1st ed. Vol. 547, Methods in Enzymology. Elsevier Inc.; 2014. 251–273 p.

28.   Gaetke LM, Chow CK. Copper toxicity, oxidative stress, and antioxidant nutrients. Toxicology. 2003;189(1–2):147–63.

29.   Zou W, Yan M, Xu W, Huo H, Sun L, Zheng Z, et al. Cobalt chloride induces PC12 cells apoptosis through reactive oxygen species and accompanied by AP-1 activation. J Neurosci Res. 2001;64(6):646–53.

30.   Pulido MD, Parrish AR. Metal-induced apoptosis: Mechanisms. Mutat Res - Fundam Mol Mech Mutagen. 2003;533(1–2):227–41.

31.   Valko M, Morris H, Cronin M. Metals, Toxicity and Oxidative Stress. Curr Med Chem. 2005;12(10):1161–208.

32.   Culotta VC, Yang M, O'Halloran T V. Activation of superoxide dismutases: Putting the metal to the pedal. Biochim Biophys acta-molecular cell Res. 2006;1763(7):747–58.

33.   Yu H, Pastor SA, Lam K, Yee RW. Ascorbate-enhanced copper toxicity on bovine corneal endothelial cells in vitro. Curr Eye Res. 1990;9(2):177–82.

34.   Lertkiatmongkol P, Liao D, Mei H, Hu Y, Newman PJ. Endothelial functions of PECAM-1 (CD31). Curr Opin Hematol. 2016;23(3):253–9.

35.   DeLisser HM, Christofidou-Solomidou M, Strieter RM, Burdick MD, Robinson CS, Wexler RS, et al. Involvement of endothelial PECAM-1/CD31 in angiogenesis. Am J Pathol. 1997;151(3):671–7.

36.   Yang S, Graham J, Kahn JW, Schwartz EA, Gerritsen ME. Functional roles for PECAM-1 (CD31) and VE-cadherin (CD144) in tube assembly and lumen formation in three-dimensional collagen gels. Am J Pathol. 1999;155(3):887–95.

37.   Cao G, O'Brien CD, Zhou Z, Sanders SM, Greenbaum JN, Makrigiannakis A, et al. Involvement of human PECAM-1 in angiogenesis and in vitro endothelial cell migration. Am J Physiol - Cell Physiol. 2002;282(5 51-5).

38.   Short SM, Talbott GA, Juliano RL. Integrin-mediated signaling events in human endothelial cells. Mol Biol Cell. 1998;9(8):1969–80.

39.   Peters K, Unger RE, Barth S, Gerdes T, Kirkpatrick CJ. Induction of apoptosis in human microvascular endothelial cells by divalent cobalt ions. Evidence for integrin-mediated

signaling via the cytoskeleton. J Mater Sci Mater Med. 2001;12(10–12):955–8.

40.   Teti G, Focaroli S, Salvatore V, Mazzotti E, Ingra L, Mazzotti A, et al. The hypoxia-mimetic agent cobalt chloride differently affects human mesenchymal stem cells in their chondrogenic potential. Stem Cells Int. 2018;2018(3237253).

41.   Stavely R, Nurgali K. The emerging antioxidant paradigm of mesenchymal stem cell therapy. Stem Cells Transl Med. 2020;9(9):985–1006.

42.   Grayson WL, Zhao F, Bunnell B, Ma T. Hypoxia enhances proliferation and tissue formation of human mesenchymal stem cells. Biochem Biophys Res Commun. 2007;358(3):948–53.

43.   Fehrer C, Brunauer R, Laschober G, Unterluggauer H, Reitinger S, Kloss F, et al. Reduced oxygen tension attenuates differentiation capacity of human mesenchymal stem cells and prolongs their lifespan. Aging Cell. 2007;6(6):745–57.

44.   Zhou J, Zhao L. Hypoxia-mimicking Co doped TiO2 microporous coating on titanium with enhanced angiogenic and osteogenic activities. Acta Biomater. 2016;43:358–68.

45.   Zhou J, Schmid T, Schnitzer S, Brüne B. Tumor hypoxia and cancer progression. Cancer Lett. 2006;237(1):10–21.

46.   Schamel M, Bernhardt A, Quade M, Würkner C, Gbureck U, Moseke C, et al. Cu2 +, Co2 + and Cr3 + doping of a calcium phosphate cement influences materials properties and response of human mesenchymal stromal cells. Mater Sci Eng C. 2017;73:99–110.

47.   Hsu SH, Chen CT, Wei YH. Inhibitory effects of hypoxia on metabolic switch and osteogenic differentiation of human mesenchymal stem cells. Stem Cells. 2013;31(12):2779–88.

48.   Chen C-T, Shih Y-R V., Kuo TK, Lee OK, Wei Y-H. Coordinated Changes of Mitochondrial Biogenesis and Antioxidant Enzymes During Osteogenic Differentiation of Human Mesenchymal Stem Cells. Stem Cells. 2008;26(4):960–8.

CHAPTER 4

First approximation of microparticle development method and their encapsulation within fibers as dual drug delivery system

CHAPTER 4. First approximation of microparticle development method and their encapsulation within fibers as dual drug delivery system

4.1.   Introduction

Bone tissue has the ability of self-regeneration in response to small size damage, although it is unable to regenerate tissue damage with a size higher than 2.5 cm (1). In this last case, clinical intervention using autologous or allogeneic bone grafts have been the gold standard treatment for a long time, although they possess some disadvantage such as availability of the graft, possible immune response and possible risk of disease transmission (2,3). Therefore, the development of synthetic grafts for bone tissue engineering (BTE) emerged as an alternative source for bone regeneration. First attempts in BTE resulted in the use of biological inert materials to just fill the bone defect volume (4). Over the years, those scaffolds have evolved to meet some characteristics: i) they should be biocompatible; ii) biodegradable, presenting predictable degradation rate similar to the regeneration rate; iii) porous, to allow cell ingrowth and nutrient and oxygen diffusion; iv) ability to promote osteogenic differentiation; and v) preferable with a customized shape in order to fill different bone defects (5,6). Moreover, because bone regeneration involves multiple steps (inflammation, angiogenesis, chemotaxis and osteogenesis) and multiple signaling molecules through them, scaffolds developed as multi drug delivery systems (DDS) have been considered more effective. More in detail, these DDS offer the possibility to deliver different therapeutic molecules encapsulated in different compartments in a time-dependent manner. Scaffold compartmentalization is achieved with core-shell microsphere or fiber structures (7) or by combining different formulations of biomaterials (nano/microparticles, fibers and hydrogels), for instance, microspheres embedded within fibers or within hydrogels, fibers within hydrogels, to mention a few (8). With these approaches, usually, the molecules incorporated in the outer part of the scaffold are firstly released, whereas molecules encapsulated in the inner part are delivered afterwards. Therefore, DDS have made possible to mimic different phases of bone regeneration. For instance, Hsu *et al*., developed poly(D,L)-lactide-*co*-glycolide (PLGA) core-shell nanofibers where vancomycin and ceftazidime, two antibiotics, were encapsulated in the shell, and the osteogenic growth factor BMP-2 in the core (9), with the scope to avoid infection and stimulate osteogenesis. Results demonstrated dual delivery of these molecules, avoiding bacteria growth and enhancing osteogenic differentiation with enhanced ALP activity. As another example, in order to stimulate angiogenesis followed by osteogenesis, Kanczler *et al*., developed alginate fibers embedded in PLA matrix containing VEGF and BMP-2, respectively

(10). VEGF was first released from day 7, and thereafter, BMP-2 was released up to 28 days, demonstrating an increased bone formation with an *in vivo* femoral bone mouse defect.

Generally, growth factors or antibiotics have been extensively incorporated in DDS. However, they have some drawbacks. More specifically, antibiotics can induce antimicrobial resistance, considered one of the biggest threats to global health according to World Health Organization (11), and growth factors have delicate handling properties and short half-life. As an alternative, some ions have been considered as another attractive option as they have been described to induce therapeutic effects, with the ability to regulate cellular functions, and at the same time, presenting higher stability (12). For instance, examples of therapeutic roles are anti-bacterial, described with silver, copper, zinc, gallium (13); anti-inflammatory, reported with magnesium or zinc (14,15); angiogenic, demonstrated with copper, cobalt and silicon (16); or osteogenic, described with silicon, zinc or strontium (12,16).

This chapter describes an alternative approach to develop osteogenic microparticles in an easy and feasible way. The diameter of microcarriers have been previously described to have an influence in cell adhesion, being the range of 100-400 µm appropriate for cell attachment (17). Moreover, we embedded them within fibers in order to develop a DDS. As a *proof of concept* of the material design as a DDS, we incorporated two different therapeutic ions, within microparticles and through the fiber, to study their behavior release, in order to stimulate early regeneration phases of bone.

4.2.   Objectives

The main objective of this chapter was to develop a dual drug delivery system. For this purpose, we first aimed to develop osteogenic alginate/hydroxyapatite (HA) composite microparticles and embed them in alginate monofibers. As a second objective, we aimed to introduce bioactive properties in this system by doping it with two therapeutic ions, subsequently modulating their dual release. Schematic representation of dual ion delivery system is shown in **Figure 1**.
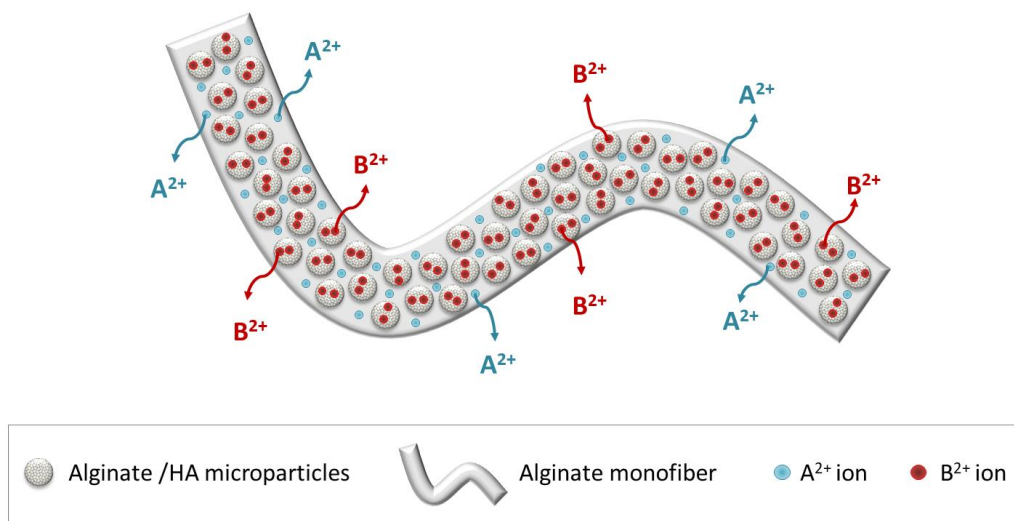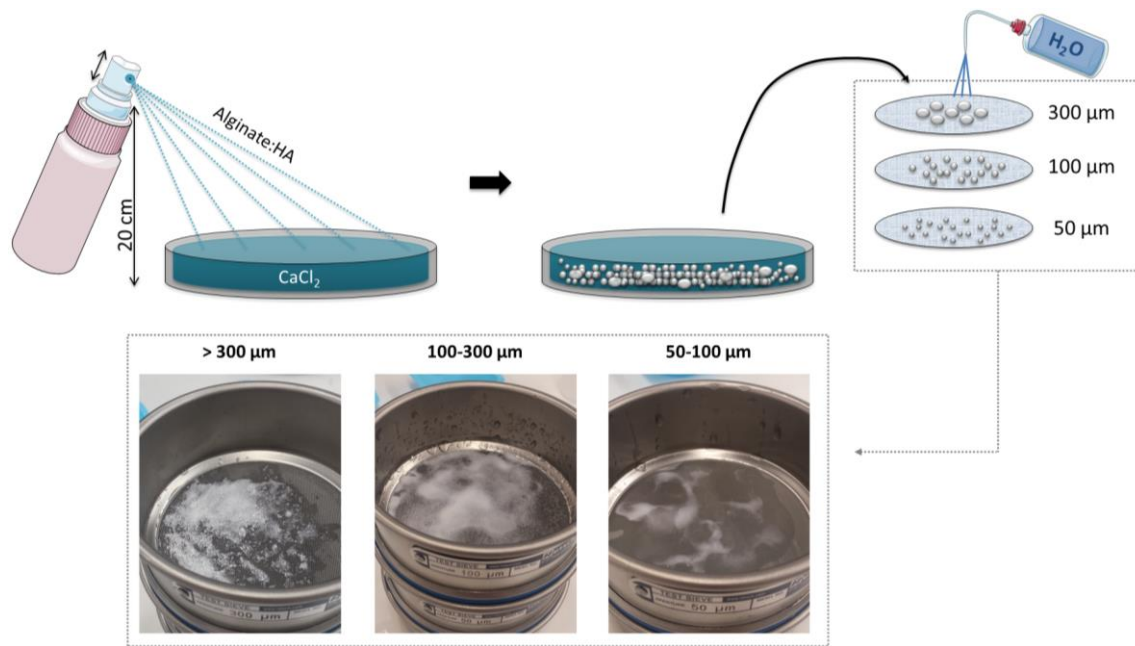
Figure 1. Schematic representation of dual ion delivery system. Alginate monofibers containing a therapeutic ion (A^{2+}) and with embedded microspheres made of hydroxyapatite (HA) and alginate blend containing another therapeutic ion (B^{2+}).

4.3.   Materials & Methods

For the development and optimization of alginate/HA microparticles and alginate monofibers, we used calcium (Ca^{2+}) as a model ion for the cross-linking. After the optimization, therapeutic ions were introduced.

4.3.1. Microparticle development

As a first step, we optimized microparticle development, composed of mixtures of alginate with hydroxyapatite (HA). To this purpose, we first determined the minimum alginate concentration that allowed microparticle gelation once in contact with $CaCl_2$ (Sigma-Aldrich) solution. Then, different amounts of hydroxyapatite (particle size 2.5 μm, Sigma-Aldrich) were added, with ratios %w/w alginate:HA of 1:0, 1:4 and 1:40, dissolved with mili-Q H_2O. The resultant mixture was introduced in a fingertip spray bottle (DDBiolab). Microparticles were generated by spraying the sample into 300 mL of 150 mM $CaCl_2$ contained within a non-adhesive circular container within 20 cm of distance (**Figure 2**). Once the sprayed solution got in contact with the surface of $CaCl_2$, instant crosslinking occurred. After 5 min of incubation, microparticles were sieved with 300, 100 and 50 μm pore size meshes (DDBiolab) and with the aid of mili-Q H_2O. Fractioned microparticles in the range of 50-100 μm and 100-300 μm were kept with mili-Q H_2O and used thereafter.

Figure 2. Schematic representation of microparticles development. A blend of alginate with hydroxyapatite is sprayed into 150 mM calcium chloride and incubated for 5 min. Then, microparticles are sieved with meshes with pore size of 300 μm, 100 μm and 50 μm.

### 4.3.2. Characterization of microparticles size distribution

The size distribution of sieved microparticles was assessed by Laser diffraction. Briefly, a laser beam passes through microparticles dispersed in mili-Q H_2O. The angle of light scattered is inversely proportional to particle size (for instance, the larger the particle size, the smaller the angle of light scattered). Initially, in order to see the particle size distribution of the prepared microparticles, we evaluated the size distribution of the different ratios tested (1:0, 1:4 and 1:40). Then, we analyzed the particle size distribution of the sieved microparticles in order to confirm that the size distribution was in the range we expected. We sprayed three times the different ratios to obtain three triplicates per condition. Samples were measured using the Universal Liquid Module of LS13320 (Beckman).

4.3.3. Fiber development

As a second step, we optimized alginate fiber development. To this purpose, we used several parameters, which included alginate concentration, syringe needle and injection speed. Schematic representation of sodium alginate fiber development is shown in **Figure 3.** First, sodium alginate (PanReac Applichem) was dissolved with mili-Q H_2O at ratios that allowed fiber shape structure when extruded and, at the same time, that allowed their handling manipulation. Then, it was loaded in a 5 mL syringe (Becton Dickinson). A volume of 0.2 mL of alginate solution was extruded in a 150 mM $CaCl_2$ crosslinking solution through different sizes

of syringe needles. More specifically, the sizes tested were 20G ($\varnothing_{out}$: 0.9 mm; $\varnothing_{in}$: 0.65 mm), 25G ($\varnothing_{out}$: 0.5 mm; $\varnothing_{in}$: 0.32 mm), 26G ($\varnothing_{out}$: 0.46 mm; $\varnothing_{in}$: 0.26 mm) and 27G ($\varnothing_{out}$: 0.4 mm; $\varnothing_{in}$:

0.22 mm) (Becton Dickinson). Different constant injection speeds (10, 50, 100 and 150 ml/h) were studied with the aid of an infusion syringe pump (KD Scientific). After 5 min of incubation with CaCl$_2$, three washes with mili-Q H$_2$O were made to remove the excess of ions. Then, they were stored with mili-Q H$_2$O. There were three triplicates per condition and captures of them were performed with Stereo Microscope (Zeiss). Ten measurements of the diameter per fiber were made to assess how the concentration of alginate, the syringe needle size and the injection speed affected the size of the fiber.
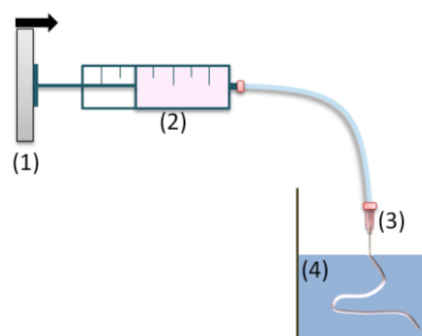
Figure 3. Schematic representation of alginate fiber development. An infusion syringe pump (1) was used to control the injection speed for the extrusion of alginate (2) through a syringe needle (3) into calcium chloride solution (4).
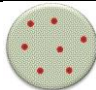
4.3.4. Development of drug delivery system

We chose copper (Cu^{2+}) (CuCl$_2$, Sigma-Aldrich) and cobalt (Co^{2+}) (CoCl$_2$, Sigma-Aldrich) as therapeutic ions to be incorporated within alginate/HA microparticles and alginate fibers, respectively. Although fiber and microparticle optimization was performed with Ca^{2+}, it was assumed the same outcome when Cu^{2+} or Co^{2+} were incorporated, as Ca^{2+} still remained as the majority ion.

For the incorporation of Cu^{2+} within alginate/HA microparticles, different combinations of Ca^{2+} and Cu^{2+} were incorporated in the crosslinking solutions, shown in **Table 1,** following the same procedure explained in *section 4.3.1*.

Table 1. Crosslinking solution composition for alginate/HA microparticle formation. Concentration of divalent cations of Ca^{2+} and Cu^{2+} was varied to crosslink alginate with HA and incorporate Cu^{2+}.
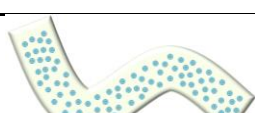
Sample code	CaCl$_2$ (mM)	CuCl$_2$ (mM)	Schematic representation
150Ca/0Cu	150	0	
149Ca/1Cu	149	1	
140Ca/10Cu	140	10	

In order to incorporate Co^{2+} within alginate fiber, different combinations of Ca^{2+} and Co^{2+} were incorporated in the crosslinking solution, shown in **Table 2**, following the procedure described in *section 4.3.3*.

Table 2. Crosslinking solution composition for alginate fiber formation. Concentration of divalent cations of Ca^{2+} and Co^{2+} was varied to crosslink alginate and incorporate Co^{2+}.
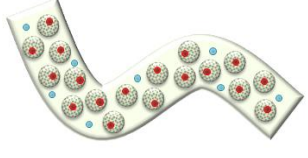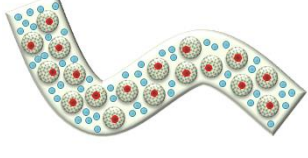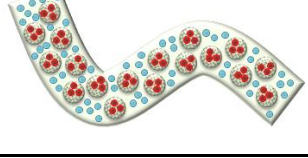
Sample code	CaCl$_2$ (mM)	CoCl$_2$ (mM)	Schematic representation
150Ca/0Co	150	0	
149Ca/1Co	149	1	
140Ca/10Co	140	10	

Different amounts of microspheres were incorporated into the fiber by mixing them with alginate fiber solution by volume (%v/v), until the alginate fiber could contain the maximum microspheres without jeopardizing the fiber structure. In all cases, the final concentration of alginate fiber was the one previously optimized that allowed its handling manipulation. The size of fibers with the maximum amount of microparticles incorporated was measured.

4.3.5. Release of cobalt and copper

The ion release of different combinations of Ca^{2+} and Cu^{2+} from alginate/HA microparticles embedded within alginate fibers cross-linked with different combinations of Ca^{2+} and Co^{2+} were studied. Different combinations of ions are shown in **Table 3**.

Table 3. Different combinations of Ca^{2+}, Cu^{2+} and Co^{2+} in crosslinking solutions of alginate/HA microparticles and alginate fibers.

Sample code	Microparticle crosslinking solution		Fiber crosslinking solution		Schematic representation
	$CaCl_2$ (mM)	$CuCl_2$ (mM)	$CaCl_2$ (mM)	$CoCl_2$ (mM)	
150Ca/0Cu – 150Ca/0Co	150	0	150	0	
149Ca/1Cu – 149Ca/1Co	149	1	149	1	
149Ca/1Cu – 140Ca/10Co	149	1	140	10	
140Ca/10Cu – 149Ca/1Co	140	10	149	1	
140Ca/10Cu – 140Ca/10Co	140	10	140	10	

The ion release study was performed under sterile conditions. Briefly, alginate and hydroxyapatite powders were sterilized under 3 rounds of 15 min each one with UV. After sterilization, they were resuspended with mili-Q H_2O previously filtered with 0.2 μm filters. Crosslinking solutions of $CaCl_2$, $CuCl_2$ and $CoCl_2$ were also filtered with 0.2 μm filters for their sterilization. The fingertip spray bottle, the mili-Q H_2O container and meshes were sterilized with gas plasma (Johnson & Johnson). The non-adhesive circular container was autoclaved.

For each condition, triplicates of 0.15 ml of alginate fibers containing microparticles were extruded and after 5 min of incubation, they were soaked 3 times with cell culture media to remove the excess of ions. Subsequently, each fiber was incubated with 1 mL of endothelial growth medium (EGM-2) (Lonza) at 37ºC for a total duration of 7 days. Supernatants were collected at 1, 3, 5 and 7 days. For their analysis, each mL of supernatant was diluted with 9 mL of 2% HNO_3 (dilution 1:10), and kept at 4ºC until analysis. The release of Ca^{2+} ions were analyzed with inductively coupled plasma – optical emission spectrometry (ICP-OES) and the release of Cu^{2+} and Co^{2+} were analyzed with inductively coupled plasma – mass spectrometry (ICP-MS). Cell culture media without fiber incubation was used as blank.

4.3.6. Statistical analysis

Statistical analysis was performed using SPSS software (SPSS v21, IBM). Kruskal-Wallis and Mann Whitney U non-parametric tests were used to compare microparticle mean size from different microparticle compositions and the size of pristine alginate fibers and fibers with the maximum microparticles incorporated. Statistically significant differences were considered with $p<0.05$.

4.4.   Results

4.4.1. Microparticle size distribution

For microparticle development, we aimed to use the minimum alginate concentration that allowed alginate microparticle formation, which was found to be 0.5% (% wt). From this point on, we increased HA amount to determine until which amount was possible to spray. We found that the ratio of alginate:HA of 1:50 presented difficulties of being sprayed and partially obstructed the fingertip spray, but up to 1:40 could be easily sprayed. To assess if this method was reproducible to develop microparticles, we analyzed triplicates of the size distribution of them with an alginate:HA ratio of 1:0, 1:4 and 1:40.

Un-sieved microparticles of ratios 1:0, 1:4 and 1:40 did not present differences in the mean size (**Figure 4**). However, sieved microparticles presented significantly differences between different microparticles compositions. More in detail, microparticles in the range 50-100 μm presented smaller mean size when HA mount was increased, whereas microparticles in the range of 100-300 μm the higher mean size was obtained with 1:4 instead of 1:0. In both size ranges, the 1:40 ratio presented the smaller mean size, being 85.3 ±2.8 μm with 50-100 μm size range and 253.6 ±2.0 μm with 100-300 μm size range. Moreover, the coefficient of

variation obtained was low in all compositions tested, indicating reproducibility of this technique.
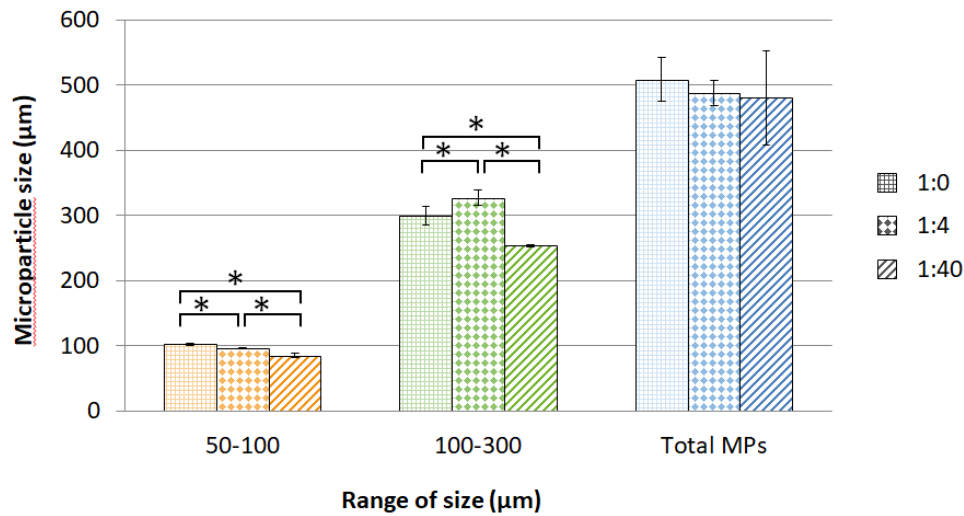
Figure 4. Mean size of microparticles. Representation of mean size of sieved and non-sieved alginate:HA microparticles with different compositions (1:0, 1:4 and 1:40). Abbreviations: MPs = microparticles.
*Statistically significant differences ($p<0.05$).

Size distributions of non-sieved and sieved microparticles showed practically an overlap between triplicates with all compositions tested (microparticles sprayed in three different times), further demonstrating the reproducibility of this technique (**Figure 5**).
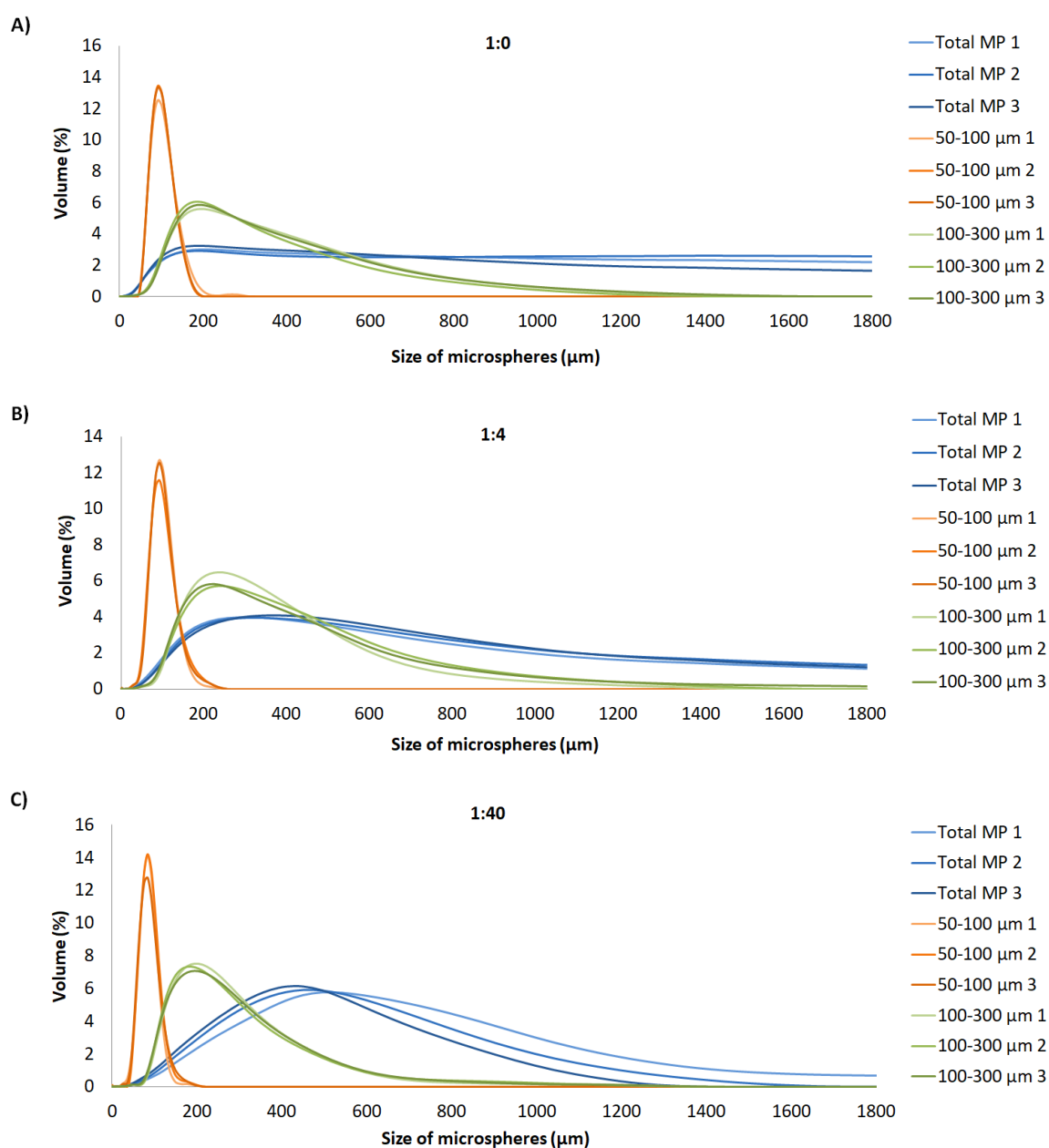
Figure 5. Alginate/HA microparticle size distribution. Triplicate size distribution of un-sieved and sieved microparticles of alginate:HA A) 1:0, B) 1:4 and C) 1:40. Abbreviations: MP = microparticle.

After sieving the microparticles, we assessed the percentage of microparticles that had a size between 50-100 µm and 100-300 µm within the microparticles obtained in the range of 50-100 µm and 100-300 µm, respectively. With the ratio 1:0, the respective amounts with 50-100 µm and 100-300 µm were 63.3 ± 1.4% and 63.1 ± 5.2%, respectively (**Figure 6**). For image capture, microparticles were stained with red ink for a better visualization.
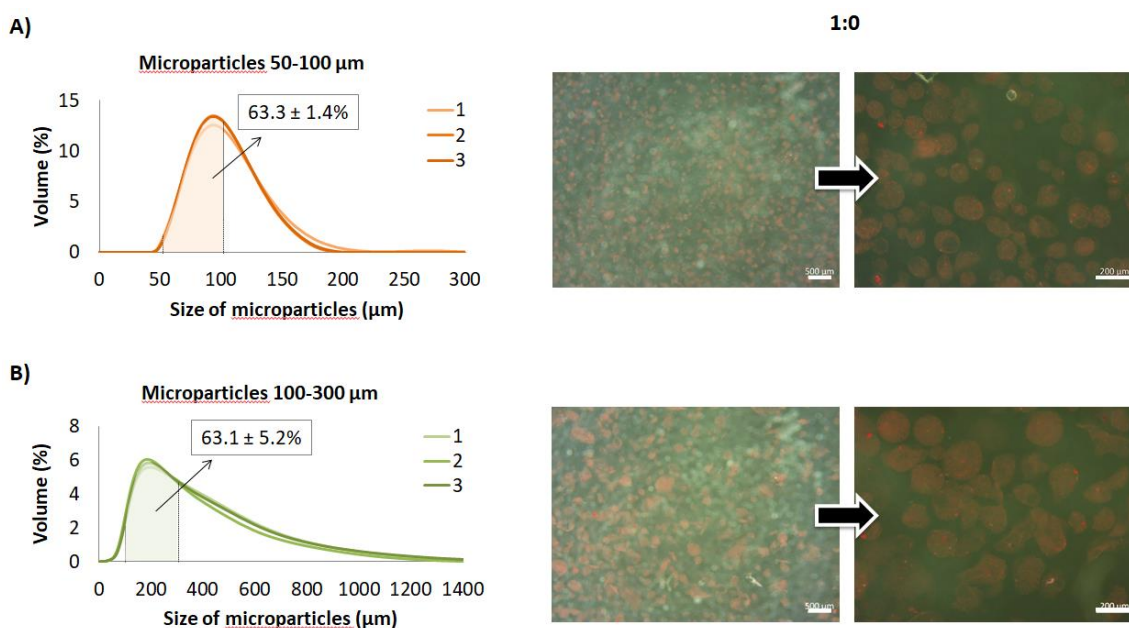
Figure 6. Sieved microparticles alginate:HA 1:0. A) Triplicates of sieved microparticles between 50-100 μm. Left: percentage of microparticles between 50-100 μm is represented in the size distribution graph. Right: stereomicroscope images of the microparticles (stained with red ink for their visualization). B) Triplicates of sieved microparticles between 100-300 μm. Left: percentage of microparticles between 100-300 μm is represented in the size distribution graph. Right: stereomicroscope images of the microparticles (stained with red ink for their visualization). Scale bar: 500 μm and for magnification 200 μm.

With the ratio 1:4, the amount obtained were 61.1 ± 3.8% and 56.9 ± 3.0% with 50-100 μm and 100-300 μm sieved microparticles, respectively (**Figure 7**).
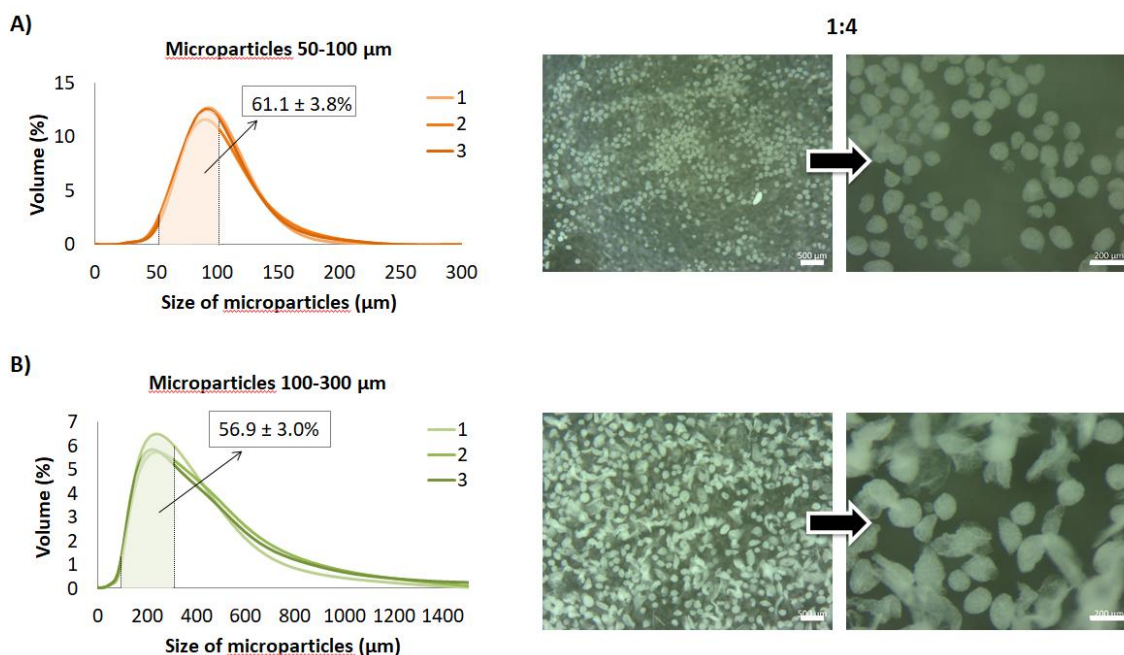
Figure 7. Sieved microparticles alginate:HA 1:4. A) Triplicates of sieved microparticles between 50-100 μm. Left: percentage of microparticles between 50-100 μm is represented in the size distribution graph.

Right: stereomicroscope images of the microparticles. B) Triplicates of sieved microparticles between 100-300 μm. Left: percentage of microparticles between 100-300 μm is represented in the size distribution graph. Right: stereomicroscope images of the microparticles. Scale bar: 500 μm and for magnification 200 μm.

Finally, with the ratio 1:40, an amount of 75.4 ± 2.1% and 71.5 ± 1.3% were obtained with 50-100 μm and 100-300 μm sieved microparticles, respectively (**Figure 8**).
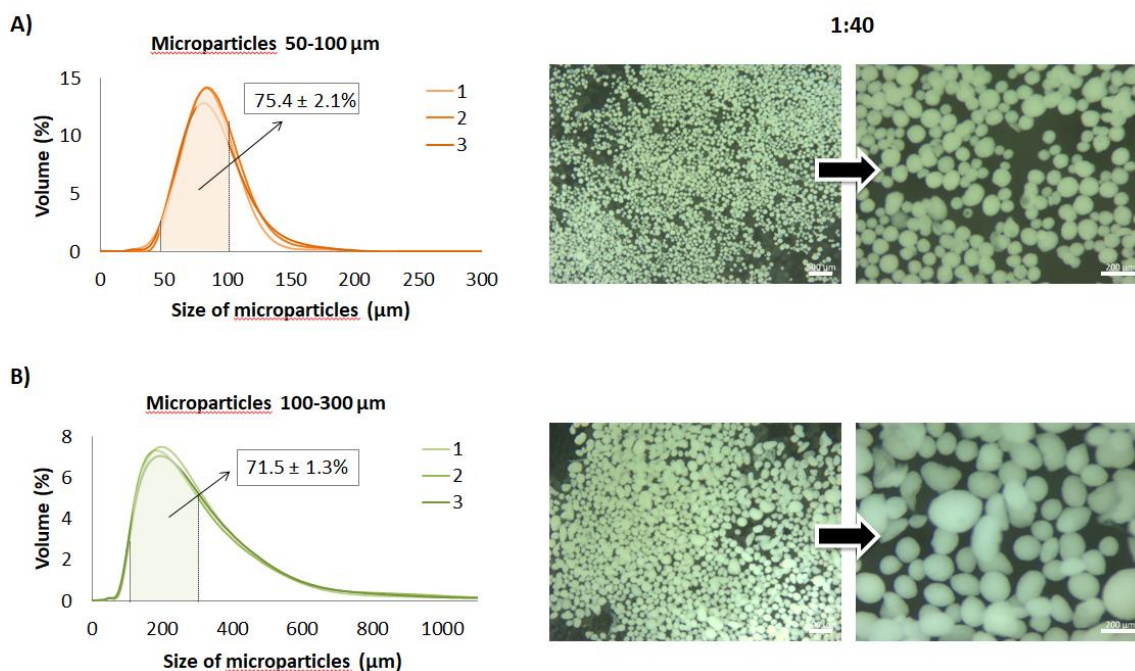
Figure 8. Sieved microparticles alginate:HA 1:40. A) Triplicates of sieved microparticles between 50-100 μm. Left: percentage of microparticles between 50-100 μm is represented in the size distribution graph. Right: stereomicroscope images of the microparticles. B) Triplicates of sieved microparticles between 100-300 μm. Left: percentage of microparticles between 100-300 μm is represented in the size distribution graph. Right: stereomicroscope images of the microparticles. Scale bar: 500 μm and for magnification 200 μm.

When observing the stereomicroscope images of the microparticles, in general 50-100 μm microparticles presented homogeneity and sphericity in all compositions (**Figure 6A, Figure 7A** and **Figure 8A**). By way of contrast, the ratio 1:40 maintained the morphology more spherical with the size range of 100-300 μm compared with 1:4 and 1:0 (**Figure 6B, Figure 7B** and **Figure 8B**). It is worth to mention that we could manipulate those microparticles without jeopardizing their structure. However, if we pressed the microparticles strongly they eventually broke, probably due to low alginate concentration.

For further experiment analysis, we considered to use the alginate:HA ratio of 1:40, as it allows the maximum hydroxyapatite incorporation. Furthermore, we selected the size range of 100-300 μm to be used for subsequently assays, as it is described to be the appropriate size to allow cell adhesion and tissue ingrowth.

4.4.2. Alginate fiber size

One of the second things that we wanted to determine was the size of alginate fibers. For this purpose, we assessed how different variables (alginate concentration, needle diameter (G) and injection speed) affected the final alginate fiber diameter, in order to choose the most appropriate parameters to encapsulate microparticles within them.

Regarding the injection speed, in general we could observe that its increase resulted in an increase of alginate fiber diameter as represented in **Figure 9**. The lowest concentration of alginate of 0.5%, in general presented higher diameters compared to 1.5% concentration. Moreover, 0.5% presented higher standard deviation and coefficient of variation in more than half of the conditions compared to 1.5%, suggesting higher homogeneity of fiber size with 1.5% alginate (**Figure 9**). Moreover, needle G also presented an effect on the final fiber diameter, obtaining the higher sizes with the higher inner diameter of the needle (20G) (**Figure 9**).
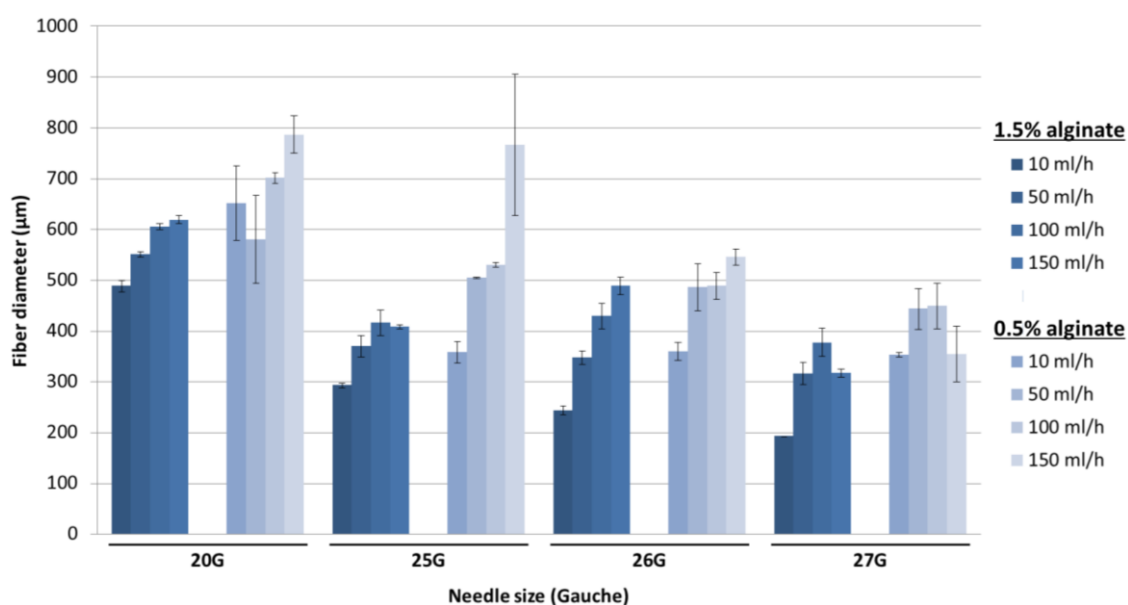
Figure 9. Alginate fiber size. Representation of alginate fiber size depending on alginate concentration, needle gauche and injection speed.

As we aimed to obtain microparticles with a maximum size of 300 μm and incorporate them within alginate fibers, we decided to use 20G needles as they have an inner diameter of 650 μm and it would avoid possible obstructions. We decided to use 1.5% alginate concentration as it presented more fiber size homogeneity and at the same time, it possessed higher mechanical properties to allow handling manipulation without breaking compared to 0.5%. Finally, as previously mentioned, we observed that alginate/HA microparticles could break

when we applied pressure on them. Therefore, 100 and 150 mL/h of injection speed were considered too high with the possibility of damaging microparticle structure when extruded due to high shear stress. Alternatively, 10 and 50 mL/h present lower and similar flow rate, so we decided to use 50 mL/h as that would be less time consuming. Additionally, the fiber size obtained with 50 ml/h is higher than 10 ml/h, specifically 550.5 µm and 488.7 µm, respectively, therefore providing more space to accommodate big size microparticles.

4.4.3. Microparticle incorporation within alginate fibers

Finally, we aimed to incorporate the maximum microparticle size of 100-300 µm with the composition 1:40 within alginate fiber. For this purpose, we started incorporating 10% (%v/v) and gradually increased the amount. An amount of 60% (% v/v) resulted in fiber rupture while extruding it and needle obstruction. A final amount of 50% (% v/v) was the maximum that could be incorporated within alginate fiber without rupture and needle obstruction, and also could maintain homogeneous diameter size as shown in **Figure 10**. The size of alginate fibers containing 50% of 1:40 microparticles was 595.8 ± 25.9 µm, which was statistically significant higher than pristine alginate fibers, which had a size of 550.5 ± 23.8 µm (p<0.01). For further experiments, we encapsulated microparticles within fibers with a ratio of 50 % (v/v). It is worth to mention that with this amount of microparticles loaded, they were close to the surface with an almost direct contact to the exterior.
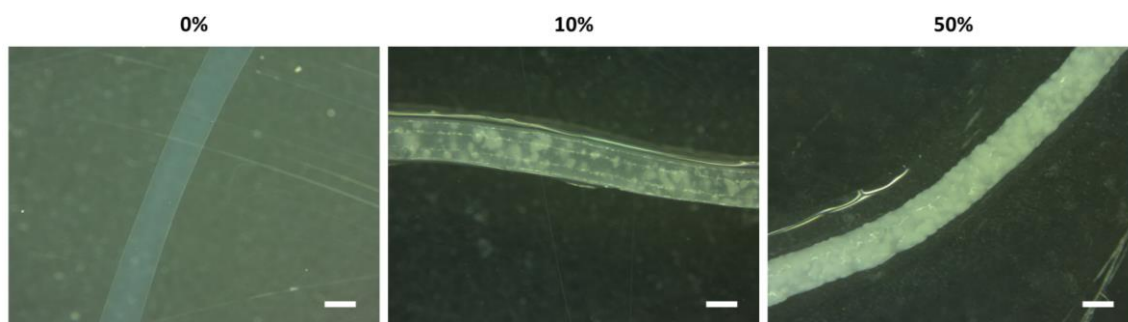
Figure 10. Incorporation of alginate/HA composite microparticles within alginate fibers. Images of pristine alginate fibers (left), the minimum (10%) amount of microparticles incorporated (% v/v) (middle) and maximum amount (50%) that could be incorporated avoiding fiber rupture (right). Scale bar = 500 µm.

4.4.4. Ion release

To further assess the possibility to use the alginate/HA composite microparticles embedded within alginate fibers as an ion delivery system, we chose Cu^{2+} and Co^{2+} as therapeutic ions to study their release, incorporating them in the crosslinking solutions as described in **Table 3.** As it was observed that microparticles were close to the fiber surface, we hypothesized that the

ion incorporated would have a direct release. Therefore, as Cu^{2+} has been described as antibacterial and Co^{2+} as angiogenic, we incorporated Cu^{2+} in the microparticles and Co^{2+} in the alginate fiber, to provide the DDS with anti-bacterial and angiogenic properties. Moreover, as Ca^{2+} was also introduced in the crosslinking solution to maintain the total ion concentration to 150 mM, its release was also studied.

In general, Ca^{2+} and Cu^{2+} presented a burst release profile, whereas Co^{2+} presented a more sustained release close to zero order kinetics. More in detail, when Co^{2+} and Cu^{2+} where not incorporated in the DDS, Ca^{2+} showed the maximum concentration delivered (**Figure 11A**). With the minimum incorporation of Co^{2+} and Cu^{2+}, specifically 1 mM in their respective crosslinking solution, the release of calcium was reduced (**Figure 11B**). Interestingly, the concentrations of Cu^{2+} delivered were higher than Co^{2+}. As expected, maintaining the concentration of Cu^{2+} and increasing the concentration of Co^{2+} to 10 mM, the concentrations of Ca^{2+} was reduced whereas the concentrations and release profile of Cu^{2+} were maintained (**Figure 11C**). Curiously, Co^{2+} presented a zero order kinetics release, with higher concentrations delivered compared to Cu^{2+} at the end of the experiment. Unexpectedly, when Cu^{2+} concentrations were increased up to 10 mM in the crosslinking solution and Co^{2+} reduced to 1 mM, the amount of Cu^{2+} released was higher than Ca^{2+} (**Figure 11D**). Moreover, the amount of Co^{2+} released was lower compared to the previous condition where the same amount of Co^{2+} was incorporated (**Figure 11B** and **D**). Finally, when the concentration of Co^{2+} was also increased up to 10 mM in the crosslinking solution, the amount and release of Cu^{2+} was maintained the same as the previous condition where the same amount was introduced (**Figure 11D** and **Figure 11E**). Additionally, the amount of Ca^{2+} was reduced compared to Cu^{2+} and all previous conditions tested. Interestingly, the release profile of Co^{2+} presented a zero order kinetics (**Figure 11E**). However, the amounts released where lower than a previous condition where the same amount was incorporated (**Figure 11C**), although in that case, the amount of Cu^{2+} incorporated was lower.
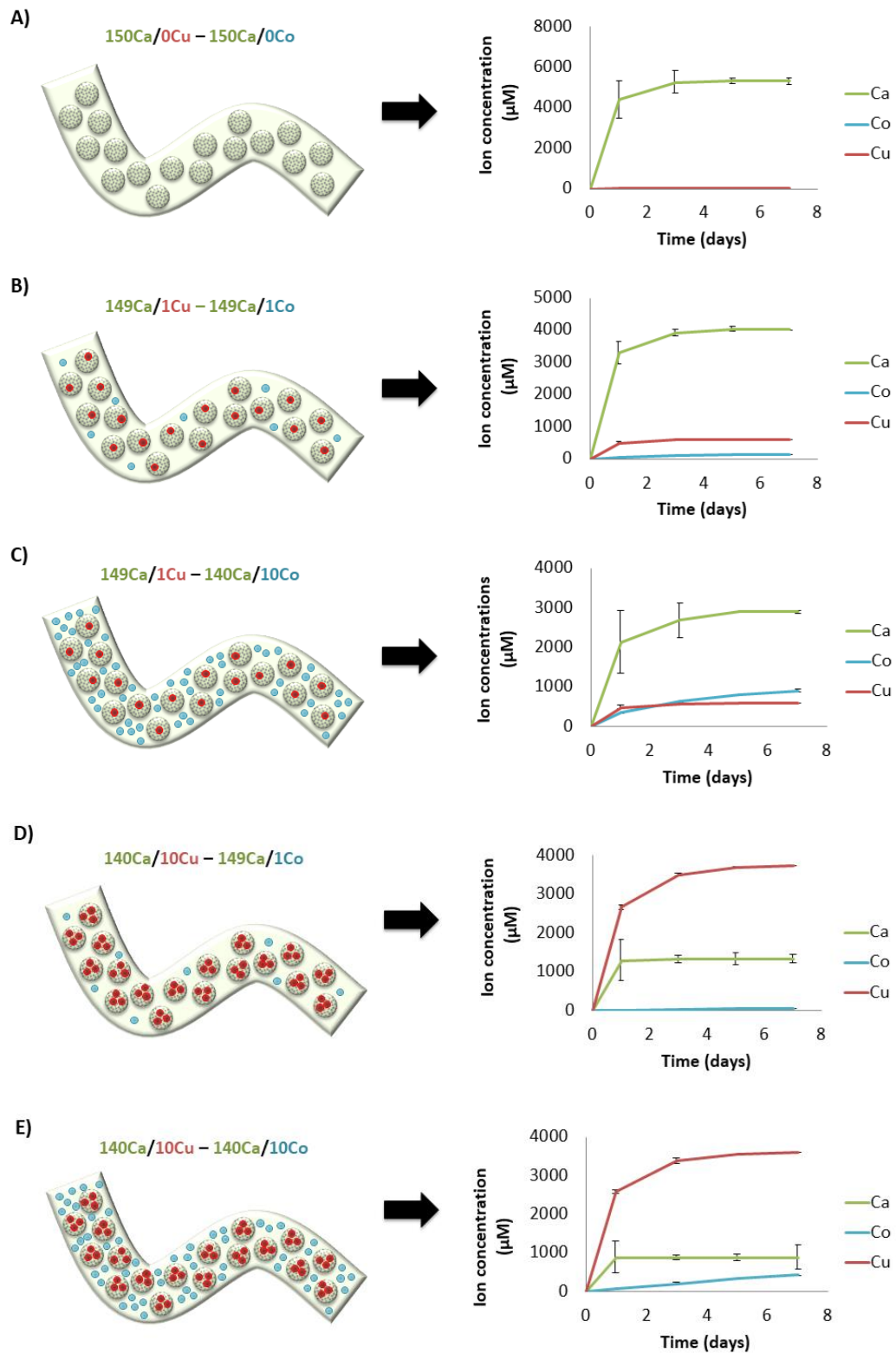
Figure 11. Sustained release of calcium, cobalt and copper ions. Different concentrations of calcium, cobalt and copper were incorporated in the dual drug delivery system using different crosslinking solutions with different ion concentrations (microparticle-fiber): A) 150Ca/0Cu – 150Ca/0Co, B) 149Ca/1Cu – 149Ca/1Co, C) 149Ca/1Cu – 140Ca/10Co, D) 140Ca/10Cu – 149Ca/1Co, E) 140Ca/10Cu – 140Ca/10Co. Release of ions measured up to 7 days.

4.5.　　　Discussion

In this study, we aimed to develop a dual DDS. For this purpose, we first aimed to develop microparticles with osteogenic composition for bone regeneration purposes and incorporate them within alginate. As a *proof of concept*, we introduced two therapeutic ions within DDS to study if the material design was appropriate to control and deliver those ions. More specifically, the ions introduced were Cu^{2+} and Co^{2+}, described to promote antibacterial and angiogenesis response, respectively.

Initially, we aimed to develop microsphere-like particles using a spraying method. Microspheres present some advantages such as the possibility to encapsulate many types of drugs, such as small molecules, proteins and even nucleic acids, being able to provide a sustained release over long periods of time (18). In the last decades, several methods have been used for microsphere development, being the most used the emulsification method (such as water-in-oil emulsion) and nozzle extrusion method (such as spray-drying or electrospraying) (19,20). Briefly, emulsification consists of stirring hydrophilic solution in a continuous hydrophobic phase. Due to immiscibility between the two phases, droplets are generated and can be separated (21). Alternatively, with nozzle extrusion method the polymer solution is discontinuously ejected as droplets using a high pressure (spray-drying) (22) or an electrical field (electrospraying) (23). Here, we aimed to use a method similar to nozzle extrusion to eject the liquid microparticle composition as droplets. In a different way, we used a fingertip spray bottle to eject the alginate/HA blend into a divalent ion crosslinking solution to instantly gel the droplets. To the best of our knowledge, there is only one study reporting this method as well, generating pure alginate microspheres containing cells (24). Our results demonstrated practically the same size distribution between triplicates with all alginate/HA blends tested (**Figure 5**), with a low coefficient of variation of the mean size (**Figure 4**), indicating high reproducibility of this method. Further, we wanted to analyze the percentage of microparticles obtained in the range of 50-100 μm and 100-300 μm after sieving them. To our surprise, not all particles were in these ranges, specifically between approximately 30 and 40% of the microparticles had higher sizes, according to the size distribution (**Figure 6, Figure 7 and Figure 8)**. When observing the stereoscope images of the microparticles (**Figure 6, Figure 7 and Figure 8**), not all of them have spherical form, presenting elongated shape. Therefore, a possible explanation is that large particles could pass through the pore meshes due to their elongated shape. Additionally, the results of how HA influences the mean size of microparticles is similar to another study, where it was also found a decrease size of alginate/HA beads when the amount of HA was increased (25).

As HA has been described to be osteoconductive and enhance osteogenic differentiation and bone formation with MSC (26–28), we aimed to introduce the maximum HA amount to improve the osteogenic properties of the microparticles and mimic the native inorganic composition of bone. We mixed HA with the minimum alginate concentration that maintained HA particles compact forming microspheres-like structures and allowed the spraying. Other studies developed alginate/HA microspheres with the ratio 1:15 (29) or with the ratios 95:5 and 50:50 (25). In this last study, *in vitro* experiments with human MSC demonstrated an enhanced osteogenic differentiation and matrix deposition with the highest amount of HA, and *in vivo* experiment with a rat femoral condyle defect resulted in a higher bone growth due to the presence of HA (25). Authors suggested that this enhancement could be due to MSC recognition to the matrix component (HA) and that HA increased roughness, facilitating cell attachment sites and interaction with proteins excreted by cells. Our microparticle composition of choice had an alginate:HA ratio of 1:40, which is higher than the previous studies mentioned. In our case, HA is the main composition of microparticles and alginate is used as a binder, with the minimum amount. In this regard, other studies used HA as the main scaffold component and demonstrated cell adhesion, proliferation (30), osteogenic differentiation and *in vivo* bone formation (31). According to these studies, our microparticles would have the potential to stimulate osteogenic response. Another advantage of 1:40 microparticle composition is that they presented a more spherical morphology compared to 1:4. Microsphere structures are described to have a high drug loading efficiency and to better control the release of molecules due to surface area-to-volume ratio (18,32). Therefore, 1:40 morphology was another reason of choice. Moreover, it is described that microspheres between 100 and 400 μm are an appropriate size for cell attachment and proliferation (17). In addition, those sizes give an appropriate porosity to the scaffold for cell infiltration and tissue ingrowth (33). At the same time, it is described that higher microsphere size have a more sustained release than smaller ones due to surface-volume ratio and diffusion based release (34). Therefore, for all these reasons, we chose microparticles of 100-300 μm to be incorporated within fibers.

As a second step, we aimed to design alginate fibers with appropriate size to incorporate microparticles within them. To this purpose, we studied how alginate concentration, needle diameter and injection speed influenced the final fiber diameter. In several of the conditions tested, the low concentration of alginate of 0.5% presented more variability in size and higher diameter, whereas with 1.5% concentration alginate fibers presented more homogeneity and lower size (**Figure 9**). A possible explanation of the higher size with lower concentration of

alginate could be due to the presence of less alginate chains to be cross-linked with, and therefore, a higher expansion of them before binding when it is extruded. Regarding the injection speed, we could observe a general increase of fiber size when increasing the flow rate, which is in accordance with a previous study (35). As expected, the diameter of the needle also influenced the final diameter of alginate fibers, obtaining the higher sizes with 20G needle. The inner diameter of 25, 26 and 27G needles does not differ considerably between them, and that can explain the similar alginate fiber sizes obtained, whereas 20G needle has an almost double diameter compared to 25G, clearly resulting in a higher fiber diameter (**Figure 9**). Taking into account these first results, we considered to use a concentration of alginate for fiber development of 1.5% as it presented proper stability to allow handling manipulation without jeopardizing its structure, and at the same time, it presented more homogenous fiber size. Moreover, as we aimed to use microparticles between 100-300 µm, we selected 20G needle as it possessed the most appropriate diameter to avoid its obstruction when encapsulating microparticles within alginate fiber. Finally, injection speeds of 100 and 150 mL/h were considered too high with the possibility to damage microparticle due to high shear stress. Between 10 and 50 ml/L we considered to use 50 mL/h as it would be less time consuming. All these selected parameters results in fiber size of 550 µm, which is similar to filament size of 3D printed scaffolds for bone tissue regeneration used by other authors (30,36).

As a final step, we aimed to develop a DDS by incorporating 1:40 microparticles doped with different amounts of Cu^{2+} within alginate fibers doped with different amounts of Co^{2+}. Their pattern release was studied together with Ca^{2+}. In general, Ca^{2+} and Cu^{2+} presented a burst release, whereas Co^{2+} presented a zero order kinetics release. Additionally, higher amounts of Cu^{2+} were released compared with Co^{2+} when same concentrations were incorporated in their respective crosslinking solutions (**Figure 11B-E**), which can be due to different reasons. One of them is that the final concentration of alginate within microparticles was 0.5%, whereas in the fiber was 1.5%. It is described that stability of alginate can be decreased when in contact with monovalent ions such as Na^+, as they can replace Ca^{2+} and unbind alginate chains (37). Since we performed the release study with cell culture media and it contains a concentration of NaCl approximately of 150 mM, alginate from microparticles (0.5%) could be degraded faster than the alginate fiber (1.5%) and release more Cu^{2+} (schematic representation in **Figure 12**). Furthermore, as alginate fibers are fully loaded with microparticles (50% v/v) and most of them reach to the fiber surface, there might be a direct delivery of Cu^{2+} ions to the medium. Moreover, we noticed that applying pressure on microparticles, they could break. Although we

used a low injection speed to reduce the shear stress applied on microparticles, it exist the possibility that some microparticles might have broken. In this line, it is described that the rate of drug release from smaller microspheres/microparticles is faster that those with higher size due to the surface area-to volume ratio of the particles (34,38). Therefore, if some microparticles were broken in small pieces, their ion delivery would have been faster, and that is another possibility that might also explain the higher and burst release of Cu^{2+}.
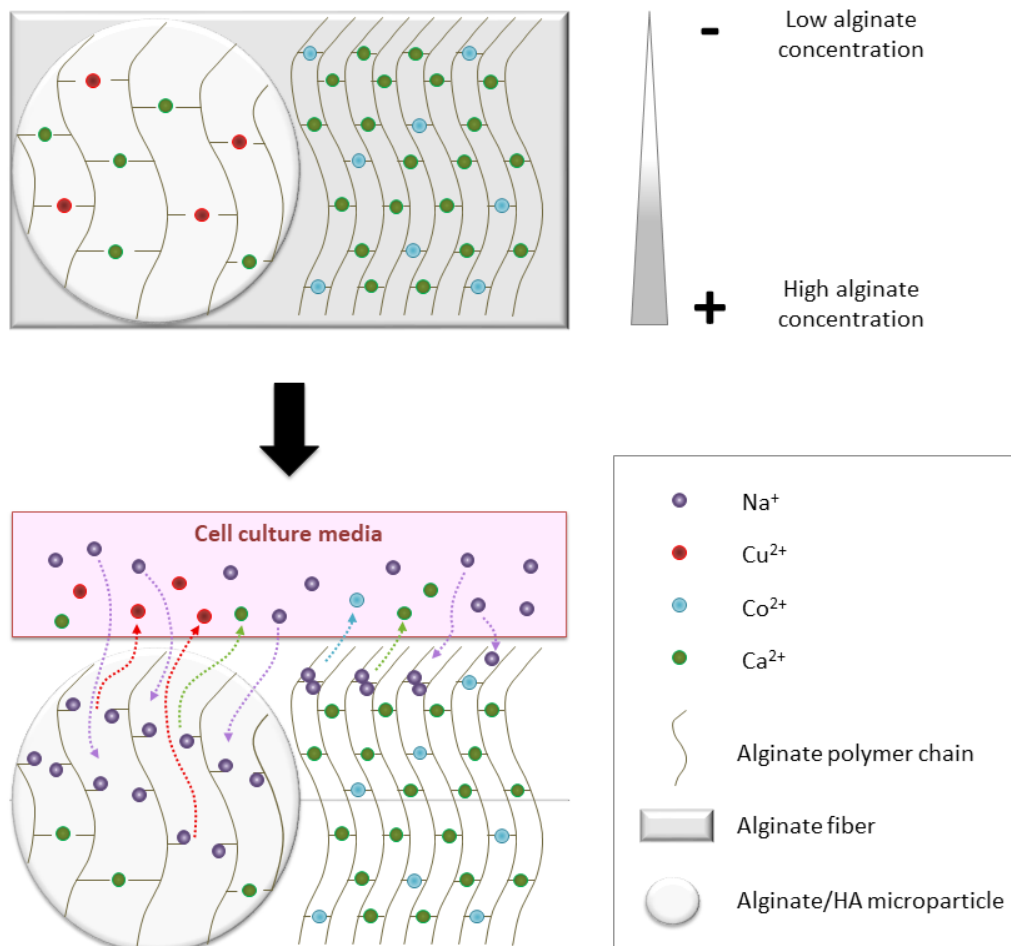
Figure 12. Effect of cell culture media on ion delivery. Na^+ is able to diffuse easily into microparticles compared to alginate fiber due to lower alginate concentration. Na^+ gradually replace divalent ions, resulting in the un-crosslinking of alginate polymer chains, facilitating the release of divalent ions.

Another observation is that Cu^{2+} seem to have an influence in Co^{2+} and Ca^{2+} release. In more detail, with the same amount incorporated of Co^{2+}, when the amount of Cu^{2+} is increased, the quantity of Co^{2+} is reduced (**Figure 11B,D** and **Figure 11C,E**). Moreover, for the same concentration of Cu^{2+} and Co^{2+} introduced in the crosslinking solutions, Cu^{2+} seemed to reduce more the delivery of Ca^{2+} (**Figure 11**). Conversely, Co^{2+} seemed to not interfere with Cu^{2+} release, as the delivery pattern was practically the same with the same amount of Cu^{2+}, independently of the Co^{2+} amount incorporated in the fibers (**Figure 11B,C** and **Figure 11D,E**).

The reason of why Cu^{2+} reduced the release of Co^{2+} and Ca^{2+} is not completely understood. However, we speculated that it could be due to ion affinity to alginate. It is described that the gel forming ability follow this order: $Cu^{2+} > Ca^{2+} > Co^{2+}$ (39,40). Therefore, we hypothesized that the delivery of Cu^{2+} from inner microparticles might further crosslink alginate chains, probably reducing the mesh size, which is described to lower the diffusion rate of the encapsulated molecules, in our case Ca^{2+} or Co^{2+} (41,42) (schematic representation shown in **Figure 13**). Interestingly, the order kinetics of Co^{2+} release was close to zero. Probably, due to the high amount of alginate/HA microparticles incorporated within alginate fiber and the higher affinity of Cu^{2+} for alginate, Co^{2+} might have had more difficulties to diffuse and, therefore, it presented a more controlled and sustained release.
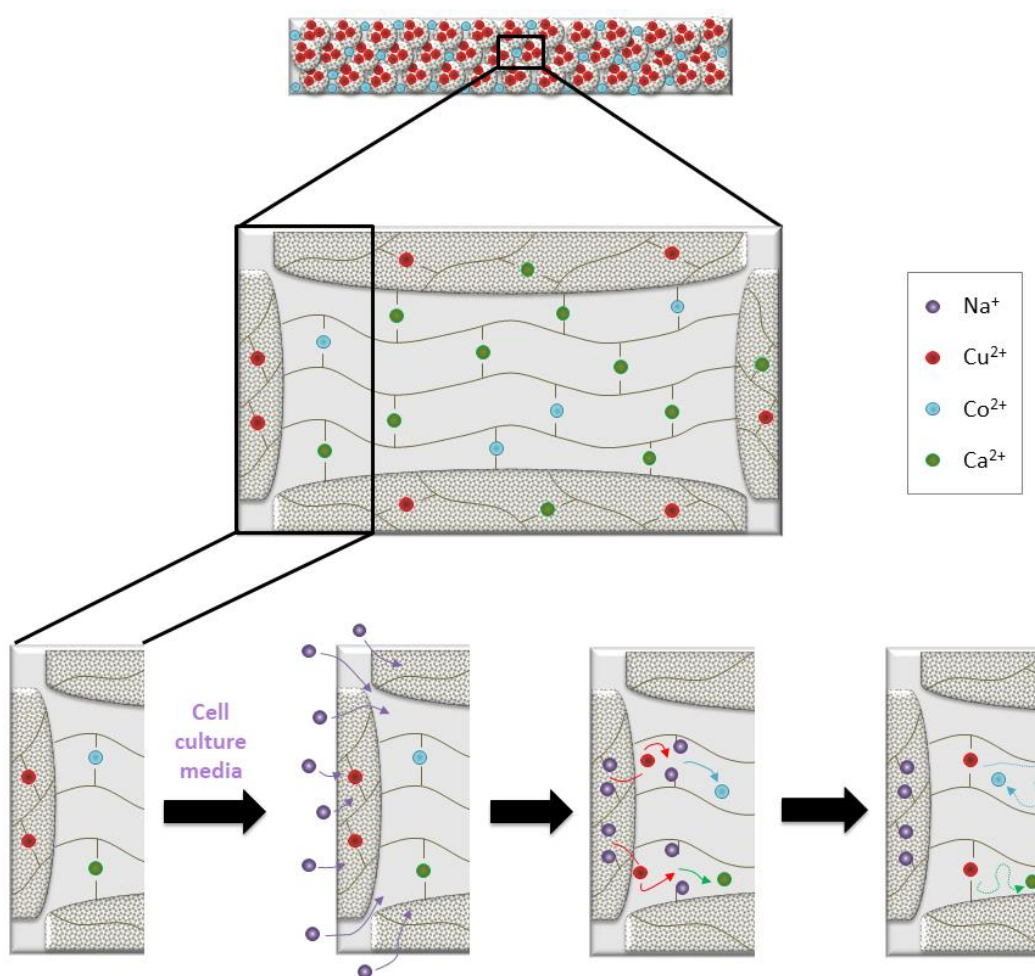
Figure 13. Influence of Cu^{2+} on Co^{2+} and Ca^{2+} release. In the presence of cell culture media, Na^{2+} replace divalent ions from microparticles and alginate fiber. The delivery of Cu^{2+} from microparticles crosslinks free alginate chains from alginate fiber due to its higher affinity. Ca^{2+} and Co^{2+} remain entrapped and have more difficulties to diffuse.

An important feature of any DDS is the amount of drug delivered, as it should be in a therapeutic range to avoid cytotoxicity or side effects. In our ion delivery system, we used Cu^{2+}

to add anti-bacterial properties (13), and Co^{2+} to potentially stimulate blood vessel formation (16). Although we used Ca^{2+} as a model ion, it has also been described to regulate biological functions, specifically it has been described to stimulate proliferation and/or osteogenic differentiation of osteoblasts (12). Therefore, the DDS developed in this study has the potential to be used as a bioactive ion delivery system for bone regeneration. Regarding the concentrations released, several Cu^{2+} concentrations are reported to be effective against different bacterial strains, from 150 to 6000 μM, approximately (43–45). It is worth to mention that the anti-bacterial effects were evident as early as 24h in all studies. In this regard, any of the conditions tested seem appropriate to avoid bacteria growth as the main concentrations are released within the first 1 to 3 days. However, higher doses can induce mammalian cell cytotoxicity. Taking this into account, the lowest dose released should be more appropriate. This would correspond to the condition where 1 mM of Cu^{2+} was incorporated in the crosslinking solution (**Figure 11B** or **C)**, where practically all Cu^{2+} (≈500 μM) was delivered within 24h. Regarding Co^{2+}, concentrations from 10 to 100 μM are reported to stimulate the angiogenic response when delivered from scaffolds (46,47). Considering our results, the condition in which 1 mM of Cu^{2+} and Co^{2+} were incorporated in the cross-linking solutions resulted in a zero order kinetics release of Co^{2+} during 7 days with constant concentrations of approximately 30-40 μM (**Figure 11B**). Therefore, this condition has the potential to stimulate the angiogenic response. Finally, considering Ca^{2+}, the maximum amount delivered was around 5 mM (**Figure 11A**), which is higher than the concentration found in blood plasma or extracellular fluids (around 2 mM). However, a previous study reported that whereas concentrations of 2-4 mM were suitable for osteoblast proliferation, concentrations from 6-8 mM enhanced osteoblast differentiation and matrix mineralization (48). Another study reported that Ca^{2+} concentrations of 6 and 8 mM increased MSC proliferation and matrix mineralization (49). Considering that Ca^{2+} concentration of the cell culture media is around 1.6 mM and physiological concentrations in blood plasma and extracellular fluids is around 2 mM, a final concentration of Ca^{2+} between 6-8 mM is achieved. Therefore, our system seems to be promising to stimulate osteogenesis when only Ca^{2+} or Ca^{2+} with the lowest concentrations of Cu^{2+} and Co^{2+} (1 mM) are incorporated in the crosslinking solutions. All in all, taking into account the different ion release profiles, the most appropriate condition to stimulate early phases of bone regeneration would be with the minimum amount (1 mM) of Cu^{2+} and Co^{2+} and 149 mM of Ca^{2+} in their respective crosslinking solutions.

4.6.   Conclusions

To summarize, we were able to develop microparticles incorporating high amount of HA with spraying method, being a high reproducible approach even using different microparticle compositions. Moreover, when incorporated within alginate fibers and doped microparticles and alginate fibers with two different ions, their release could be modulated through their concentrations in the crosslinking solution in a dose-dependent manner. With the lowest concentrations of Cu^{2+} and Co^{2+} incorporated, we could develop a DDS with potential to stimulate early phases of bone regeneration, specifically with an initial anti-bacterial effect followed by an angiogenic stimulation phase. Eventually, the release of Ca^{2+} and the presence of HA could potentially enhance osteogenic differentiation and bone formation. Moreover, as the DDS is fiber-based, it could be adapted to 3D printing technology to custom-shape scaffolds.

4.7.   References

1.   Schemitsch EH. Size Matters: Defining Critical in Bone Defect Size! J Orthop Trauma. 2017;31(10):S20–2.

2.   Henkel J, Woodruff MA, Epari DR, Steck R, Glatt V, Dickinson IC, et al. Bone Regeneration Based on Tissue Engineering Conceptions — A 21st Century Perspective. Bone Res. 2013;1(3):216–48.

3.   Roberts TT, Rosenbaum AJ. Bone grafts, bone substitutes and orthobiologics: the bridge between basic science and clinical advancements in fracture healing. Organogenesis. 2012;8(4):114–24.

4.   Dorozhkin S V. A detailed history of calcium orthophosphates from 1770s till 1950. Mater Sci Eng C. 2013;33(6):3085–110.

5.   Gao C, Deng Y, Feng P, Mao Z, Li P, Yang B, et al. Current progress in bioactive ceramic scaffolds for bone repair and regeneration. Int J Mol Sci. 2014;15(3):4714–32.

6.   Sheikh Z, Najeeb S, Khurshid Z, Verma V, Rashid H, Glogauer M. Biodegradable materials for bone repair and tissue engineering applications. Materials (Basel). 2015;8(9):5744–94.

7.   Perez RA, Kim HW. Core-shell designed scaffolds for drug delivery and tissue engineering. Acta Biomater. 2015;21:2–19.

8.   Pérez RA, Won JE, Knowles JC, Kim HW. Naturally and synthetic smart composite biomaterials for tissue regeneration. Adv Drug Deliv Rev. 2013;65(4):471–96.

9.   Hsu YH, Lin CT, Yu YH, Chou YC, Liu SJ, Chan EC. Dual delivery of active antibactericidal agents and bone morphogenetic protein at sustainable high concentrations using biodegradable sheath-core-structured drug-eluting nanofibers. Int J Nanomedicine.

2016;11:3927–37.

10. Kanczler JM, Ginty PJ, White L, Clarke NMP, Howdle SM, Shakesheff KM, et al. The effect of the delivery of vascular endothelial growth factor and bone morphogenic protein-2 to osteoprogenitor cell populations on bone formation. Biomaterials. 2010;31(6):1242–50.

11. World Health Organization. Antibiotic resistance [Internet]. 2020. Available from: https://www.who.int/news-room/fact-sheets/detail/antibiotic-resistance

12. Perez RA, Seo SJ, Won JE, Lee EJ, Jang JH, Knowles JC, et al. Therapeutically relevant aspects in bone repair and regeneration. Mater Today. 2015;18(10):573–89.

13. Gugala N, Lemire JA, Turner RJ. The efficacy of different anti-microbial metals at preventing the formation of, and eradicating bacterial biofilms of pathogenic indicator strains. J Antibiot (Tokyo). 2017;70(6):775–80.

14. Bonaventura P, Benedetti G, Albarède F, Miossec P. Zinc and its role in immunity and inflammation. Autoimmun Rev. 2015;14(4):277–85.

15. Nielsen FH. Magnesium deficiency and increased inflammation: Current perspectives. J Inflamm Res. 2018;11:25–34.

16. O'Neill E, Awale G, Daneshmandi L, Umerah O, Lo KWH. The roles of ions on bone regeneration. Drug Discov Today. 2018;23(4):879–90.

17. Malda J, Frondoza CG. Microcarriers in the engineering of cartilage and bone. Trends Biotechnol. 2006;24(7):299–304.

18. Kim KK, Pack DW. Microspheres for Drug Delivery. In: BioMEMS and Biomedical Nanotechnology. 2006. p. 19–50.

19. Perez RA, Jung CR, Kim HW. Biomaterials and Culture Technologies for Regenerative Therapy of Liver Tissue. Adv Healthc Mater. 2017;6(2).

20. Wee CY, Yang Z, Thian ES. Past, present and future development of microspheres for bone tissue regeneration: a review. Mater Technol. 2020;

21. Perez RA, Altankov G, Jorge-Herrero E, Ginebra MP. Micro- and nanostructured hydroxyapatite-collagen microcarriers for bone tissue-engineering applications. J Tissue Eng Regen Med. 2013;7(5):353–61.

22. Zhou P, Wu J, Xia Y, Yuan Y, Zhang H, Xu S, et al. Loading BMP-2 on nanostructured hydroxyapatite microspheres for rapid bone regeneration. Int J Nanomedicine. 2018;13:4083–92.

23. Workman VL, Tezera LB, Elkington PT, Jayasinghe SN. Controlled generation of microspheres incorporating extracellular matrix fibrils for three-dimensional cell culture. Adv Funct Mater. 2014;24(18):2648–57.

24. Bigdeli S, Dettloff RO, Frank CW, Davis RW, Crosby LD. A simple method for encapsulating single cells in alginate microspheres allows for direct PCR and whole genome amplification. PLoS One. 2015;10(2):1–15.

25. Wang MO, Bracaglia L, Thompson JA, Fisher JP. Hydroxyapatite-doped alginate beads as scaffolds for the osteoblastic differentiation of mesenchymal stem cells. J Biomed

Mater Res - Part A. 2016;104(9):2325–33.

26.   Mygind T, Stiehler M, Baatrup A, Li H, Zou X, Flyvbjerg A, et al. Mesenchymal stem cell ingrowth and differentiation on coralline hydroxyapatite scaffolds. Biomaterials. 2007;28(6):1036–47.

27.   Kim K, Dean D, Lu A, Mikos AG, Fisher JP. Early osteogenic signal expression of rat bone marrow stromal cells is influenced by both hydroxyapatite nanoparticle content and initial cell seeding density in biodegradable nanocomposite scaffolds. Acta Biomater. 2011;7(3):1249–64.

28.   Wang H, Li Y, Zuo Y, Li J, Ma S, Cheng L. Biocompatibility and osteogenesis of biomimetic nano-hydroxyapatite/polyamide composite scaffolds for bone tissue engineering. Biomaterials. 2007;28(22):3338–48.

29.   Costa Cuozzo R, Da Rocha Leão MHM, De Andrade Gobbo L, Da Rocha DN, Mohammed Elmassalami Ayad N, Trindade W, et al. Zinc alginate-hydroxyapatite composite microspheres for bone repair. Ceram Int. 2014;40(7 PART B):11369–75.

30.   Leukers B, Gulkan H, Irsen S, Milz S, Tille C, Schieker M, et al. Hydroxyapatite scaffolds for bone tissue engineering made by 3D printing. J Mater Sci Med. 2005;16(12):1121–4.

31.   Ren X, Tuo Q, Tian K, Huang G, Li J, Xu T, et al. Enhancement of osteogenesis using a novel porous hydroxyapatite scaffold in vivo and vitro. Ceram Int. 2018;44(17):21656–65.

32.   Wang H, Leeuwenburgh SCG, Li Y, Jansen JA. The use of micro-and nanospheres as functional components for bone tissue regeneration. Tissue Eng - Part B Rev. 2012;18(1):24–39.

33.   Aronin CEP, Sadik KW, Lay AL, Rion DB, Tholdpady SS, Ogle RC, et al. Comparative effects of scaffold pore size, pore volume, and total void volume on cranial bone healing patterns using microsphere-based scaffolds. J Biomed Mater Res Part A. 2009;89A(3):632–41.

34.   Chen W, Palazzo A, Hennink WE, Kok RJ. Effect of particle size on drug loading and release kinetics of gefitinib-loaded PLGA microspheres. Mol Pharm. 2017;14(2):459–67.

35.   Perez RA, Kim M, Kim T-H, Kim J-H, Lee JH, Park J-H, et al. Utilizing Core–Shell Fibrous Collagen-Alginate Hydrogel Cell Delivery System for Bone Tissue Engineering. Tissue Eng Part A. 2014;20(1–2):103–14.

36.   Jeon HJ, Lee M, Yun S, Kang D, Park K ho, Choi S, et al. Fabrication and characterization of 3D-printed biocomposite scaffolds based on PCL and silanated silica particles for bone tissue regeneration. Chem Eng J. 2019;360:519–30.

37.   Lee KY, Mooney DJ. Alginate: Properties and biomedical applications. Prog Polym Sci. 2012;37(1):106–26.

38.   Varde N, Pack D. Microspheres for controlled release drug delivery. Expert Opin Biol Ther. 2004;4(1):35–51.

39.   Wang Z -Y, Zhang Q -Z, Konno M, Saito S. Sol–Gel transition of alginate solution by the addition of various divalent cations: A rheological study. Biopolymers. 1993;33(4):703–11.

40. Agulhon P, Robitzer M, Habas JP, Quignard F. Influence of both cation and alginate nature on the rheological behavior of transition metal alginate gels. Carbohydr Polym. 2014;112:525–31.

41. Reinhart CT, Peppas NA. Solute diffusion in swollen membranes. Part II. Influence of crosslinking on diffusive properties. J Memb Sci. 1984;18:227–39.

42. Carbinatto FM, de Castro AD, Evangelista RC, Cury BSF. Insights into the swelling process and drug release mechanisms from cross-linked pectin/high amylose starch matrices. Asian J Pharm Sci. 2014;9(1):27–34.

43. Bari A, Bloise N, Fiorilli S, Novajra G, Vallet-Regí M, Bruni G, et al. Copper-containing mesoporous bioactive glass nanoparticles as multifunctional agent for bone regeneration. Acta Biomater. 2017;55:493–504.

44. Abou Neel EA, Ahmed I, Pratten J, Nazhat SN, Knowles JC. Characterisation of antibacterial copper releasing degradable phosphate glass fibres. Biomaterials. 2005;26(15):2247–54.

45. Benhalima L, Amri S, Bensouilah M, Ouzrout R. Antibacterial effect of copper sulfate against multi-drug resistant nosocomial pathogens isolated from clinical samples. Pakistan J Med Sci. 2019;35(5):1322–8.

46. Perez RA, Kim JH, Buitrago JO, Wall IB, Kim HW. Novel therapeutic core-shell hydrogel scaffolds with sequential delivery of cobalt and bone morphogenetic protein-2 for synergistic bone regeneration. Acta Biomater. 2015;23:295–308.

47. Quinlan E, Partap S, Azevedo MM, Jell G, Stevens MM, O'Brien FJ. Hypoxia-mimicking bioactive glass/collagen glycosaminoglycan composite scaffolds to enhance angiogenesis and bone repair. Biomaterials. 2015;52(1):358–66.

48. Maeno S, Niki Y, Matsumoto H, Morioka H, Yatabe T, Funayama A, et al. The effect of calcium ion concentration on osteoblast viability, proliferation and differentiation in monolayer and 3D culture. Biomaterials. 2005;26(23):4847–55.

49. Lee MN, Hwang HS, Oh SH, Roshanzadeh A, Kim JW, Song JH, et al. Elevated extracellular calcium ions promote proliferation and migration of mesenchymal stem cells via increasing osteopontin expression. Exp Mol Med. 2018;50(11):1–16.

CHAPTER 5

Direct extrusion of individually encapsulated endothelial and smooth muscle cells mimicking blood vessel structures and vascular native cell alignment

CHAPTER 5. Direct extrusion of individually encapsulated endothelial and smooth muscle cells mimicking blood vessel structures and vascular native cell alignment

5.1.   Introduction

As reported by the World Health Organization (WHO), 31% of global death is due to cardiovascular diseases (CVDs), considered the principal cause of worldwide death (1). The main etiology of CVDs is the narrowing and occlusion of blood vessels as a result of atherosclerotic plaque formation in the inner layer of arteries, known as atherosclerosis, which impedes the blood flow and eventually leads to tissue ischemia (2). Up to now, the gold standard strategies to treat CVDs have been the use of stents or blood vessel replacement by bypass surgery. The use of stents can induce endothelial damage triggering a cascade of events that leads to the re-narrowing of the vessel, known as restenosis (3). Although stents have been improved over time to reduce restenosis (4), it still remains a problem in real world practice (5). The alternative strategy for blood vessel replacement generally considers autologous source, such as saphenous vein or mammary artery (6,7). However, because of the inherent disease of the patient or due to previous harvest, the autologous source offers a limited solution. The use of decellularized xenogeneic vessels has also been proposed to surpass this problem, and also because they can preserve the extracellular matrix (ECM) of native vessels allowing cell migration, proliferation and survival. However, the complete removal of immunogenic molecules still remains a challenge and can trigger an immune response (8). Due to the aforementioned issues, significant efforts are steering in developing tissue engineered blood vessels (TEBV) as an alternative graft source for bypass surgery.

To bioengineer a TEBV, it is important to mimic to the highest extent the architecture and the structural components of a blood vessel. Higher caliber vessels, such as arteries, are composed of two main functional layers: tunica intima and tunica media. Tunica intima is the closest to the blood and it is comprised of a confluent monolayer of endothelial cells (ECs) aligned in the direction of the blood flow (9). Tunica media is composed of smooth muscle cells (SMCs) which are concentrically arranged, being rich in collagen type I and elastin. Several mechanical functionalities of the blood vessel, such as the vasoactivity (contraction and dilation) are mainly related with SMCs alignment, (10,11), and for this reason, special attention is focused in achieving a proper alignment of these cells when developing a TEBV. Therefore, as a first step

139

to develop a TEBV, the earliest achievements to accomplish in vascular engineering should be: i) proper mechanical stability of the construct to allow handling and perfusion; ii) obtaining a multilayered structure resembling the native arrangement; iii) the allocation of vascular specific cell types in their respective layer, with a proper ECM allowing their survival; iv) and concentric orientation of SMCs.

To achieve mechanical stability of the constructs, the use of synthetic biodegradable polymers has been proposed due to their inherent mechanical properties. In general, these synthetic polymers present adequate mechanical properties but limited biological activity. A commonly used method using synthetic materials is sheet rolling, that uses a biomaterial sheet on top of which ECs and/or SMCs can be seeded. The sheet is then rolled over a mandrel to form a tubular structure (12), with the possibility to form more than one layer (13). To further guide cells and orientate them on the desired direction, surface patterning can be performed either by lithography based techniques or by electrospinning (14). Actually, the latter technology itself can be used to obtain tubular constructs by simply electrospinning onto small rotating mandrels (15), where SMCs are seeded on the top of the construct and ECs in the inner surface. Using both approaches, it takes several steps and time to obtain a vascular construct, especially with sheet rolling, as cells have to be seeded on the surface of 2D biomaterial and allow their proliferation (12), before rolling it to obtain a tubular structure. Furthermore, the released products from synthetic materials degradation have been shown to alter the contract phenotype of SMCs (16).

For this reason, alternative materials and technologies are needed to provide a more natural environment for cells, that allows forming layered structures incorporating different cell types with enough mechanical stability. For this purpose, extrusion based system of natural materials, with concentric nozzles has recently shown interesting results, allowing the fabrication of core shell layered fibers in a one step process (17). This core-shell technology has allowed the encapsulation of cell types in the inner layer, being sheathed by an acellular hydrogel layer, generally alginate, as it provides mechanical stability (18). Despite these systems may eventually allow the encapsulation of cells in different compartments, their use as a blood vessel is very limited due to the absence of the lumen. To further mimic a blood vessel, other studies have incorporated a water soluble polymer in the inner layer to obtain a hollow fiber, allowing the encapsulation of vascular related cells on the outer layer (17,19). The main limitation of this system is the limited functionality due to the presence of one individual layer where cells can be placed. An added value of the extrusion based process is the ability to align cells based on the shear stress applied, avoiding the use of patterning and

electrospinning techniques. In a previous study, alignment of mesenchymal stem cells (MSCs) was demonstrated due to the shear stress during extrusion (20). Moreover, it is described that the shear stress of the blood flow can induce the parallel alignment of EC (21), and SMCs can be aligned in a shear-stress dependent manner (22), being perpendicular with low shear stress. Therefore, the shear stress generated during the extrusion process might induce a specific cell alignment.

5.2.   Objectives

In this chapter, we aimed at using a triple concentric nozzle to form dual-layered blood vessel-like structure encapsulating human umbilical vein endothelial cells (HUVECs) and human aortic smooth muscle cells (HASMCs) in their respective layers. Furthermore, we expected that the shear stress applied during the extrusion based process would allow the alignment of HUVECs parallel to the direction of the TEBV whereas HASMCs would align perpendicular to the TEBV.

5.3.   Materials & Methods

5.3.1. Collagen type I isolation

Collagen type I was isolated from bovine tendons obtained from an abattoir and all the isolation process was based on well-established protocols (23). First, tendon was separated from the surrounding fascia and was cut to small pieces with the aid of a blender, followed by three washes with phosphate buffered saline (PBS). Then, the sliced tendon was dissolved with 1M acetic acid under agitation for 72h. Enzymatic digestion was performed using porcine gastric mucosa pepsin (Sigma-Aldrich) at 40U/mg of tendon under stirring, 2h at room temperature (<20 ºC) and 72h at 4ºC. The resultant enzymatic digestion was filtered to obtain pepsin soluble collagen and was purified by salt precipitation (0,9 M NaCl) during 24h. The precipitated collagen was collected and dissolved with 1M acetic acid under stirring for 5 days. Finally, collagen solution was dialyzed (MW 8,000 cut off) repeatedly against 1mM acetic acid and the dialyzed collagen solution was kept at 4ºC. Collagen concentration was determined using dry weight and collagen purity was evaluated using sodium dodecyl sulfate polyacrylamide gel electrophoresis (SDS-PAGE) followed by Coomassie staining and densitometry analysis with ImageJ software.

5.3.2. Cell culture

Human umbilical vein endothelial cells (HUVECs) (Lonza) and human aortic smooth muscle cells (HASMCs) (ATCC) were used. For cell expansion, HUVEC were seeded at a density of 2500 cells/cm^2 with endothelial growth medium-2 bulletkit (EGM-2) (Lonza) containing VEGF, rhFGF-B, rhEGF, r-IGF-1, hydrocortisone, ascorbic acid, gentamicin sulfate, amphotericin-B and 2% of FBS. HASMC were seeded at a density of 2500 cells/cm^2 with vascular cell basal medium supplemented with vascular smooth muscle cell growth kit (ATCC) containing 5 ng/mL rh-FGF-basic, 5 µg/mL rh-Insulin, 50 µg/mL ascorbic acid, 10 mM L-glutamine, 5 ng/mL rh EGF, 5% FBS and 1% Penicillin-streptomycin. When both cell types reached 70-85% confluence, they were passaged using 0,25% Trypsin-EDTA (Gibco) or they were ready to be used for TEBV development. All cells were cultured in standard cell culture conditions (37ºC and 5% CO$_2$).

5.3.3. Endothelial cell encapsulation in core-shell fibers

The methodology to obtain a core-shell fiber was followed from a previous study (24). Briefly, a dual concentric nozzle (23G inner and 17G outer) was used to obtain a core-shell fiber in which two different biomaterials were extruded: alginate (Panreac Applichem) at a ratio of 1,5% (%wt) in the outer layer and 2 mg/mL of collagen type I in the core. The concentric flows were extruded at 50 mL/h into a 150 mM calcium chloride (CaCl$_2$) (Sigma) solution and incubated for 5 min. After that, fibers were rinsed with H$_2$O miliQ. In order to verify if our initial hypothesis was viable, allowing the alignment of HUVEC on the direction of a core shell fiber as previously observed with mesenchymal stem cells (24), a small preliminary experiment was performed. Furthermore, due to the higher sensitivity of HUVEC compared to MSC, we also aimed exploring if cell concentration could have an effect on cell alignment and survival as well as to verify if the shear stress caused during the extrusion process could jeopardize cell viability. Different amounts of HUVEC (1x10^5, 1x10^6 and 2x10^6 cells/mL) were loaded in the core with collagen type I. After the incubation with 150 mM of CaCl$_2$, three washes with fresh cell culture media were performed to remove the excess of calcium and, finally, they were cultured with EGM-2 medium (Lonza) up to 7 days and optical images were acquired.

5.3.4. Core-shell hollow fiber fabrication

To develop a dual layer hollow fiber as a tissue engineered blood vessel (TEBV) structure, a triple concentric nozzle (23G inner, 17G middle and 13G outer) (NanoNC) was used. Schematic representation of the method is shown in **Figure 1**. The nozzle was fed with the help of injection pumps with three different materials placed in syringes to allow the formation of the

tri-concentric fiber. The inner syringe was loaded with a 25% wt Pluronic F-127 (Sigma) aqueous solution, as a sacrifice material. The middle syringe was loaded with the previously extracted collagen type I. In order to maximize the stability of the tubular structure, different collagen concentrations ranging from 2 to 5 mg/mL were tested. To mimic the native conditions of blood vessels and to present an adequate environment for cell survival, collagen was self-assembled by adding 200 μL of 10x PBS and the necessary amount of NaOH, 1M or 5M, was added to 2 mL of collagen. The outer syringe was loaded with a mix of sodium alginate (A3249, Panreac Applichem) and collagen type I. In this case, the concentration of each biomaterial was optimized by maximizing the collagen presence without jeopardizing the mechanical stability of the fiber provided by the alginate. The injection speed was varied between 25 and 50 ml/h to study the effect of the injection speed on the general parameters of the blood vessel like structure, mainly shell thickness and fiber size. All the loaded syringes were kept at 4ºC. The tip of the nozzle was placed in contact with a 150 mM calcium chloride bath at 37ºC, where calcium allowed an instant crosslinking of the outer layer containing alginate, providing stability to the fiber structure, whereas the increased temperature allowed collagen self-assembling contributing to the stabilization of both the outer and middle layer. The tri-layered structures were maintained in the crosslinking solution during 10-15 minutes. After collagen gelation, the tri-layered fiber was placed in H_2O miliQ and was cut to a length of 1 cm. Pluronic was removed from the inner core by dissolution with H_2O miliQ during 5 minutes, obtaining the TEBV structure. The outer and the inner diameter of TEBV were measured for each injection speed. Additionally, manual perfusion with red food ink was performed to confirm the hollow structured vessel and to qualitatively assess the sufficient mechanical stability of the vessel to withstand perfusion of liquids without bursting the structure or leaking the perfused liquids.
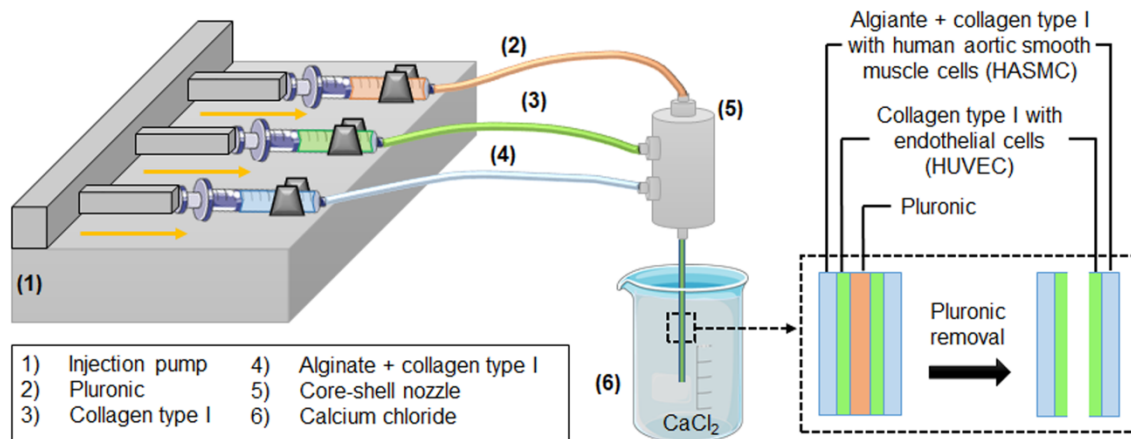
Figure 1. Schematic representation of TEBV development through extrusion method. Pluronic (2), collagen (3) and alginate mixed with collagen (4) are injected into a triple concentric nozzle (5) in the inner, middle and outer layer, respectively. These biomaterials are extruded in a constant injection speed controlled by an injection pump (1) into a crosslinking solution of calcium chloride (6). The fibers are incubated at 37ºC in order to allow collagen gelation and then, pluronic is removed from the inner core, obtaining a hollowed dual layer tubular structure.

5.3.5. Individual cell encapsulation within tissue engineered blood vessel structures (TEBV)

Initially, in order to assess the individual behavior of each cell type encapsulated within its designated compartment, hollow fibers encapsulating HUVEC or HASMC were prepared. All the procedure was performed under sterile conditions. Pluronic and sodium alginate powders were sterilized with UV. Then, they were mixed with sterile mili-Q water to achieve 25 and 5% (% wt) of Pluronic and alginate, respectively. For the encapsulation of cells, the previously described procedure was followed using 50 ml/h as the injection speed. For TEBV containing only HUVEC (TEBV-HUVEC), a small volume of culture media containing 15×10^6 HUVEC cells/mL were loaded in the collagen syringe after pH neutralization. Based on our preliminary results, this cell concentration was used to achieve, within the middle layer, at least a continuous cell monolayer that would allow a continuous endothelial cell layer that would mimic the native structure of blood vessels. For TEBV containing only HASMC (TEBV-HASMC), 2 ml of 5% alginate and 3 ml of 5 mg/mL of collagen (previous neutralized) were mixed to achieve a final concentration of 2% and 3 mg/mL of alginate and collagen, respectively. Then, based on previous works (25), a small volume of culture media containing 10×10^6 HASMC cells/mL was added. Once complete crosslinking of alginate and gelation of collagen was achieved, the TEBVs were rinsed three times with fresh cell culture medium to remove the excess of $CaCl_2$.

Then, TEBV were cut to a length of 1 cm and, finally, each cell type was cultured with each specific cell culture medium mentioned.

5.3.6. Co-encapsulation of HUVECs and HASMCs within tissue engineered blood vessel structures (TEBV)

For the co-culture assay (TEBV-co), HUVEC were loaded into the collagen syringe (middle layer) and HASMC were loaded into the alginate mixed with collagen syringe (outer layer), following a similar cell encapsulation method as the one performed for individual cell encapsulation. In a similar way, after alginate crosslinking and collagen gelation, the TEBVs were rinsed three times with fresh cell culture medium to remove the excess of CaCl$_2$.
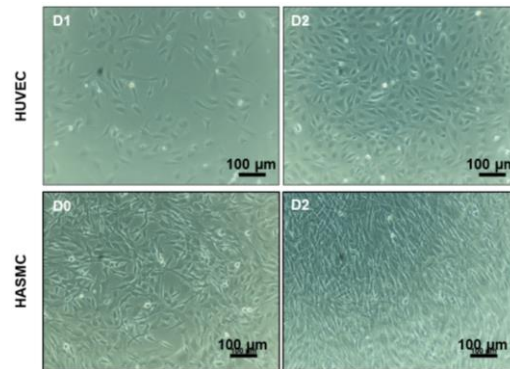
Figure 2. HUVEC and HASMC grown with 50% HUVEC cell culture medium and 50% HASMC cell culture medium**.**

Then, TEBV were cut to a length of 1 cm and 50% of each cell culture media was used (both cell types proved to survive and proliferate as shown in **Figure 2**).

5.3.7. Cell viability analysis

The cell viability of HUVEC, HASMC or both in co-culture was assessed at 24h, to quantitatively assess cell survival after the shear stress produced by the extrusion method, and at 20 days, to prove if cells could survive after a long cell culture period within the TEBV structure. The LIVE/DEAD cell imaging kit (Invitrogen) was used following manufacturer's instructions. Briefly, the methodology consists of a live component which stains live cells giving a uniform green fluorescence (excitation/emission wavelengths were 488/515 nm) and a dead component which stains death cells producing a nuclear red fluorescence (excitation/emission wavelengths were 570/602 nm). Equal volumes of both components were added in the cell culture medium with TEBVs reaching a final concentration of 1x. After 15 minutes of incubation protected from light, cells were imaged with a laser scanning confocal microscope (Leica SP8, LAS X software version 3.5.5.19976). As a positive control for cell death, some TEBV were prior treated with 4% PFA at room temperature during 30 min followed by an incubation with 1x PBS/0,5% triton X-100 during 10 min. Three samples per time point were analyzed and three captures at different plans per sample were acquired. Images were analyzed using ImageJ software (ImageJ 1.52a) and live and dead cells were counted for each one. Viability

was calculated as number of live cells divided per total number of cells (live and dead), as a percentage.

5.3.8. Cell proliferation assay

To assess the proliferation of cells, quantification of double-stranded DNA (dsDNA) using fluorimetric dsDNA quantification kit (Quant-It Picogreen dsDNA assay Kit, Invitrogen) was performed according manufacturer's instructions. Time points were at 0, 2, 5, 12 and 20 days for TEBV-HUVEC and TEBV-HASMC and at 0, 2, 8, 12 and 20 days for TEBV-co. Because there was not a big difference between day 2 and 5 when cells were cultured separately, we decided to assess it at day 8 in co-culture conditions instead of day 5. Three samples per time point were analyzed. Briefly, each sample was collected with 100 µL of 1x Tris-EDTA (TE) buffer and submitted to a three cycles of freezing and defrosting to lyse the cells. Between cycles, samples were mechanically disrupted by pipetting to allow the release of DNA from TEBV structures. After spin centrifugation, 100 µL of the supernatant was transferred into an opaque 96-well plate and mixed with 100 µL of diluted Picogreen (1:200). The plate was incubated 5 min at room temperature protected from light. Then, samples were excited at 480 nm and fluorescence intensity was measured at 520 nm using a spectrofluorometer (Synergy H1 microplate reader, BioTek). A standard curve was plotted using λ DNA standard from 0 to 1000 ng/mL and DNA amount of the samples were calculated from the standard curve.

5.3.9. Cell morphology of individual cell encapsulation and alignment

In order to assess the organization and alignment of cells in TEBV-HUVEC and TEBV-HASMC, actin filaments (F-actin) were stained with phalloidin (Acti-stain 488 fluorescent phalloidin, Cytoskeleton, Inc) at the end of experiment, day 20, and at earlier time points, day 9 for HASMC and day 16 for HUVEC. Briefly, TEBV were rinsed with PBS prior the fixation with 4% PFA during 20 min at room temperature. After three washes of PBS, TEBV were permeabilized with 0,5% Triton-100x/PBS for 10 min. Afterwards, TEBV were rinsed three times with PBS and then incubated at room temperature with 100 nM Acti-stain 488 phalloidin protected from light for 30 min. Upon PBS washing, samples were incubated with DAPI (NucBlue Fixed Cell stain DAPI, LifeTechnologies) for 5 min. Finally, samples were kept with PBS and visualized by confocal laser microscopy (Leica SP8, LAS X software version 3.5.5.19976) (excitation/emission wavelengths were 480/520 nm for phalloidin and 405/460 for DAPI). Images processing and 3D reconstruction were performed with IMARIS software (Imaris 8.2, Bitplane and Oxford Instruments).

The alignment of HASMC was assessed measuring the alignment of actin filaments using the freely OrientationJ plugin for Fiji/ImageJ, based on the analysis of pixel-by-pixel vector field from the intensity gradient in the vertical and horizontal directions of the image, as further detailed in http://bigwww.epfl.ch/demo/orientation/ (26) . Different representative regions of different TEBV were analyzed. The percentage of alignment between |0±45º| and |90±45º| was calculated for each time point as a way to quantify the parallel alignment of HUVEC and perpendicular and diagonal alignment of HASMC within TEBV, respectively.

5.3.10. Cell morphology of co-cultured encapsulated cells in tissue engineered blood vessels (TEBV)

Finally, in order to understand if the co-culture would disrupt the cell morphology as well as if the cells could be allocated on their respective compartments, each cell type was stained with different colored cell tracker fluorescence probes previous the development of TEBV structures. HUVEC cells were stained with Green CMFDA (Invitrogen) and HASMC were stained with Red CMTPX (Invitrogen), emitting a green and red signal, respectively. Each cell tracker was added in the specific cell culture media at a final concentration of 10 µM and incubated with cells during 45 min at 37 ºC in 5% CO_2 protected from light. After incubation, cells were detached with Trypsin-EDTA (Gibco), centrifuged at 150xg for 3 min and used for blood vessel formation. Once TEBV were developed, they were imaged at 5 days by a confocal laser microscopy (Leica SP8, LAS X software version 3.5.5.19976). The excitation/emission wavelengths were 492/517 for Green CMFDA and 577/602 for Red CMTPX. Images were processed and 3D reconstruction was performed with IMARIS software (Imaris 8.2, Bitplane and Oxford Instruments).

5.3.11. Statistical analysis

Statistical analysis was performed using SPSS software (SPSS v21, IBM). Kruskal-Wallis and Mann Whitney U non parametric tests were used to compare the diameters of the TEBV at different injections speeds (data represented as mean ± standard deviation; n=10) and the DNA amount of cells at different time points (values of all time points were compared to day 0) (n=3). P-value of less than 0.05 was considered statistically significant.

5.4. Results

5.4.1. Concentration and purity of isolated collagen

After isolating the collagen, we measured its concentration by dry weight and obtained a concentration of 5.7 mg/mL. We further assessed the purity of collagen by SDS-PAGE as shown in **Figure 3** comparing it with a commercial type I collagen. The purity obtained was > 95%.
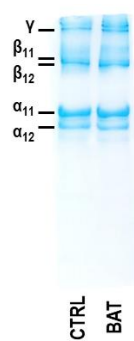
Figure 3. Collagen purity assessed by SDS-PAGE. CTRL: Type I collagen from BD Bioscience; BAT: Bovine Aquiles Tendon type I collagen.

5.4.2. Development of acellular TEBV-like structure

Maintaining a tubular structure is one of the first requisites to develop a TEBV-like structure. Experiments showed that the best conditions to maintain a tubular conformation were: 5 mg/mL of collagen in the middle layer, which could maintain the structure once Pluronic was removed (**Figure 4A**); and a final concentration of 2% of alginate and 3 mg/mL of collagen in the outer layer, in which HASMC stretching and orientation was observed. These conditions allowed a stable dual-layered tubular construct that could easily be handled.

Results showed a direct relation between the injection speed and the diameter of the construct, showing smaller diameters of the TEBV-like structures with the lower injection speed (**Figure 4B**). The outer and inner diameter were 1683.5 ± 45.7 µm and 1453.7 ± 55.8 µm for 50 mL/h and 1474.3 ± 60.4 and 1286.7 ± 61.6 µm for 25 mL/h, being statistically significant the differences between the two injection speeds ($p < 0.01$). The wall thickness was 114.9 ± 13.7 µm and 93.8 ± 10.5 µm for 50 and 25 mL/h respectively, also presenting statistically significant differences between them ($p < 0.01$). It is also worth highlighting the low variability in the different measurements, which are related with the fabrication of homogenous sized TEBVs.
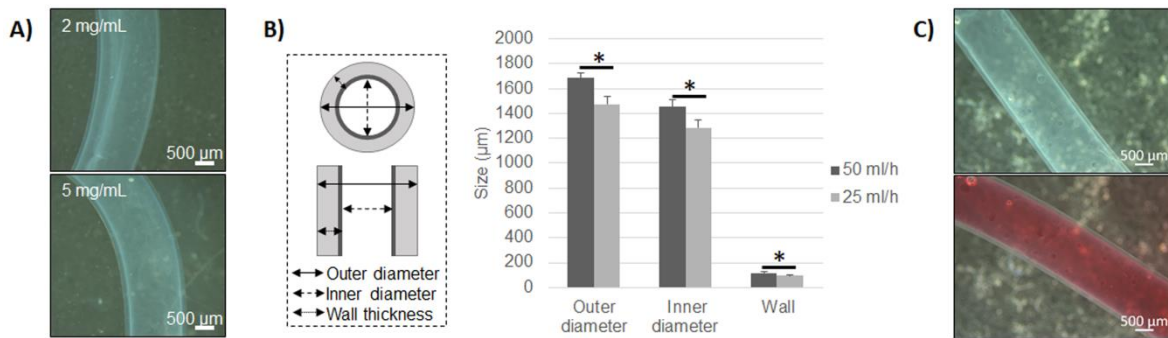
Figure 4. Characterization of tissue engineered blood vessels. (A) Optical images of collagen core optimization of TEBV with 2 and 5 mg/mL, above and below, respectively. (B) Outer and inner diameter and wall thickness of TEBV in response to 25 and 50 mL/h injection speed (n=10) (*= p<0.01). (C) Optical images of TEBV before (above) and after (below) manual perfusion with red ink.

Furthermore, the openness of TEBV-like structures and its perfusion was assessed using manual perfusion with red food ink, demonstrating a free flow through de TEBV, as shown in **Figure 4C**.

5.4.3. Proof of concept: alignment of HUVEC cells

A preliminary study was performed to validate if HUVEC cells were able to align into the longitudinal core-shell fiber axis. **Figure 5** displays representative phase contrast microscope images of HUVEC during culture for up to 3 days when encapsulated within core-shell collagen-alginate fibers. First of all, the lowest cell density ($1x10^5$ cells/mL) induced large zones without cells which maintained the rounded morphology overtime. Although this large zones without cells were smaller for the intermediate cell density ($1x10^6$ cells/mL), HUVEC cells maintained rounded morphology with negligible cell-to-cell interaction. Nevertheless, the highest cell density ($2x10^6$ cells/mL) induced reduction of distance between cells at day 0 and cell spreading at day 3, as shown in **Figure 5**. Moreover, HUVEC cells were aligned parallel to the core-shell fiber with the highest cell density at day 3.
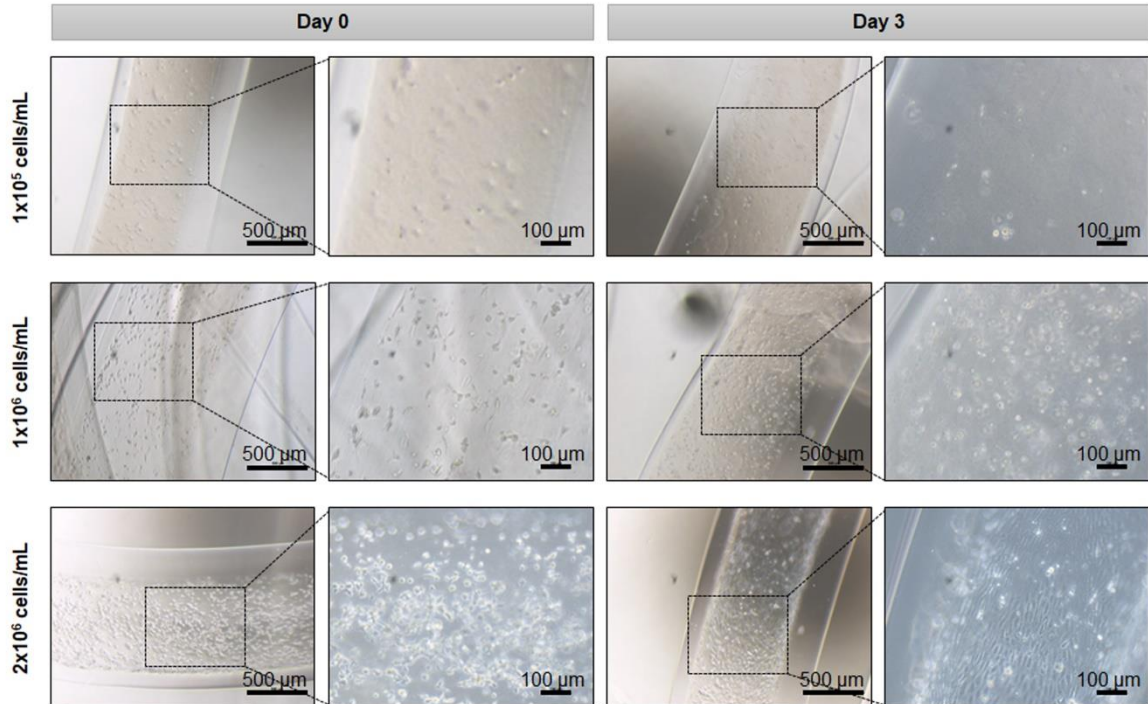
Figure 5. HUVEC density optimization in core-shell fibers. Different amount of HUVEC cells ($1x10^5$, $1x10^6$ and $2x10^6$ cells/mL) loaded in the core of core-shell fibers made of 1.5% alginate in the shell and 2 mg/mL of collagen. Images of cell culture at day 0 and 3.

5.4.4. Proliferation and viability of individual HUVEC and HASMC encapsulation within tissue engineered blood vessels (TEBVs)

After the preliminary results, in which the non-hollowed core shell fibers proofed the alignment of HUVEC on the direction of the fiber as well as the need to encapsulate high cell density within the fibers, we proceeded to encapsulate the cells in the hollowed TEBV like structure. The encapsulation of HUVEC in the middle layer (TEBV-HUVEC) resulted in HUVEC stretching within 24h, mostly with a parallel alignment and practically covering the entire core with a monolayer within 2 days (**Figure 6A**). A significant increase of DNA content arising from HUVEC was observed between day 0 and day 2 ($p<0.05$), remaining stable for the rest of the time points suggesting that HUVEC could proliferate within TEBV-like structure and that they reached confluence at day 2 (**Figure 6B**). Furthermore, live/dead assays revealed higher rates of cell survival, being near to 95% at 24h and 20 days (**Figure 6C**).
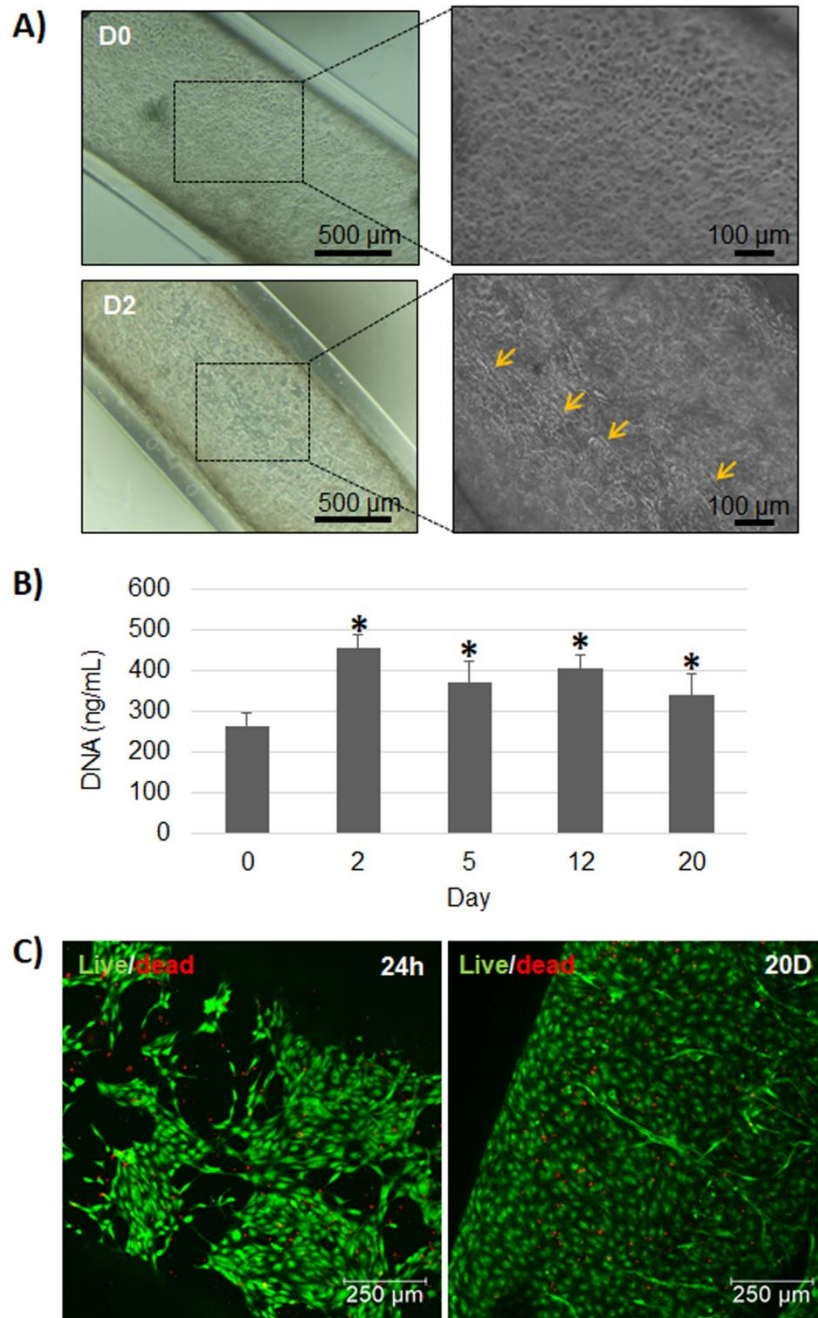
Figure 6. Encapsulation of HUVEC in TEBV (TEBV-HUVEC). (A) Optical microscope images of TEBV with HUVEC in the core at day 0 and 2. Arrows indicate some aligned cells. (B) HUVEC DNA content in TEBV at day 0, 2, 5, 12 and 20 (n=3, * p<0.05; day 0 was compared to the rest of the groups). (C) Live/dead assay performed on TEBV with HUVEC at 24h and day 20. Live cells (green) and dead cells (red).

When HASMC were encapsulated in the outer layer (TEBV-HASMC), cells started to lengthen at day 2 and covered the tubular wall structure at day 13 showing signs of perpendicular alignment respect TEBV direction (**Figure 7A**). There was a significant gradual increase of the DNA content from HASMC that could be observed at all time points compared to day 0 (p<0.05), suggesting that these cells could also proliferate within the construct (**Figure 7B**).

Similar to HUVEC, HASMCs showed high rates of cell survival after 24 hours and 20 days, being close to 95% in both cases (**Figure 7C**).
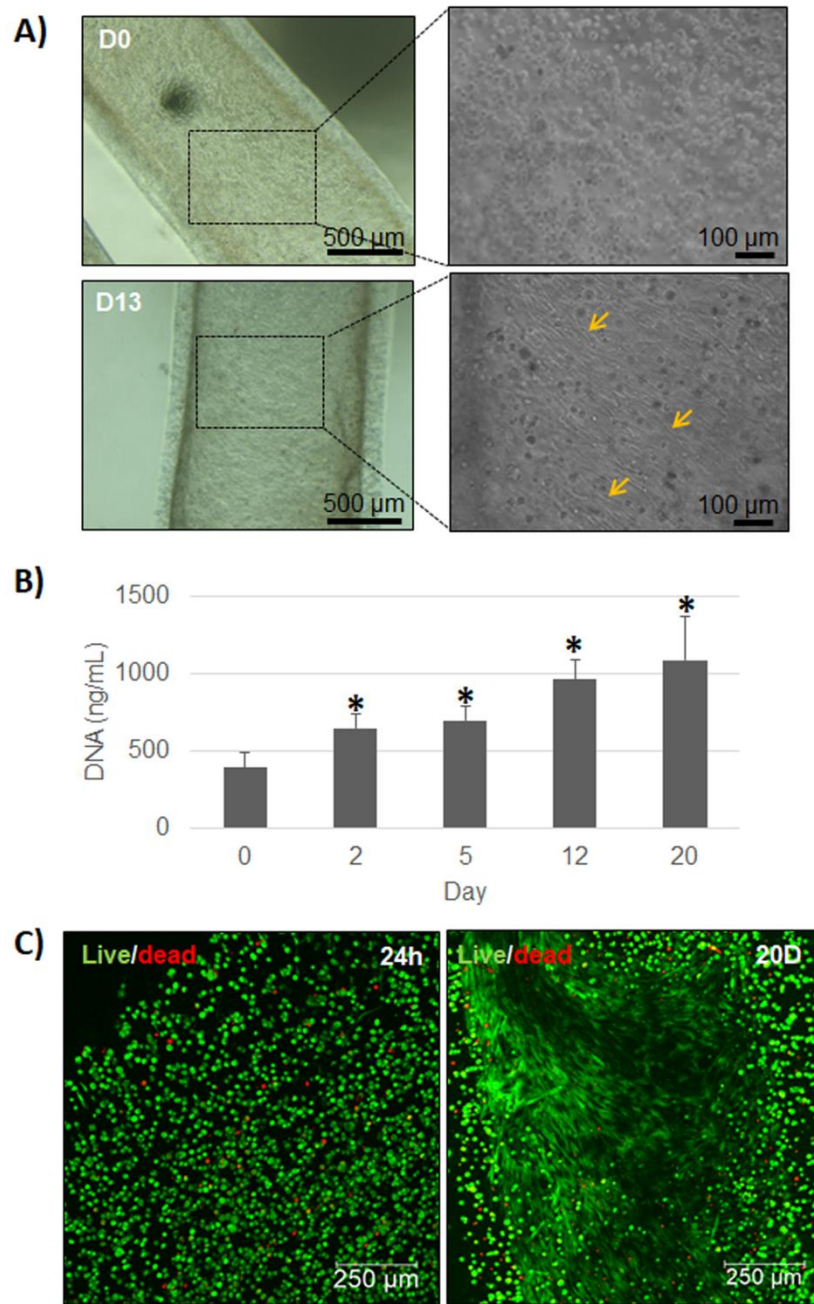
Figure 7. Encapsulation of HASMC in TEBV (TEBV-HASMC). (A) Optical microscope images of TEBV with HASMC in the shell at day 0 and 13. (B) HASMC DNA content in TEBV at day 0, 2, 5, 12 and 20 (n=3, * p<0.05; day 0 was compared to the rest of the groups). (C) Live/dead assay performed on TEBV with HASMC at 24h and at day 20. Live cells (green) and dead cells (red).

5.4.5. Organization and alignment of HUVEC and HASMC when encapsulated individually in tissue engineered blood vessel (TEBV) structures

In order to confirm the homogenous coverage of each individual cell type within the blood vessel like structure, a 3D reconstruction with phalloidin and DAPI was performed. Until day 16, TEBV-HUVEC formed a monolayer (**Figure 8A)**, but at the final time point, cells reorganized over it (**Figure 8B and C**). Unlike HUVEC, HASMC could proliferate forming a dense layer observed from day 9 (**Figure 8D**) to day 20 (**Figure 8E and F**). Cell alignment analysis showed 74% and 17% of HUVEC cells aligned between 0 and 45º respect to TEBV direction at day 16 and 20, respectively (**Figure 9A-D**). The reduction of a more parallel alignment might be due to the reorganization of cells over the monolayer and the difficulty to analyze the cells that were below it. The alignment of HASMC between 45 and 90º respect the direction of TEBV was 73% and 51% at day 9 and day 20, respectively (**Figure 10A-D**). This diagonal-perpendicular alignment was consistent with the optical microscope images of TEBV-HASMC (**Figure 8A**) and 3D reconstruction with phalloidin (**Figure 8D-F**), resembling natural alignment of native vessels.
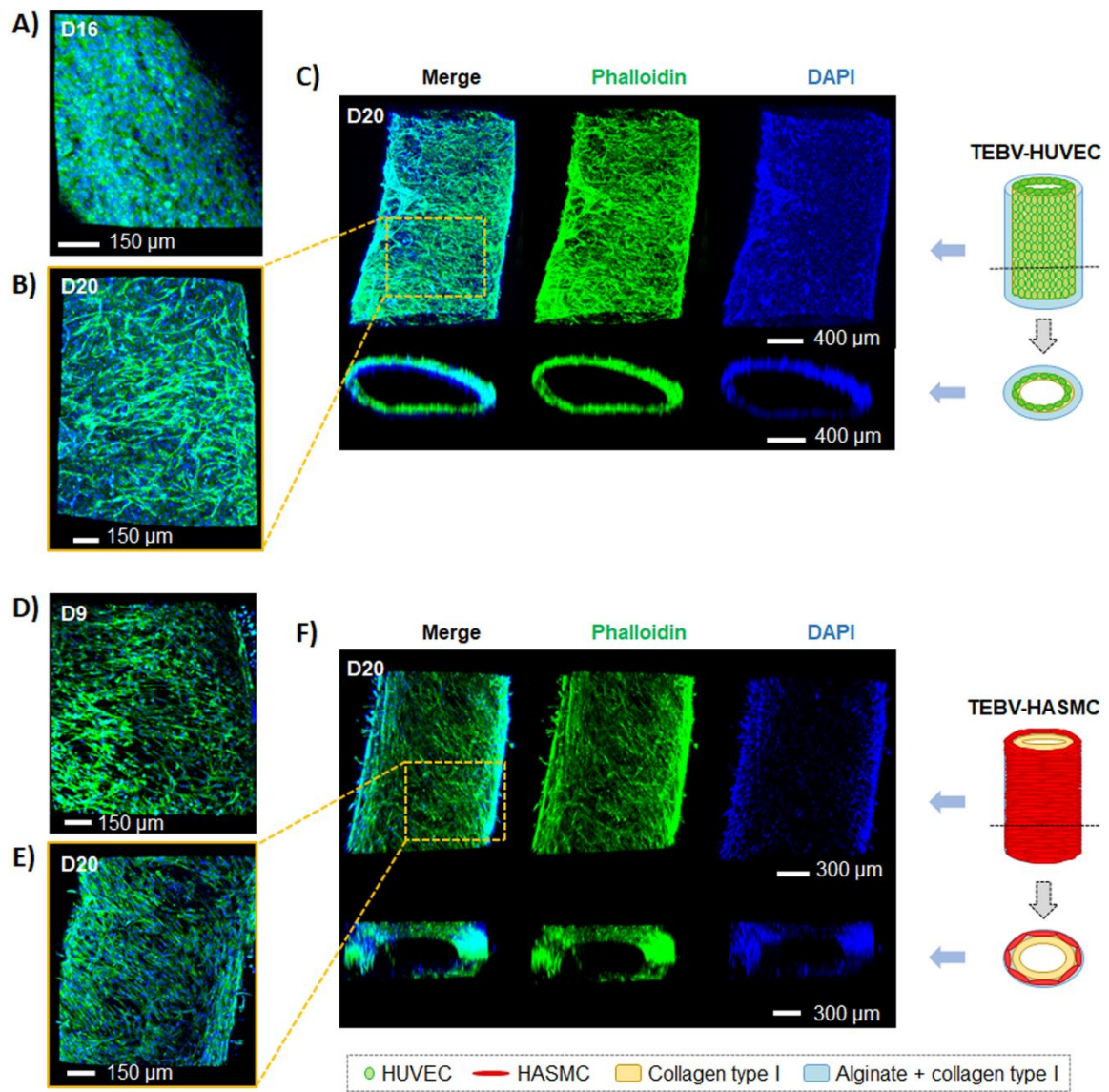
Figure 8. Confocal microscope reconstruction of TEBV-HUVEC or TEBV-HASMC. Phalloidin immunofluorescence staining of TEBV-HUVEC at day 20 (A) and 16 (B) and TEBV-HASMC at day 20 (C) and day 9 (D).
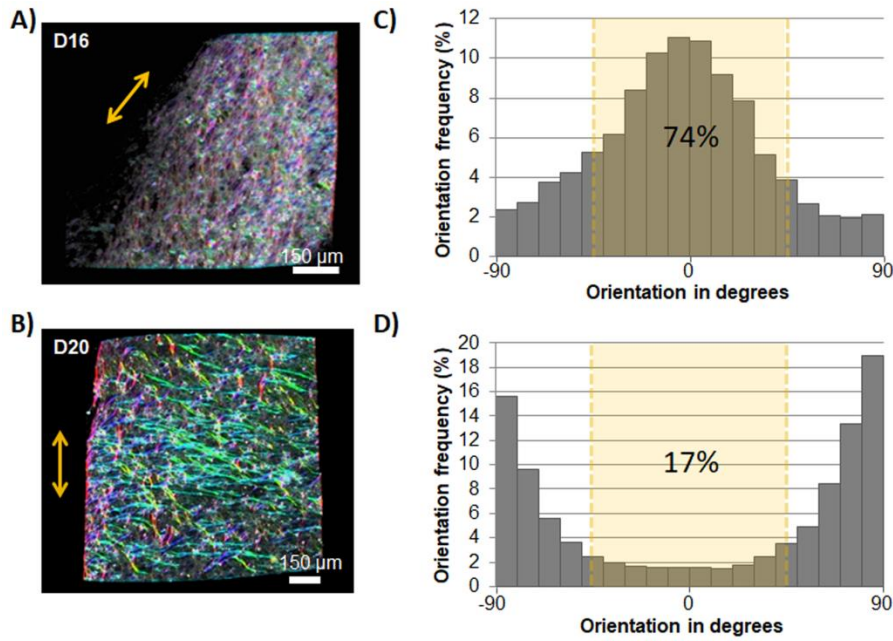
Figure 9. Orientation of HUVEC. Cell color coded orientation of TEBV-HUVEC at day 16 (A) and day 20 (B) showing the directionality of HUVEC. Cells with the same angle alignment are colored the same. Orientation of TEBV is indicated by the double headed arrow. Histograms showing the distribution of cell orientation at day 9 (C) and day 20 (D), were the direction of the TEBV was established as 0º.
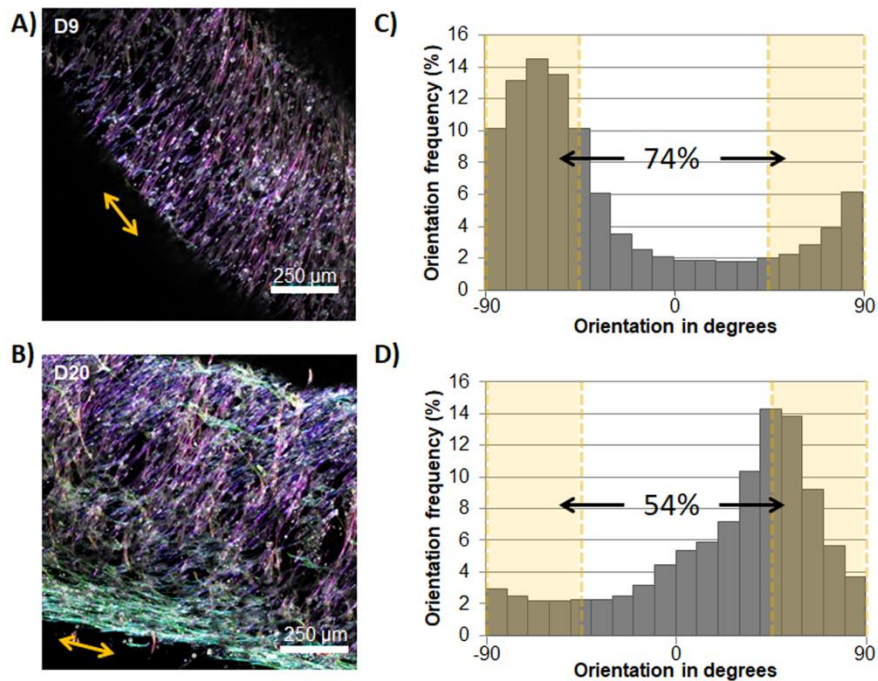
Figure 10. Orientation of HASMC. Cell color coded orientation of TEBV-HASMC at day 9 (A) and day 20 (B) showing the directionality of HASMC. Cells with the same angle alignment are colored the same. Orientation of TEBV is indicated by the double headed arrow. Histograms showing the distribution of cell orientation at day 9 (C) and day 20 (D), were the direction of the TEBV was established as 0º.

5.4.6. Co-culture within TEBV-like structure

The following step was to assess the behavior of HUVEC and HASMC once they were co-cultured within TEBV-like structure (TEBV-co). The live/dead assay confirmed high cell viability at 24h and at 20 days, showing over 96% and 94%, respectively (**Figure 11A**). However, the amount of DNA remained constant until day 12, followed by a moderate increase in DNA content ($p<0.05$) (**Figure 11B**).
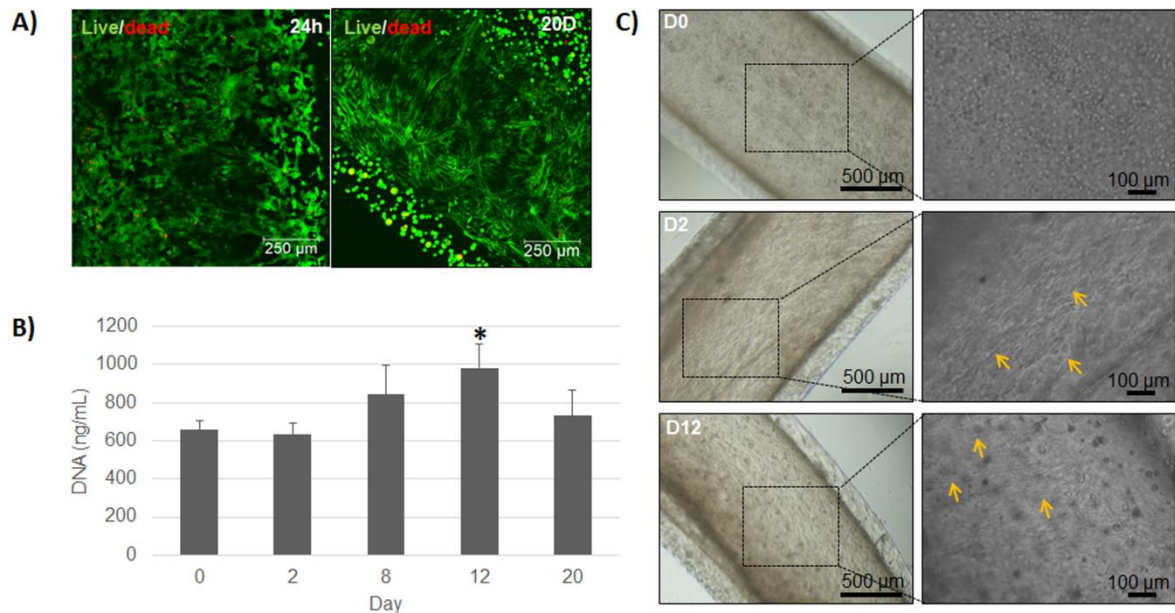
Figure 11. Co-culture of HUVEC and HASMC in TEBV (TEBV-co). (A) Live/dead assay performed on TEBV-co at 24h and at day 20. Live cells (green) and dead cells (red). (B) HUVEC and HASMC DNA content in TEBV at day 0, 2, 8 and 12 (n=3, * $p<0.05$; day 0 was compared to the rest of the groups). (C) Optical microscope images of co-culture of HUVEC and HASMC in TEBV at day 0, 2 and 12.

Optical microscope images showed stretched cells in the inner layer at day 2 and stretched cells in the outer layer from day 12 (**Figure 11C**). Visualizing the different cell types in co-culture was difficult with optical microcopy as well as with phalloidin and DAPI staining. Therefore, cells were stained with cell trackers in order to identify the two different cell types. At day 5, HUVEC were forming a monolayer, whereas HASMC remained with a round morphology (**Figure 12A and B**). It is important to note that both cell types remained in their respective cell layers. Short after, cell tracker fluorescence decayed, not allowing imaging and performing the 3D reconstruction with confocal microscope.
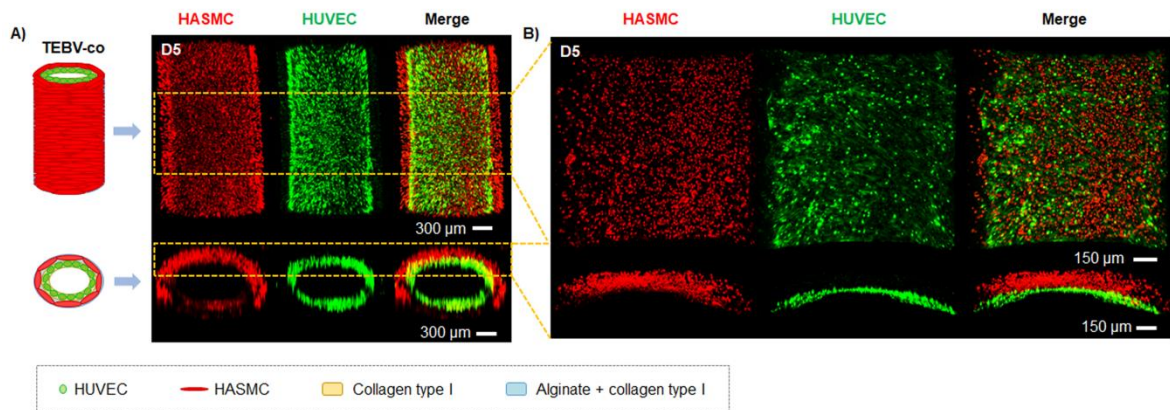
Figure 12. TEBV-co cell tracker reconstruction with confocal microscope at day 5. (A) Each color indicates different cell type: hSMCs in red and HUVEC cells in green at day 5. (B) Magnification of images shown in (A).

5.5.   Discussion

In order to bioengineer blood vessels *in vitro,* it is important to reproduce their native architecture to obtain a proper function once cells are embedded. In this study, we have developed a stable TEBV through an extrusion technique. This structure was composed, from inside to outside, by a hollowed layer followed by a layer of collagen sheathed by an outer layer made of alginate and collagen. Due to the property of alginate to instantly crosslink when being in contact with divalent ions (27), an alginate solution could maintain the tubular structure when extruded within a calcium chloride. Moreover, Pluronic was able to gel at 37 ºC (28) and it could maintain collagen into a tubular structure until it was gelled. When Pluronic was removed from the inner core by dissolution, a stable dual-layered hollow construct was obtained.

A part from reproducing the architecture of a blood vessel, another important characteristic to take into account is the biomaterials used. Two of the major components of an artery are collagen and elastin. More specifically, the most prevalent extracellular matrix (ECM) protein is collagen, specially type I, distributed in all three tunica (intima, media and adventitia) (29). For this reason, predominantly collagen type I was used to develop our TEBV. When testing which concentration of collagen type I provided the maximum tubular stability in the inner layer, we found that 5 mg/mL was the optimum condition, as shown in **Figure 4A**. A part from collagen, alginate was elected as the main component for the outer layer to give stability to our TEBV, which we previously showed to be an interesting hydrogel for core shell fiber formation. Nevertheless, the absence of functional domains could prevent HASMCs stretching and hence was combined with collagen. It was determined to use a final concentration of 2% alginate,

which conferred stability to our TEBV once it was extruded in calcium chloride solution, and 3 mg/mL of collagen on the outer layer, in which it could be observed HASMC lengthening (**Figure 7A**).

An interesting feature of the extrusion method used in the present work was that TEBV diameters obtained were dependent to the injection speed, obtaining higher calibers with higher injections speeds, as well as higher wall thickness. With 50 mL/h the outer diameter was around 1700 μm and the inner diameter around 1500 μm, whereas with 25 mL/h the outer and inner diameter were around 1500 and 1300 μm, respectively. The obtained results are similar to a previous study where it was observed an increase of the shell width when using the extrusion method, although their structures were non-hollowed core-shell constructs (24). These sizes correspond to the range of arteries, as they are described to be within 100 μm to 10 mm (30). Moreover, there was a lower coefficient of variation (less than 5%) for outer and inner diameter, indicating homogeneity between TEBV and a high reproducibility using this technique. Since the differences between the TEBV sizes extruded at 25 and 50 mL/h were very subtle, we decided to use the highest injection speed as it would take half the time to obtain the TEBV, hence increasing the chances of cell survival during extrusion process.

Due to the high injection speed chosen, we wanted to evaluate if cells could survive the shear stress suffered from the extrusion process at short time points. Furthermore, in order to guarantee nutrients and oxygen diffusion to the cells we also assessed cell survival at longer time points within the TEBV construct. We first encapsulated HUVEC in the inner layer (consisting of collagen) and HASMC in the outer layer (composed of alginate and collagen), in independent TEBV before performing a co-culture study. Both cell types exhibited high levels of viability during all time course of the experiment, being above 90% (**Figure 6C and 7C**). These results suggest that the extrusion method was not harmful for these cells and they could survive within the TEBV construct. This is a positive result taking into account that the viability of cells using microextrusion bioprinting technique is described to be between 40 and 86% (31,32). Moreover, there was an increase of DNA content of HUVEC cells from day 2 compared to day 0 (**Figure 6B**), suggesting that these cells had the proper 3D ECM conditions to proliferate. The content of DNA remained constant from day 2 to the end of experiment, implying that HUVEC cells may have reached confluence in an early stage, probably due to the high amount of cells initially incorporated. With HASMC, a gradual and significant increase of DNA content was observed during the course of the experiment (**Figure 7B**), suggesting that these cells also presented proper conditions to proliferate within TEBV structure. In this

particular case, lower amounts of HASMC were loaded compared to HUVEC due the different cell size, being HASMC three times the size of HUVEC (33).

More interestingly, with F-actin staining, HUVEC were observed to be covering the entire inner tubular structure, forming a monolayer of cells at day 16 (**Figure 8A**), although some cells grew over the monolayer at the end of experiment (**Figure 8B**). A parallel alignment was also observed for HUVEC in TEBV during the initial days after extrusion (**Figure 6A**) and persisted at day 16 (**Figure 9A and C**) but this arrangement was not consistent at the end of TEBV culture (**Figure 8B and C and Figure 9B and D**). In physiological conditions, endothelial cells (EC) are submitted through a shear stress from the blood flow, which is described to induce the alignment of EC parallel to the vessel (21). The extrusion method also applies a shear stress on the cells once they are extruded, and this could explain the initial parallel alignment of HUVEC. Because TEBV were cultured under static conditions, cells were not exposed to a laminar flow shear stress and this could explain the loss of their parallel alignment at the end of the experiment. A part from that, blood flow is needed to induce vessel maturation, which leads the quiescence of endothelial cells (34,35), amongst others, and this would also explain why HUVEC cells kept reorganizing over the monolayer when they reached confluence.

Similarly, F-actin staining of HASMC, showed cells covering the outer layer of TEBV (**Figure 8E and F**), having as well more cells at the end of the experiment compared with an early stage, such as day 9 (**Figure 8D**), consistent with DNA content. More interestingly, the percentage of aligned cells between 45º and 90º (perpendicular arrangement) was 73% and 51% at day 9 and 20, respectively, suggesting a diagonal-perpendicular alignment of these cells resembling the perpendicular alignment found in native arterial blood vessels (**Figure 8D-F and Figure 10A-D**)(10). This alignment is consistent with previous reports showing that vascular smooth muscle cells (VSMC) aligns in a shear-stress-dependent manner, being their orientation perpendicular with low shear stress (36). This alignment is of special interest as several mechanical functionalities of blood vessels, such as tensile strength, compliance and vasoactivity response, are mainly related to this conformation (37). To our knowledge, this is the first time that HUVEC and HASMC can be aligned in a parallel and diagonal-perpendicular way without perfusion, respectively, without inducing a patterning modification to the biomaterial, as has been performed with other methodologies such as sheet rolling (13,14) or electrospinning (38). To our knowledge, the only study that also encapsulated HUVEC and HASMCs using triple co-axial nozzle did not achieved a native cell alignment in static conditions and could only achieved it after perfusion (39). It is worth to mention that the collagen used was non-commercial and we isolated by ourselves. Although we demonstrated purity over

95%, we cannot exclude the possibility of the presence of other bioactive factors within the collagen that might have helped to promote the perpendicular alignment of HASMCs.

Finally, after ensuring HUVEC and HASMC survival within the TEBV structure, we wanted to validate if they could behave in a similar way once they were co-cultured (TEBV-co). Cells exhibited a high percentage of viability as shown in **Figure 11A**, being above 90%, at 24h and 20 days. These results suggest that both cell types could survive in co-culture within the TEBV construct, even at the end of the experiment where more cells were present. Optical microscope images (**Figure 11C**) showed cell lengthening in the inner layer at day 2, and cell lengthening in the outer layer at day 12, although both cells types could not be distinguished. Because of this, each cell type was stained with specific cell tracker previous to TEBV development in order to distinguish them within the structure. In an early stage of cell culture, a monolayer of lengthened HUVEC cells was observed, whereas HASMC presented a round morphology (**Figure 12A and B**). However, with the images obtained with the live/dead assay at 20 days we could observe that most of the cells were stretched (**Figure 11A**). The differences in cell stretching could be related with the decreased content of collagen in the HASMC layer compared to the HUVEC layer. Further experiment are required to increase the collagen content in the outer layer to enhance cell-matrix interaction as well as perfusion culture, as it has been previously shown to induce to a greater extent the cell arrangement of HUVEC parallel to the flow and perpendicular arrangement of HASMC perpendicular to the flow (21,40). Moreover, it has been reported that perfusion of blood vessels also induces ECM deposition by HASMC (40,41), further increasing their mechanical properties (42), and also enhance their maturation and functionality in terms of vasoactivity and permeability (40,43,44). Therefore, further studies should include assessment of mechanical properties and functionality of these TEBVs.

5.6.   Conclusions

In summary, it could be developed a TEBV-like structure in the range of arteries with this simple and low cost extrusion method in one step procedure, presenting high homogeneity between TEBV constructs leading to a high reproducibility of this technique. Moreover, it can be adapted to obtain TEBVs of higher caliber just changing the size of the triple concentric nozzle. The TEBVs obtained could be easily handled and can be potentially perfused. Furthermore, these TEBVs constructs were able to encapsulate HUVEC and HASMC, allowing their survival and proliferation within it. Additionally, HASMC showed a diagonal-perpendicular

alignment, resembling the alignment of smooth muscle cells in native arterial blood vessels, whereas HUVEC cells presented parallel alignment. Further experiments are required using perfusion culture to maintain the proper cell alignment and induce maturation and functionality of the construct.

5.7. References

1. World Health Organization. Cardiovascular diseases (CVDs) [Internet]. 2017. Available from: https://www.who.int/news-room/fact-sheets/detail/cardiovascular-diseases-(cvds)

2. Libby P, Buring JE, Badimon L, Hansson GK, Deanfield J, Bittencourt MS, et al. Atherosclerosis. Nat Rev Dis Prim. 2019;5(56):1–18.

3. Chaabane C, Otsuka F, Virmani R, Bochaton-Piallat ML. Biological responses in stented arteries. Cardiovasc Res. 2013;99(2):353–63.

4. McKavanagh P, Zawadowski G, Ahmed N, Kutryk M. The evolution of coronary stents. Expert Rev Cardiovasc Ther. 2018;16(3):219–28.

5. Kokkinidis DG, Waldo SW, Armstrong EJ. Treatment of coronary artery in-stent restenosis. Expert Rev Cardiovasc Ther. 2017;15(3):191–202.

6. Sabik JF. Understanding saphenous vein graft patency. Circulation. 2011;124(3):273–5.

7. Gu CX, Yang JF, Zhang HC, Wei H, Li LK. Off-pump coronary artery bypass grafting using a bilateral internal mammary artery Y graft. J Geriatr Cardiol. 2012;9(3):247–51.

8. Rieder E, Steinacher-Nigisch A, Weigel G. Human immune-cell response towards diverse xenogeneic and allogeneic decellularized biomaterials. Int J Surg. 2016;36:347–51.

9. Truskey GA. Endothelial cell vascular smooth muscle cell co-culture assay for high throughput screening assays for discovery of anti-angiogenesis agents and other therapeutic molecules. Int J High Throughput Screen. 2010;2010(1):171–81.

10. O'Connell MK, Murthy S, Phan S, Xu C, Buchanan J, Spilker R, et al. The Three-Dimensional Micro- and Nanostructure of the Aortic Medial Lamellar Unit Measured Using 3D Confocal & Electron Microscopy Imaging. Matrix Biol. 2008;27(3):171–81.

11. M M, S. S. Tubular hydrogels of circumferentially aligned nanofibers to encapsulate and orient vascular cells. Biomaterials. 2013;33(23):5713–22.

12. Jung Y, Ji H, Chen Z, Fai Chan H, Atchison L, Klitzman B, et al. Scaffold-free, Human Mesenchymal Stem Cell-Based Tissue Engineered Blood Vessels. Sci Rep. 2015;5(15116):1–9.

13. Yuan B, Jin Y, Sun Y, Wang D, Sun J, Wang Z, et al. A Strategy for Depositing Different Types of Cells in Three Dimensions to Mimic Tubular Structures in Tissues. Adv Mater. 2012;24(7):890–6.

14. Chen M, Li L, Xia L, Zhang F, Jiang S, Hu H, et al. Temperature Responsive Shape-Memory Scaffolds with Circumferentially Aligned Nanofibers for Guiding Smooth

Muscle Cell Behavior. Macromol Biosci. 2020;20(2):1–11.

15. Horakova J, Mikes P, Lukas D, Saman A, Jencova V, Klapstova A. Electrospun vascular grafts fabricated from poly (L- lactide-co-ε-caprolactone) used as a bypass for the rabbit carotid artery Electrospun vascular grafts fabricated from poly (L -lactide-co- ε - caprolactone) used as a bypass for the rabbit carotid a. Biomed Mater. 2018;13(065009).

16. Higgins SP, Solan AK, Niklason LE. Effects of polyglycolic acid on porcine smooth muscle cell growth and differentiation. J Biomed Mater Res - Part A. 2003;67(1):295–302.

17. Gao G, Lee JH, Jang J, Lee DH, Kong JS, Kim BS, et al. Tissue Engineered Bio-Blood-Vessels Constructed Using a Tissue-Specific Bioink and 3D Coaxial Cell Printing Technique: A Novel Therapy for Ischemic Disease. Adv Funct Mater. 2017;27(33):1–12.

18. Onoe H, Okitsu T, Itou A, Kato-Negishi M, Gojo R, Kiriya D, et al. Metre-long cell-laden microfibres exhibit tissue morphologies and functions. Nat Mater. 2013;12(6):584–90.

19. Zhang Y, Yu Y, Akkouch A, Dababneh A, Dolati F, Ozbolat IT. In vitro study of directly bioprinted perfusable vasculature conduits. Biomater Sci. 2015;3(1):134–43.

20. Perez RA, Kim M, Kim TH, Kim JH, Lee JH, Park JH, et al. Utilizing core-shell fibrous collagen-alginate hydrogel cell delivery system for bone tissue engineering. Tissue Eng - Part A. 2014;20(1–2):103–14.

21. Li Y, Huang G, Zhang X, Wang L, Du Y, Lu TJ, et al. Engineering cell alignment in vitro. Biotechnol Adv. 2014;32(2):347–65.

22. Deng X, Liao D, Wang G, Qiu J, Fan Y, Zheng Y, et al. Biomechanical regulation of vascular smooth muscle cell functions: from in vitro to in vivo understanding. J R Soc Interface. 2013;11(90):20130852–20130852.

23. Delgado LM, Shologu N, Fuller K, Zeugolis DI. Acetic acid and pepsin result in high yield, high purity and low macrophage response collagen for biomedical applications. Biomed Mater. 2017 Oct;12(6):65009.

24. Perez RA, Kim M, Kim T-H, Kim J-H, Lee JH, Park J-H, et al. Utilizing Core–Shell Fibrous Collagen-Alginate Hydrogel Cell Delivery System for Bone Tissue Engineering. Tissue Eng Part A. 2014;20(1–2):103–14.

25. Gui L, Dash BC, Luo J, Qin L, Zhao L, Yamamoto K, et al. Implantable tissue-engineered blood vessels from human induced pluripotent stem cells. Biomaterials. 2016;102:120–9.

26. Mohammed M, Thurgood P, Gilliam C, Nguyen N, Pirogova E, Peter K, et al. Studying the Response of Aortic Endothelial Cells under Pulsatile Flow Using a Compact Microfluidic System. Anal Chem. 2019;91(18):12077–84.

27. Kuen Yong Lee, David J. Mooney. Alginate: Properties and Biomedical Applications. Prog Polym Sci. 2012;37(1):106–26.

28. Gioffredi E, Boffito M, Calzone S, Giannitelli SM, Rainer A, Trombetta M, et al. Pluronic F127 Hydrogel Characterization and Biofabrication in Cellularized Constructs for Tissue Engineering Applications. Procedia CIRP. 2016;49:125–32.

29. Miranda-Nieves D, Chaikof EL. Collagen and Elastin Biomaterials for the Fabrication of Engineered Living Tissues. ACS Biomater Sci Eng. 2017;3(5):694–711.

30. Tortora GJ, Derrickson BH. Chapter 21. The cardiovascular system: Blood Vessels and Hemodynamics. In: Principles of anatomy & physiology. JSTOR; 2011. p. 740–807.

31. Bishop ES, Mostafa S, Pakvasa M, Luu HH, Lee MJ, Moriatis J, et al. 3-D bioprinting technologies in tissue engineering and regenerative medicine : Current and future trends. Genes Dis. 2017;4(4):185–95.

32. Chang R, Nam JAE, Sun WEI. Effects of Dispensing Pressure and Nozzle Diameter on Cell Survival from Solid Freeform Fabrication - Based Direct Cell Writing. Tissue Eng Part A. 2008;14(1):41–8.

33. Heydarkhan-Hagvall S, Helenius G, Johansson BR, Li JY, Mattsson E, Risberg B. Co-culture of endothelial cells and smooth muscle cells affects gene expression of angiogenic factors. J Cell Biochem. 2003;89(6):1250–9.

34. Carmeliet P, Jain RK. Molecular mechanisms and clinical applications of angiogenesis. Nature. 2011;473(7347):298–307.

35. Paszkowiak JJ, Dardik A. Arterial wall shear stress: Observations from the bench to the bedside. Vasc Endovascular Surg. 2003;37(1):47–57.

36. Qiu J, Zheng Y, Hu J, Liao D, Gregersen H, Deng X, et al. Biomechanical regulation of vascular smooth muscle cell functions : from in vitro to in vivo understanding. J R Soc Interface. 2014;11(90).

37. Chan-Park MB, Shen JY, Cao Y, Xiong Y, Liu Y, Rayatpisheh S, et al. Biomimetic control of vascular smooth muscle cell morphology and phenotype for functional tissue-engineered small-diameter blood vessels. J Biomed Mater Res - Part A. 2009;88(4):1104–21.

38. Wu T, Zhang J, Wang Y, Li D, Sun B, El-Hamshary H, et al. Fabrication and preliminary study of a biomimetic tri-layer tubular graft based on fibers and fiber yarns for vascular tissue engineering. Mater Sci Eng C. 2018;82:121–9.

39. Gao G, Kim H, Kim BS, Kong JS, Lee JY, Park BW, et al. Tissue-engineering of vascular grafts containing endothelium and smooth-muscle using triple-coaxial cell printing. Appl Phys Rev. 2019;6(4).

40. Eoh JH, Shen N, Burke JA, Hinderer S, Xia Z, Schenke-layland K, et al. Enhanced elastin synthesis and maturation in human vascular smooth muscle tissue derived from induced-pluripotent stem cells. Acta Biomater. 2017;52:49–59.

41. Oikonomou E, Tsalamandris S, Mourouzis K, Tousoulis D. Biology of the Vessel Wall. Coronary Artery Disease. Elsevier Inc.; 2017. 3–12 p.

42. Fernandez CE, Yen RW, Perez SM, Bedell HW, Povsic TJ, Reichert WM, et al. Human vascular microphysiological system for in vitro drug screening. Sci Rep. 2016;6(21579).

43. Price GM, Wong KHK, Truslow JG, Leung AD, Tien J. Effect of mechanical factors on the function of engineered human blood microvessels in microfluidic collagen gels. Biomaterials. 2011;31(24):6182–9.

44.   Ando J, Yamamoto K. Effects of Shear Stress and Stretch on Endothelial Function. Antioxid Redox Signal. 2011;15(5):1389–403.

CHAPTER 6

Mechanical and functional assessment of tissue engineered blood vessels (TEBV)

CHAPTER 6. Mechanical and functional assessment of tissue engineered blood vessels (TEBV)

The present chapter is the result of the collaboration with Truskey's lab led by Professor George Truskey from Biomedical Engineering Department of Duke University (Durham, North Carolina, USA). This work was developed during a PhD research stay for 6 months.

6.1.   Introduction

Vascular tissue engineering (VTE) has emerged in the last decades as an alternative of blood vessel replacement with autologous or xenogeneic source grafts for the treatment of cardiovascular diseases (CVDs) such as atherosclerosis or aneurysms. Before the use of vascular grafts in the clinics, several testing and criteria must be achieved, briefly summarized as: i) proper cell distribution and organization mimicking the architecture of native vessels; ii) proper maturation and functionality, including endothelial barrier function and vasoactivity and iii) proper mechanical stability to withstand physiological flow conditions (1).

In chapter 5, we described the use of a triple co-axial extrusion method to develop tissue engineered blood vessels (TEBVs) and demonstrated that cells were able to remain in their respective layers (endothelial cells (ECs) in the inner layer and smooth muscle cells (SMCs) in the outer layer). Remarkably, both cell types presented similar alignment to native blood vessels, although this arrangement was less consistent after 20 days of culture, specifically with ECs. Moreover, it is worth to mention that these TEBVs were not functional as they were cultured in static conditions. In order to achieve a functional degree in TEBVs, they need to be mechanically stimulated, similar to *in vivo* conditions (2). In this regard, perfusion bioreactors have been extensively used, as they allow the homogenous distribution of oxygen and biochemical factors, along all TEBV structure and, at the same time, provide biomechanical signals, specially laminar shear stress, which mimics physiological conditions inducing TEBV maturation (3,4).

It is worth to mention that the vascular system is exposed to different shear stress levels, and this should be taken into account for the perfusion of TEBVs. In physiological conditions, arterial shear stress is described to generally be between 10 and 70 dynes/cm^2, whereas vein shear stress is reported to be between 1 and 6 dynes/cm^2 (5,6). Several previous studies with

TEBVs with arterial size between 800 and 2000 μm, a shear stress between 6.8 and 15 dynes/cm^2 were applied, demonstrating functionality (7–10).

More in detail, it has been described that the laminar shear stress induced by TEBV perfusion tends to align EC parallel to the direction of the vessel (11), suppresses EC proliferation and induces them to a quiescence state (12). Moreover, it induces the expression of surface adhesion markers (13), establishing cell to cell adhesion increasing the selective permeability of the endothelium. It also stimulates the synthesis of NO, which is involved in vascular tone, specifically in vasodilation response, amongst other functions (14). At the same time, perfusion induces circumferential alignment of SMCs (15), inhibits their proliferative phenotype and triggers them to differentiate to a senescence contractile phenotype, with the ability to contract in response to vasoconstrictors (8,16). Additionally, it has been reported in the literature that perfusion activates vascular remodeling and stimulates cells to synthesize and deposit extracellular matrix (ECM), increasing their mechanical properties over culture perfusion time compared to TEBV cultured in static conditions (4,8,17).

Given all these mentioned properties of shear stress, maturation and functionality of perfused TEBVs can be studied *in vitro* by assessing vasoactivity response with the presence of vasoconstrictors and vasodilators. Additionally, endothelium permeability can also be assessed through the infusion of a labeled molecule and determining if its diffusion through the vessel wall is reduced through time. Furthermore, mechanical tests can provide more information about the increase of mechanical properties of TEBVs through time-perfusion.

All in all, these results published in the literature imply the need to perfuse TEBV in order to induce their maturation with proper functionality and adequate mechanical properties as a previous step for *in vivo* applications.

6.2.   Objectives

The aim of this chapter is to set up a perfusion system with appropriate conditions to perfuse our TEBVs. Moreover, this chapter seeks to address if perfusion of our TEBVs can increase mechanical properties as well as induce vessel functionality in terms of vasoactivity and barrier function.

6.3. Materials & Methods

For the tissue engineered blood vessel (TEBV) development, the procedure explained in the previous chapter (chapter 5) in sections 5.3.4, 5.3.5 and 5.3.6 was followed, with few modifications. Instead of using human aortic smooth muscle cells (HASMCs) encapsulated in the outer layer, human neonatal dermal fibroblasts (hNDF) were used. Additionally, alginate coupled with RGD sequences was used as outer layer composition.

6.3.1. Cell culture

Human umbilical vein endothelial cells (HUVECs) (Lonza Clonetics) and human neonatal dermal fibroblasts (hNDF) (Lonza Clonetics) were used. For expansion, HUVEC were seeded at a density of 2500 cells/cm^2 with endothelial cell growth medium (Cell Applications), supplemented with 5 mL of Antimycotic/Antibacterial (Gibco). hNDF were seeded at a density of 3500 cells/cm^2 and maintained with high glucose DMEM (Gibco) supplemented with 0.1% β-mercaptoethanol (Gibco), 1% Antimycotic/Antibacterial (Gibco), 1x Non-essential amino acids (NEAA, Gibco), 1x GlutaMax (Gibco), 1x Sodium Pyruvate (Gibco), and 10% Heat Inactivated FBS (Gibco). Both cell types were passaged at 80% confluence using 0.05% trypsin/EDTA (Sigma-Aldrich) and neutralized 1:1 with cell culture media. All cells were cultured in standard cell culture conditions (37ºC and 5% CO_2). For TEBV development, a final concentration of 15x10^6 HUVEC/mL and 10x10^6 hNDF/mL were used.

6.3.2. Setting up the perfusion system

6.3.2.1. Attachment of tissue engineered blood vessels (TEBV) to the chamber perfusion

For the perfusion of TEBVs, we used a chamber perfusion designed by Truskey's Lab (**Figure 1**).
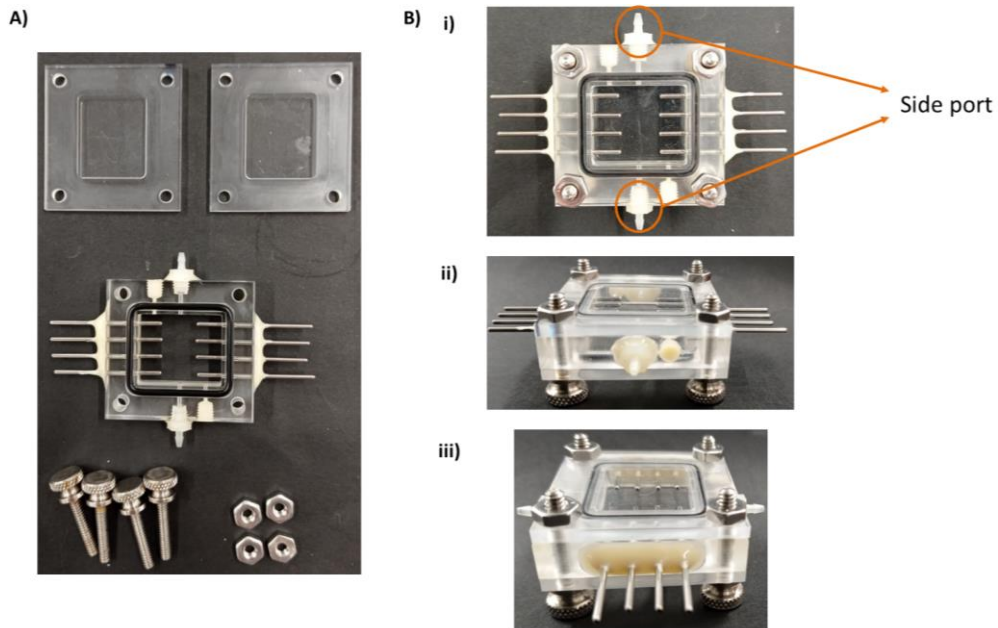
Figure 1. Perfusion chamber. A) Parts of the perfusion chamber disassembled. B) Mounted perfusion chamber, with i) upper view and ii-iii) side view.

In order to attach TEBVs to the mandrels of the perfusion chamber, we tested two different approaches. One of them was to suture TEBVs with 4-0 Silk Black Braided non-absorbable sutures (VWR) with one knot (**Figure 2A**). The other strategy consisted of attaching more surface of TEBV to avoid cutting it. In more detail, rectangular molds were developed with a silicone-based material (EcoFlex 00-30). Then, they were attached in the inner surface of the lids of the perfusion chamber. Finally, when the perfusion chamber was sealed with the lids, TEBVs were attached by pressure (schematic representation of this process is shown in **Figure 2B**).
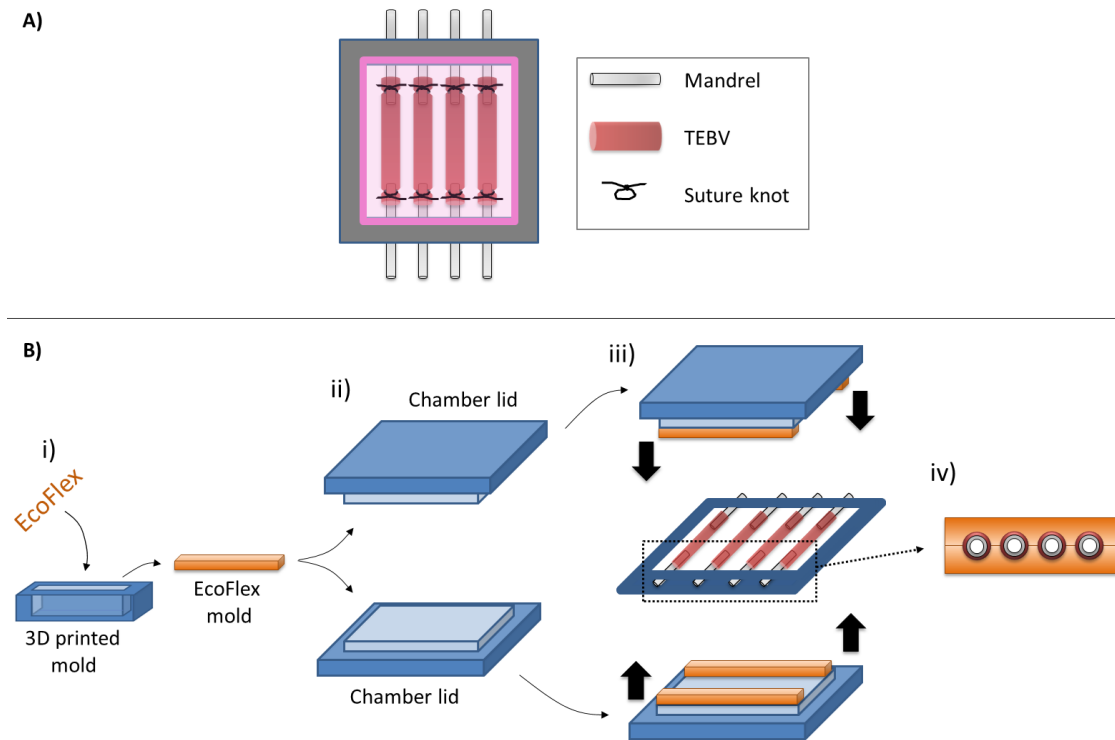
Figure 2. Approaches to attach TEBVs to perfusion chamber. A) TEBVs attached to the mandrels of the perfusion chamber using suture knots. B) i) EcoFlex molds are fabricated and ii) attached in the inner surface of chamber's lids to iii-iv) attach TEBV by pressure.

6.3.2.2. Flow rate parameters and components of perfusion system

First of all, the appropriate flow rate was calculated in order to apply an arterial shear stress, which was decided to be 10 dynes/cm^2 according to previous studies. For this purpose, we used the Poiseuille equation:

$$SS = \frac{4\mu Q}{\pi r^3}$$

Where *SS* is the shear stress, μ is the viscosity of the fluid, *Q* is the fluid rate and *r* is the radius of the vessel.

Then, a closed flow loop perfusion system was set up as schematically shown in **Figure 3.** Briefly, a masterflex peristaltic pump (Cole-Parmer) was used to drive the cell culture media from the reservoir to the pulsation dampener, then through the perfusion chamber and finally to the cell culture media reservoir again. All the main components were connected through L/S 16 platinum-cured silicone tubing (Masterflex, Cole-Parmer), with an exception on the input and output of the perfusion chamber, where L/S 13 platinum-cured silicone tubing (Masterflex, Cole-Parmer) was used. The perfusion chamber contained 8 stainless steel

mandrels (4 in each side), which matched the lumen diameter of the vessels, allowing the attachment of 4 TEBVs. This system allowed the perfusion of TEBV while maintaining the medium outside the TEBVs static, mimicking *in vivo* conditions.
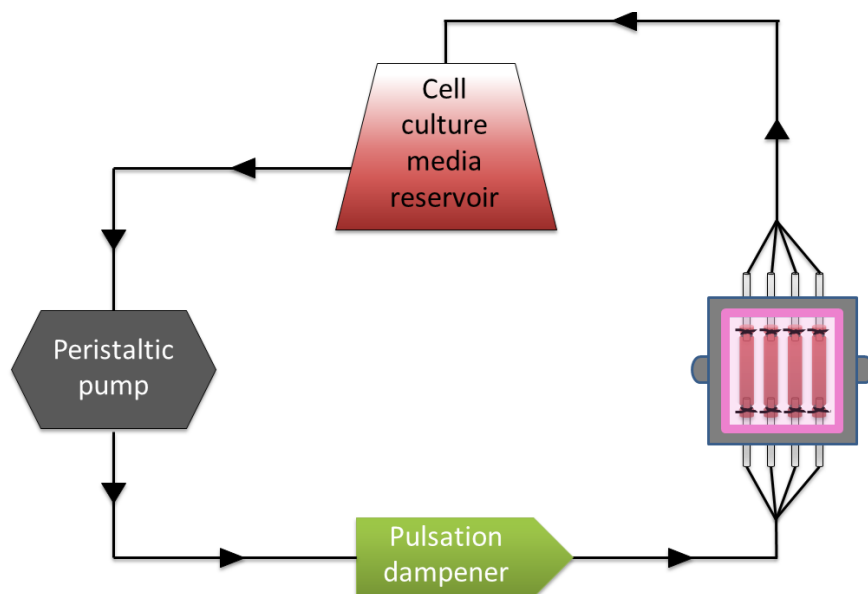
Figure 3. Schematic representation of the perfusion system. The system consists of a closed flow loop where the peristaltic pump drives the cell culture media from the reservoir to the perfusion chamber, which contains 4 TEBVs. To maintain a continuous flow, a pulsation dampener is added between the pump and the perfusion chamber.

The peristaltic pump used in this system induced a pulsatile flow rate, generating a cyclic stretch on TEBVs. Although it has been previously demonstrated that pulsatile flow enhances considerably TEBV maturation (4,17), it is difficult to establish the appropriate cyclic stretch according to TEBV size. Additionally, previous studies also reported that continuous flow induced TEBV maturation and functionality (7,8). Therefore, it was decided to establish a continuous flow as a first approach for the assessment of TEBV maturation. For this purpose, a pulsation dampener was added into the perfusion system to ensure a continuous and stable flow rate through TEBVs. Generally, a pulsation dampener consist of a closed chamber containing air with an inlet, where cell culture media enters, and an outlet, where cell culture media leaves (**Figure 4A**). Briefly, when cell culture media enters in to the pulsation dampener, the air contained within absorbs the pulsatile wave, resulting in a continuous flow when leaving through the outlet. Here, we developed ourselves a hand-made pulsation dampener. For this purpose, we used a 50 mL syringe (Becton Dickinson, VWR) and pulled out the plunger of the syringe without removing it completely. Then, with the help of a drill, we drilled the syringe transversely including the plunger and fixed it with a screw, as shown in **Figure 4B**. Finally, we sealed the plunger borders with Loctite Epoxy (M-121HP, McMaster Carr), to avoid

the escape of air or liquid. The 4 way stopcock (Cole-Parmer) was left open to allow the fluid flow to enter inside the pulsation dampener and attenuate the pulsatile flow. In our pulsation dampener, the inlet and outlet are the same orifice.
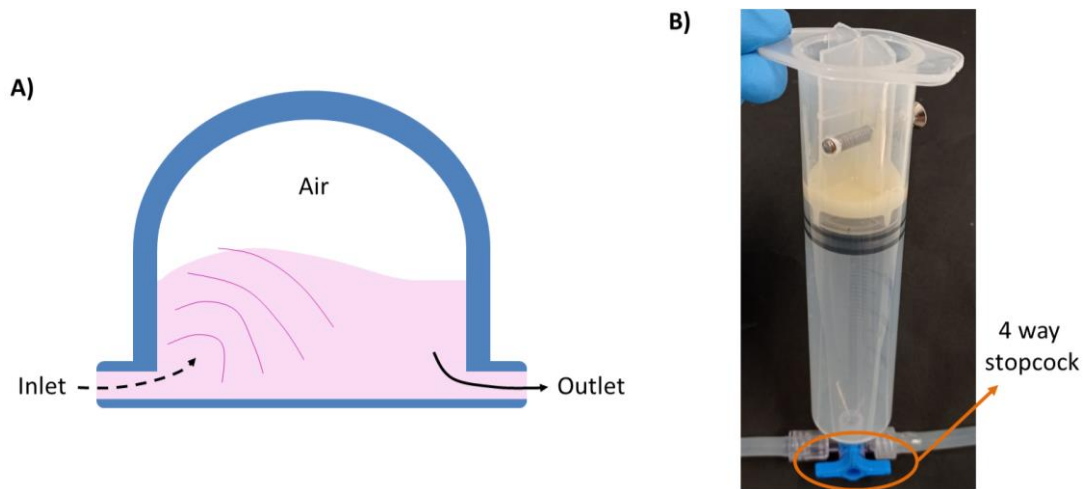
Figure 4. Pulsation dampener. A) Schematic representation of a pulsation dampener: the pulsation flow enters into the pulsation dampener, where the pulsatile wave is attenuated by the air, leading to a continuous flow when cell culture media leaves through the outlet. B) Image of the hand-made pulsation dampener developed and used in our perfusion system.

Once the perfusion system was set up, it was first tested by perfusing cell-free TEBVs with distilled water to ensure there was no leakage through all the system. Moreover, to ensure that there were no TEBV leakages, we stained the perfused distilled water with a blue ink while maintaining the water in the perfusion chamber un-stained. Then, we repeated the same procedure using cell culture media to confirm if TEBVs could be perfused with a flow rate inducing a shear stress of 10 dynes/cm^2.

Experiments of TEBV containing HUVEC and hNDF with their subsequently perfusion were performed in sterile conditions. All the tubing parts of the perfusion system were autoclaved, whereas the rest of the parts were sterilized with ethylene oxide. Cell culture media was replaced every other day from all the perfusion system, including the perfusion chamber using the side ports. Peristaltic pump was maintained outside the incubator whereas the perfusion system was maintained inside (**Figure 5**) with normal cell culture conditions, at 37ºC and 5% CO_2. TEBVs were perfused with the endothelial cell growth medium (Cell Applications) described in *section 6.3.1*.

Figure 5. Pictures of the perfusion system with the incubator. Peristaltic pump was placed outside the incubator whereas the rest of the perfusion system was placed inside.

6.3.3. Mechanical assessment

For mechanical assessment, burst pressure and ultimate tensile strength were measured and calculated, respectively.

Burst pressure is defined as the maximum pressure that a TEBV can withstand before rupture. In order to measure it, TEBVs were attached in the perfusion chambers with one end sealed and the other connected to a differential pressure gauge (Keller). PBS was injected through TEBVs until failure and the maximum pressure achieved was recorded. All the process was recorded in order to measure the diameters and wall thickness of TEBV to calculate the ultimate tensile strength. For this purpose, it was used a stereoscope (Amscope) connected to a video camera with ISCapture software. Burst pressure was performed with cell-free TEBVs with distilled water and with cell-loaded TEBVs with cell culture media. A total of four TEBVs were analyzed in each case.

Ultimate tensile strength (UTS) is defined as the peak stress that a TEBV can withstand while being stretched before failure. Burst pressure was used to calculate the UTS based on the law of Laplace using the following formula:

$$UTS = P \cdot \frac{D}{2t}$$

Where P is the value of the burst pressure, D is the inner diameter of the TEBV and t is the wall thickness. The same TEBVs that were used to measure the burst pressure were also used to calculate the UTS (n=4).

6.3.4. Understanding TEBV mechanical properties based on ion cell culture composition.

Cell-free TEBVs were developed and maintained with distilled H_2O prior to analysis. Three different experiments were performed to assess how sodium and calcium affected TEBV mechanic stability, measured by burst pressure. Sodium (NaCl, Sigma-Aldrich) and calcium ($CaCl_2$, Sigma-Aldrich) were prepared with distilled H_2O.

6.3.4.1. Incubation of TEBVs with sodium

TEBVs were placed and sutured within chamber perfusion with distilled H_2O. Then, the distilled H_2O was removed and TEBVs were incubated with sodium during 10 minutes. Concentrations tested were: 0, 10, 50, 150 and 300 mM NaCl (0 mM was distilled H_2O). Just thereafter the incubation time, burst pressure analysis was performed. Schematic representation of the procedure is shown in **Figure 6.**
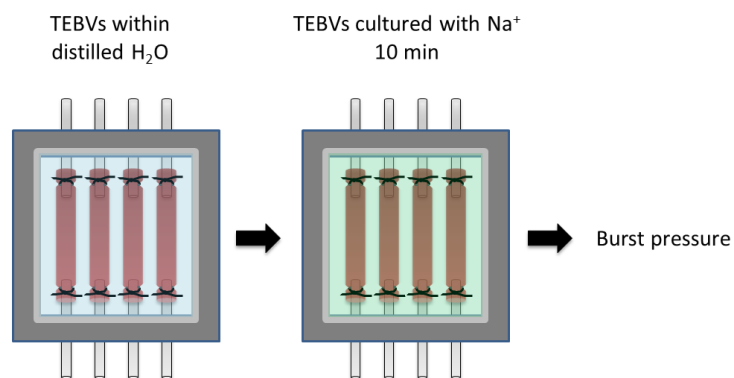
Figure 6. TEBVs cultured with sodium. After placing TEBVs in the perfusion chamber and suturing them, distilled H_2O was removed and replaced with a sodium-containing solution. After 10 minutes of incubation, burst pressure was performed.

6.3.4.2. Simultaneous incubation of sodium and calcium with TEBVs

The same procedure explained before (*section 6.1.1.1.1.*) was followed, but in this case, the combination of different concentrations of sodium and calcium were tested (see **Table 1** for concentrations tested). Schematic representation of the procedure is shown in **Figure 7.**

Table 1. Concentrations of sodium and calcium tested.

NaCl (mM)	CaCl$_2$ (mM)
10	300
50	300
150	300
300	300
10	50
50	50
150	50
300	50

Figure 7. TEBVs cultured with sodium and calcium solution. After placing TEBVs in the perfusion chamber and suturing them, distilled H$_2$O was removed and replaced with a sodium and calcium-containing solution. After 10 minutes of incubation, burst pressure was performed.

6.3.4.3. Sequential incubation of TEBVs with sodium and calcium

The same procedure explained before (*section 6.1.1.1.1.*) was followed with small changes. A concentration of 300 mM of sodium was removed after 10 min of incubation. Then, TEBVs and the chamber perfusion were washed three times with distilled H$_2$O. Afterwards, 300 mM of calcium was added and incubated for 10 more minutes. Just thereafter, burst pressure analysis was performed. Before and after sodium and calcium incubation, captures of TEBVs were taken. Schematic representation of the procedure is shown in **Figure 8.**

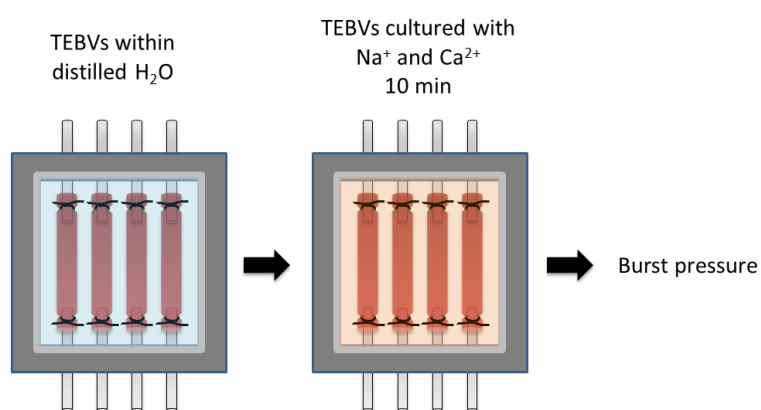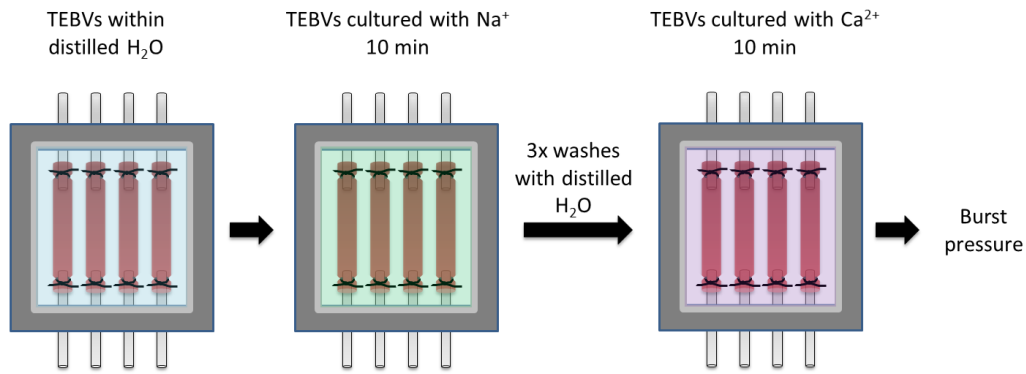**Figure 8. TEBVs cultured with sodium followed by calcium solution.** After placing TEBVs in the perfusion chamber and suturing them, distilled H_2O was removed and replaced with a sodium-containing solution. After 10 minutes of incubation, three washes were made with distilled H_2O. Then, TEBVs were incubated with calcium solution for 10 more min. After the incubation, burst pressure was performed.

6.3.5. Functional assessment

6.3.5.1. Vasoactivity

Vasoactivity assay consists on perfusing TEBVs with the presence of a vasoconstrictor (e.g. phenylephrine) or vasodilator (e.g. acetylcholine) and measure the diameter change. Phenylephrine interacts directly with hNDF to induce a vasoconstriction response, whereas acetylcholine interacts with endothelial cells, increasing their NO synthesis. Then, NO diffuses and interact with hNDF inducing a vasodilation response. Therefore, acetylcholine elicits an endothelium-dependent vasodilation through NO release. Phenylephrine and acetylcholine demonstrated to induce a diameter change in a dose-response manner from 1 to 100 µM (8).

Vasoactivity assay was measured with cell-loaded TEBVs at day 7 and day 14 (n=2). The same two TEBVs were analyzed per time point. Vasoactivity assay was measured at room temperature with the same perfusion circuit where TEBVs were cultured. Briefly, TEBVs attached in the perfusion chamber were located under a stereoscope (Amscope) connected to a video camera and were recorded with ISCapture software. First, the video recording was run for 30 sec to establish TEBV baseline diameter. Then, 1 or 10 µM of phenylephrine (Sigma-Aldrich) was injected into the flow circuit to assess the vasoconstriction response of TEBVs. After 5 min, 1 or 10 µM of acetylcholine (Sigma-Aldrich) was added into the perfusion system to study the vasodilation response. After 5 more minutes, the video recording was stopped. Images of TEBV from baseline, vasoconstriction and vasodilation were obtained from the video recorded and were analyzed using Image J. Four measurements per TEBV were performed using the same *x* or *y* positions for baseline, vasoconstriction and vasodilation. Changes in

outer diameter were expressed as percent change from the baseline outer diameter (% vasoconstriction) and percent change from the outer vasoconstriction diameter (% vasodilation).

6.3.5.2. Permeability

Permeability assay consist of infusing a labeled molecule with specific molecular weight through TEBV. The rate of diffusion of the molecule through the vessel wall can be calculated and be compared through perfusion time. Generally, TEBV perfusion induces maturation of them, which induces cell-to-cell adhesion and hence, selective permeability of molecules through vessel wall, avoiding the diffusion of high molecular weight molecules. Therefore, a reduction of diffusion rate is indicative of an increased selective permeability of endothelium.

For permeability assay, TEBVs were transferred and cannulated in a homemade perfusion device as schematized in **Figure 9**. FITC labeled dextran, with molecular weight of 500 KDa (FD500S, Sigma-Aldrich) or 20 KDa (FD20, Sigma-Aldrich) was injected into the lumen of TEBV, at a concentration of 2 mg/mL. We aimed to use a molecular weight of dextran that allowed its diffusion through the TEBV wall to further assess how its diffusion was decreased with perfusion time as a signal of a proper barrier function of our TEBVs. For his reason, we tested two molecular weights. The release of FITC-dextran through the wall of the TEBV increased the background fluorescent signal with time. Visualization was performed using a fluorescent microscope (Nikon ECLIPSE TE2000-U) for a maximum of 50 min.
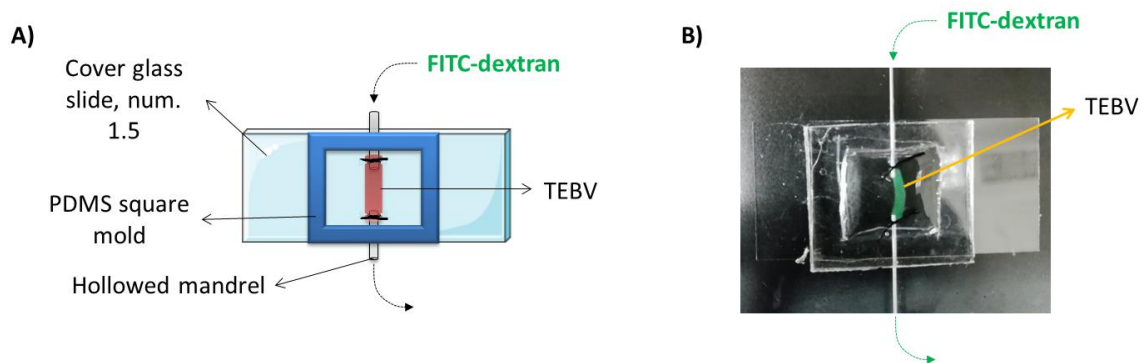
Figure 9. Hand-made permeability assessing device. A) PDMS hollowed square mold was attached on the surface of a cover glass slide together with two mandrels. TEBVs were sutured with the ends of the mandrels and FITC-dextran was perfused into the lumen. B) An image of the real device used for the permeability assays, containing 500 KDa FITC-dextran into the lumen of the TEBV.

The diffusion rate (P) of FITC-dextran with time was calculated using the following formula:

$$P = \frac{1}{\Delta I}\left(\frac{dI}{dt}\right)_0 \frac{r}{2}$$

Where:

- ΔI is the change in total fluorescent intensity upon adding labeled molecule.

- $\left(\frac{dI}{dt}\right)_0$ is the initial rate of increase of fluorescence out of the vessel lumen. This can be approximated as $\left(\frac{dI}{dt}\right)_0 \approx \frac{I_t - I_{t=0}}{t}$, where I_t is the intensity outside the vessel at time t, $I_{t=0}$ is the intensity outside the vessel at time 0.

- r is the radius of the lumen, estimated from width/2 of fluorescent region at t=0.

We aimed to measure permeability at day 0, 7 and 14, analyzing three TEBVs per time point.

6.3.6. Statistical analysis

Statistical analysis was performed using SPSS software (SPSS V21, IBM). Mann-Whitney U non-parametric test was used to compare the burst pressure of cell-free TEBV with distilled water and cell-loaded TEBV with cell culture medium at day 0 (n=3). Mann-Whitney U non-parametric test was also used to compare the burst pressure of TEBVs incubated with different concentrations of sodium respect to 0 mM of NaCl (n=3). Kruskal-Wallis and Mann-Whitney U non-parametric test were performed to analyze the differences of TEBV burst pressure comparing 0 to 10, 50, 150 and 300 mM of $CaCl_2$ for each NaCl concentration, and comparing 0 to 10, 50, 150 and 300 mM of NaCl for each $CaCl_2$ concentration. Data were represented as mean with standard deviation, analyzing 3 TEBVs per condition. P<0.05 was considered statistically significant.

6.4.   Results

6.4.1. Setting up the perfusion system

6.4.1.1.   Attachment of TEBVs to the chamber perfusion

In order to ensure TEBV immobilization within perfusion chamber, we first tried to attach them with hollowed mandrels using sutures. When we sutured them with cell culture media, TEBV were cut at the point of the suture with time, as shown in **Figure 10A**. As a second option, we tried to attach them by pressure using EcoFlex molds, but TEBV slipped away from the mandrels and could not be maintained straight (**Figure 10B**). Finally, we tried to combine both methods. More in detail, we first sutured TEBV with a weak knot that allowed TEBV to be maintained in specific position. Then, we applied pressure with EcoFlex molds resulting in straight TEBV conformation, as shown in **Figure 10C**.
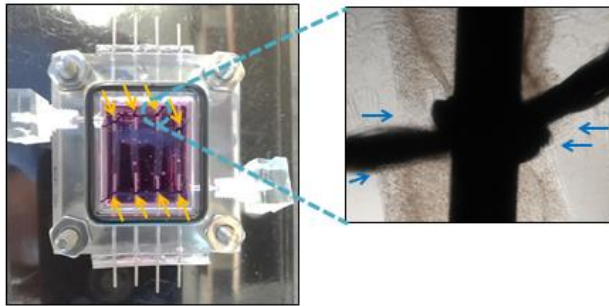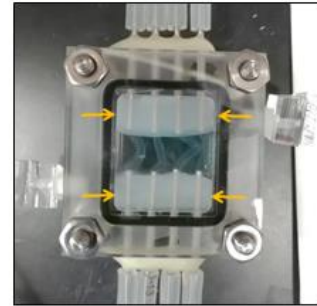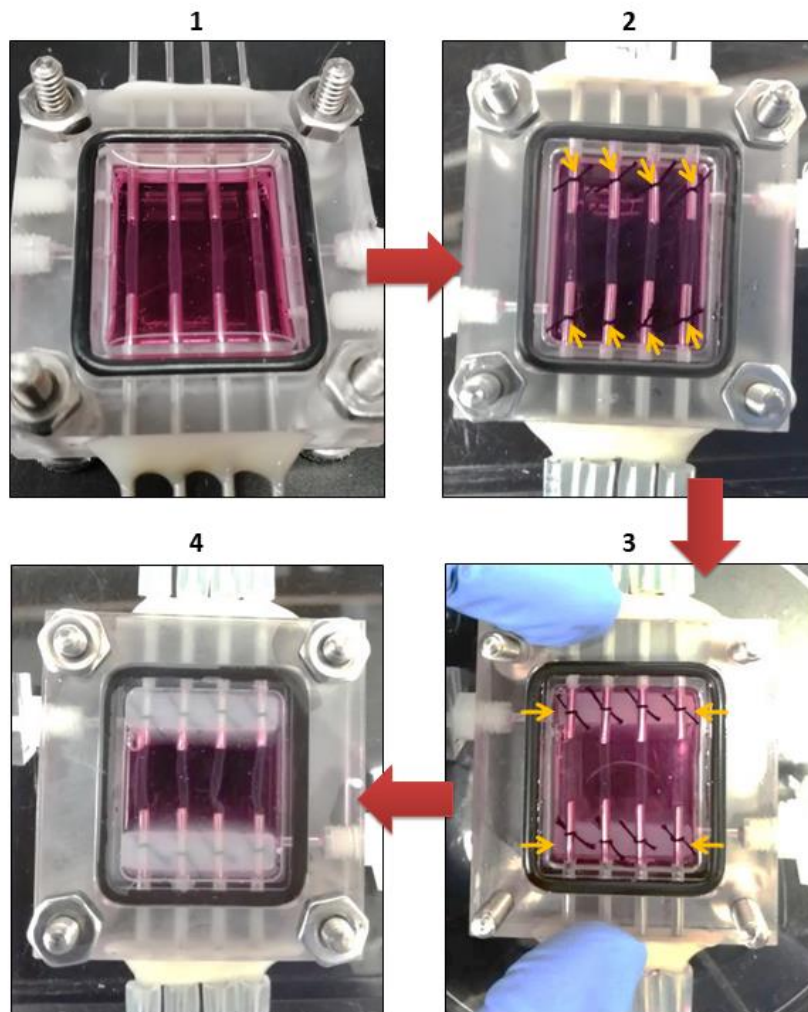
Figure 10. TEBVs attachment to perfusion chamber. TEBV attachment with A) sutures (orange arrows indicate the sutures; blue arrows shows points of TEBV break), B) EcoFlex molds (indicated with orange arrows) or C) a combination of sutures with EcoFlex molds, suturing them first and applying pressure with the EcoFlex molds thereafter.

6.4.1.2. Flow rate parameters

After adapting the chamber and perfusion system to the size of TEBVs, we first tried to perfuse them with distilled H_2O colored with blue ink to assess if they were able to withstand a minimum shear stress of 10 dynes/cm^2 and confirm that there were no leakages in the perfusion system. Remarkably, TEBVs could stand shear stress at least to 20 dynes/cm^2, with no leakage (**Figure 11A**). We decided to use 10 dynes/cm^2 for the perfusion experiments. However, when we perfused TEBVs with cell culture media, TEBVs seemed to be weaker and broke at the point of attachment. As a consequence, we reduced the flow rate, reducing the shear stress down to 4.8 dynes/cm^2, which showed to maintain TEBV integrity after 24h of perfusion with cell culture media with non-sterile conditions (**Figure 11B-C**).
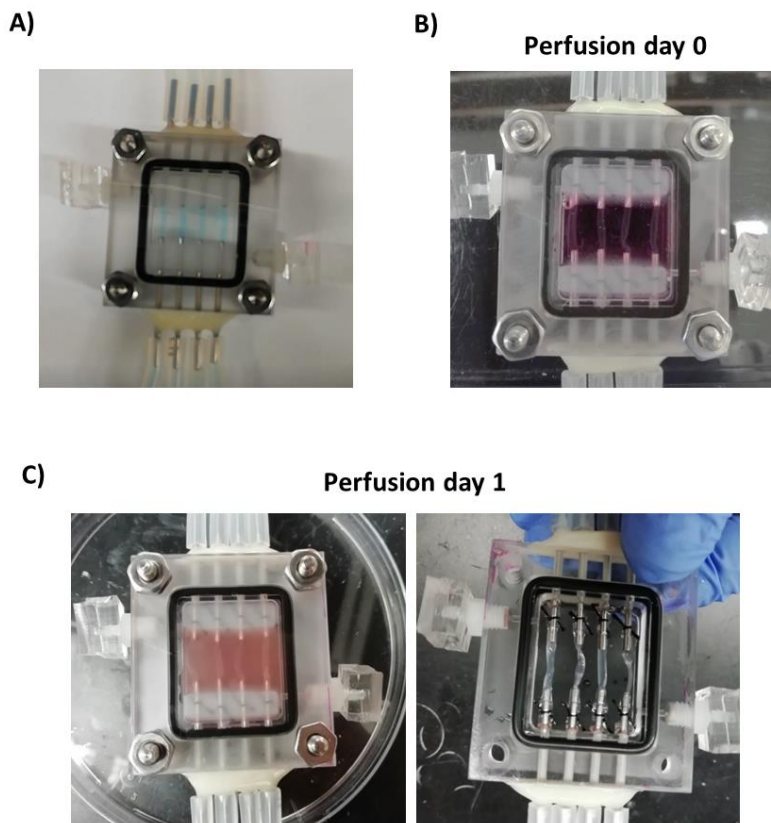
Figure 11. TEBV perfusion. A) TEBVs perfused with distilled H_2O colored with blue ink at 10 dynes/cm^2. B) Image of TEBV perfused with cell culture media at day 0 and C) at day 1 at 4.8 dynes/cm^2 (left: TEBVs within perfusion chamber with cell culture media; right: TEBVs without cell culture media maintaining the structure).

6.4.2. Mechanical assessment of TEBVs

Burst pressure and UTS were measured and calculated to evaluate the mechanical strength and stability of our TEBVs. We first measured the mechanical properties of cell-free TEBVs, obtaining a burst pressure of 1.77 ± 0.12 Bar (**Table 2**) and UTS of 1.01 MPa.

Table 2. Burst pressure results of cell-free TEBV with distilled H_2O.

Sample	Burst pressure (Bar)
TEBV-1	1.94
TEBV-2	1.74
TEBV-3	1.72
TEBV-4	1.68
Mean	**1.77**
± SD	0.12
CV (%)	6.56

Then, we repeated the measures with freshly develop TEBV containing HUVEC and hNDF (day 0) with cell culture media, obtaining a statistically significantly reduction of burst pressure with a value of 1.06 ± 0.03 Bar (**Table 3**) and a reduction of UTS of 0.37 MPa. From this time point on, no other analysis could be performed at day 7 or 14 as TEBVs had to be transferred into permeability chamber device and be sutured for burst pressure analysis, and they broke at the point of suture before being able to run the test.

Table 3. Burst pressure results of cellular TEBVs at day 0 with cell culture media.

Sample	Burst pressure (Bar)
TEBV-1	1.03
TEBV-2	1.06
TEBV-3	1.09
TEBV-4	1.04
Mean	**1.06**
± SD	0.03
CV (%)	2.51

6.4.3. TEBV stability with the presence of cell culture media ions

We realized that TEBVs become weaker in terms of mechanical properties when they were maintained with cell culture media, especially at the point of attachment of TEBVs with the perfusion chamber. This was not observed when TEBVs were maintained with distilled H_2O (**Figure 12A-B).**

Figure 12. A) Cell-free TEBVs attached with sutures within permeability chamber device in contact with distilled H_2O. B) Cellular TEBV after 7 days of perfusion in contact with cell culture media. Red arrows show break points of TEBVs.

In the cell culture media used, the concentration of sodium was 155 mM, whereas calcium was 1.8 mM. As both ions can affect the crosslinking of alginate, we proceeded to incubate TEBVs with different concentrations of them and assess TEBV stability.

6.4.3.1. TEBV cultured with different concentrations of sodium

As observed in **Figure 13**, the increase of sodium concentration reduced the burst pressure in a likely dose-concentration manner. The concentration of sodium present in the cell culture media used (155 mM, marked with red arrows in the graph) corresponded to a burst pressure around 1 Bar, which is in concordance with the burst pressure of cell loaded TEBVs at day 0 with cell culture media reported in section 6.4.2. This value corresponds to a reduction of 44.5% compared to burst pressure with 0 mM of sodium.
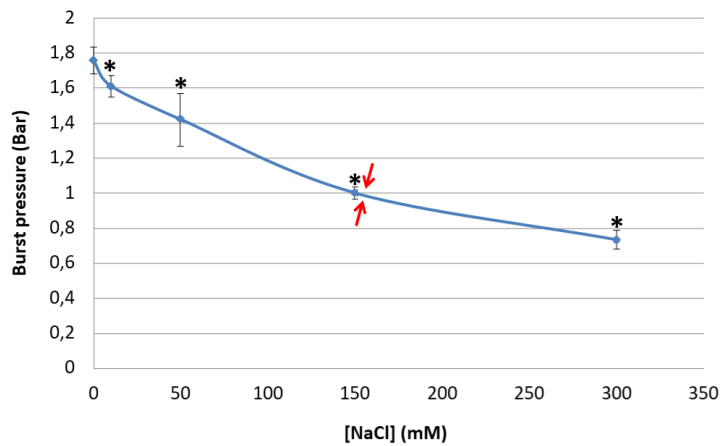
Figure 13. Burst pressure of TEBV cultured with different concentrations of sodium. Arrows indicate the concentration of sodium in cell culture media used for TEBV culture perfusion. Mean burst pressures with standard deviations are represented (n=3 per condition).
*Statistically significant differences of TEBV burst pressure compared with TEBVs incubated with 0 mM of sodium (p<0.05).

6.4.3.2. Simultaneous incubation of sodium and calcium with TEBVs

Then, we wanted to assess how different concentrations of both ions affected TEBV stability. As observed in **Figure 14**, without any concentration of sodium and increasing the concentration of calcium, burst pressure was maintained around 1.8 Bar. When concentration of sodium was increased, the burst pressure was reduced, but it could be increased at some extend increasing at the same time the concentration of calcium. Again, the approximate concentration of sodium and calcium in the cell culture media used was pointed out in the graph, which corresponded a burst pressure around 1 Bar.
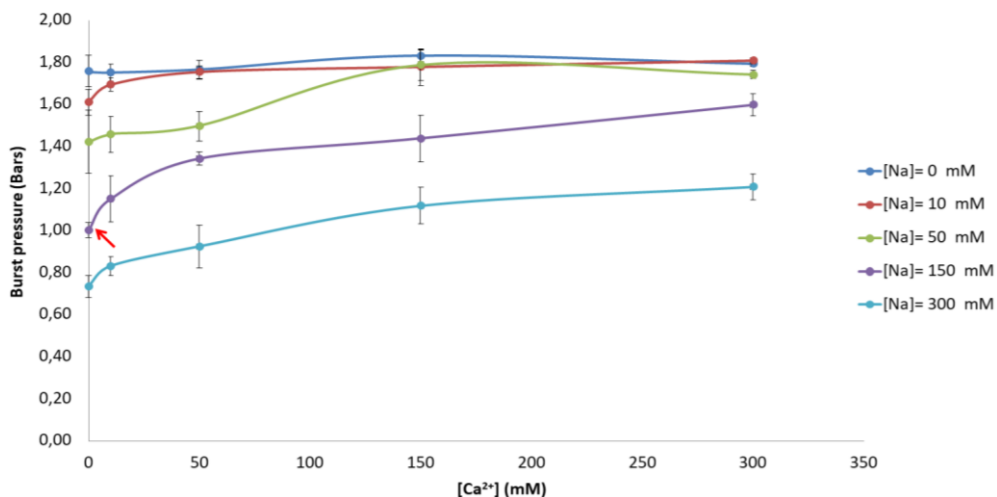
Figure 14. Burst pressure of TEBV cultured with different concentrations of sodium and calcium. Red arrow indicates the approximate concentration of sodium and calcium of cell culture media used to perfuse TEBV. Mean burst pressure with standard deviation is represented per condition (n=3).

The summarized statistical analysis results are in **Table 4** and **Table 5.**

Table 4. Significant statistical differences between 0 and 10, 50, 150 and 300 mM of CaCl$_2$ for each sodium concentration. Mann-Whitney U non-parametric test; n=3 per condition; *=p<0.05; ns =p>0.05.

		[CaCl$_2$] (mM)			
		10	**50**	**150**	**300**
[NaCl] (mM)	**0**	ns	ns	ns	ns
	10	*	*	*	*
	50	ns	ns	*	*
	150	*	*	*	*
	300	ns	*	*	*

Table 5. Significant statistical differences between 0 and 10, 50, 150 and 300 mM of NaCl for each calcium concentration. Mann-Whitney U non-parametric test; n=3 per condition; *=p<0.05; ns =p>0.05.

		[NaCl] (mM)			
		10	**50**	**150**	**300**
[CaCl$_2$] (mM)	**0**	*	*	*	*
	10	ns	*	*	*
	50	ns	*	*	*
	150	ns	ns	*	*
	300	ns	*	*	*

6.4.3.3.   Sequential incubation of TEBVs with sodium and calcium

As a final test, we proved if mechanical properties could be reversed. For this purpose, we incubated TEBVs with sodium and then with calcium. As shown in **Figure 15,** when TEBVs were incubated with 300 mM of sodium, they lost their straight integrity. Interestingly, after a second incubation with 300 mM of calcium, TEBVs could recover they straight structure and obtained a burst pressure of 1.8 ± 0.03 Bar.
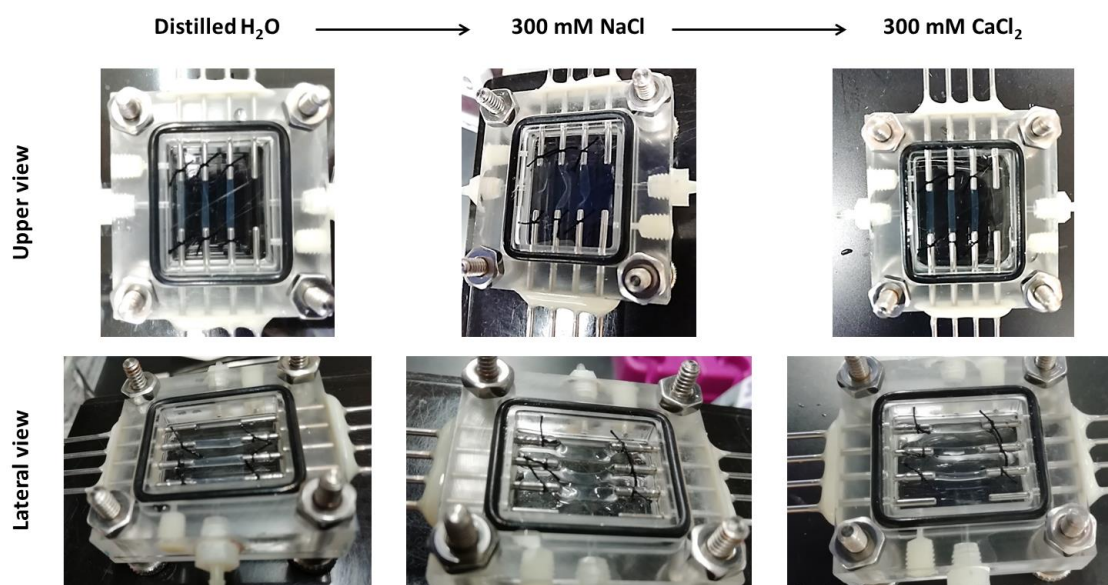
Figure 15. Captures of TEBVs incubated with distilled H_2O (left), after 10 min incubation with 300 mM of NaCl (middle) and after 10 min incubation with 300 mM $CaCl_2$ (right). Images from the above row are TEBVs in contact with their respective solutions, whereas images from the below row are TEBVs after removing their respective solutions.

6.4.4. Functionality of TEBVs

Although previous results showed a reduction of TEBV burst pressure with cell culture media, we proceeded to perfuse them with 4.8 dynes/cm^2, as previously shown to maintain their integrity at least for 1 day.

With a view to elucidate if TEBVs acquired some functionality due to perfusion, we analyzed their vasoactive response with the presence of phenylephrine as a vasoconstrictor and acetylcholine as a vasodilator. Moreover, we aimed to analyze the barrier function of the TEBVs by measuring the diffusion of dextran through the wall.

6.4.4.1. Vasoactivity response

After several attempts, only two TEBVs could withstand perfusion and reach up to day 7 and day 14. Despite the low number of samples analyzed, they seemed to present some vasoactivity in a dose-response manner, as observed in **Figure 16**. At day 7, an increase of contraction was obtained from -0.8 ± 0.4% to -1.62 ± 0.2% with 1 and 10 µM of phenylephrine, respectively (**Figure 16A**). In a similar way, an increase of dilation was observed from 0.9 ± 0.8% to 2.1 ± 0.4% with 1 and 10 µM of acetylcholine, respectively. At day 14, the contraction response with phenylephrine was reduced compared to day 7, being -0.6 ± 0.1 and -0.8 ± 0.8 with 1 and 10 µM, respectively (**Figure 16B**). Conversely, the vasodilation response seemed to

186

be slightly higher compared to day 7, being 1.22 ± 0.8% and 2.56 ± 1.4% with 1 and 10 μM, respectively.
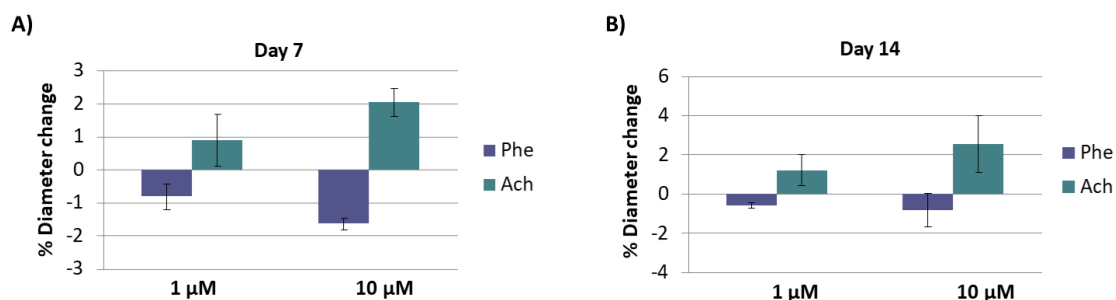
Figure 16. Vasoactivity of TEBVs. A) Vasoactive response of TEBVs at A) day 7 and B) day 14. Mean of % change is represented with standard deviation (n=2).

6.4.4.2. Permeability of endothelium

In order to assess the barrier function of endothelium, we first needed to select a proper molecular weight of dextran that diffused freely through TEBV wall in the absence of cells. This allows to further analyze if the diffusion is reduced with the presence of cells submitted to perfusion stimulus, as a sign of enhancing barrier function, reducing the random permeability of molecules through the vessel wall.

Dextran with a molecular weight of 500 KDa could not diffuse through the wall even after 50 min (**Figure 17A**). Conversely, 20 KDa could diffuse through the TEBV wall, as observed in **Figure 17B**, with a diffusion rate of 1×10^{-5}, 6.7×10^{-6} and 3.1×10^{-6} cm/s at 5, 10 and 20 min, respectively. Therefore, we selected 20 KDa of FITC-Dextran to perform permeability assay with cellular TEBVs. Interestingly, the diffusion rate of dextran obtained with freshly developed TEBV (day 0) containing HUVEC and hNDF was initially reduced, being $1.7\times10^{-5} \pm 4.9\times10^{-6}$, $1.2\times10^{-6} \pm 2.9\times10^{-6}$ and $7.2\times10^{-6} \pm 1.3\times10^{-6}$ cm/s at 5, 10 and 20 minutes, respectively (**Figure 17C**), which was lower than cell-free TEBVs. No further analysis could be performed beyond day 0, as TEBV had to be transferred from perfusion chamber into TEBV permeability perfusion device and be sutured. All of them broke in the point of suture, resulting in FITC-dextran leakage outside the vessel making it impossible to measure the diffusion through the wall.
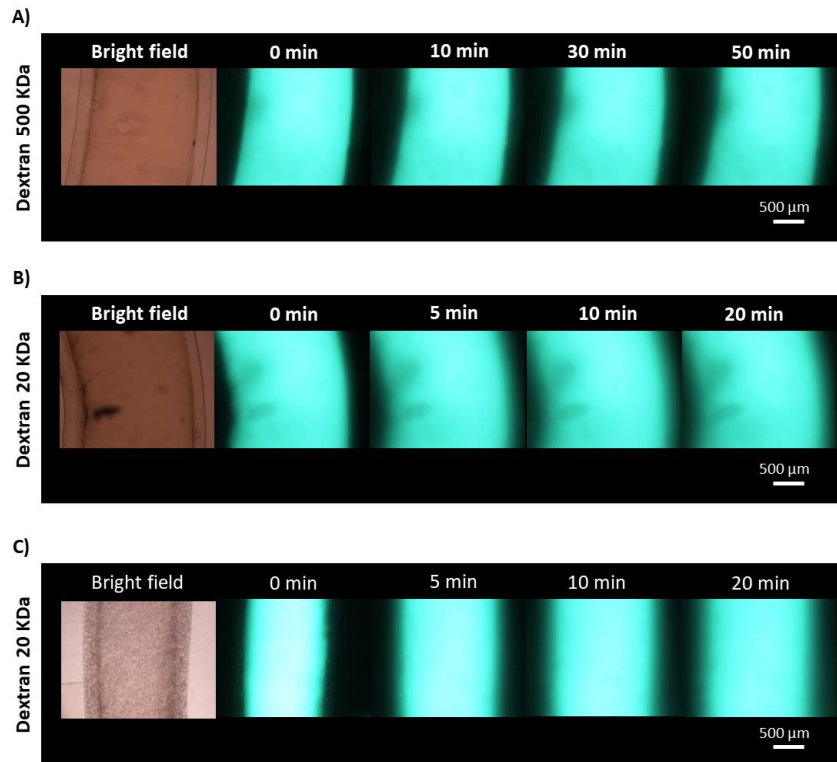
Figure 17. Permeability assay of TEBVs. Perfusion of cell-free TEBVs with A) 500 KDa and B) 20 KDa of FITC-Dextran. C) Perfusion of cellular TEBV with 20 KDa dextran at day 0.

6.5.   Discussion

In this chapter, the perfusion of TEBVs was performed to address if mechanical properties and functionality of TEBVs could be improved during perfusion time course. Initially, once the perfusion system was adapted to the size of our TEBVs, we perfused them to assess if they could withstand physiological flow rates which induced arterial shear stress. It is described that, generally, the shear stress in native arteries is between 10 and 70 dynes/cm^2, whereas in veins is reported to be among 1 to 6 dynes/cm^2 (5,6). Moreover, the size of arteries is described to be between 0.1 and 10 mm (18). Therefore, as our TEBVs had an approximately inner diameter of 1400 μm, which is in the low range of artery size, we decided to induce them a lower shear stress of 10 dynes/cm^2, which is in accordance with the shear stress applied in other studies with similar TEBVs sizes (9,10). Remarkably, when cell-free TEBVs were perfused with distilled H$_2$O to test the perfusion system, they could withstand at least a shear stress of 20 dynes/cm^2. However, when perfused with cell culture media, TEBVs become weaker and broke at the point of attachment. After reducing the shear stress, TEBVs could only maintain their integrity applying a shear stress of 4.8 dynes/cm^2 for at least 24h (**Figure 11**). Therefore, we used this low shear stress for the subsequent assays. Previous studies could demonstrate

TEBV maturation and functionality with shear stress of 6.8 dynes/cm^2 (7,8). Moreover, other studies demonstrated that EC and SMCs could mature with even lower shear stress, specifically with 2.5 and less than 1 dyne/cm^2 (17,19). Therefore, we considered that some functionality could be achieved with 4.8 dynes/cm^2.

After developing TEBVs and mature them with perfusion stimulus, mechanical properties of them are expected to be at least similar to native vessels. For instance, burst pressure of internal mammary artery is 3200 mmHg (4.2 Bars) and saphenous vein is 1600 mmHg (2.1 Bars) (20), having diameters of 1.9-2.6 mm and 3.1-8.5 mm, respectively (21). When we performed the burst pressure of cell-free TEBV with distilled water, we obtained a burst pressure of 1327.6 ± 87 mmHg (1.77 Bars) (**Table 2**), which is a little lower than saphenous vein. However, a study reported an increase of burst pressure during perfusion time due to extracellular matrix deposition by cells (22), therefore, we considered they were good initial mechanical properties with potential to be increased throughout perfusion time. Moreover, we obtained UTS of 1.01 MPa, which is a little above from native arteries, which is described to be around 0.5-0.8 MPa (23,24). However, when we incorporated cells to our TEBVs and performed burst pressure at day 0 with cell culture media, burst pressure and UTS drastically drop, specifically obtaining 791.3 ± 22.5 mmHg (1.06 Bars) and 0.37 MPa (**Table 3**). As previously mentioned, cell culture media seemed to weaken our TEBVs, and this could explain the reduction of burst pressure and UTS.

After observing the evident weakening of TEBVs when placed or being in contact with cell culture media, we checked cell culture media composition and noticed that it contained an elevated concentration of sodium (around 155 mM) compared to calcium (around 2 mM), which is consistent with the concentrations of these ions found in human blood (25). We conducted experiments were cell-free TEBV were incubated with different concentrations of sodium and with a combination of different concentrations of sodium and calcium, to test how sodium ions affected TEBV stability. The increase of sodium decreased the burst pressure of TEBVs (**Figure 13**), being with 150 mM of sodium almost a reduction of 50% compared with 0 mM of sodium. Moreover, when calcium was increased with the presence of sodium, it could increase to some extend the burst pressure (**Figure 14**). Interestingly, TEBV incubation with calcium after sodium, recovered burst pressure to 1.8 Bar. These results suggested that sodium and calcium might compete for alginate, and sodium might be able to replace calcium from alginate when found in higher concentrations, destabilizing the crosslinking of alginate. Therefore, these results can explain why we had more difficulties to perfuse TEBVs with cell culture media. These findings are in agreement with prior papers published in the literature.

Alginate has been previously described with a limited long-term stability when placed with physiological fluids due to exchange of calcium with monovalent ions (26). However, it is worth to mention that considering TEBVs developed with alginate, our TEBVs presented higher mechanical properties, with an UTS of 0.37 MPa, compared to TEBVs developed with 4% alginate by other authors, reporting an ultimate strength of 0.18 MPa (27). That might be due to the presence of collagen in our TEBVs. Other studies report difficulties in manipulating alginate-TEBVs with low mechanical properties, but presenting promising results when implanted *in vivo*. For instance, Gao *et al.* developed a TEBV with and hybrid bioink composed of a mixture of alginate with vascular-tissue-derived decellularized extracellular matrix and implanted in an *in vivo* mouse ischemic limb model. Authors mentioned as a limitation the weak mechanical strength of their TEBVs hampering their surgical anastomosis with the host vessel in the implantation process. However, they could demonstrate an improvement of neovascularization in the ischemic limb after TEBV implantation (28).

Although TEBVs presented low mechanical properties, we decided to perfuse the cell loaded TEBVs with the lower shear stress of 4.8 dynes/cm^2, in which TEBVs seem to withstand for at least 24h during the setting up of perfusion system. During perfusion time, the chances of TEBVs to maintain their integrity at the point of attachment up to 7 or 14 days were low. Regarding vasoactivity assay, we could analyze two TEBVs at both time points. The preliminary results were promising, demonstrating some functionality, with the capability of TEBVs to respond to phenylephrine and acetylcholine, a vasoconstrictor and vasodilator, respectively. TEBVs seemed to respond in a dose-dependent manner, with the maximum contraction achieved of -1.62% and a maximum dilation of 2.56% (**Figure 16**). The vasoactive response was close to the physiological range of human native arteries, since for instance, human radial arteries dilate between 3-10% (29). It is likely that the lower values are due to the low flow rate and shear stress applied, which were characteristic from veins. Moreover, given that our findings are based on a limited number of TEBVs, the results from such analyses should therefore be treated with caution. In relation to endothelial barrier function, 500 KDa FITC-dextran could not diffuse through cell-free TEBVs, whereas 20KDa could freely pass through vessel wall (**Figure 17**). These are interesting results, as suggests that alginate itself is able to reduce the freely diffusion of molecules with high molecular weight. In addition, these results are in agreement with a previous study, where the same molecular weights of molecule were tested (30). Specifically, 500 KDa could not diffuse through a 2.5% alginate vessel wall, a concentration similar of our TEBVs, which was 2%. Authors suggested that the highest molecular weight could not diffuse due to mesh pore size, being lower molecular weight

tested smaller and, therefore, being able to rapidly invade the alginate wall. Interestingly, diffusion rate of dextran through cell-loaded TEBVs at day 0 was slightly reduced compared to cell-free TEBVs, indicating that the presence of cells ameliorated the barrier function. However, although we were able to obtain three TEBVs up to day 7 and 14, we could not evaluate if the diffusion rate was reduced from day 0 on due to technical problems. More specifically, TEBVs had to be transferred into permeability chamber device and be sutured for the assay, resulting in TEBV break at the point of suture leading to FITC-dextran leakage.

6.6.   Conclusions

In summary, TEBVs presented low mechanical properties when placed with cell culture media, due to the presence of higher concentrations of sodium compared to calcium, which affected alginate crosslinking stability. This conditions lead to perfuse our TEBVs with a flow rate inducing low shear stress. Nonetheless, preliminary results of vasoactivity assay showed that TEBVs were able to constrict and dilate in a dose-dependent response with the presence of phenylephrine and acetylcholine. Future work is required in the improvement of TEBV attachment to the perfusion chamber to avoid TEBV break. Alternatives should include, for example, the use of a mesh around all TEBV structure.

6.7.   References

1.   Niu G, Sapoznik E, Soker S. Bioengineered blood vessels. Expert Opin Biol Ther. 2014;14(4):403–10.

2.   Tresoldi C, Pellegata AF, Mantero S. Cells and stimuli in small-caliber blood vessel tissue engineering. Regen Med. 2015;10(4):505–27.

3.   Huang AH, Niklason LE. Engineering biological-based vascular grafts using a pulsatile bioreactor. J Vis Exp. 2011;(52).

4.   Syedain ZH, Meier LA, Bjork JW, Lee A, Tranquillo RT. Implantable arterial grafts from human fibroblasts and fibrin using a multi-graft pulsed flow-stretch bioreactor with noninvasive strength monitoring. Biomaterials. 2011;32(3):714–22.

5.   Paszkowiak JJ, Dardik A. Arterial wall shear stress: Observations from the bench to the bedside. Vasc Endovascular Surg. 2003;37(1):47–57.

6.   Papaioannou TG, Stefanadis C. Vascular wall shear stress: Basic principles and methods. Hell J Cardiol. 2005;46(1):9–15.

7.   Jung Y, Ji H, Chen Z, Fai Chan H, Atchison L, Klitzman B, et al. Scaffold-free, Human Mesenchymal Stem Cell-Based Tissue Engineered Blood Vessels. Sci Rep. 2015;5:1–9.

8.   Fernandez CE, Yen RW, Perez SM, Bedell HW, Povsic TJ, Reichert WM, et al. Human vascular microphysiological system for in vitro drug screening. Sci Rep. 2016;6(21579).

9.   Strobel HA, Hookway TA, Piola M, Fiore GB, Soncini M, Alsberg E, et al. Assembly of Tissue-Engineered Blood Vessels with Spatially Controlled Heterogeneities. Tissue Eng - Part A. 2018;24(19–20):1492–503.

10.   Han HC, Ku DN. Contractile responses in arteries subjected to hypertensive pressure in seven-day organ culture. Ann Biomed Eng. 2001;29(6):467–75.

11.   Li Y, Huang G, Zhang X, Wang L, Du Y, Lu TJ, et al. Engineering cell alignment in vitro. Biotechnol Adv. 2014;32(2):347–65.

12.   Deanfield JE, Halcox JP, Rabelink TJ. Endothelial function and dysfunction: Testing and clinical relevance. Circulation. 2007;115(10):1285–95.

13.   Allen JB, Khan S, Lapidos KA, Ameer GA. Toward engineering a human neoendothelium with circulating progenitor cells. Stem Cells. 2010;28(2):318–28.

14.   Ando J, Yamamoto K. Effects of Shear Stress and Stretch on Endothelial Function. Antioxid Redox Signal. 2011;15(5):1389–403.

15.   Shyu KG. Cellular and molecular effects of mechanical stretch on vascular cells and cardiac myocytes. Clin Sci. 2009;116(5):377–89.

16.   Beamish JA, He P, Kottke-Marchant K, Marchant RE. Molecular regulation of contractile smooth muscle cell phenotype: Implications for vascular tissue engineering. Tissue Eng - Part B Rev. 2010;16(5):467–91.

17.   Eoh JH, Shen N, Burke JA, Hinderer S, Xia Z, Schenke-layland K, et al. Enhanced elastin synthesis and maturation in human vascular smooth muscle tissue derived from induced-pluripotent stem cells. Acta Biomater. 2017;52:49–59.

18.   Tortora GJ, Derrickson BH. Chapter 21. The cardiovascular system: Blood Vessels and Hemodynamics. In: Principles of anatomy & physiology. JSTOR; 2011. p. 740–807.

19.   Kim DH, Heo SJ, Kang YG, Shin JW, Park SH, Shin JW. Shear stress and circumferential stretch by pulsatile flow direct vascular endothelial lineage commitment of mesenchymal stem cells in engineered blood vessels. J Mater Sci Mater Med. 2016;27(60):1–11.

20.   Konig G, Mcallister TN, Ph D, Dusserre N, Garrido S a, Iyican C, et al. Mechanical properties of completely autologous human tissue engineered blood vessels compared to human saphenous vein and mammary artery. 2009;30(8):1542–50.

21.   Canham PB, Finlay HM, Boughner DR. Contrasting structure of the saphenous vein and internal mammary artery used as coronary bypass vessels. Cardiovasc Res. 1997;34(3):557–67.

22.   Fernandez CE, Yen RW, Perez SM, Bedell HW, Povsic TJ, Reichert WM, et al. Human vascular microphysiological system for in vitro drug screening. Sci Rep. 2016;6(21579):1–14.

23.   Gauvin R, Guillemette M, Galbraith T, Bourget JM, Larouche D, Marcoux H, et al. Mechanical properties of tissue-engineered vascular constructs produced using arterial

or venous cells. Tissue Eng - Part A. 2011;17(15–16):2049–59.

24. Claes E, Atienza JM, Guinea G V., Rojo FJ, Bernal JM, Revuelta JM, et al. Mechanical properties of human coronary arteries. In: 2010 Annual International Conference of the IEEE Engineering in Medicine and Biology Society, EMBC'10. 2010. p. 3792–5.

25. Oyane A, Kim H, Furuya T, Kokubo T, Miyazaki T, Nakamura T. Preparation and assessment of revised simulated body fluids. J Biomed Mater Res Part A. 2003;65A(2):188–95.

26. Lee KY, Mooney DJ. Alginate: Properties and biomedical applications. Prog Polym Sci. 2012;37(1):106–26.

27. Gao Q, Liu Z, Lin Z, Qiu J, Liu Y, Liu A, et al. 3D Bioprinting of Vessel-like Structures with Multi-level Fluidic Channels 3D Bioprinting of Vessel-like Structures with Multi-level Fluidic Channels. ACS Biomater Sci Eng. 2017;3(3):399–408.

28. Gao G, Lee JH, Jang J, Lee DH, Kong JS, Kim BS, et al. Tissue Engineered Bio-Blood-Vessels Constructed Using a Tissue-Specific Bioink and 3D Coaxial Cell Printing Technique: A Novel Therapy for Ischemic Disease. Adv Funct Mater. 2017;27(33):1–12.

29. Tilling L, Hunt J, Donald A, Clapp B, Chowienczyk P. Arterial injury and endothelial repair: Rapid recovery of function after mechanical injury in healthy volunteers. Cardiol Res Pract. 2014;2014.

30. Andrique L, Recher G, Alessandri K, Pujol N, Feyeux M, Bon P, et al. A model of guided cell self-organization for rapid and spontaneous formation of functional vessels. Sci Adv. 2019;5(6).

CHAPTER7

Extrusion of high concentrated collagen for tissue engineering blood vessel development

CHAPTER 7. Extrusion of high concentrated collagen for tissue engineering blood vessel development

7.1.   Introduction

The choice of the biomaterial for developing a tissue engineered blood vessel (TEBV) is of special importance, as it should recreate the native extracellular matrix to allow cell attachment and spreading and, at the same time, it should possess enough mechanical stability to withstand physiological flow rates. Regarding the achievement of biological properties, natural polymers have gained special attention. Amongst them, collagen has been considered a good candidate as it is the most prevalent extracellular matrix (ECM) protein found in all three tunica (intima, media and adventitia) of native arteries (1). The first attempt in developing a three-layered TEBV was performed with collagen by Weinberg and Bell in 1986 using matrix molding approach (2). However, those TEBVs did not present adequate mechanical properties, even when a Dacron mesh was added as structural support to further enhance their mechanical stability, obtaining burst strength of 120-180 mmHg. These values were significantly lower in comparison to 2000-3000 mmHg obtained with physiological vessels such as saphenous vein and internal mammary artery (3).It is worth to mention that concentration of collagen used was below 2 mg/mL and Dacron mesh was the one providing most of the structural support. In the last years, different strategies have been followed to increase the mechanical properties of collagen gel for TEBV development. For instance, Li *et al* developed 1 mm inner diameter vessel with a final collagen concentration of 6.3 mg/ml using the matrix molding approach. After collagen gelification, the vascular conduit was dried overnight at 37ºC to increase collagen density. The day after, the TEBV was rehydrated and crosslinked with genipin. This process resulted in an increase of mechanical properties with a burst pressure of 1300 mmHg (4). In a slightly different approach, enhancement of mechanical strength of TEBVs through collagen fiber densification was achieved by plastic compression. More in detail, this process consists on removing the water content of collagen TEBV (with an initial collagen concentration of 2 mg/mL) using absorbing sterile kimwipes. Following this process, the TEBVs with an inner diameter of 800 μm achieved a burst pressure of 1600 mmHg (5), comparable to saphenous vein. In this last case, matrix molding approach was also used for the development of vascular conduit. Generally, when collagen is used for TEBV manufacturing, some support is necessary to avoid its spreading and to maintain tubular shape while being gelled. In this regard, matrix molding is the method of choice, although it can be

limited for developing more sophisticated structures. In this regard, the ability to create complex structures such as bifurcated vessels with collagen, has recently been demonstrated using 3D printing method (6). In more detail, they could print small coronary artery-scale comparable to left anterior descending artery of 9 mm length, 1.4 mm of inner diameter and a wall thickness of 300 μm. To allow collagen integrity during 3D printing process, the authors extruded a high concentration collagen (24 mg/mL) into a gelatin microparticle support bath. In another study, slightly higher concentrations of collagen (30 mg/mL) were used for the development of different a-cellular tissue-like structures such as blood vessels (7). In this second study, the authors used a pre-shaped print head according to the tissue they aimed to develop. Moreover, the collagen was directly printed into DMEM, being able to preserve its structure. These recent contributions demonstrate the possibility to extrude pure collagen while preserving its structure by using high concentrations.

Previously, in chapter 5, we described a method to develop tissue engineered blood vessels (TEBV) using a triple co-axial nozzle. It would be interesting to use the same method to develop in one step procedure TEBVs with high concentrations of collagen, incorporating specific vascular cell types. To the best of our knowledge, this has not been performed before using our extrusion co-axial approach, and would significantly reduce manufacturing steps compared to matrix molding.

7.2.   Objectives

The aim of this chapter is the development of tissue engineered blood vessels (TEBV) in one step procedure using high concentrations of collagen with our triple co-axial nozzle extrusion method. We also aim to incorporate specific vascular cell types and assess their viability and also to assess the feasibility of TEBV perfusion with arterial shear stress.

7.3.   Materials & Methods

7.3.1. Isolation of collagen type I

Collagen type I was isolated from bovine tendons obtained from an abattoir and all the isolation process was based on well-established protocols (8). First, tendon was separated from the surrounding fascia and was cut to small pieces with the aid of a blender, followed by three washes with phosphate buffered saline (PBS). Then, the sliced tendon was dissolved with 1M acetic acid under agitation for 72h. Enzymatic digestion was performed using porcine

gastric mucosa pepsin (Sigma-Aldrich) at 40U/mg of tendon under stirring, 2h at room temperature (<20 ºC) and 72h at 4ºC. The resultant enzymatic digestion was filtered to obtain pepsin soluble collagen and was purified by salt precipitation (0,9 M NaCl) during 24h. The precipitated collagen was collected and dissolved with 1M acetic acid under stirring for 5 days. Finally, collagen solution was dialyzed (MW 8,000 cut off) repeatedly against 1mM acetic acid and the dialyzed collagen solution was kept at 4ºC. Collagen concentration was determined using dry weight and collagen purity was evaluated using sodium dodecyl sulfate polyacrylamide gel electrophoresis (SDS-PAGE) followed by Coomassie staining and densitometry analysis with ImageJ software.

7.3.2. Obtaining high concentrations of collagen

Once collagen was isolated and its purity assessed (performed in chapter 5), it was then frozen at -20ºC for at least 24h, followed by lyophilization (Cryodos-80, Telstar). Afterwards, lyophilized collagen (**Figure 1 i)** was cut into small pieces (**Figure 1 ii**) and dissolved with cold 50 mM acetic acid to the desired concentration (**Figure 1 iii**). Specifically, we dissolved collagen at concentration of 10 and 20 mg/mL.
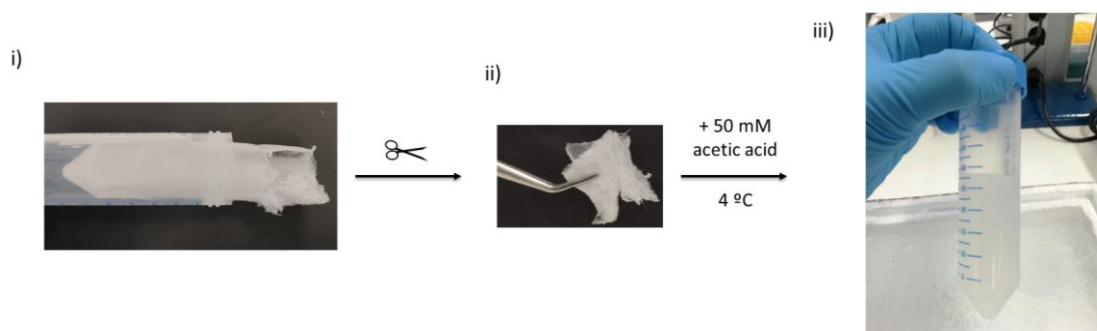

Figure 1. Obtaining high concentration of collagen. i) After collagen lyophilization, it is cut ii) to small pieces and then iii) dissolved with cold 50 mM acetic acid. Picture on the right (iii) shows 20 mg/mL of collagen type I dissolved.

7.3.3. Development of gelatin microparticles support bath

Schematic representation of gelatin microparticles support bath is shown in **Figure 2.** First, a solution containing a final concentration of 2% (w/v) gelatin Type B (Sigma-Aldrich), 0.25% (w/v) Pluronic F-127 (Sigma-Aldrich) and 0.1% (w/v) gum arabic (Sigma-Aldrich) in 1L of 50% (v/v) ethanol (PanReac AppliChem) was heated to 45ºC. The pH was adjusted to 6.25 with 1M hydrochloric acid (HCl). Then, the beaker was placed on stirrer (MS-H-S, Dlab), sealed with parafilm to avoid solution evaporation and cooled at room temperature while stirring overnight for microparticle formation. To compact the gelatin microparticles, the slurry was

divided with 50 mL conical tubes and centrifuged at 300g for 5 min. After removing the supernatant, the microparticles were resuspended with 1x phosphate buffered saline (1x PBS) at pH 7.4 (washing solution) and centrifuged at 1000g for 2 min. This washing step was repeated three times. Then, the gelatin microparticle slurry was kept at 4ºC with 1x PBS in its uncompacted state (they could be stored up to 1 month at 4ºC). Prior to TEBV extrusion, gelatin microparticles were compacted by centrifuging them at 2000g for 5 min. Supernatant was removed and gelatin slurry was transferred into a petri dish.
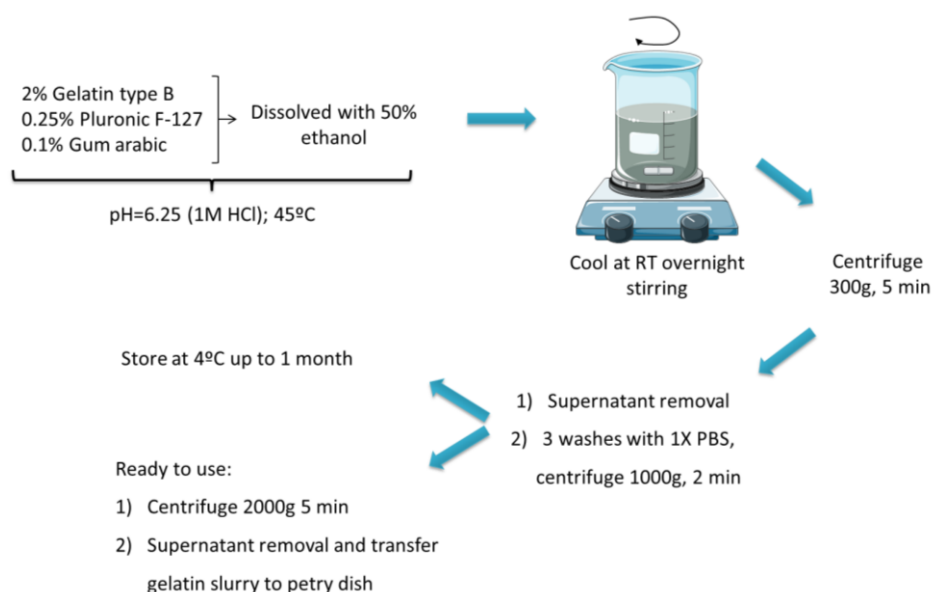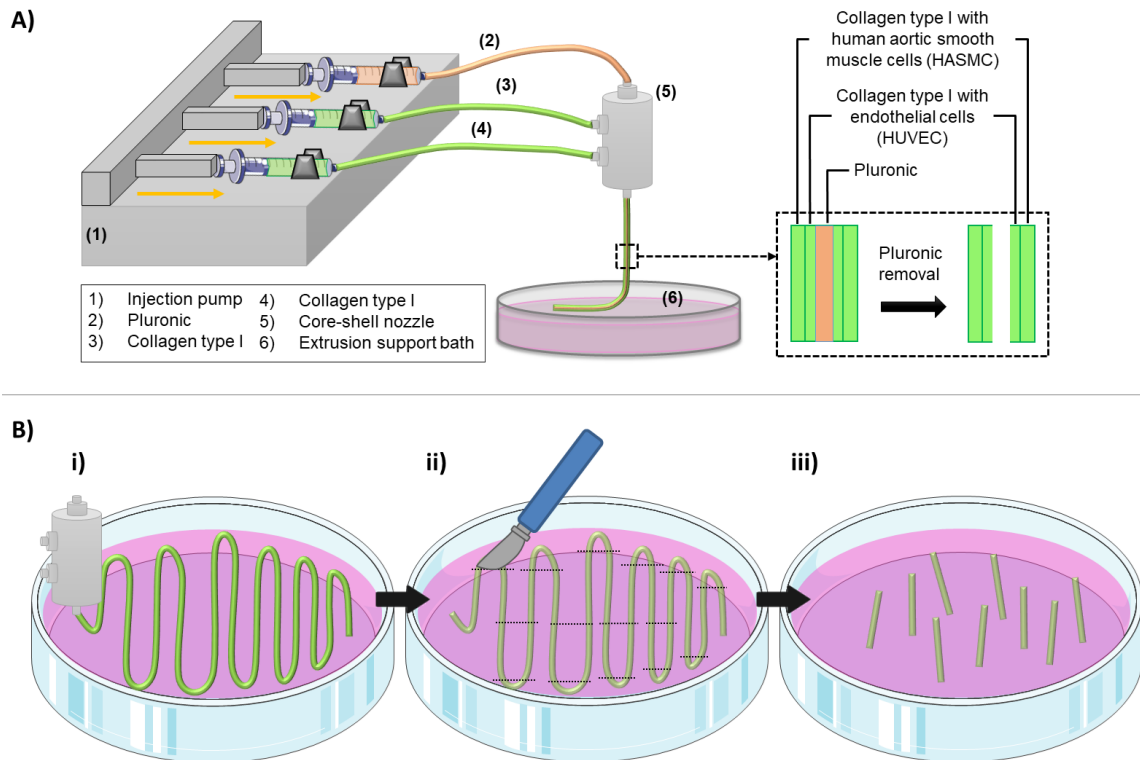

Figure 2. Schematic representation of gelatin microparticle extrusion support development.

7.3.4. Cell culture

Human umbilical vein endothelial cells (HUVECs) (Lonza) and human aortic smooth muscle cells (HASMCs) (ATCC) were used. For cell expansion, HUVEC were seeded at a density of 2500 cells/cm^2 with endothelial growth medium-2 bulletkit (EGM-2) (Lonza) containing VEGF, rhFGF-B, rhEGF, r-IGF-1, hydrocortisone, ascorbic acid, gentamicin sulfate, amphotericin-B and 2% of FBS. HASMC were seeded at a density of 2500 cells/cm^2 with vascular cell basal medium supplemented with vascular smooth muscle cell growth kit (ATCC) containing 5 ng/mL rh-FGF-basic, 5 μg/mL rh-Insulin, 50 μg/mL ascorbic acid, 10 mM L-glutamine, 5 ng/mL rh EGF, 5% FBS and 1% Penicillin-streptomycin. When both cell types reached 70-85% confluence, they were passaged using 0,25% Trypsin-EDTA (Gibco) or they were ready to be used for TEBV development. All cells were cultured in standard cell culture conditions (37ºC and 5% CO$_2$).

7.3.5. Collagen tissue engineered blood vessel (TEBV) development

The procedure explained in chapter 5 (section 5.3.4 and 5.3.5) was followed with some modifications. Schematic representation of the method is shown in **Figure 3A**. A triple concentric nozzle (23G inner, 17G middle and 13G outer) (NanoNC) was fed with the help of injection pumps with two different materials placed in three syringes to allow the formation of tricentric fiber. The inner syringe was loaded with 25% wt Pluronic F-127 (Sigma-Aldrich) aqueous solution, as a sacrifice material. The middle and outer syringes were loaded with the previously extracted collagen type I at a concentration of either 10 or 20 mg/mL. Collagen was self-assembled by adding 200 µL of 10x DMEM (Sigma-Aldrich) and the necessary amount of NaOH, 1M or 5M, was added to 2 mL of collagen. Three injection speeds were tested (10, 25 and 50 ml/h) for two main purposes: i) to study the effect of the injection speed on the general parameters of the blood vessel-like structure, mainly shell thickness and inner and outer diameter and ii) to determine which injection speed would allow us to control more uniformly the movement of the triple co-axial nozzle along the petri dish, facilitating the development of straight TEBVs (see **Figure 3Bi** for the extrusion pattern to follow). All the loaded syringes were kept at 4ºC. Then, the solutions were extruded at the same time in a petri dish containing an extrusion bath. Specifically, two types of extrusion baths were tested: gelatin microparticles slurry (at room temperature, approximately 20 ºC), or endothelial growth medium-2 (EGM-2, Lonza) (both at 37ºC). The purpose of testing gelatin microparticles slurry as a support bath was to ensure structural support to the extruded collagen, allowing its gelification without spreading. We also wanted to test if collagen could maintain its structure once extruded into EGM-2 medium without the need of structural support, as previously reported with higher collagen concentrations (7). After 10 min of the extrusion, the petri dish was placed at 37ºC, which further allowed collagen gelification and, in the case of gelatin microparticle, allowed their melting leaving behind collagen vessel gelled. Afterwards, TEBVs were cut to the desired length (**Figure 3Bii-iii)** and pluronic was removed from the inner core by dissolution with cell culture media during 5 min, obtaining TEBV structure. To assess the feasibility of perfusion of TEBVs, they were cut to 2.5 cm length, the appropriate size to incorporate them in the perfusion chamber.

Figure 3. Schematic representation of collagen TEBV development through triple concentric extrusion method. A) Pluronic (2) and collagen type I (3 and 4) are injected into a triple concentric nozzle (5) in the inner, middle and outer layer, respectively. These biomaterials are extruded in a constant injection speed controlled by an injection pump (1) into a petri dish containing an extrusion support bath (6). The fibers are incubated at room temperature (approximately 20ºC) for 10 min followed by an incubation at 37ºC for 10-15 min to allow collagen gelation. Then, pluronic is removed from the inner core, obtaining a hollowed dual layer tubular structure. B) i) Once TEBVs are extruded and gelled, ii-iii) the straight parts are cut to the desired length.

For cell encapsulation, HUVEC cells were added at a concentration of 15×10^6 cells/mL in the middle collagen syringe, and HASMCs were added at a concentration of 10×10^6 cells/mL in the outer collagen syringe. For cell viability and 3D reconstruction assays, TEBV were cut to a length of 1 cm.

7.3.6. Cell viability assay

Viability of HUVEC and HASMCs incorporated within in collagen TEBV was assessed at 24h, to quantitatively assess cell survival after the shear stress produced by the extrusion method with two high concentrations of collagen, specifically 10 and 20 mg/mL. The LIVE/DEAD cell imaging kit (Invitrogen) was used following manufacturer's instructions. Briefly, the methodology consists of a live component which stains live cells giving a uniform green fluorescence (excitation/emission wavelengths were 488/515 nm) and a dead component which stains death cells producing a nuclear red fluorescence (excitation/emission wavelengths were 570/602 nm). Equal volumes of both components were added in the cell culture medium with

TEBVs reaching a final concentration of 1x. After 15 minutes of incubation protected from light, cells were imaged with a laser scanning confocal microscope (Leica SP8, LAS X software version 3.5.5.19976). As a positive control for cell death, some TEBV were prior treated with 4% PFA at room temperature during 30 min followed by an incubation with 1x PBS/0,5% triton X-100 during 10 min. Three samples per time point were analyzed and three captures at different plans per sample were acquired. Images were analyzed using ImageJ software (ImageJ 1.52a) and live and dead cells were counted for each one. Viability was calculated as number of live cells divided per total number of cells (live and dead), as a percentage.

7.3.7. 3D reconstruction of tissue engineered blood vessels loaded with fluorescent labeled HUVECs and HASMCs

In order to check if HUVEC and HASMCs could remain in their respective layers once extruded, inner and outer layers, respectively, each cell type was stained with different colored cell tracker fluorescence probes previous the development of TEBV structures. HUVEC cells were stained with Green CMFDA (Invitrogen) and HASMC were stained with Red CMTPX (Invitrogen), emitting a green and red signal, respectively. Each cell tracker was added in the specific cell culture media at a final concentration of 10 µM and incubated with cells during 45 min at 37 ºC in 5% CO_2 protected from light. After incubation, cells were detached with Trypsin-EDTA (Gibco), centrifuged at 150xg for 3 min and used for blood vessel formation. Once TEBV were developed, they were imaged at 2 days by a confocal laser microscopy (Leica SP8, LAS X software version 3.5.5.19976). The excitation/emission wavelengths were 492/517 for Green CMFDA and 577/602 for Red CMTPX. Images were processed and 3D reconstruction was performed with the same confocal software.

7.3.8. Proof of concept of tissue engineered blood vessel perfusion

Finally, after checking the viability and allocation of cells within collagen TEBV structure, we wanted to check if these TEBVs were able to withstand physiological flow rate with an arterial shear stress of 10 dynes/cm^2 to perform functional assays in the future. To this purpose, we calculated the appropriate flow rate according to our TEBVs size with Poiseuille formula (described in chapter 6, section 6.3.2.2). We tested if they could withstand physiological arterial shear stress with cell free TEBV containing collagen at a concentration of 20 mg/mL and perfuse with endothelial cell growth medium-2 (EGM-2, Lonza) with non-sterile conditions. The same perfusion system described in chapter 6 (section 6.3.4) was used.

7.3.9. Statistical analysis

Statistical analysis was performed using SPSS software (SPSS v21, IBM). Kruskall-Wallis and Mann Whitney U non parametric test were used to compare if there were differences between the outer diameter, inner diameter and wall thickness of TEBVs extruded with different injection speeds and between collagen concentrations. Data was represented as mean ± standard deviation; n=8. P-value of less than 0.05 was considered statistically significant.

7.4. Results

7.4.1. Optimal conditions for high concentration collagen tissue engineered blood vessel (TEBV) development

We wanted to assess first which extrusion bath was more appropriate for the extrusion of collagen TEBV. Then, we assessed how the injection speed influenced the size of TEBVs and which one facilitated the printing process.

The size of gelatin microparticles was around 100 µm as illustrated in **Figure 4A.** For testing different support baths, TEBVs were extruded using a concentration of 10 mg/mL of collagen. Gelatin microparticle slurry allowed the extrusion of TEBVs maintaining their tubular structure (**Figure 4B**). More interestingly, the high concentration of collagen provided enough stability to allow the extrusion of TEBV in cell culture media while preserving the tubular structure without spreading, as illustrated in **Figure 4C**. Taking into account that vascular cells would be incorporated within TEBV structure, we decided to use cell culture media as the support bath for the subsequently assays, as it would provide a more cell friendly environment for their survival. At the same time, this would require less manufacturing steps.
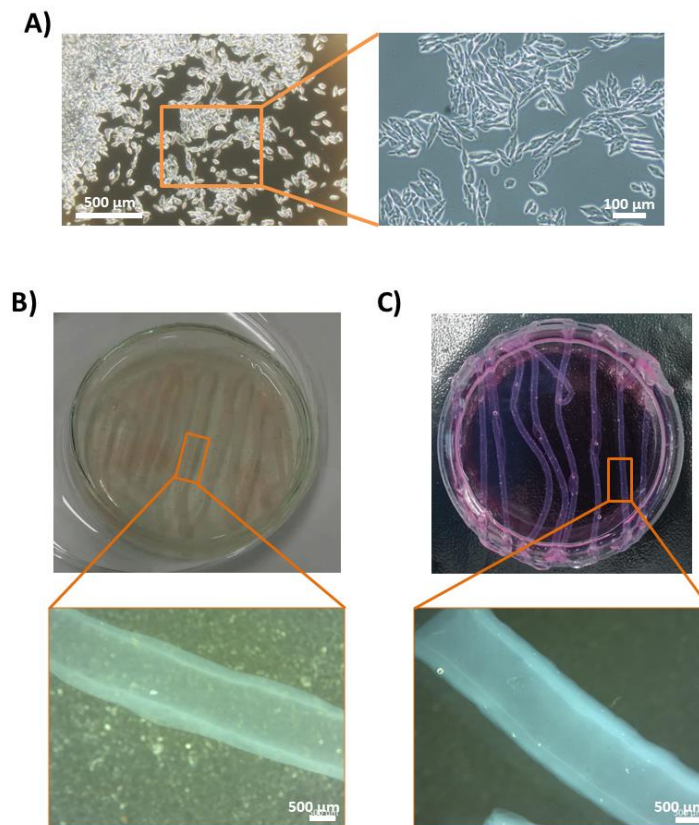
Figure 4. A) Optical images of gelatin microparticles support bath. TEBVs extruded with collagen concentration of 10 mg/mL in B) gelatin microparticles or C) in cell culture media, with 25 mL/h as injection speed.

Results of sizes of TEBVs (outer diameter, inner diameter and wall thickness) depending on the injection speed and collagen concentration are represented in **Figure 5**. In general, when comparing how injection speed influenced the sizes for each collagen concentration, they were reduced with 10 mg/mL and increased with 20 mg/mL as injection speed was increased. Nonetheless, the inner diameter remained the same with 10 mg/mL for all injection speeds tested. It is worth to highlight that wall thickness was significantly higher with 10 mg/mL of collagen for the injection speeds of 10 and 25 mL/h.
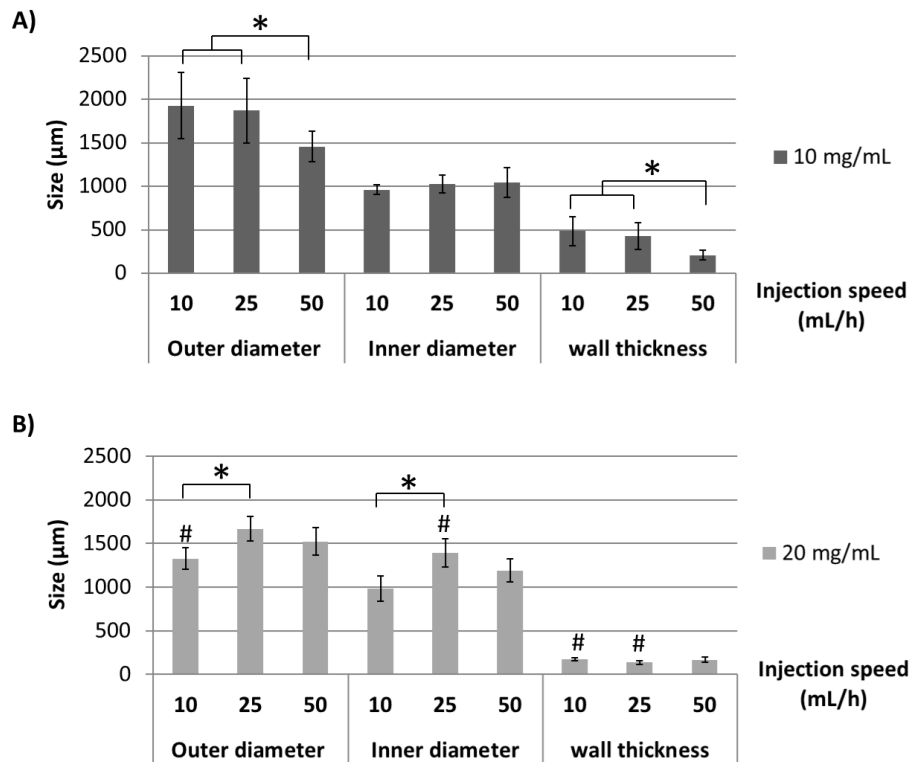
Figure 5. TEBVs size. Size of outer diameter, inner diameter and wall thickness depending on the injection speed with collagen at A) 10 mg/mL and B) 20 mg/mL. Data represented as mean with standard deviation (n=8 per condition).

*=statistically significant differences between injection speeds for the same collagen concentration (p<0.05); #= statistically significant differences between collagen concentrations for the same injection speed.

We also calculated the coefficient of variation (CV) of wall thickness. With 10 mg/mL, the coefficient of variation for 10, 25 and 50 mL/h were 34.5, 36.8 and 25.7%, respectively. With 20 mg/mL, the CV were 10.8, 17.1 and 17.9% for 10, 25 and 50 mL/h, respectively, suggesting a more wall thickness homogeneity with higher collagen concentration.

As we had to move the triple co-axial nozzle manually during extrusion along the petri dish, we decided to use 25 mL/h as injection speed for the rest of the experiments. This velocity allowed us to control the movement of the triple co-axial nozzle more uniformly, facilitating the formation of straight TEBVs. With 50 mL/h we had some difficulties and 10 mL/h was too slow.

7.4.2. Viability of HUVEC and HASMC extruded within TEBVs

We wanted to assess if cells would be able to survive within both high collagen concentrations once extruded, specifically with 10 and 20 mg/mL. After 24h of extrusion, viability of cells was 86.0% and 85.8% for 10 and 20 mg/mL of collagen, respectively (**Figure 6**). At this point, as both concentrations presented similar high viability, we decided to use the highest

concentration of collagen for the subsequently assays, as it would provide more mechanical stability.
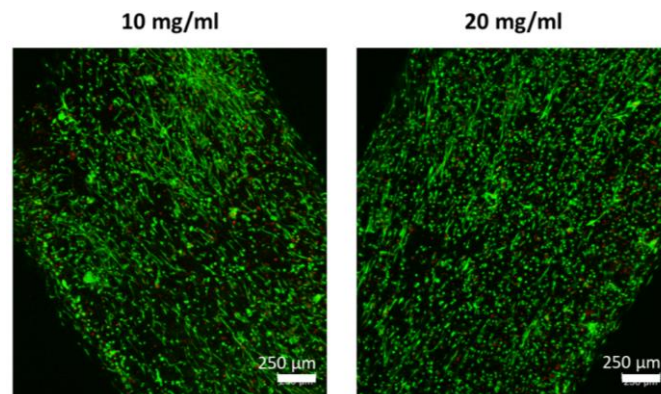
Figure 6. Vascular cell viability. Live/dead assay performed on TEBV containing HUVEC and HASMCs in co-culture at 24h after extrusion. Live cells (green) and dead cells (red).

During cell culture of TEBVs with 20 mg/mL of collagen, some cells started to proliferate within few hours, as shown in **Figure 7A.** After 2 days, practically all cells were lengthened (**Figure 7B**), and from day 5, TEBVs started to fold (**Figure 7C**) due to cell stretching. Each cell type could not be distinguished during culture time. However, these observations were consistent throughout all TEBV 3D structure plans.
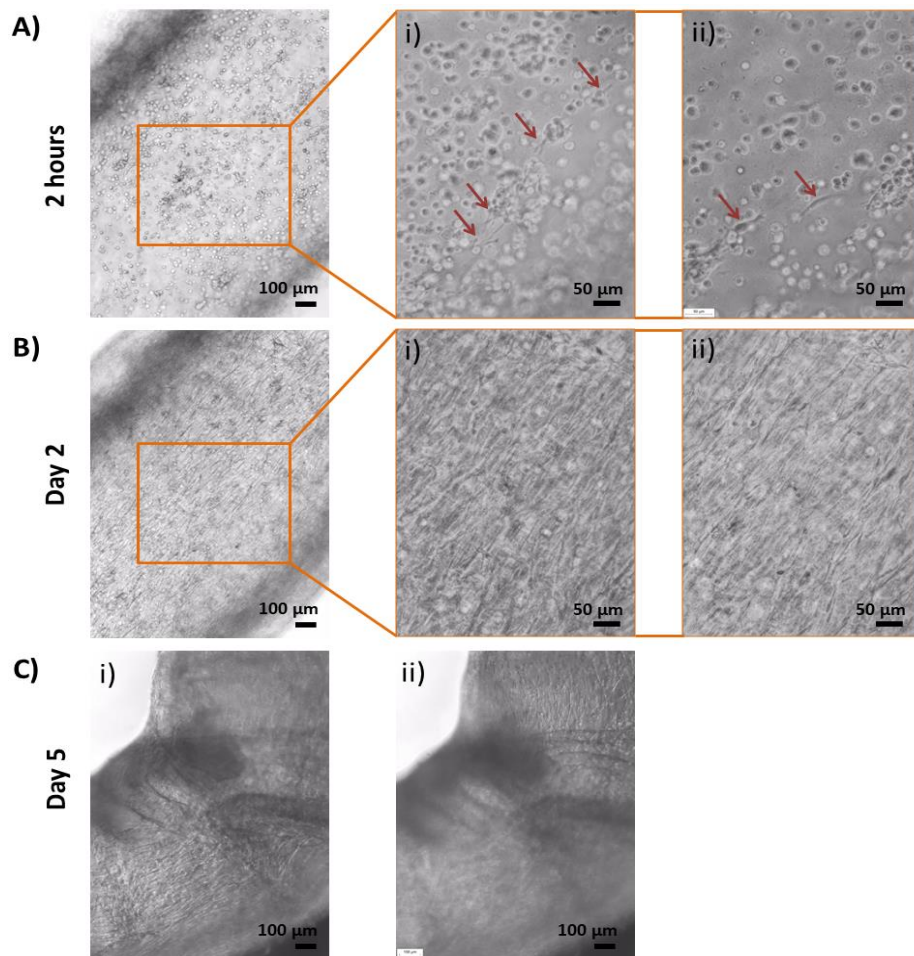
Figure 7. Images of TEBVs with HUVEC and HASMC in co-culture. A) First cells spreading after 2h of TEBV culture. On the right are presented magnifications at two different plans with red arrows pointing out stretched cells. B) Practically all cells were lengthened within 2 days of TEBV culture. On the right are magnifications at two different plans. C) TEBVs started to blend from day 5. Images from two different plans.

7.4.3. 3D reconstruction of collagen tissue engineered blood vessel

HUVEC and HASMCs were stained with specific cell tracker (color green and red, respectively) in order to visualize and confirm if cells were allocated in their respective layers within TEBV construct. As can be observed in **Figure 8**, cells covered all tubular structure within 2 days of culture. It is worth to mention that few HASMCs were visualized in HUVECs layer in the upper part, and some HUVECs in the SMCs layer in the bottom part.
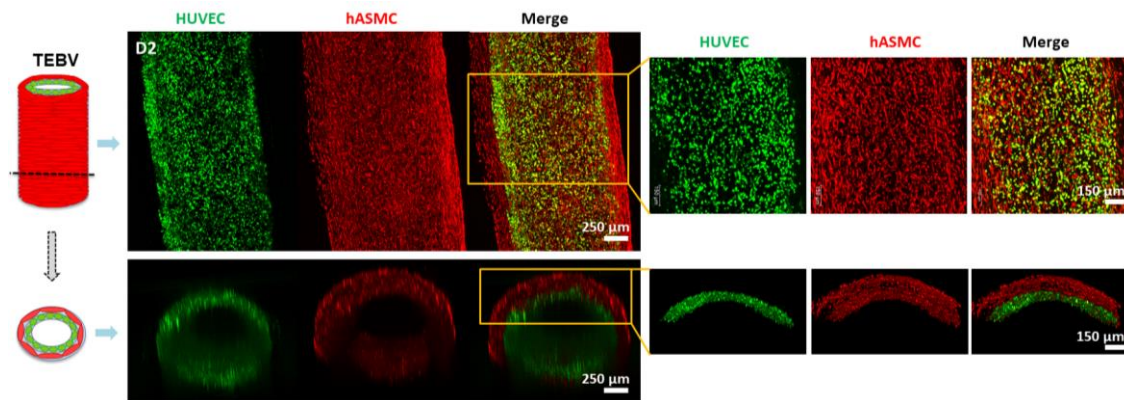
Figure 8. TEBV cell tracker reconstruction with confocal microscope at day 2. Each color indicates different cell types: HUVEC in green and HASMCs in red at day 2. On the right there is a magnification of the TEBV.

7.4.4. Preliminary results of tissue engineered blood vessels (TEBVs) perfusion

As a final experiment, we wanted to assess if these TEBVs with a collagen concentration of 20 mg/mL were able to withstand physiological flow rate equivalent to arterial shear stress of 10 dynes/cm^2. To this purpose, we attached them in the perfusion chamber and perfused them with
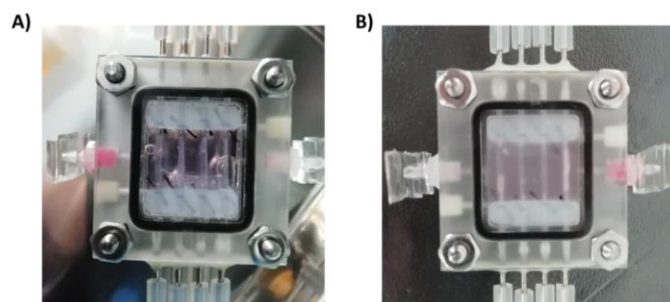
Figure 9. Cell-free TEBVs perfusion. 20 mg/mL of collagen cell-free TEBVs perfused with cell culture media. Images correspond to A) 4h perfusion and B) 3 days perfusion.

cell culture media at 37ºC with non-sterile conditions. After 3 days, cell-free TEBVs were able to withstand arterial flow rate and shear stress corresponding to 10 dynes/cm^2, as shown in **Figure 9**. Perfusion was stopped at this point due to contamination.

7.5. Discussion

In this chapter, we aimed to extrude TEBVs with high concentration of collagen type I as the unique biomaterial composition and assess if cells were able to survive within them and if they had enough mechanical properties to withstand perfusion equivalent to arterial shear stress. To this purpose, we first tested two different support baths for their extrusion. One of them was gelatin microparticles, based on a previous study (6), to give structural support to extruded collagen to avoid its spreading. The gelatin microparticle size reported in this study

was approximately 25 μm, whereas we obtained microparticle size around 100 μm (**Figure 4A**). Nonetheless, the size we obtained allowed us to print collagen TEBVs while maintaining their tubular structure (**Figure 4B**). Remarkably, the high concentrations of collagen tested also allowed maintaining the tubular structure when extruded in cell culture media solutions without spreading (**Figure 4C**), demonstrating that no structural support was needed to extrude TEBVs. Therefore, we finally chose cell culture media as a support bath for collagen TEBV extrusion, as it would ameliorate cell survival due to the presence of nutrients and growth factors, and at the same time, it would reduce one step the TEBV manufacturing process, avoiding the need to previously fabricate a support bath.

Following the optimization of extrusion bath, we wanted to elucidate how the injection speed influenced TEBVs size in both collagen concentrations, and which injection speed facilitated the uniform movement of triple co-axial nozzle while extruding. Interestingly, wall thickness was in general higher when 10 mg/mL was used compared to 20 mg/mL (**Figure 5**). Lower collagen concentration tested had lower consistency, and therefore, during the transition from liquid to gel state, it might spread more resulting in a higher wall thickness. This reason might also explain thinner wall thickness of TEBVs when 20 mg/mL was used, presenting lower coefficient of variation, which was indicative of more homogeneous wall size. In general, there were no big differences in TEBV size between both collagen concentrations. Similarly to TEBVs from Chapter 5, the outer and inner diameters of TEBVs obtained were in the range of arteries, as described to be within 100 μm and 10 mm (9). Between the three injection speeds tested, 25 mL/h was the one which facilitated us the most uniformly movement of the triple co-axial nozzle when extruding the TEBVs.

As a next step, we wanted to choose one collagen concentration to develop TEBVs for the subsequent assays. To this purpose, we encapsulated both HUVEC and HASMCs within TEBVs and tested two concentrations, 10 and 20 mg/mL, to assess if cells were able to survive through extrusion process and within these high collagen concentrations as ECM. After 24h of extrusion and culture, viability was 86.0% and 85.8% for 10 and 20 mg/mL, respectively (**Figure 6**). These are positive results, as it has been previously described that, generally, viability of cells using microextrusion bioprinting is between 40 and 86% (10,11). However, other studies reported higher viability specifically using high collagen concentrations. For instance, Lee *et* obtained a viability of approximately 96% using 24 mg/mL of collagen, although they used a different cell type, cardiomyocytes, and assessed the viability after 1h of printing (6). Another study reported viability of approximately 90% using ECs and liver cells (HepG2), up to day 5 of culture (7). More recently, other authors reported viability of NIH 3T3 to be 97, 95 and 87%

with 20, 30 and 40 mg/mL after 7 days culture (12). Nonetheless, our results indicate that the extrusion method is not harmful for these cells and cells could survive in both collagen concentrations. When 20 mg/mL of collagen was used, spreading of cells was observed as early as 2h, and practically all cells were stretched within 2 days (**Figure 7**). Furthermore, TEBV folding was observed at day 5, probably due to the strength of cells when adhering and spreading, suggesting a proper environment for their adhesion and proliferation. Accordingly to these results, we decided to use 20 mg/mL of collagen concentration for TEBV development as it allowed cell survival and it would provide more mechanical stability due to the presence of more collagen fibers compared to 10 mg/mL.

Remarkably, with specific HUVEC and HASMC staining with cell trackers, we could confirm that cells were distributed along all tubular structure (**Figure 8**). Unexpectedly, we also observed the presence of some HASMCs in HUVEC's inner layer, and *vice versa*, few HASMCs in HUVEC's layer, which there might be a possible explanation for this. Just after TEBV extrusion, there is the possibility that during the transition of collagen containing cells from a liquid to gel state, cells might have moved due to gravity. Therefore, HASMCs and HUVEC might have been in contact with its adjacent layer. Although some cells could not be allocated in their respective layers, that might not be considered a bad outcome. A previous study reported the extrusion of endothelial cells (ECs) and smooth muscle cells (SMCs) in the same layer, demonstrating that these cells were able to self-organize (13). More specifically, ECs could form an endothelium with the presence of tight junctions in the inner lumen core, whereas SMCs were allocated in the adjacent layer. Moreover, evidence of cells self-organization ability has also been previously reported (14). Therefore, with the perfusion of our TEBVs, we would expect as well a self-organization triggered by flow rate and shear stress stimulus.

Finally, we could prove that TEBVs developed with 20 mg/mL of collagen could withstand flow rates inducing arterial shear stress of 10 dynes/cm^2, at least up to 3 days, which is similar shear stress used in previous studies with similar TEBV sizes (15,16). This positive result opens the possibility to perfuse vascular cell loaded TEBVs and perform mechanical and functional assays.

7.6.   Conclusions

To conclude, in this chapter we were able to extrude collagen TEBV structures without structural support, previously reported to be necessary to print collagen structures with similar concentration. Moreover, vascular cells were able to survive through the manufacturing process and even with high concentrations. Strikingly, 20 mg/mL collagen TEBV could withstand physiological flow rates equivalent to arterial shear stress, opening the possibility to perfuse them to induce their maturation and functionality.

7.7.   References

1.   Miranda-Nieves D, Chaikof EL. Collagen and Elastin Biomaterials for the Fabrication of Engineered Living Tissues. ACS Biomater Sci Eng. 2017;3(5):694–711.

2.   Weinberg CB, Bell E. A blood vessel model constructed from collagen and cultured vascular cells. Science (80-). 1986;231(4736):397–400.

3.   Konig G, McAllister TN, Dusserre N, Garrido SA, Iyican C, Marini A, et al. Mechanical properties of completely autologous human tissue engineered blood vessels compared to human saphenous vein and mammary artery. Biomaterials. 2009;30(8):1542–50.

4.   Li X, Xu J, Nicolescu CT, Marinelli JT, Tien J. Generation, Endothelialization, and Microsurgical Suture Anastomosis of Strong 1-mm-Diameter Collagen Tubes. Tissue Eng - Part A. 2017;23(7–8):335–44.

5.   Fernandez CE, Yen RW, Perez SM, Bedell HW, Povsic TJ, Reichert WM, et al. Human vascular microphysiological system for in vitro drug screening. Sci Rep. 2016;6(21579):1–14.

6.   Lee A, Hudson AR, Shiwarski DJ, Tashman JW, Hinton TJ, Yerneni S, et al. 3D bioprinting of collagen to rebuild components of the human heart. Science (80-). 2019;365(6452):482–7.

7.   Kang D, Ahn G, Kim D, Kang HW, Yun S, Yun WS, et al. Pre-set extrusion bioprinting for multiscale heterogeneous tissue structure fabrication. Biofabrication. 2018;10(3).

8.   Delgado LM, Shologu N, Fuller K, Zeugolis DI. Acetic acid and pepsin result in high yield, high purity and low macrophage response collagen for biomedical applications. Biomed Mater. 2017 Oct;12(6):65009.

9.   Tortora GJ, Derrickson BH. Chapter 21. The cardiovascular system: Blood Vessels and Hemodynamics. In: Principles of anatomy & physiology. JSTOR; 2011. p. 740–807.

10.   Bishop ES, Mostafa S, Pakvasa M, Luu HH, Lee MJ, Moriatis J, et al. 3-D bioprinting technologies in tissue engineering and regenerative medicine : Current and future trends. Genes Dis. 2017;4(4):185–95.

11.   Chang R, Nam JAE, Sun WEI. Effects of Dispensing Pressure and Nozzle Diameter on Cell Survival from Solid Freeform Fabrication - Based Direct Cell Writing. Tissue Eng Part A. 2008;14(1):41–8.

12. Osidak EO, Karalkin PA, Osidak MS, Parfenov VA, Sivogrivov DE, Pereira FDAS, et al. Viscoll collagen solution as a novel bioink for direct 3D bioprinting. J Mater Sci Mater Med. 2019;30(3).

13. Andrique L, Recher G, Alessandri K, Pujol N, Feyeux M, Bon P, et al. A model of guided cell self-organization for rapid and spontaneous formation of functional vessels. Sci Adv. 2019;5(6):1–12.

14. Jakab K, Norotte C, Marga F, Murphy K, Vunjak-Novakovic G, Forgacs G. Tissue engineering by self-assembly and bio-printing of living cells. Biofabrication. 2010;2(2).

15. Han HC, Ku DN. Contractile responses in arteries subjected to hypertensive pressure in seven-day organ culture. Ann Biomed Eng. 2001;29(6):467–75.

16. Strobel HA, Hookway TA, Piola M, Fiore GB, Soncini M, Alsberg E, et al. Assembly of Tissue-Engineered Blood Vessels with Spatially Controlled Heterogeneities. Tissue Eng - Part A. 2018;24(19–20):1492–503.

CHAPTER 8

General conclusions and Future perspectives

CHAPTER 8. General conclusions and future perspectives

8.1.   Conclusions

Copper and cobalt as potential inducers of angiogenesis and osteogenesis

Angiogenic response

1. Concentrations of Cu^{2+} up to 10 µM and Co^{2+} up to 50 µM were non-toxic for HUVEC cells.

2. High concentrations of Cu^{2+} (10 µM) enhanced an early angiogenic response, whereas lower concentrations (0.1 and 1 µM) improved it in a later stage.

3. High concentrations of Co^{2+} (25 and 50 µM) improved the angiogenic response at early and late times.

4. There was a strong correlation between HIF-1α and VEGF expression with Co^{2+} supplementation, but not with Cu^{2+}.

5. The combination of Cu^{2+} and Co^{2+} were toxic for HUVEC and did not enhance the angiogenic response.

Osteogenic response

6. Concentrations of Cu^{2+} up to 10 µM and Co^{2+} up to 100 µM were non-toxic for hBM-MSC.

7. The early gene expression induced by Cu^{2+} and Co^{2+} indicated an early commitment of hBM-MSC to osteogenic differentiation, but later gene expression suggested and impairment.

First approximation of microparticle development method and their encapsulation within fibers as dual drug delivery system

1. Using spraying method, microparticles containing ions could be developed.

2. Spraying method was a technic with high reproducibility allowing the extrusion of alginate combined with hydroxyapatite (HA) up to 1:40 ratio.

3. The ratio selected of 1:40 resulted in a more spherical-like morphology.

4. The ion release from our ion delivery system was influenced by the ion concentration in the crosslinking solutions. Moreover, the release of Cu^{2+} also had an influence in the release of Ca^{2+} and Co^{2+}.

5. Co^{2+} presented a zero order kinetic release whereas Ca^{2+} and Cu^{2+} presented a burst release.

6. The minimum concentration of Cu^{2+} and Co^{2+} incorporated allowed a proper release with potential anti-bacterial properties and stimulation of blood vessel formation.

Direct extrusion of individually encapsulated endothelial and smooth muscle cells mimicking blood vessel structures and vascular native cell alignment

1. The extrusion method using a triple coaxial nozzle allowed the formation of tissue engineered blood vessel (TEBV) in one step procedure, with different diameters depending on the injection speed. The sizes of the vessels obtained were in the range of arteries.

2. After extrusion and up to 20 days of culture, viability of cells was higher than 90% even in co-culture conditions.

3. HUVEC and HASMCs could proliferate in their own layer.

4. HUVEC and HASMCs could mimic the native vascular cell alignment.

Mechanical and functional assessment of tissue engineered blood vessels (TEBV)

1. TEBV placed with distilled H_2O presented enough burst pressure and UTS being able to withstand arterial shear stress.

2. TEBVs placed with cell culture media presented a reduced burst pressure and UTS.

3. TEBV become weaker with cell culture media due to high concentration of Na^+ and low concentration of Ca^{2+}, which allowed a lower flow rate with a shear stress of 4.8 dynes/cm^2.

4. TEBVs showed a low vasoactivity, which can be due to the low flow rate and low shear stress, but they showed a dose-concentration response.

5. Other alternatives to attach the TEBVs in the perfusion chamber are needed to allow perfusion with arterial shear stress.

Extrusion of high concentrated collagen for tissue engineering blood vessel development

1. It was possible to extrude TEBVs with high concentration of collagen through extrusion method using a triple co-axial nozzle.

2. The two extrusion baths tested allowed the extrusion of collagen TEBVs.

3. TEBVs could be extruded maintaining tubular structure with high collagen concentrations (10 and 20 mg/mL).

4. Both 10 and 20 mg/mL of collagen with an extrusion injection speed of 25 mL/h allowed HUVEC and HASMCs survival (≈85%).

5. TEBVs developed with 20 mg/mL of collagen could withstand physiological flow rates with an arterial shear stress of 10 dynes/cm^2 when perfused with cell culture media.

8.2.   Future perspectives

The results obtained in the present doctoral thesis are encouraging in the field of vascular tissue engineering. On one side, we defined a range of therapeutic concentrations of copper and cobalt during time course that could induce angiogenesis and could potentially be included in scaffolds to induce blood vessel network formation. As we studied the ions effect in a gene expression level, further experiments are required to confirm that they have also an effect in a protein expression level. To be able to increase their potentially in tissue engineering and tissue regeneration, it could be interesting to combine these ions with other molecules to elucidate if together they can have synergistic effects requiring lower doses of them.

Regarding the drug delivery system, we were able to introduce potential anti-bacterial and angiogenic properties, showing promising results. A first release of antimicrobial ion followed by a sustained release with zero order kinetics of blood vessel formation ion was achieved, both within therapeutic doses. Moreover, the composition of the system had the potential to stimulate osteogenesis differentiation. These results open the possibility to use this system for bone regeneration, mimicking early phases of regeneration. Moreover, as the system is fiber-based, it could potentially be adapted with 3D printing technology and be used for custom-shape scaffolds to fill bone defects.

Another interesting result in this thesis is derived from tissue engineered blood vessel (TEBV) development. We were able to develop TEBVs mimicking the native architecture and vascular cell alignment, with high percentages of viability and presenting some vasoactive response. Furthermore, we were able to improve their mechanical properties using high concentration of collagen, allowing their perfusion with arterial shear stress for further maturation. Further experiments are required to confirm their functionality and degree of maturation. The present developed TEBVs could have significant clinical relevance if their functionality is achieved. For instance, it could be used as blood vessel replacement in some cardiovascular diseases such as atherosclerosis or aneurisms. Nevertheless, it would be necessary to demonstrate their functionality and patency in *in vivo* studies prior to clinical applications. Moreover, if cells from patients with specific illness are reprogrammed and subsequently differentiated in vascular cell types, they could be incorporated within TEBVs structure as vascular model disease. In addition, this would not only serve as an *in vitro* model which reproduce key features of specific illness, but it could also be used to test drug effectiveness and toxicity, which would reproduce a more human physiological response compared to 2D cell culture or animal

models. Alternatively, these TEBVs could be incorporated within scaffolds, which would allow a direct perfusion once implanted if they are anastomosed with the vasculature of the patient. Therefore, the development of TEBVs opens a wide range of clinical relevant applications.

Supplementary data

Supplementary data

Ethics comitee approval

APROVACIÓ PROJECTE PEL CER/ APROBACIÓN PROYECTO POR EL CER

Codi de l'estudi / *Código del estudio*: IMR-2017-02
Versió del protocol / *Versión del protocolo*: 1.0
Data de la versió / *Fecha de la versión*: 25/10/2017
Títol / *Título*: Core shell designed system for the encapsulation of cells and biological molecules for tissue regeneration

Sant Cugat del Vallès, 6 de febrer de 2018

Investigadora: Èlia Bosch Rué
Director de Tesi: Román Pérez Antoñanzas

Títol de l'estudi / *Título del estudio*: Core shell designed system for the encapsulation of cells and biological molecules for tissue regeneration

Benvolgut/da,

Valorat el projecte presentat, el CER de la Universitat Internacional de Catalunya, considera que, el contingut de la investigació, no implica cap inconvenient relacionat amb la dignitat humana, tracte ètic per als animals ni atempta contra el medi ambient, ni té implicacions econòmiques ni conflicte d'interessos, **però no s'han valorat els aspectes metodològics del projecte de recerca degut a que tal anàlisis correspon a d'altres instàncies.**

Per aquests motius, el Comitè d'Ètica de Recerca, RESOLT FAVORABLEMENT, emetre aquest CERTIFICAT D'APROVACIÓ, per que pugui ser presentat a les instàncies que així ho requereixin.

Em permeto recordar-li que, si en el procés d'execució es produís algun canvi significatiu en els seus plantejaments, hauria de ser sotmès novament a la revisió i aprovació del CER.

Atentament,

Apreciada,

*Valorado el proyecto presentado, el CER de la Universidad Internacional de Catalunya, considera que, el contenido de la investigación, no implica ningún inconveniente relacionado con la dignidad humana, trato ético para los animales, ni atenta contra el medio ambiente, ni tiene implicaciones económicas ni conflicto de intereses, **pero no se han valorado aspectos metodológicos del proyecto de investigación debido a que tal análisis corresponde a otras instancias.***

Por estos motivos, el Comitè d'Ètica de Recerca, RESUELVE FAVORABLEMENTE, emitir este CERTIFICADO DE APROBACIÓN, para que pueda ser presentado a las instancias que así lo requieran.

Me permito recordarle que si el proceso de ejecución se produjera algún cambio significativo en sus planteamientos, debería ser sometido nuevamente a la revisión y aprobación del CER.

Atentamente,

Dr. Josep Argemí
President CER-UIC

Research stage certificate

GEORGE A. TRUSKEY, PROFESSOR
DEPARTMENT OF BIOMEDICAL ENGINEERING
1427 FCIEMAS, BOX 90281

TELEPHONE: (919) 660-5147
FAX: (919) 684-4488

March 4, 2020

This letter is to certify that Ms. Èlia Bosch Rué, a PhD student in the Bioengineering Institute of Technology (BIT) at the Universitat Internacional de Catalunya did research related to her dissertation in my laboratory at Duke University. She was in the laboratory from June 27, 2019 through the end of December 2019. She learned a number of fabrication techniques to prepare and characterize tissue engineered blood vessels and she is now incorporating them into her research.

Sincerely,

George A. Truskey, PhD
R. Eugene and Susie E. Goodson
Professor of Biomedical Engineering
Senior Associate Dean,
Pratt School of Engineering